COASTAL AND OCEANOGRAPHIC ENGINEERING LABORATORY

College of Engineering
University of Florida
Gainesville, Florida

TECHNICAL REPORT NO. 15

LITTORAL DRIFT COMPUTATIONS ALONG THE COAST OF FLORIDA BY MEANS OF SHIP WAVE OBSERVATIONS

by

Todd L. Walton, Jr.

Prepared Under
Grant No. NG-3-72
National Oceanic and Atmospheric
Administration Sea Grant Program
Washington, D. C.
February, 1973

COASTAL AND OCEANOGRAPHIC ENGINEERING LABORATORY

University of Florida
Gainesville, Florida

Technical Report No. 15

LITTORAL DRIFT COMPUTATIONS ALONG THE COAST OF FLORIDA BY MEANS OF SHIP WAVE OBSERVATIONS

By

Todd L. Walton, Jr.

Prepared Under
Grant No. NG-3-72
National Oceanic and Atmospheric
Administration Sea Grant Program
Washington, D. C.
February, 1973

ACKNOWLEDGEMENTS

The author is indebted to Dr. R. G. Dean for his guidance and valuable comments throughout the project which led to this report. The encouragement given by him during the writing of this report is also deeply appreciated. The author also wishes to thank Dean M. P. O'Brien for his valuable suggestions, and review of the report.

In addition, thanks go to Mrs. Susan Phillips and Mrs. Marilyn Morrison for the typing of the rough draft, and to Mrs. Jeanne Ojeda for typing of the final manuscript. Thanks are also extended to Bruce Heinly and Denise Frank who did much of the drafting and plotting of various diagrams.

Appreciation is also extended to the Coastal Engineering Research Center, U. S. Army Corps of Engineers, for the use of compiled wave data taken from shore wave gauges operated by CERC in Florida, the results of which have been summarized in this report.

The work presented in this report was conducted under the National Oceanic and Atmospheric Administration Sea Grant Program, Grant No. NG-3-72, a program entitled "Nearshore Circulation, Littoral Drift, and the Sand Budget of Florida." The support of the Sea Grant Foundation is greatly appreciated.

The facilities of the University of Florida Computer Center were utilized for the computations in this study.

TABLE OF CONTENTS

TABLE OF CONTENTS (CONTINUED)

LIST OF TABLES

LIST OF FIGURES

LIST OF FIGURES (CONTINUED)

LIST OF FIGURES (CONTINUED)

LIST OF SYMBOLS

C wave celerity

C_b wave celerity at breaking

C_g wave group velocity

C_{go} deep water wave group velocity

C^* a constant

E surface energy density of a wave train

E_a longshore energy, longshore energy flux

$E_a(t)$ differential amount of longshore energy (flux)

E_{a+} longshore energy (flux) in positive direction

E_{a-} longshore energy (flux) in negative direction

E_o deep water surface energy density

E_o^* surface energy density contained in one wavelength

F energy flux

$f = f(H_o,T,\theta)$ frequency of time that a wave having characteristic values of H_o, T, θ acts during a period of time

f' friction factor

$f_{18} = f_{18}(H_o,\theta)$ frequency of time that a wave having characteristic values of H_o, θ acts during a period of time

$f_{19} = f_{19}(H_o,T)$ frequency of time that a wave having characteristic values of H_o, T acts during a period of time

g acceleration of gravity

H wave height

LIST OF SYMBOLS (CONTINUED)

H_b	breaking wave height
H_o	deep water wave height
H_o^*	a specific wave height
H_o'	$H_o \cdot K_r$ deep water wave height times the refraction coefficient
H_{rms}	root mean square wave height
$H_{1/3}$	significant wave height
h	depth of water below Mean Sea Level
h_b	depth of water below MSL at point of breaking
h_s	depth below MSL to which friction, percolation, and refraction are considered
K	wave number = $2\pi/L$
K_{fp}	friction-percolation coefficient
K_{fp_b}	friction-percolation coefficient at breaking
K_o	deep water wave number = $2\pi/L_o$
K_r	refraction coefficient
K_{r_b}	refraction coefficient at breaking
Ks	shoaling coefficient
L	wave length
n	ratio of group velocity to wave celerity
n_o	ratio of group velocity to wave celerity in deep water = 1/2
n_p	porosity
Q_ℓ	volume transport rate of littoral drift
$Q_{\ell net}$	net volume transport rate of littoral drift
$Q_{\ell -}$	total volume transport rate of littoral drift in negative direction
$Q_{\ell +}$	total volume transport rate of littoral drift in positive direction

LIST OF SYMBOLS (CONTINUED)

$(Q_{\ell net})_R$	net volume transport rate of littoral drift on right side of inlet
$(Q_{\ell net})_L$	net volume transport rate of littoral drift on left side of inlet
$(Q_{\ell -})_R$	total volume transport rate of littoral drift in negative direction on the right side of inlet
$(Q_{\ell -})_L$	total volume transport rate of littoral drift in negative direction on left side of inlet
$(Q_{\ell +})_R$	total volume transport rate of littoral drift in positive direction on right side of inlet
$(Q_{\ell +})_L$	total volume transport rate of littoral drift in positive direction on left side of inlet
T	wave period in seconds
t	a time
t*	a specific time interval of consideration
dt	a small time interval
W_ℓ	immersed weight transport rate of littoral drift
α	angle of wave approach to shoreline
α_b	angle of wave approach to shoreline at point of breaking
α_o	deep water angle of wave approach to shoreline
γ	specific weight of seawater
Δb	a length of beach corresponding to $\Delta\ell$
$\Delta\ell$	a length measured along a wave crest in feet
θ	azimuth angle of wave approach to shoreline

LIST OF SYMBOLS (CONTINUED)

θ_n	azimuth angle of outward normal to the shoreline
$(\theta_n)_R$	azimuth angle of outward normal to the shoreline on right side of inlet
$(\theta_n)_L$	azimuth angle of outward normal to the shoreline on left side of inlet
ρ_f	fluid density of seawater
ρ_s	sediment density

ABSTRACT

At present, the reliability of littoral drift magnitude and direction estimates along the coast of Florida are inadequate for rational coastal engineering design. The available values of littoral drift have been estimated from various dredging and sand pumping operations at inlets, and from relatively short periods of wave observations; thus, these values may contain significant uncertainties and depart from long-term average conditions by a considerable amount.

The present study utilizes a large data source of ship wave ovservations for the computation of littoral drift along segments of Florida's coast. Wave transformation from the observation site to a section of shore includes effects of shoaling, refraction, friction, and percolation. Assumptions are made that limit the analysis to an ideal beach with no anomalies in offshore topography. The results of the study are presented in a series of littoral drift roses which make it possible to find annual rates of littoral drift for sections of Florida having sandy shorelines. A comparison of computed values of drift with existing estimated values is made for specific locations. Results of the comparison confirm most of the estimated drift directions, however the drift magnitudes differ significantly.

CHAPTER I

INTRODUCTION

A. Introductory Note

Florida's shoreline, with its numerous beautiful sandy beaches has long enjoyed great popularity with both the residents of the state, and the enormous influx of tourists seeking out these vacation meccas. It has long been recognized that these same beaches, an increasing source of income for Florida's citizens, are in serious trouble due to erosion. Preservation of these beaches is not only desirable aesthetically, but is also an economic necessity.

The economic significance of the erosion problem can be seen from costs shared between the State of Florida and the Federal Government in order to preserve the State's beaches. As of 1970, estimated first costs of authorized Federal beach improvement projects in Florida amounted to over 76 million dollars for 108 miles of beach. Estimated first costs to correct all the existing erosion problems in Florida (includes authorized and unauthorized projects) amounted to over 113 million dollars for 209 miles of ocean shoreline [1].

Of approximately 1000 miles of sandy beaches in Florida (see Figure 1), the annual quantity of erosion in the nearshore area has been estimated at 15,000,000 cu. yds. per year, with over 20% of the beach shoreline in a critical state of erosion. Factors that influence

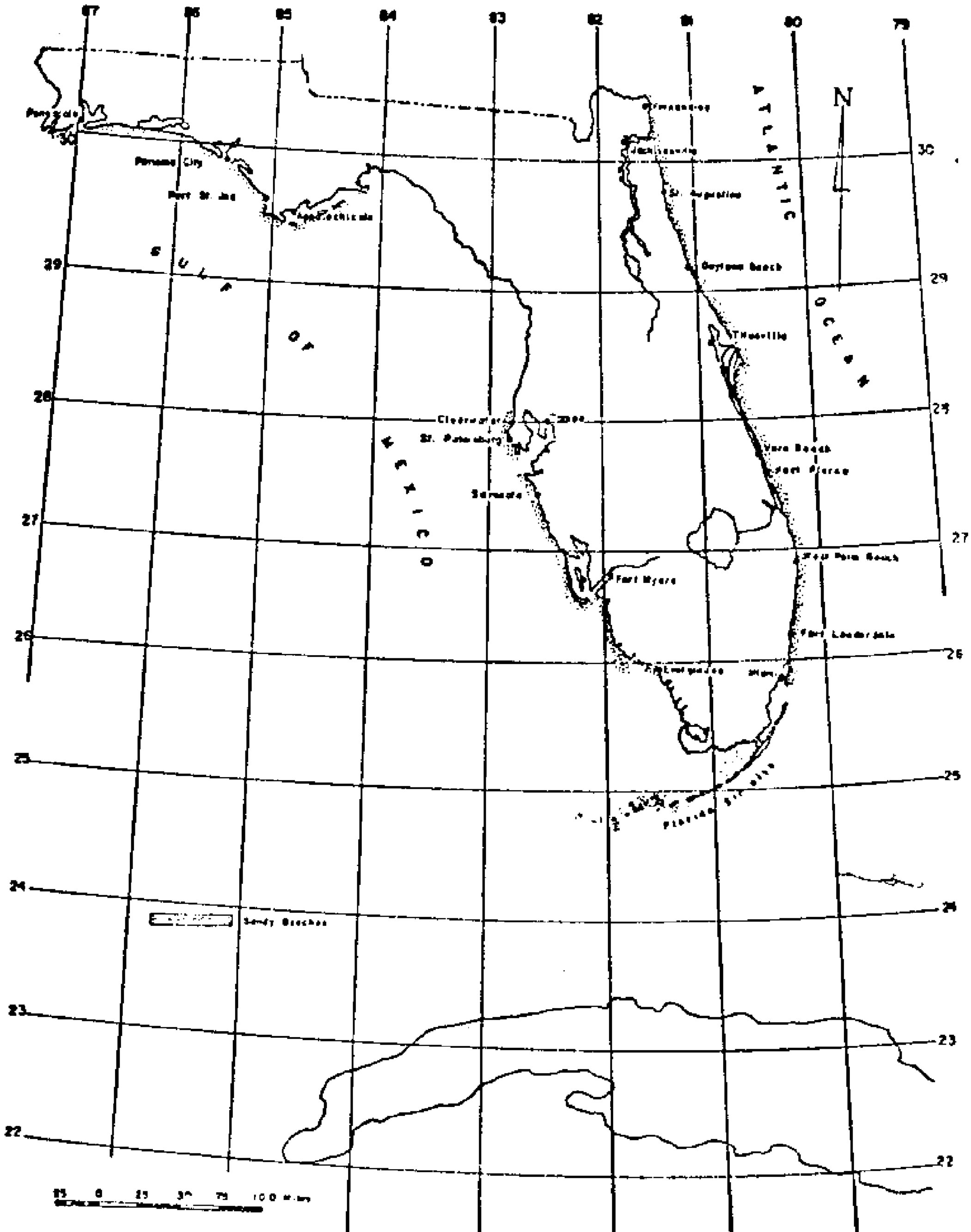

FIGURE I. LOCATION OF SAND BEACHES IN FLORIDA beach erosion are mean water level, tides, local winds, wave height, and wave steepness, wave refraction, diffraction, hydrography, land mass forms, source and characteristics of beach material, ground water table and others. For a further view of the present situation of Florida's shoreline and its history of erosion, see References [1], [2], and [3].

B. Statement of Problem

The major causes of erosion are threefold:

(1) Eustatic rise of sea level

(2) Intense meteorological disturbances, more commonly tropical cyclones (hurricanes)

(3) Interference in the littoral regime, natural or manmade.

The first of these, is well covered in Reference [4] and mean sea level recordings at various stations are shown in Reference [1]. Tropical cyclones (or hurricanes), the second listed cause of erosion, have made tremendous shoreline changes in a short time. Listings of tropical cyclones in Florida and some of their effects upon the shoreline can be found in References [1], and [2]. The third cause of erosion, interference in the littoral regime, is probably the most significant in regard to the possibility of economically halting erosion problems. In the past, man has induced considerable erosion due to his lack of understanding and consideration of the "littoral regime." Of the previously quoted figure of 15,000,000 cu. yds. per year of sand eroded annually from Florida's beaches, it is estimated that one-third or 5,000,000 cu. yds. per year of this is due to manmade erosion. Much has been written on this subject and additional references are available in [5], [6], and [7].

Although the first and second listed causes of erosion are not yet within total economic feasibility of correction, the third type of erosion problem is on the verge of solvability. A major obstacle in the past has been a lack of good quantitative values on factors of the littoral regime, the main one being "littoral drift," the amount of sediment (sand and shell) transported in the longshore direction due to wave action and wave-induced currents.

This report is an attempt to place some specific values on littoral drift along Florida's coastline, and thus, hopefully, provide criteria upon which future decisions will be made in regard to erosion problems of type three.

CHAPTER II

THEORETICAL BACKGROUND AND APPLICATION OF DATA

A. Sand Transport in the Nearshore Coastal Zone

Sand can be transported in the onshore-offshore direction or the longshore direction. This report, as stated previously, deals with the longshore motion, more commonly called littoral drift. The mechanisms causing transport in any direction are much the same though. The sediment is moved either in suspension or as bed load (bottom moving or saltation). Bed load is caused by high shear on the bottom which is in turn caused by high orbital velocities outside the zone of breaking and high mass transport velocities inside the breaker zone. This type of transport usually predominates outside the surf zone and is responsible for the movement of the coarser grains inside the surf zone. Suspended load moves as part of the regular fluid mass transport; a mechanism must first be present to entrain this sediment into the flow, after which relatively low velocities can carry the sediment from its place of entrainment. The entrainment mechanism is provided by high orbital velocities up to the zone(s) of breaking and turbulent dissipation of wave energy in the breaking zone(s). Mass transport currents then transport the sediment.

These two types of transport "drive" the sediment with the net movement having both an onshore-offshore and a longshore component (littoral drift). Both components are seasonal in nature with the offshore direction being the dominant of the offshore-onshore component in winter due to higher winter waves, and, along the Florida East coast, the southward littoral movement being the dominant direction of the longshore component in winter due to the predominance of waves propagating from the Northeast. The trends for each are reversed in the summer months. The actual mechanics of the surf zone are very complex due to non-uniform topography, and often-present rip currents (see Figure 2). Distribution of current and sediment transport also vary widely across the surf zone (see Figure 3) with most of the transport taking place over the bars in the surf zone. The factors mentioned above make a mathematical model of the surf zone an extremely complex three dimensional problem, one which to date has not been solved completely. Thus, prediction formulas for drift all have an empirical basis out of necessity. For a much more complete discussion of the sand transport in the coastal zone, the reader is referred to References [6], [8], and [9].

B. Methods of Computing Littoral Drift

Presently, there are a number of methods for the calculation of littoral drift, two of which are predominant in the literature and will be discussed. One method is established by computing values of the longshore current from wave and beach parameters and correlating them with measured amounts of sand transported, thus arriving at an empirically derived law of littoral drift. The second method, a more popular one, is established by computing the so called "longshore

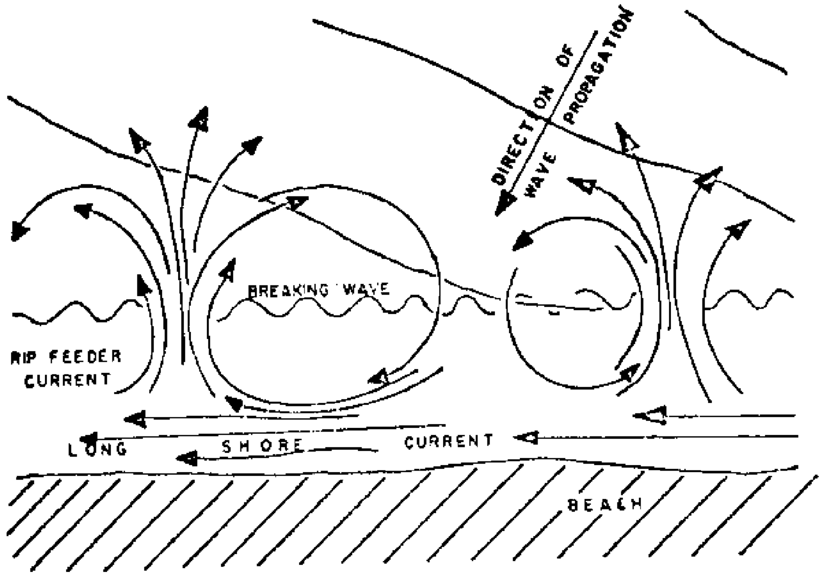

FIGURE 2. COMPLEX LITTORAL SYSTEM

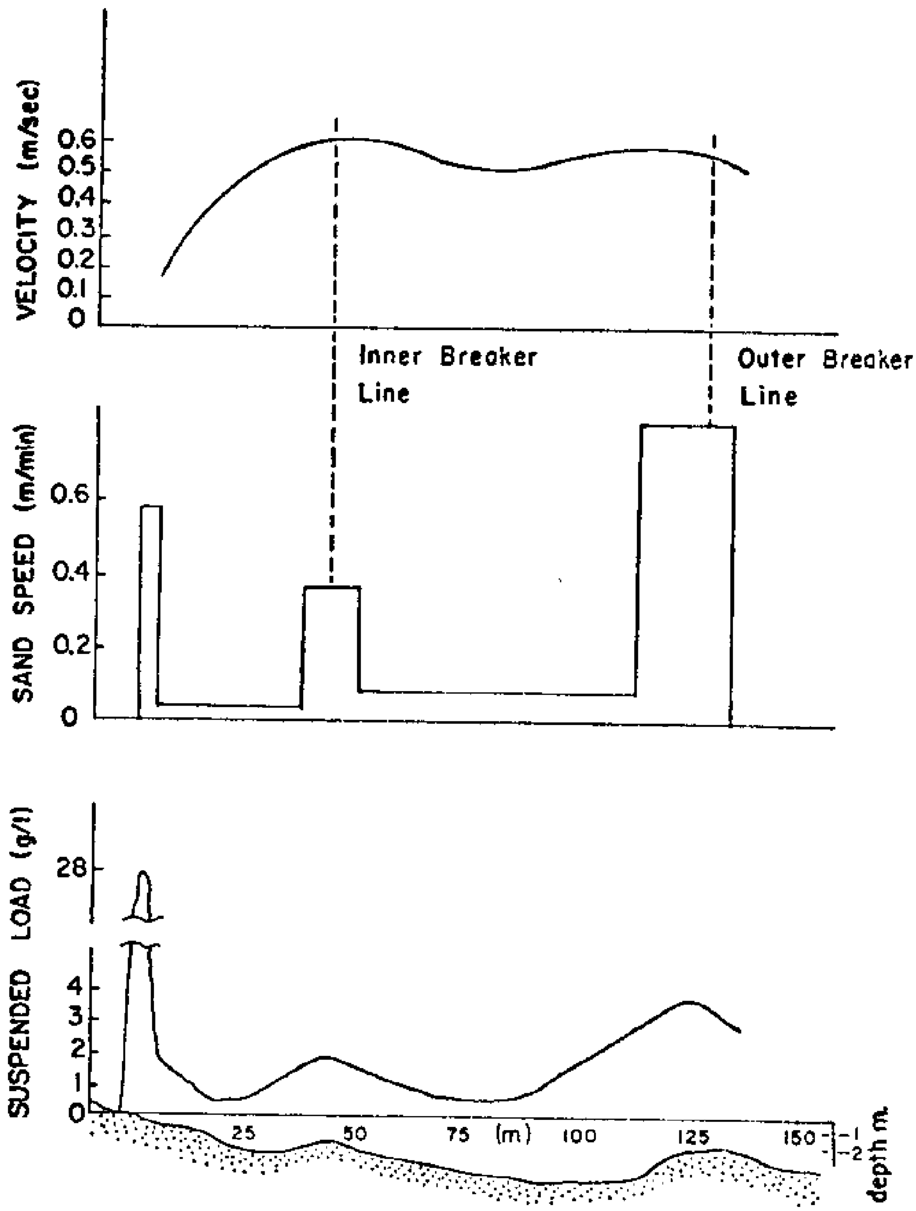

FIGURE 3. DISTRIBUTION OF LONGSHORE VELOCITY AND SEDIMENT TRANSPORT ACROSS THE SURF ZONE (AFTER ZENKOVITCH [9])

energy flux, E_a, a function of wave and beach parameters, and correlating it with measured amounts of sand transport, thus giving an empirical formula. These two methods are related (see Reverence [10]) as would be expected due to the physical nature of the problem. In the literature, the second type of empirical correlation has been used much more extensively (see References [11], [6], and [7]), and it is this correlation of longshore energy flux with littoral drift that is used in this report.

C. Correlation of Longshore Energy Flux with Littoral Drift

Littoral drift rate, Q_ℓ, the longshore volume transport rate of sand in cubic yards per day, has been correlated with longshore energy flux to give an empirical curve as shown in Figure 4. The relationship is linear and is described by the equation (see Reference [11], pg. 175):

$$Q_\ell = 125\ E_a \tag{1}$$

with Q_ℓ in cubic yards per day

E_a in millions of ft.-lbs. per day per ft. of beach.

Data points for the curve are shown and referenced to the original reports. In addition, data points from studies of Fairchild [20], Moore and Cole [21], and Komar [10] have been included on the graph although they were not included in the original correlation which established Equation (1). It is noted that Komar's data points were based on the root mean square wave height rather than on significant wave heights. This difference will be discussed later. A summary of the different methods in which Q_ℓ and E_a values were obtained for the data points is presented in Reference [22].

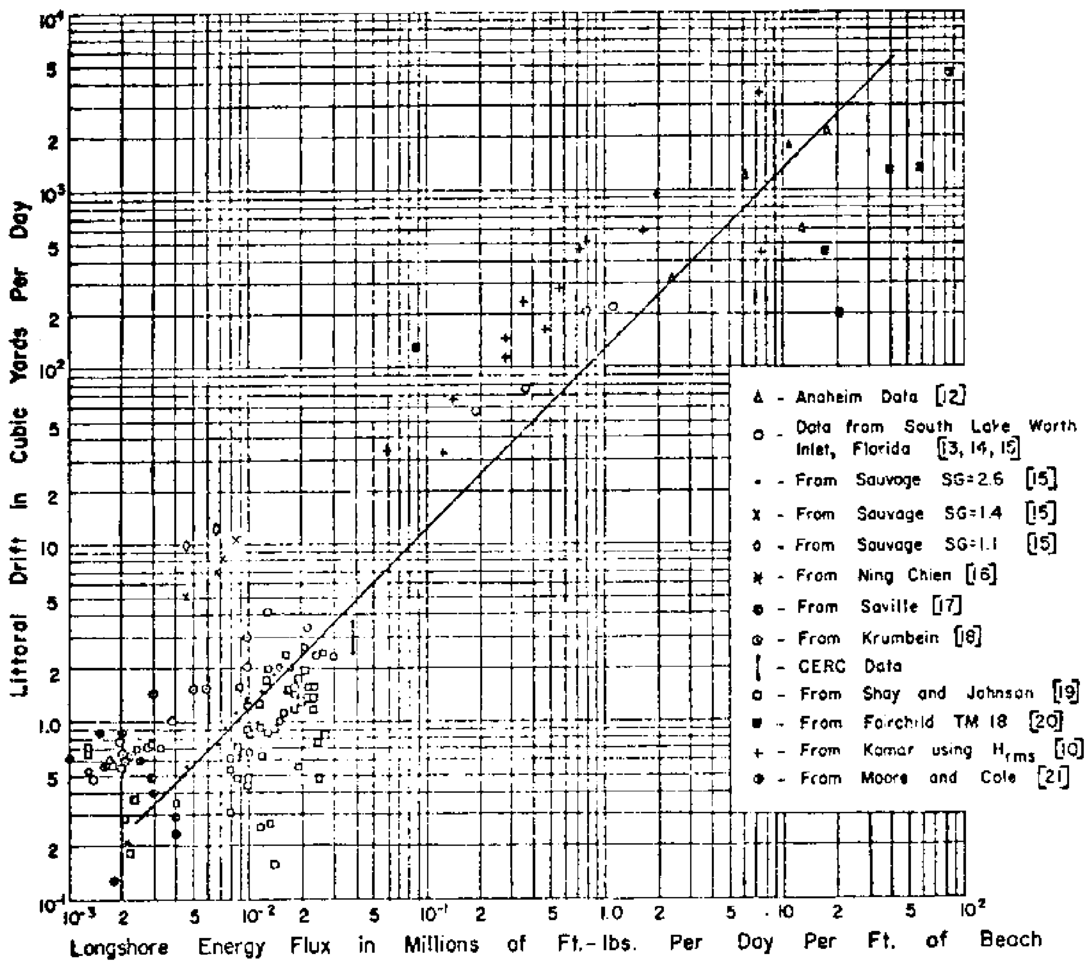

FIGURE 4. LONGSHORE ENERGY FLUX VERSUS LITTORAL DRIFT RELATIONSHIP (FROM REFERENCE [11])

Reference [11] states that the above relationship of littoral drift to longshore energy flux is an <u>order of magnitude</u> approximation to the true value. It is believed by the author that in light of more recent field measurements by Komar [10], the above relationship is well within this limit and may be considerably better.

Many different forms for the equation of longshore energy flux have been presented in the literature. The longshore energy flux E_a, due to a wave system, is

$$E_a = (E_o C_{go} \cos \alpha_o) K_{fp}^2 \sin \alpha_b \cdot \frac{24(3600)}{10^6} \tag{2}$$

where E_a = longshore energy flux in millions of ft.-lbs. per day per foot of beach

$E_o = \frac{\gamma H_o^2}{8}$ = the deep water surface energy density

H_o = deep water wave height in feet

γ = specific weight of seawater

= 64 lbs./cu. ft.

C_{go} = deep water wave group velocity in feet per second

= 1/2 C_o where C_o is the deep water wave celerity in feet per second

α_o = deep water angle of wave approach to coastline

α_b = angle formed by breaking wave crest with coastline

K_{fp} = friction-percolation coefficient; see Ref. [24]

A derivation of this formula along with the more common derivations of longshore energy found in the literature is given in Appendix I. The field data used in the Q_ℓ versus E_a correlation is based on significant wave heights, $H_{1/3}$, rather than root mean square wave heights,

H_{rms}, and, thus, the energy computed is really not "true" longshore energy flux, but rather a "significant" longshore energy flux. When using Equation (1), data used should include significant wave heights rather than root mean square heights, the ratio of corresponding values of E_a predicted being $\left(\frac{H_{1/3}}{H_{rms}}\right)^2 \approx 2.00$, when assuming a narrow energy spectrum. In particular, in Equation (1), the empirical constant would be greater by a factor of 2 if root mean square wave heights had been used in the data correlation rather than significant wave heights, and if one and only one dominant frequency were present.

Assumptions inherent in the above calculation of longshore energy flux and consequent littoral drift are as follows:

(1) Linear theory is valid for the wave transformation process and the wave energy present in the wave system;

(2) Assumptions in calculation of K_{fp} are not violated (see Reference [24];

(3) Bottom topography is composed of straight and parallel bottom contours;

(4) No drastic changes in the bottom profile are encountered in the shallow areas seaward of the breaker line up to the beach;

(5) Adequate sources of sand are available.

Item (1) refers to the mathematical formulation of the problem and its relation to physical reality. This assumption is reasonably good up to the region of breaking waves where it departs drastically from the physical situation. Item (2) assumptions will be discussed later. Assumption (3) is necessary for the simple application of Snell's Law of Refraction used in this report and does not require a monotonic decrease in depth toward shore, but only the aforementioned relationship between bottom contours. Assumption (4) is necessary due to the use of offshore wave conditions for the computation of longshore energy rather than nearshore conditions. Thus, rock or coral reef might cause a large dissipation or reflection of energy before the wave reaches the computed breaker zone, which would not be apparent in the equation of E_a formulated above. An additional assumption inherent in the presented correlation between Q_ℓ and E_a is Item (5), the availability of sand to be moved. This is dependent on the geologic processes acting in the area, and the natural or man-made conditions present. Along much of the Gulf shoreline of Florida there is a lack of sand, predominantly in areas having extremely low wave energy, and in areas which are drained by rivers containing mostly silt and organics rather than coarse alluvial materials. Rivers, inlets, jetties, groins, seawalls, prominent headlands, and submarine ridges and valleys can also cause a lack of sand in an area downdrift of the obstacle. A lack of sand supply causes erosion and in turn a depleted sand reservoir, with less sand available for the transport downdrift of the barrier.

Many of the factors upon which littoral drift depends are not contained explicitly in the equation presented for longshore energy. Wind, which has been found as a major drift factor in some studies due to its effect on the littoral current, is not present at all. Additionally, grain size, beach slope, bottom friction, etc., are factors which probably affect the longshore current and thus the littoral drift. Except for K_{fp} and $\sin \alpha_b$, the other variables in the longshore energy equation presented are totally dependent on deep water conditions.

The drift can also be expressed in terms of immersed weight transport rate rather than a volume transport rate as follows:

$$W_\ell = (\rho_s - \rho_f)\ g(1-n_p)\ Q_\ell \cdot 27 \qquad (3)$$

where

ρ_s = sediment density in slugs/ft.^{3}

ρ_f = fluid density (seawater) in slugs/ft.^{3}

g = acceleration of gravity in ft./sec.^{2}

n_p = porosity $\doteq$ 0.4 for beach sand

Q_ℓ = volume transport rate in cubic yards/day

W_ℓ = immersed weight transport rate in lbs./day

Due to the present more popular method of expressing the transport rate as a volume rate, this report will use values of Q_ℓ in cubic yards per day.

D. Data Source

The wave data used in the computation of longshore energy flux and consequent littoral drift in this report can be found in the U. S. Naval Weather Service Command--Summary of Synoptic Meteorological Observations, Volumes 4 and 5 [23], hereafter referred to as SSMO. These volumes are a compilation of meteorological and sea state observations taken from ships travelling through "Data Squares" defined by their latitude and longitude boundaries. The percent frequency of wind direction versus sea heights can be found in Table 18 for different data squares on a monthly and annual basis. The percent frequency of wave height versus wave period for both sea and swell observations can be found in Table 19 for different squares on a monthly and annual basis. Computations of drift use the data from both of these tables. Necessary assumptions made in the use of SSMO data are presented and discussed below.

In the use of Table 18 the assumptions have been made that (1) swell waves are in the same direction as the sea waves, which in turn correspond to the wind direction; and (2) waves are propagating in one direction only, the observed direction, in any specific time interval. In applying Table 19, the assumptions are made that (1) sea and swell waves of the same period and height can be treated alike, and will not lose energy to the atmosphere between the point of observation and the portion of coastline considered; (2) no other wave heights or periods are present during the observation of a recorded wave with a given height and period; and (3) all observations were made in "deep water" ($h \geq 2.56T^2$ in ft.) for the wave periods recorded.

Correlation between the ranges of wave heights, periods, and directions given in the SSMO data volumes and the corresponding values used in the calculations of drift can be found in Appendix II. Due to the nature of human observation of waves, the heights and periods found in the data tables should be considered as significant heights and periods, and are correct for use in the empirical correlation of longshore energy flux with littoral drift presented.

E. Analysis of Wave Data to Compute Longshore Energy Flux

Longshore energy, or more properly, longshore energy flux, is given in Equation (2) for one specific wave train. In foot-pound-second units this can be expressed as:

$$E_a = \left(\frac{\gamma H_o^2}{8} C_{go} \cos \alpha_o\right) K_{fp}^2 \sin \alpha_b \tag{4}$$

where E_a is now given in ft.-lbs. per second per foot of beach. Note that in this report, the terms "longshore energy" and "longshore energy flux" are used interchangeably, although, in reality, significant physical difference is attached to each. In the literature, both terminologies are used, longshore energy being the more common one, while longshore energy flux is the more proper one.

Considering a continuously changing state of offshore wave conditions, heights, periods, and directions, the total longshore energy would consist of a summation of differential amounts of longshore energy each having a value $E_a(t)$ for a representative wave height, period and direction where:

$$E_a(t) = \left(\frac{\gamma H_o^2}{8} C_{go} \cos \alpha_o\right) K_{fp}^2 \sin \alpha_b \tag{5}$$

Thus, for continuously changing wave conditions, the total longshore energy as averaged over a time interval t* would be

$$E_a = \frac{1}{t^*} \int_{t=0}^{t=t^*} E_a(t)\ dt = \int_{t=0}^{t=t^*} E_a(t)\ \frac{dt}{t^*} \qquad (6)$$

The value $\frac{dt}{t^*}$ can be thought of as the fraction of time over which a specific wave having a certain height, period, and direction is being generated during the period t*. Expressing these results in finite intervals:

$$f(H_o,T,\theta) = \text{frequency} = \frac{dt}{t^*} \qquad (7)$$

and

$$E_a = \sum_{t=0}^{t=t^*} E_a(t)\cdot f(H_o,T,\theta) \qquad (8)$$

where

$$\sum_{H_o=0}^{H_o=\infty} \sum_{T=0}^{T=\infty} \sum_{\theta=0}^{\theta=2\pi} f(H_o,T,\theta) = 1.00 \qquad (9)$$

with θ equal to the azimuth of the direction from which the wave is propagating. It is related to α_o by the equation: $\alpha_o = \theta_n - \theta$ where θ_n is the azimuth of the perpendicular to the shoreline (see Figure 5).

For waves reaching the coast, the summation would be as follows with $\theta = \theta_n - \alpha_o$ and α_o ranging from -90° to +90°;

$$\sum_{H_o=0}^{H_o=\infty} \sum_{T=0}^{T=\infty} \sum_{\theta=\theta_n-\frac{\pi}{2}}^{\theta=\theta_n+\frac{\pi}{2}} f(H_o,T,\theta) < 1.00 \qquad (10)$$

Note that in the above summation, when waves are being propagated away from the coast, that no longshore energy will be available for transport. Therefore the total longshore energy becomes;

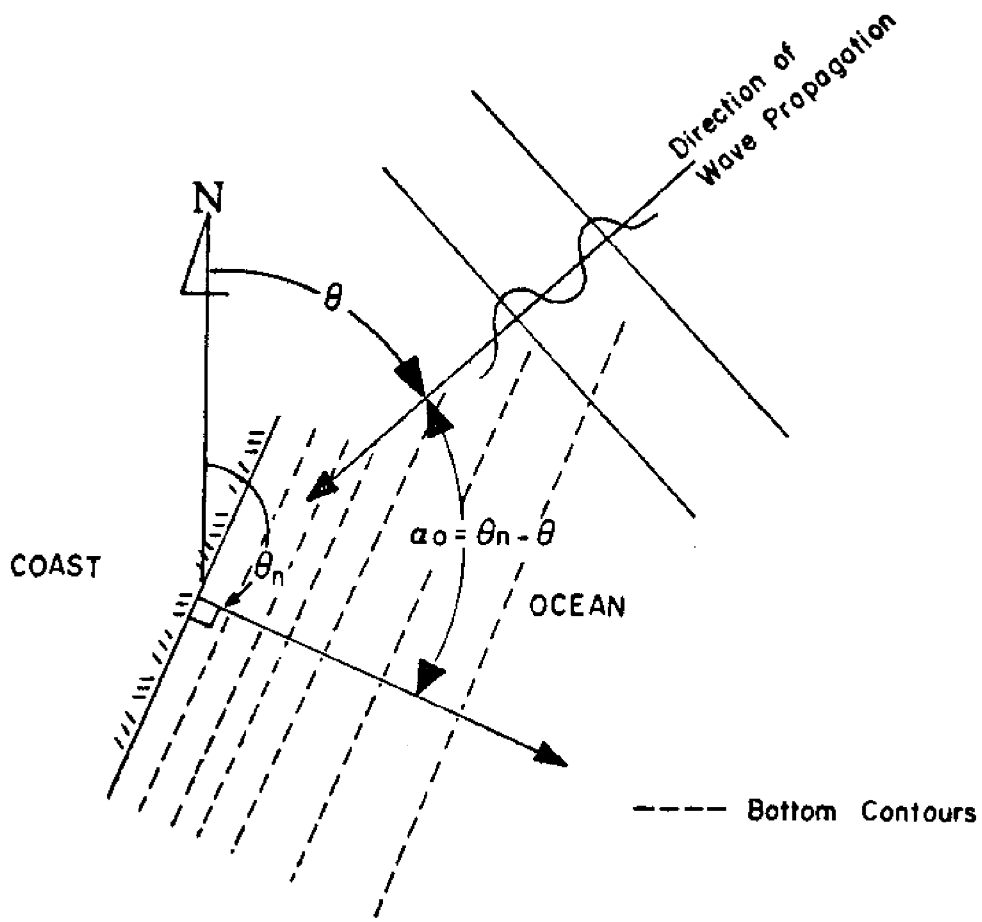

FIGURE 5. DEFINITION OF AZIMUTH ANGLE NORMAL TO SHORE θ_n, AND AZIMUTH ANGLE OF WAVE PROPAGATION θ

$$E_a = \sum_{H_o=0}^{H_o=\infty} \sum_{T=0}^{T=\infty} \sum_{\theta=\theta_n-\frac{\pi}{2}}^{\theta=\theta_n+\frac{\pi}{2}} E_a(t)\cdot f(H_o,T,\theta) \tag{11}$$

The value of $f(H_o,T,\theta)$ can be computed by means of SSMO Tables 18 and 19. From Table 19 a value of $f_{19}(H_o,T)$ is obtained such that

$$\sum_{H_o=0}^{H_o=\infty} \sum_{T=0}^{T=\infty} f_{19}(H_o, T) = 1.00 \tag{12}$$

From Table 18 a value $f_{18}(H_o,\theta)$ can be obtained corresponding to a wave height range in Table 19 such that

$$\sum_{\theta=0}^{2\pi} f_{18}(H_o^*,\theta) = 1.00 \tag{13}$$

where the * represents the correspondence of H_o in Table 18 to the same range in Table 19. Multiplying these two factors together gives the desired frequency as a function of wave height, period, and direction.

$$f(H_o,T,\theta) = f_{18}\cdot f_{19} \tag{14}$$

By the use of Equation (11), the longshore energy can be obtained in millions of ft-lbs per day, as averaged over any given period of wave observations. As mentioned previously, the representative values of H_o,T,θ for the ranges given in SSMO are discussed in Appendix II.

The procedure for the calculation of a differential amount of longshore energy = $E_a(t)\cdot f(H_o,T,\theta)$ is as follows:

(1) Compute the quantity $\left(\frac{\gamma H_o^2}{8} C_{go} \cos \alpha_o\right)$ from deep water conditions, that is, the representative conditions for given wave height, period, and direction ranges.

(2) Compute the quantity K_{fp}^2 to a shallow water depth, h_s, outside the zone of breaking waves by numerical integration procedure of Ref. [24] (along the coast of Florida this depth was normally taken as 10 feet).

(3) Compute the refraction coefficient K_r to this same depth h_s.

(4) Calculate the value $\frac{H_o'}{L_o}$, a function of the deep water wave steepness, where $H_o' = H_o \cdot K_{fp} \cdot K_r$. Based on $\frac{H_o'}{L_o}$, a judgement is made as to whether the wave breaks by solitary theory or by linear theory (see Figure 10, page 30, of Reference [26]). If $\frac{H_o'}{L_o}$ is > 0.02, linear theory is used, otherwise solitary theory is used to predict the breaking wave height.

(5) Calculate an approximate breaking depth and height based on appropriate wave theory as mentioned in step (4) (see Appendix III for calculation of breaking wave conditions). In both wave theories the relationship between breaking wave height H_b and breaking wave depth h_b is, $H_b = 0.78\ h_b$.

(6) Calculate sin α_b by Snell's Law (see Appendix III for this relationship).

(7) Find f_{18} and f_{19} values in SSMO Tables 18 and 19 as mentioned previously, and calculate $f = f_{18} \cdot f_{19}$.

Calculation of E_a is then a simple summation process in which the data must be put through a "filter" to eliminate all differential bits of energy with azimuth directions θ that are less than -90° or greater than +90° to the coastline azimuth θ_n. When looking offshore a positive value of $E_a = E_{a+}$ is recorded for waves propagating from the left side and causing longshore energy flux to the right; and likewise, a negative value of $E_a = E_{a-}$ is recorded for waves propagating from the right and causing longshore energy flux to the left (see Figure 6). By summing the positive, negative, and total values of longshore energy, positive, negative, and net values of Q_ℓ can be found equal to $Q_{\ell+}$, $Q_{\ell-}$, $Q_{\ell net}$, respectively.

Additional assumptions used in the preceding method of calculation which were not previously discussed are:

(1) There is no loss of energy through friction or percolation between h_s, the shallow water depth at which K_{fp} is calculated, and the breaking depth.

(2) No refraction occurs between h_s and the breaker line.

Computation of K_{fp} and K_r both involve linear theory. Since linear theory is violated upon approaching the breaker line, it is felt that to compute K_{fp} and K_r beyond the limit of its validity would be unjustified in light of present theory. Refraction beyond this limit can be shown insignificant for the majority of the waves if calculated by linear theory.

(3) K_{fp} is calculated using a bottom profile perpendicular to the stretch of shoreline considered rather than the actual profile over which the waves travel. Inherent in this procedure is an additional assumption that the wave climate used occurs at a point offshore perpendicular to the portion of coastline considered.

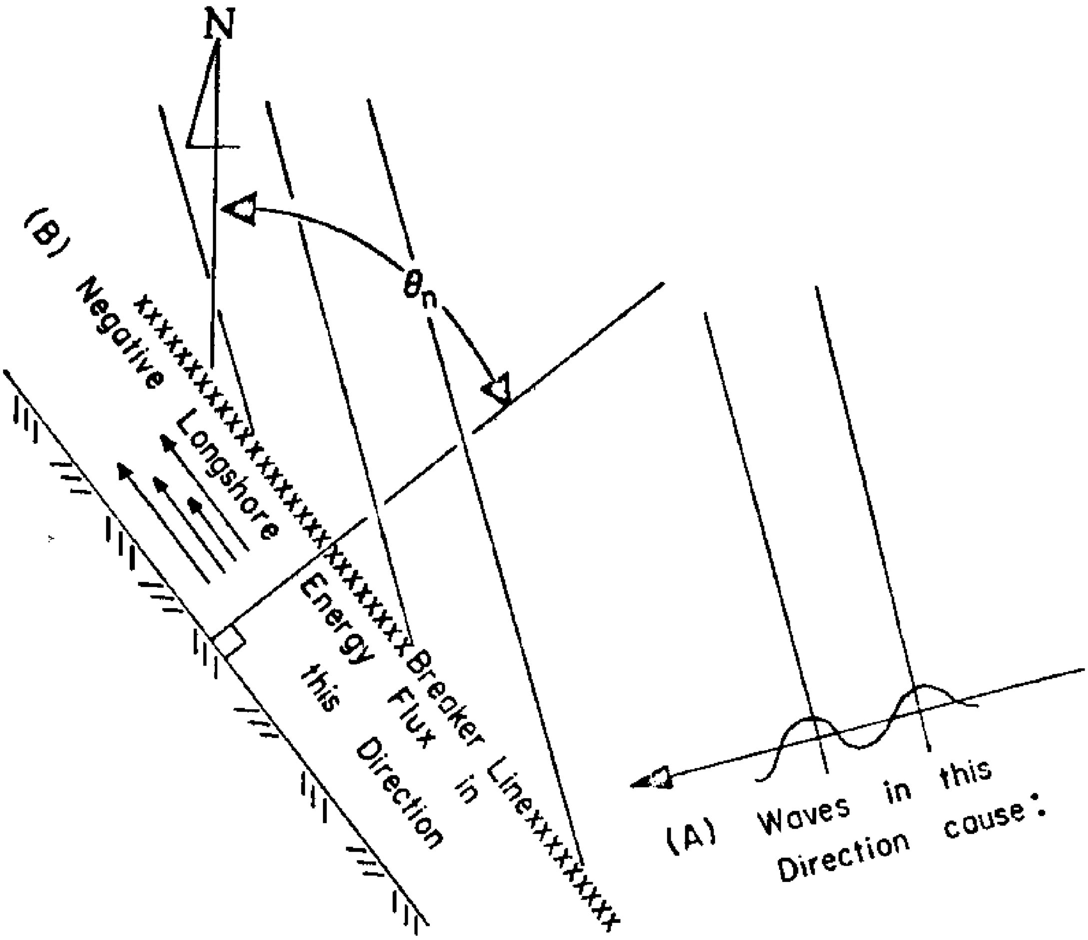

FIGURE 6. RELATIONSHIP BETWEEN DIRECTION OF WAVE PROPAGATION AND DIRECTION OF LONGSHORE ENERGY FLUX

(4) The effect of refraction on the value of K_{fp} is considered insignificant. (Refraction effect on K_{fp} can be seen in Plate IV, Page 32, Reference [24].)

(5) Loss of energy due to permeability which is included in factor K_{fp} is theoretically based on a depth of sand bed ≥ 0.3 L where L is the wave length [24].

Assumptions (3), (4) and (5) are all pertinent to the computation of the K_{fp} value. Assumption (5) is inherent in the theoretical solution to the problem of K_{fp} while (3) and (4) have been assumed by the author for shortening computational time.

So far, computation of longshore energy pertains to the wave data contained in one SSMO square. Application of this data to sections of shoreline will now be considered.

F. Data Weighting from Adjacent SSMO Squares

The SSMO squares used in this report are shown in Figure 7. For a section of coast along which a value of drift is to be computed, wave data from two adjacent squares are linearly proportioned to obtain a "weighted" value of E_a. This is done in the following manner:

(1) The midpoint of each square is determined with respect to a North-South or East-West direction depending on the orientation of the segment considered.

(2) The midpoint of the shore segment considered is found in the same manner as above.

(3) The representative location of the wave data for a Data Square is assumed to be the midpoint of that square.

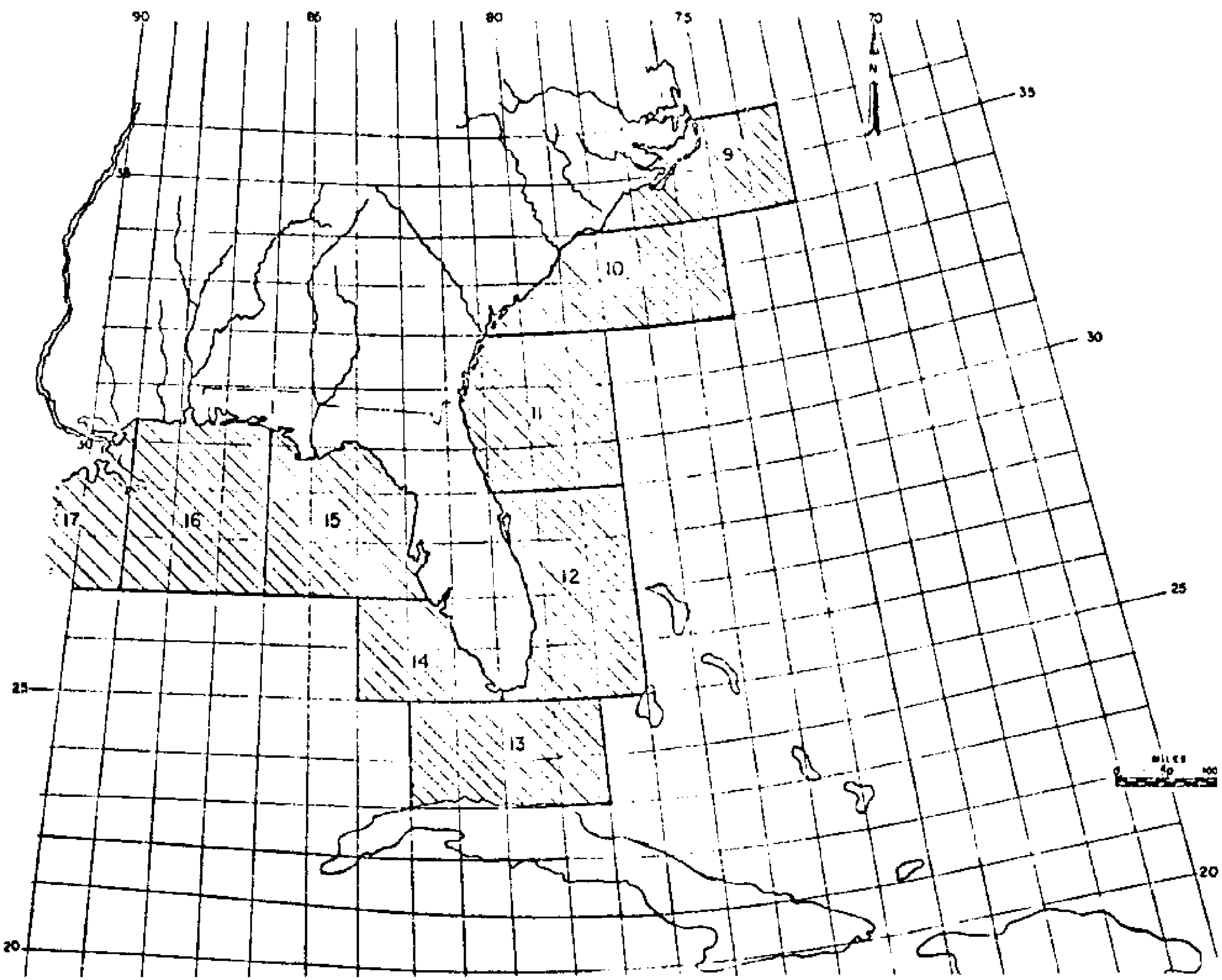

FIGURE 7. LOCATION OF SSMO DATA SQUARES ADJACENT TO THE FLORIDA PENINSULA

(4) At the boundary between two squares, the wave climate is weighted equally on both Data Squares.

(5) Linear interpolation for the dependence of wave climate on either square is made between these points.

(6) The longshore energy for a section of coastline is then calculated for each wave climate and weighted by a factor determined as described above. The results are added to obtain E_a at the site in question.

Graphically the procedure is shown in Figure 8. The example given is for the segment of beach from St. Augustine Inlet to Ponce de Leon Inlet and the weight factors are 0.67 and 0.33, for Squares 11 and 12 respectively.

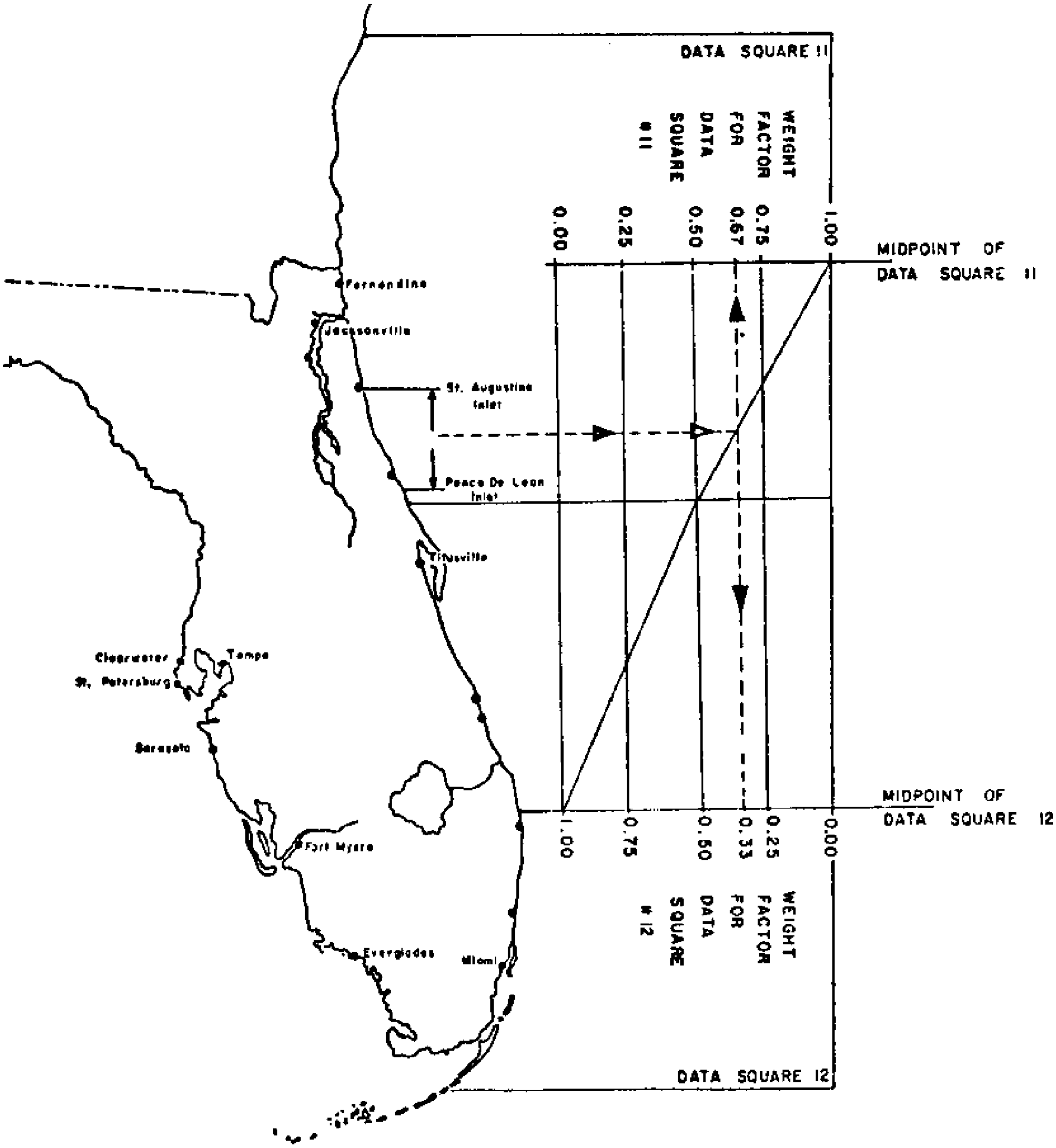

FIGURE 8. PROCEDURE FOR LINEAR INTERPOLATION OF WAVE CLIMATE FROM ADJACENT SSMO DATA

CHAPTER III

RESULTS

A. Results of Study

Littoral drift "roses" with annually averaged values of littoral drift in cubic yards per day have been computed using the SSMO annual data summary tables along sections of Florida's sandy shores. These are presented in Figures A1 through A52. Because of the large number of these figures they are located with the Appendicies section of this report. An annually averaged net drift rose is presented for each section of coast considered, with the frequency of onshore waves superimposed on the same diagram. A second littoral drift rose diagram for each section of coast considered gives the annually averaged total positive and negative drift. Positive values of littoral drift refer to drift moving toward the right when looking offshore, and conversely, negative values of drift are quantities of drift moving to the left defined similarly to positive and negative longshore energy flux. On the East Coast of Florida a positive value of drift would thus represent Southward drift, while on the Gulf Coast, the reverse would be true; that is, a negative value of drift would represent Southward drift on the Gulf Coast. The net drift values represent the difference between the Southward and Northward total values of drift with the direction of the drift indicated by its sign as described above. Although the littoral drift has been computed for coastline orientations ranging over 360° of the compass, in actuality, the coastline orientations range at most over 180° for any given section and have been presented showing the maximum practical range plus or minus 20° for local anomalies.

As mentioned previously, these values of littoral drift are for stretches of coast exposed to the ocean wave climate as represented by SSMO data. They are not valid for bays, lagoons, or estuaries, where the shoreline is not exposed to a wave climate represented by the SSMO data.

Wave climate is presented in the form of wave height and period roses for each SSMO data square to show the average offshore conditions existing annually as recorded by SSMO. Wave height and period roses are given in Figures B1 through B12. These Figures are also located following the Appendices section of this report.

Using the SSMO data monthly summaries, monthly averaged littoral drift roses are presented for the section of beach between Fort Pierce Inlet and St. Lucie Inlet and are given in Figures C1 through C24. Offshore wave climate on a monthly basis is given for SSMO Data Square Nos. 11 and 12 on which the drift values were computed. Wave climate roses are given in Figures D1 through D48. The wave data from Square 11 was "weighted" with a factor of .08 and Square 12 with a factor of .92.

B. Use of a Littoral Drift Rose

Use of a littoral drift rose is as follows:

(1) Determine the orientation of coastline at which a drift is desired.

(2) Using the azimuth of the seaward directed normal to the coastline at the location, find the value of net drift associated with this azimuth angle on the proper drift rose corresponding to the desired location.

(3) If the net drift value is positive, the net drift will be to the right when looking offshore; if negative, the net drift will be to the left.

(4) Find the total positive drift, total negative drift, and the frequency of onshore waves in the same manner (the use of this frequency value will be discussed later).

To demonstrate the method, values of net drift at Ponte Vedra Beach, south of Jacksonville are found from Figures 9 and 10. The azimuth angle of the perpendicular to the shoreline is 76°-30' as shown in Figure 9. Thus, the total Southward drift is 1600 cubic yards per day, and the total Northward drift is 810 cubic yards per day from Figure 10. The net littoral drift is 790 cubic yards per day or 288,000 cubic yards per year to the South. The frequency of onshore waves as predicted by the method of SSMO data analysis used is .54.

Limitations in the simple procedure for calculating drift values in the above manner will be discussed, taking into account some of the data limitations and data bias.

C. Possible Sources of Error

1. Errors in the Data

In the SSMO data, possible sources of error include:

(1) Human error and bias in the observation and recording of the wave data.

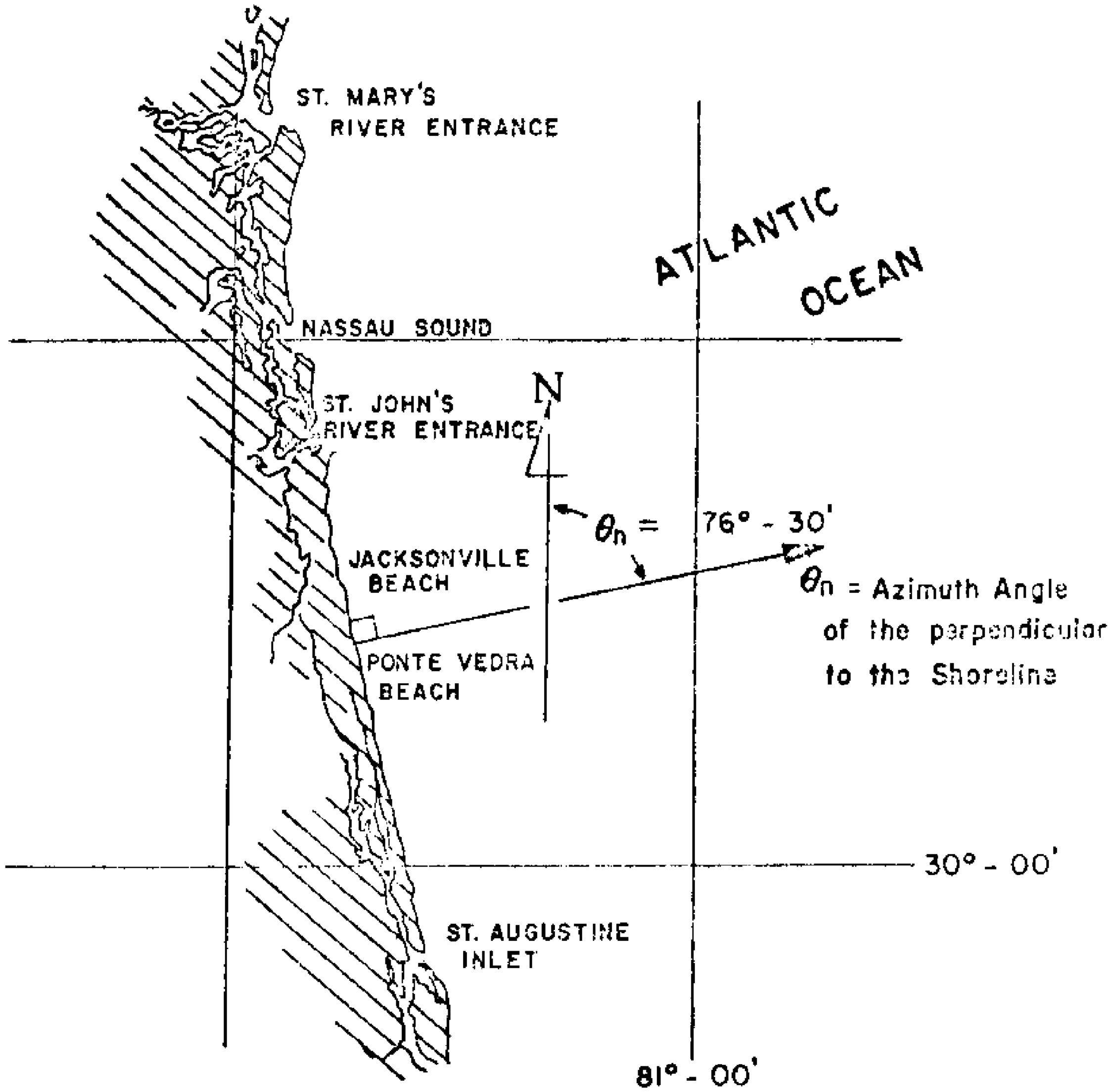

FIGURE 9. AZIMUTH OF NORMAL TO SHORELINE AT PONTE VEDRA BEACH, FLORIDA

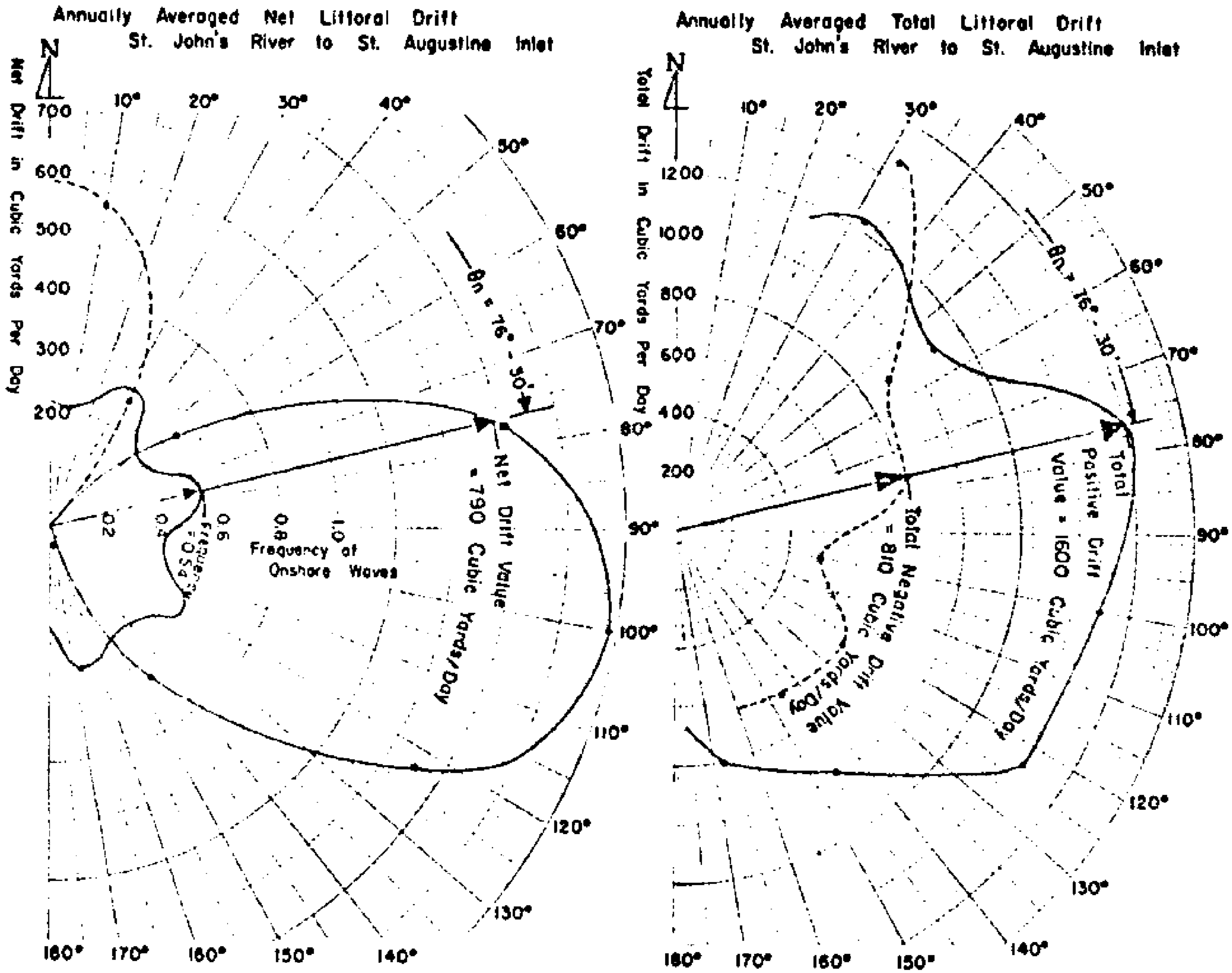

FIGURE 10. DETERMINATION OF NET AND TOTAL LITTORAL DRIFT AT PONTE VEDRA BEACH, FLORIDA

(2) Absence of extreme wave conditions due to routing of ships out of bad weather.

(3) Inaccuracies introduced due to the lack of swell direction data.

(4) Inadequate resolution of wave data in directions.

(5) Inaccurate wave height recording due to wave observation in a strong ocean current.

Error sources (1) and (2) are self-explanatory. In regard to (1), it has been shown that a large bias is introduced in the directional data due to the observer tendency toward recording of wave directions along the four cardinal and four intercardinal points of the compass. This effect can be seen in the littoral drift and onshore frequency roses. It is felt that the bias should not significantly affect the results presented here though, since wave directions used in the computations were reduced to the eight points of the compass in the SSMO volumes. If it is assumed that the waves were recorded to the nearest point of the compass (on an eight point system), the maximum error between a recorded wave direction and its true direction would be 22-1/2°. It is recommended that values of drift in a range of azimuth angles ± 11-1/4° to the actual coastline azimuth be considered as the range of possible drift values, thus covering a 22-1/2° range of possible directional error.

A general idea of the reliability of the data source is obtained by viewing the annual offshore wave height and wave period roses in the different data squares. In many of the data squares, notably Data Square 11, the wave periods are often larger in the offshore direction, contrary to expected larger periods in onshore direction due to larger fetch distance. Also, wave heights follow the same pattern contrary to physical reasoning. In Data Square 13, the observations show a majority of waves, along with the highest waves and the largest period waves, to be propagating out of the East, Northeast, and Southeast. This is as expected, since the Florida Keys shelter ship channels from waves approaching from the Gulf of Mexico. Comparing the annual wave height roses from Data Squares 11 and 12 shows that the wave climate in each is not significantly different. This is certainly contrary to what one would expect considering that most of the wave observations in Data Square 12 would be expected to show effects of sheltering from the Bahama Banks.

The question of reliability of wave climate in these two blocks might be resolved by an analysis of offshore wave climate in smaller data squares if the data become available in a convenient form at some later time. Wave data in the Gulf of Mexico is thought to be less questionable, since the fetch distance is closer to being equal in the onshore and offshore directions with regard to the shipping lanes.

The original method of reducing the data from 36 points of the compass to 8 points of the compass given in the SSMO volumes introduced a skew of the data by an angle of ten (10) degrees clockwise. This has been compensated for in the littoral drift roses and offshore wave climate roses by shifting rose azimuth angles ten (10) degrees counterclockwise.

As mentioned earlier, the lack of swell direction data, and distinction between sea and swell, cause the assumption to be made that swell waves are being propagated in the same direction as the local wind waves (which is the recorded wind direction). It is unlikely that swell is always in the same direction as the local seas and this could lead to considerable error in the computation of longshore energy. In regard to Item (4), since longshore energy is dependent on wave direction due to refraction process, the method of computing wave energy by using only eight points of the compass poses a question as to the magnitude of error possible in the results. It can be shown that the maximum error introduced by this approach as compared to spreading the energy evenly over all directions within an octant is ten (10) percent. Due to the uncertainty of wave directional data such a refinement was felt unjustified.

In regard to Item (5), wave heights are affected by strong currents, and have the tendency to steepen when propagating against an opposing current and are reduced in height by a following current. This effect is noted on the Southeast coast of Florida where the Gulf Stream is very close to shore. Due to the fact that shipping lanes run through and along the Gulf Stream, it is felt that many of the observed waves approaching shore have recorded wave heights higher or lower than would be experienced on the shoreward side of the Gulf Stream in comparatively still water. This effect would cause the computed Southward drift values to be higher than the actual drift values and Northward drift values to be lower.

2. Errors in Longshore Energy Flux Analysis

Methods of computation of longshore energy may lead to inaccuracies in drift predictions. The author believes the largest source of error comes from the assumption mentioned earlier that waves are considered to be propagating in one direction at one time. That is, it is assumed that when waves are moving away from the coast, there are no waves reaching the coast, and thus there is also no longshore energy at the coast. This is an unreasonable assumption since waves are known to propagate in many directions at the same time. From the SSMO wave data, a frequency of onshore waves is calculated for each orientation of coastline and thus can be compared to a wave record at the location in question to determine a better estimate of the true onshore frequency of waves, and, in turn, drift. For example, if the frequency of onshore waves is 40% from the littoral drift rose, and a wave record at the site has recorded waves > 1.0 feet for 80% of the time, a better estimate of the true drift might be $\frac{0.80}{0.40} = 2.0$ times the value on the given drift rose. It is believed that this factor of 2.0 is high because the periods of higher littoral drift undoubtedly coincide with periods of observed onshore-propagating waves.

Other possible sources of error which involve the computation of longshore energy flux are assumptions in the calculation of the friction-percolation coefficient and the violation of Snell's law with regard to the bottom contours.

The modification of wave height due to friction and percolation effects as the wave propagates across the continental shelf has five factors which could contribute to inaccuracies:

(1) Violation of the 0.3 L depth of permeable bed material

(2) Friction coefficient

(3) Permeability coefficient

(4) Method of taking profile for a coastline section

(5) Neglecting friction, percolation, and refraction effect beyond a certain depth, = h_s

The first of these assumptions is certainly violated in places off the East Coast of Florida, especially on the lower East Coast where much of the bottom is underlaid by hard limestone rock and reefs, at shallow depths (see Reference [29]).

The friction coefficient used in this study was constant, equal to 0.01 (see Reference [11]), but is known to be a function of bottom roughness, which in turn depends on wave height, and water depth. Thus, friction is not constant, but varies with time. A sensitivity test was done using three friction factors; 0.005, 0.01, and 0.015, for the location of coastline which best represents an average profile from Fort Pierce Inlet to St. Lucie Inlet to compute values of drift. Each drift rose is plotted on the same diagram and shown in Figure 11. Assuming that the friction factor 0.01 is correct, a value of f = 0.015 gives drift values approximately 20% lower and a value of f = 0.005 gives drift values approximately 22% higher. The sensitivity would be much greater on a broader shelf width as in North Florida on the East Coast, and much smaller on a narrow shelf width as encountered in the southern limits of Florida on the East Coast. In two sections of Florida the friction-percolation wave modification was calculated to the 5 foot contour. These sections are known to be extremely low energy sections of coastline along which little sand is available for transport. Drift diagrams were not computed in these sections, only a relative energy index.

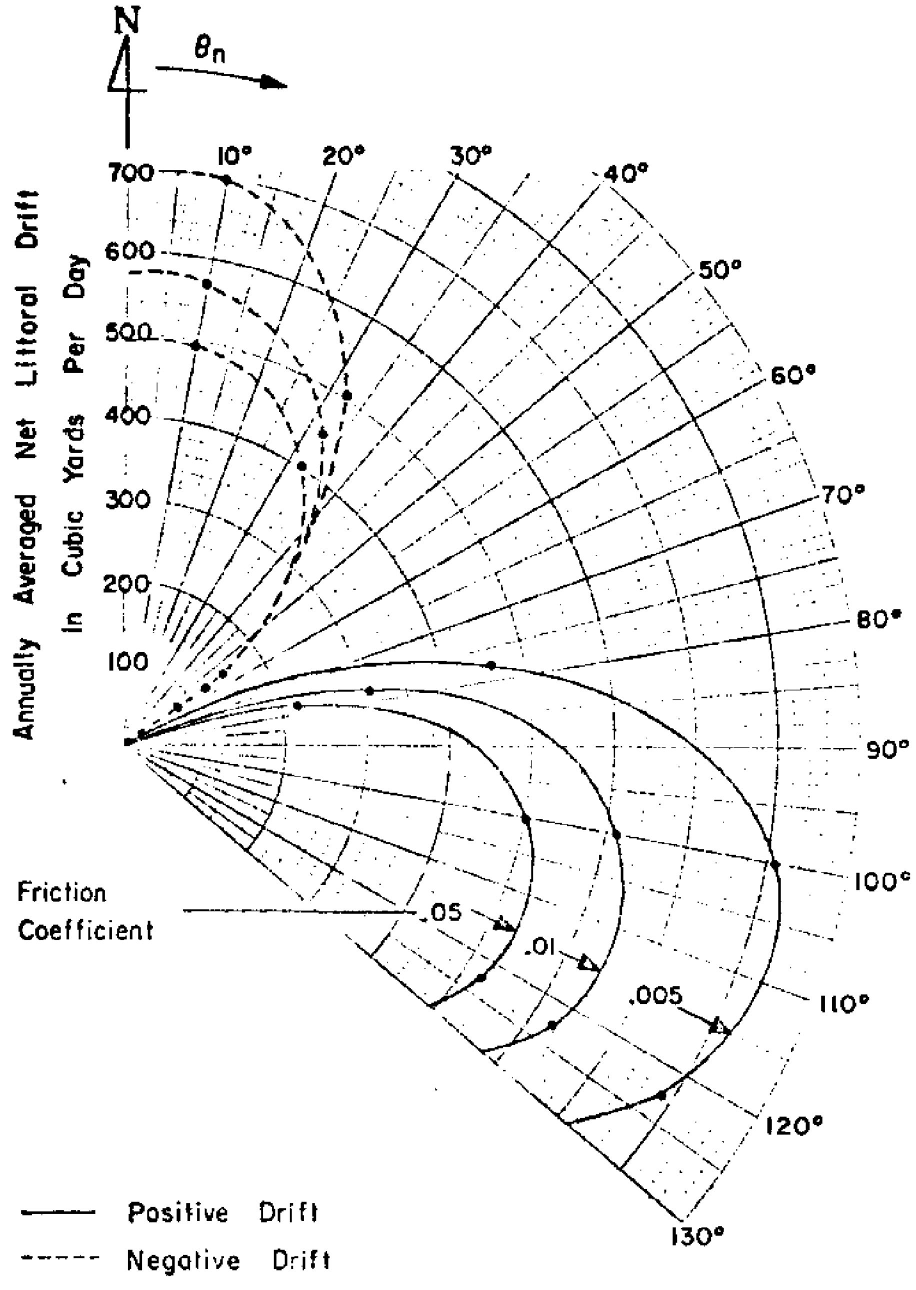

FIGURE 11. VARIABILITY OF NET LITTORAL DRIFT WITH FRICTION COEFFICIENT BETWEEN FORT PIERCE INLET AND ST. LUCIE INLET, FLORIDA

The intrinsic permeability of the offshore material has been assumed as 10 Darcys on the East coast of Florida which is consistent with an offshore sand size of 0.10-0.12 mm. On the Gulf Coast, where the bottom is composed of find sand, silt, and organic muds, the intrinsic permeability was assumed equal to 1 Darcy. To see the effect that permeability has on drift values, a sensitivity test was conducted for permeability on the same Fort Pierce-St. Lucie section with intrinsic permeability equal to 100 Darcys, 10 Darcys, and 1 Darcy, being plotted on the same diagram, shown as Figure 12. The difference in values computed using 1 and 10 Darcys is negligible, while the difference in computed values using 10 Darcys and 100 Darcys is approximately 20%. Thus, for higher permeabilities, the analysis is sensitive to this factor also. Due to the lack of offshore sand deposits to a thickness equal to 0.3 times the wave length (the assumption used in theoretical analysis of permeability modification of waves), this factor is not felt to influence the values of drift because effective permeability would probably be on the low side of 10 Darcys.

The method of taking a profile perpendicular to the stretch of shoreline considered leads to high K_{fp} values which would tend to overestimate the wave height and longshore energy flux since refraction effectively causes waves to travel over a longer profile than the one used. In view of the fact that locations of the individual wave data observations are unknown, the method of using a profile along the perpendicular to shore seems a reasonable approximation though, except where waves are likely to be coming from a different direction.

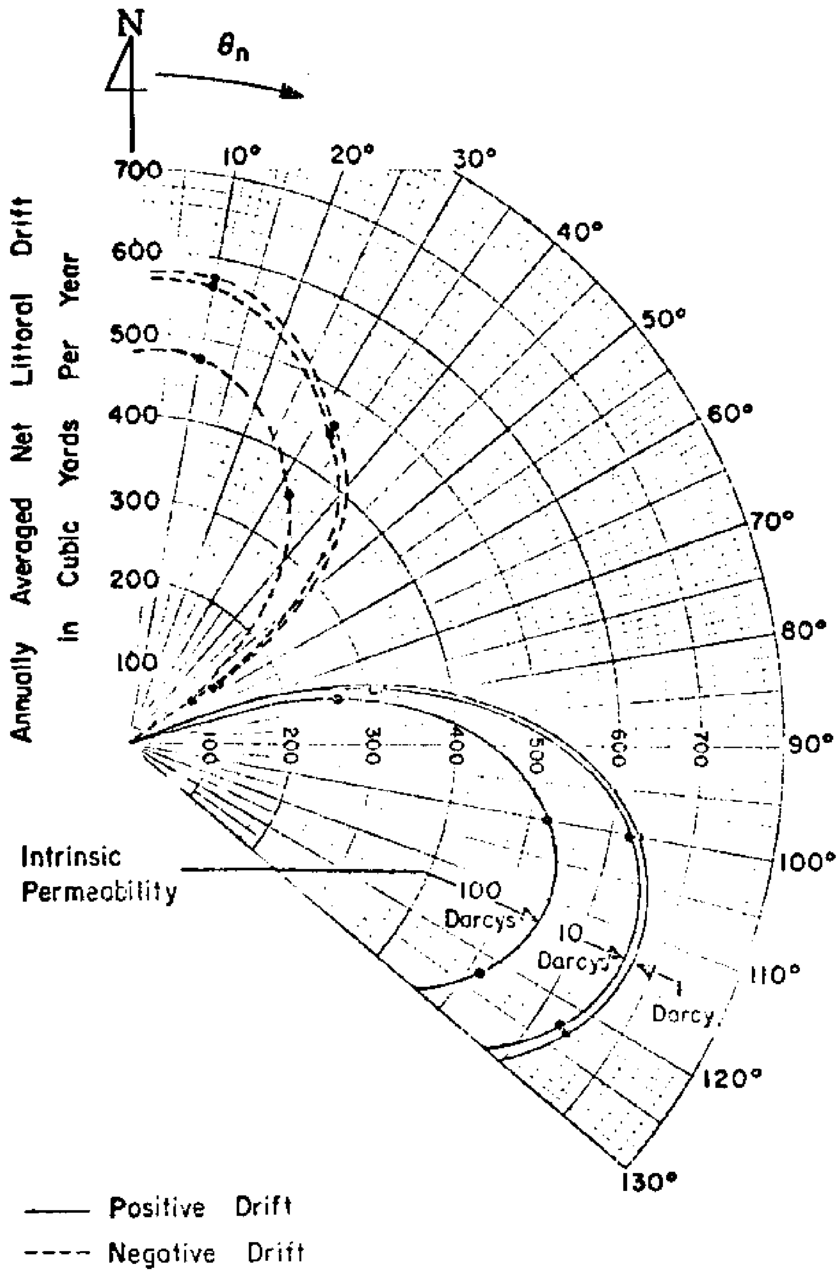

FIGURE 12. VARIABILITY OF NET LITTORAL DRIFT WITH PERMEABILITY BETWEEN FORT PIERCE INLET AND ST. LUCIE INLET, FLORIDA

One such case where a profile along the perpendicular is questionable is the stretch of shore from Cape St. George to Lighthouse Point. Figure 13 shows a sketch of this shoreline with three (3) lines along which profiles have been taken and net drift values computed. The results of the drift values for the different profiles are summarized on a net drift rose shown as Figure 14.

Assumption (5) which was mentioned earlier is made because the value of K_{fp} is based on linear wave theory, and, near breaking conditions in shallow water, the wave form no longer corresponds to linear theory. In addition, the beach is in a dynamic state at shallow depths which would make assumptions regarding slopes in this region invalid during part of the year. Assumption (5) is adequate provided that the slope is relatively steep beyond h_s. Along most of the coast of Florida, including the whole East Coast, it seems reasonable to invoke this assumption at the 10 foot depth contour. Along the Gulf Coast of Florida, from Cape Sable to Cape Romano and from Anclote Keys to Lighthouse Point, an extremely mild slope is encountered, and here the computation of friction-percolation is carried to the 5 foot contour as mentioned previously. In these sections though, the waves have a long distance to travel (5 to 10 nautical miles) before reaching shore even after propagating to the 5 foot contour. Certainly the friction effect on the waves between the 5 foot contour and the shore which is not calculated would be of considerable magnitude, but due to possible violation of the linear assumption necessary in computation of K_{fp}, this dissipation of energy was not calculated. Also, since

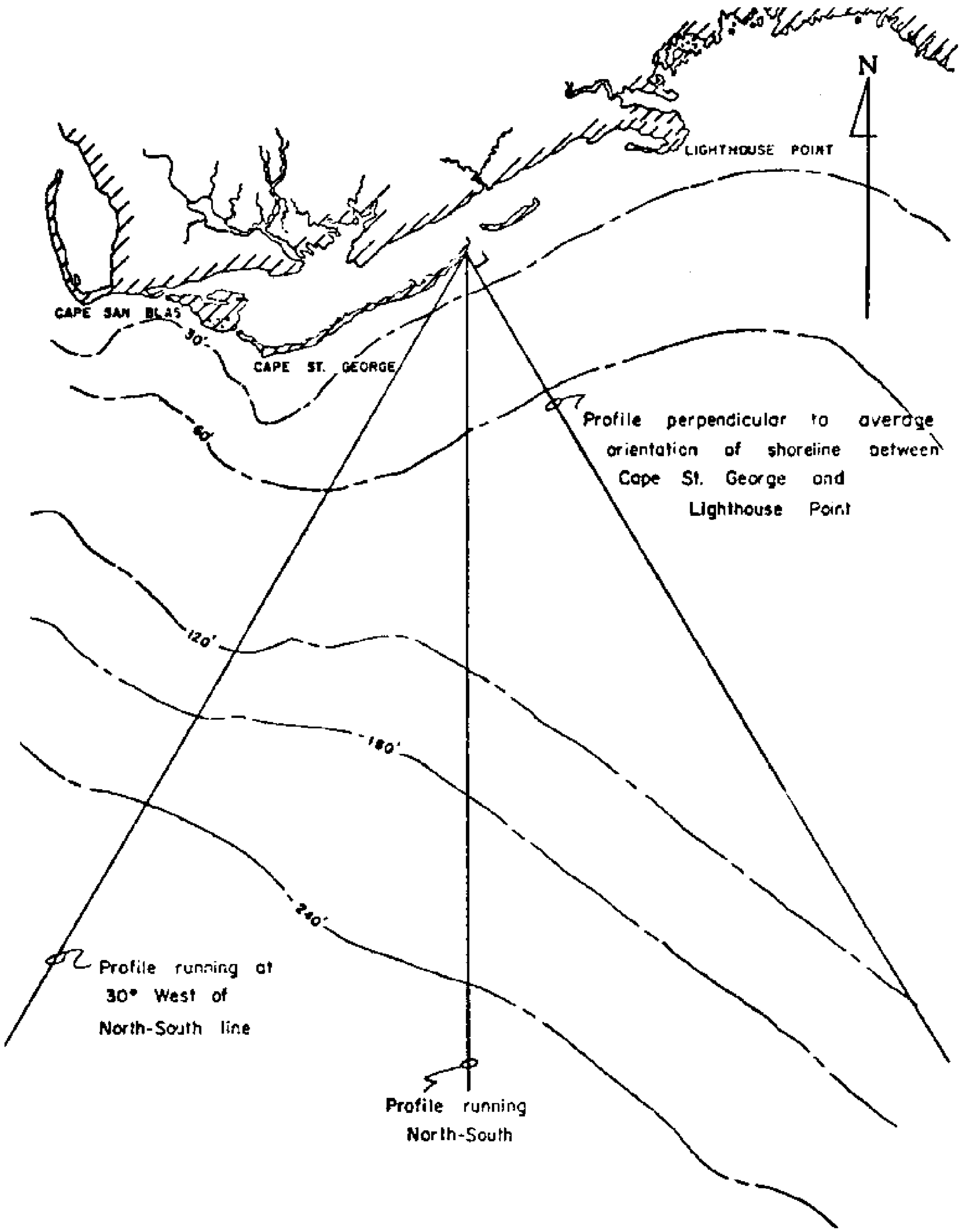

FIGURE 13. PROFILES USED IN MODIFICATION OF OFFSHORE WAVE CLIMATE BETWEEN CAPE ST. GEORGE AND LIGHTHOUSE POINT, FLORIDA

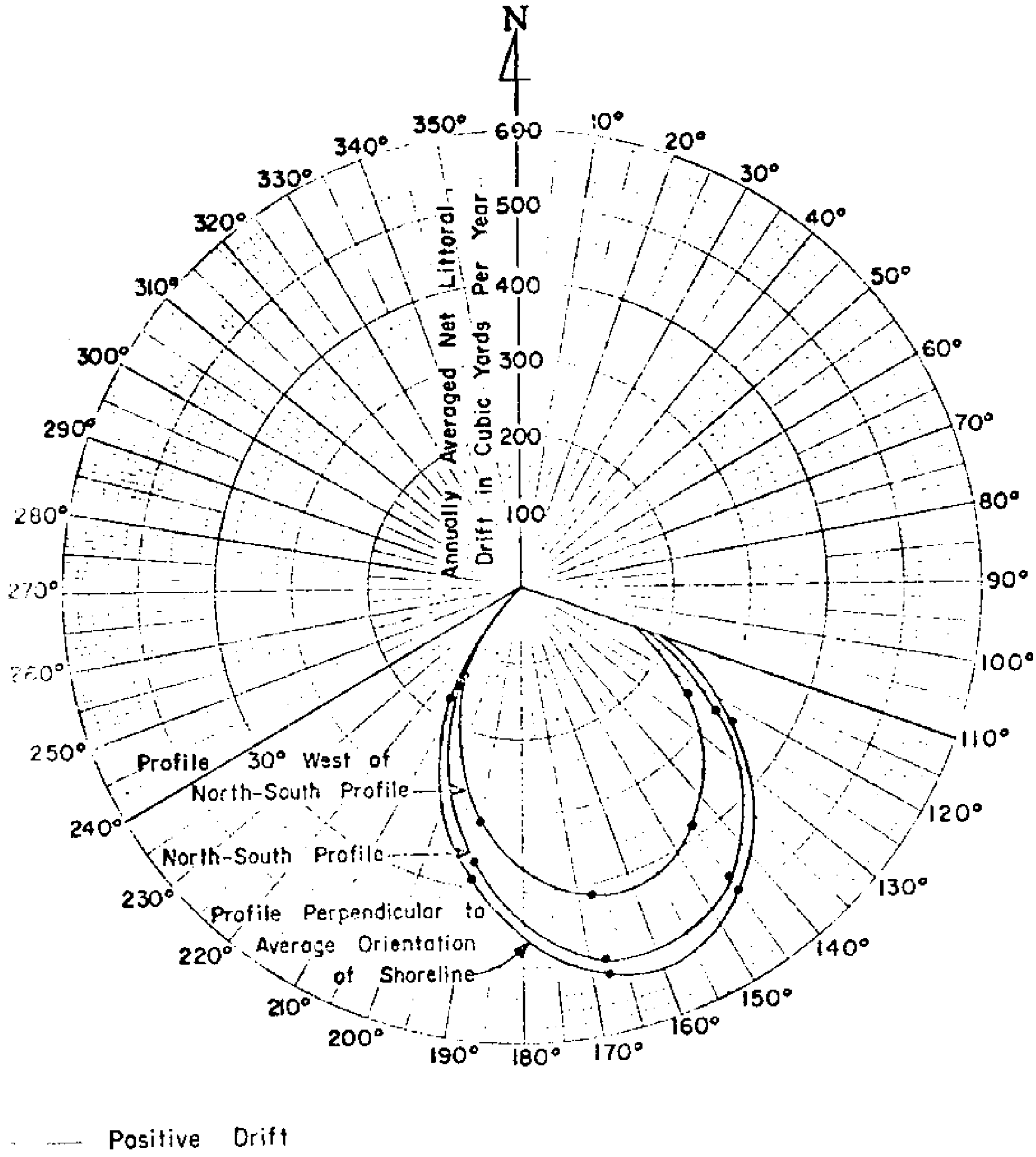

FIGURE 14. VARIABILITY OF NET LITTORAL DRIFT WITH ORIENTATION OF PROFILE BETWEEN CAPE ST. GEORGE AND LIGHTHOUSE POINT, FLORIDA

sand is lacking in these areas, the results were used only to calculate a relative magnitude of energy and not littoral drift.

In line with Assumption (5), further effects of refraction beyond h_s were not computed either. For the majority of waves considered, those with $\alpha_o \leq 67\text{-}1/2°$, $T \geq 5.5$ seconds, the further effect of refraction is insignificant. At most, for a very few waves this further effect of refraction changes the wave height by a maximum of 7% and thus wave energy by a maximum of 14.5%.

In areas of complex topography, the violation of Snell's law may lead to inaccuracies in computed longshore energy. For the majority of Florida's coastline though, this error is believed negligible when compared to other sources of error already considered.

To give an idea of the relative wave energy reaching the shore, a relative energy index has been calculated along the coast of Florida and plotted on Figure 15. This relative energy index consists of the mean square breaking wave height divided by the frequency of onshore waves, thus assuming an onshore wave frequency of 1.00. Note that direction and wave group velocity have not been included in this diagram, and, thus, this is not the available energy flux for longshore transport.

3. Errors in the Correlation with Littoral Drift

Thus far, sources of error inherent in the method used for computation of longshore energy flux (or longshore energy) and in the data source have been considered.

Certainly an important question which should be asked is whether the present linear correlation of Q_ℓ with E_a is valid. In view of the

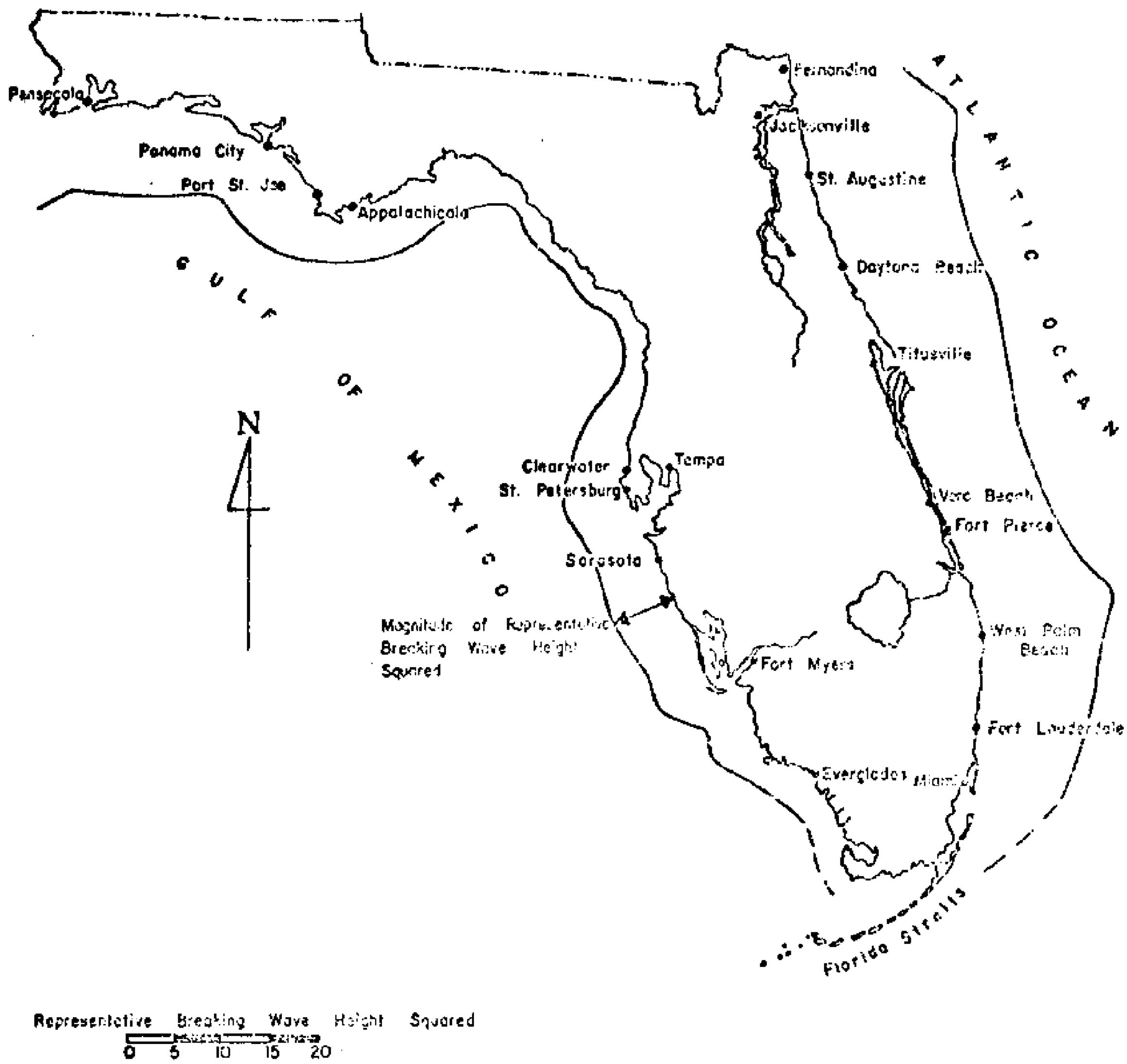

FIGURE 15. RELATIVE WAVE ENERGY AT SHORELINE ALONG THE FLORIDA PENINSULA AS COMPUTED USING THE SSMO DATA

more recent data [10] the linear relationship seems valid, and the main question relates to the value of the constant in the equation $Q_\ell = C^* E_a$. The author has mentioned previously that Reference [11] states the present correlation to be an <u>order of magnitude</u> approximation.

Many of the data points in the original field studies on which the empirical curve depends were calculated with breaking wave conditions as suggested by the equation for computation of E_a. Also, the model data points contain considerable scatter due to inherent littoral transport modeling problems [17]. In addition, there seems to be confusion due to the different methods of computing energy, one method by the root mean square wave height and one by significant wave height. In this study it was assumed that all the original data point computations of longshore energy were made using significant wave heights rather than root mean square wave heights, which to the author's best knowledge is the situation. Thus, the correlation constant between drift and longshore energy presented in this report is adequate for the purposes of this study.

4. Other Errors

Other factors which certainly have a bearing on littoral drift in an area but which were not accounted for in the present computations include:

(1) Wind effect on littoral current and corresponding drift.

(2) Sheltering effects of reefs, rock outcroppings, large submerged sand ridges, etc.

(3) Interference in littoral regime due to jetties, inlets, rivers, sand sources, sand sinks, etc.

Factor (1) has been found to be of major significance in some studies. The present correlation of longshore energy with littoral transport contains this factor to some degree, and, thus, the true effect of wind cannot be separated out.

The sheltering effect of reefs and rock outcroppings is certainly a factor affecting littoral drift along the southeast coast of Florida. Many rock outcroppings and reefs exist in the littoral regime and definitely influence drift values. In places such as Cape Kennedy where a large underwater sand ridge exists, the drift pattern is altered by the sheltering effect of the ridge which prevents some northeasterly waves from reaching the southern shore and some southeasterly waves from reaching the northern shore; thus, to an extent, the ridge tends to be a self-perpetuating littoral barrier.

Jetties, inlets, rivers, submarine valleys, etc. all influence the pattern of drift to alter it from the idealized model used to compute values of drift; these influences must be recognized when applying drift values derived by the approach presented.

CHAPTER IV

LITTORAL DRIFT COMPARISONS

A. Comparison of Calculated Littoral Drift Rates with Previously Estimated Values

Comparisons of the present study results with estimated values of net drift compiled by the U.S. Army Corps of Engineers are summarized in Table 1. The Corps of Engineers values were determined by various methods which include analysis of dredging records, volumetric surveys, and pumping records at existing by-pass plants. Computed values of drift by the present method provide both an "expected" value of drift and, to illustrate the sensitivity of drift to coastline orientation, a range of drift values which encompass ± 11 1/4° span of azimuths to the actual coastline azimuth, θ_n, at a given location. Total positive and negative drift rates with the corresponding ranges of values are summarized in Table 2.

The manner in which these littoral drift rates were computed from the drift roses is best explained by the following examples.

1. Littoral Drift Computations at Inlets

For an inlet, a material balance was made on a section of beach containing the inlet and the beach adjacent to the inlet for distances updrift and downdrift such that all local effects of erosion and accretion caused by the inlet's presence are contained within the

TABLE 1

COMPARISON OF ANNUAL AVERAGE NET LITTORAL DRIFT RATES AS ESTIMATED BY THE U.S. ARMY CORPS OF ENGINEERS AND AS CALCULATED IN THE PRESENT STUDY

Location	Estimated by Corps of Engineers: Annual Average Net Drift Rate in Cubic Yards Per Year ÷ 10^3	Estimated by Corps of Engineers: Direction	Computed Using SSMO Data: Annual Average Net Drift Rate in Cubic Yards Per Year ÷ 10^3	Computed Using SSMO Data: 11 1/4° Range	Computed Using SSMO Data: Direction
Atlantic Coast					
St. John's River	500	South	257	217-321	South
St. Augustine Inlet	400-500	South	293	195-251	South
Ponce de Leon Inlet	500	South	76.7	4-181	South
Canaveral Harbor	350	South	241	201-277	South
Sebastian Inlet	-	South	12.8	(39)-119	South
Fort Pierce Inlet	200-250	South	53.0	(21)-142	South
St. Lucie Inlet	230	South	94.1	(18)-177	South
Lake Worth Inlet	230	South	336	265-351	South
Hillsboro Inlet	120	South	315	261-347	South
Port Everglades	50	South	259	66-313	South
Miami Harbor Entrance	10	South	363	332-392	South
Lower Gulf Coast					
Gordon Pass	66	South	71.2	54.5-93.5	South
Ft. Myers Beach	22	North	21.9	0-58.2	North
Venice Inlet	40	South	86.9	58.1-108.5	South
New Pass	40	South	27.5	(7)-61.3	South
Anna Maria Island	-	North	0-80.3	(44.1)-109.6	South
Treasure Island	50	South	(40.2)-58.4	(58.4)-73.0	South
Clearwater Pass	10	South	76.7	55.8 -90.9	South
Upper Gulf Coast					
Perdido Pass (Ala.)	65 [(a)]	West	274	234-281	West
Pensacola Pass	65	West	292	234-320	West
East Pass	150	East	254	195-307	West

Parentheses ( ) indicate a drift rate in the opposite sense of the recorded direction.

(a) This drift rate is quoted as 130 x 10^3 cubic yards per year in summarized drift rates given in Table Reference [1], but given correctly as 65 x 10^3 in latter portion of the volume.

TABLE 2

COMPARISON OF ANNUAL AVERAGE TOTAL LITTORAL DRIFT RATES AS ESTIMATED BY THE U.S. ARMY CORPS OF ENGINEERS AND AS CALCULATED IN THE PRESENT STUDY

Location	Estimated by Corps of Engineers: Total Northerly (or Westerly) Drift Rate in Cu. Yds. per year ÷ 10^3	Estimated by Corps of Engineers: Total Southerly (or Easterly) Drift Rate in Cu. Yds. per year ÷ 10^3	Computed Using SSMO Data: Total Northerly (or Westerly) Drift Rate in Cu. Yds. per year ÷ 10^3	11 1/4° Range	Computed Using SSMO Data: Total Southerly (or Easterly) Drift Rate in Cu. Yds. per year ÷ 10^3	11 1/4° Range
Atlantic Coast						
St. John's River	100	600	222	169-250	479	467-490
St. Augustine Inlet	100	600	270	221-301	563	496-572
Ponce de Leon Inlet	100	600	309	307-360	386	364-488
Canaveral Harbor			197	168-215	438	416-445
Sebastian Inlet			272	272-285	285	246-391
Fort Pierce Inlet			281	245-281	334	260-387
St. Lucie Inlet			303	237-304	397	286-414
Lake Worth Inlet			213	211-276	549	541-562
Hillsboro Inlet			198	190-250	513	511-587
Port Everglades			234	183-423	493	489-496
Miami Harbor Entrance			186	179-201	549	533-571
Lower Gulf Coast						
Gordon Pass			43.8	36.5-47.5	115	102-130
Ft. Myers Beach			80.3	62.1-102	58.4	43.8-62.1
Venice Inlet			68.6	59.5-75.9	155.5	134-168
New Pass			93.1	77.7-114	120.6	107-139
Anna Maria Island			73-110	58.4-139	110-153	94.9-168
Treasure Island			73-124	65.7-131	84-131	73-139
Clearwater Pass			55.8	51.1-76.7	132.5	132.5-142
Upper Gulf Coast						
Perdido Pass (Ala.)			387	358-391	113	110-124
Pensacola Pass			417	361-429	125	109-127
East Pass			361	321-409	107	102-126

section. In this manner, the values of drift computed are not related to the local inlet configuration. Figure 16 provides a pictorial representation of the method.

Considering only the littoral transport through the "control" section, a value of $(Q_{\ell\ net})_R$ associated with $(\theta_n)_R$ will be entering or leaving the control section on the right side of the inlet in the positive or negative direction depending on sign, and $(Q_{\ell\ net})_L$ associated with $(\theta_n)_L$ will be entering or leaving the control section on the left side of the inlet in the positive or negative direction depending on sign. The average of these values should give an estimate of the net drift in the vicinity of the control section. Note that this method may not give rates which correspond to the drift rates as computed by the Corps of Engineers, since the Corps rates were estimated by volumetric changes of shoreline within the control section and dredging and pumping records for the inlet. A better representation would be given by the net drift value on the side of the inlet in which the volumetric changes were measured. For example, if the net drift on the left side (when looking offshore) of the inlet is positive, an accumulation of drift would be experienced at a jetty, and possibly a small amount of erosion would occur up drift from the accretion as shown in Figure 16. A net gain in sand would be measured if volumetric surveys on this side of the inlet were taken. It is this net gain that should be computed for a better comparison with Corps estimated values, but, due to a lack of data on the method by which the Corps values were obtained, the net drift comparisons could not be made in this manner.

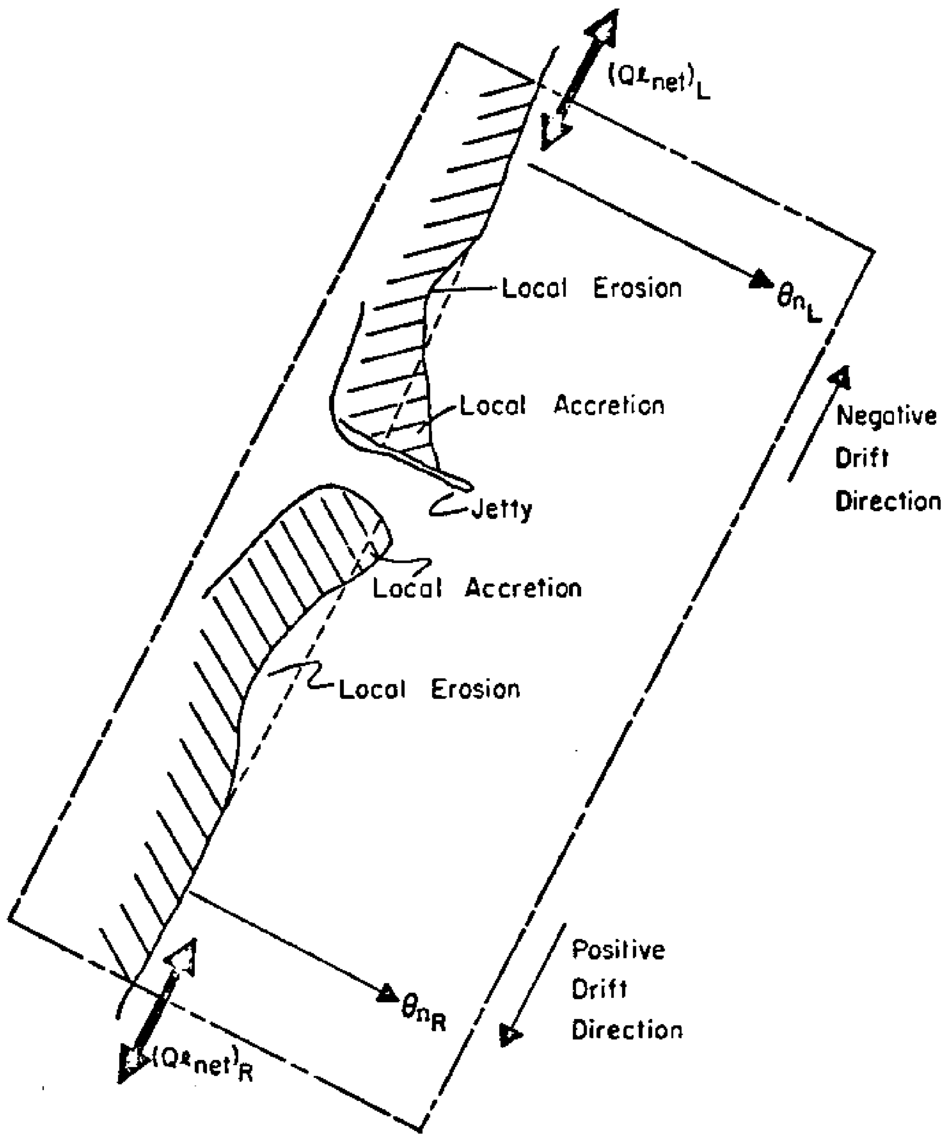

FIGURE 16. CONTROL SECTION FOR CALCULATION OF DRIFT AT AN INLET

Total positive and negative drift rates were also computed by averaging the respective positive and negative drift rates on each side of the inlet.

The difference between the net drift on the updrift side of an inlet and the net drift on the downdrift side would be the amount of sand lost to the inlet system control volume. This rate of sand gain or loss by the inlet system is the overall effect of accumulations at the jetties and in the bay and ocean shoals, and of erosion normally encountered downdrift of the inlet. Values of sand losses or gains calculated in this manner are given in Table 3.

Application of these methods to inlets within segments of the coast for which a drift rose was calculated are based on the one corresponding drift rose for that section. Where inlets are at the boundary of shoreline segments, the drift data obtained from the drift roses corresponding to each side of the inlet are weighted equally, with average values being computed for each drift direction and azimuth angle considered. Rational judgement should dictate whether or not it is necessary to use one or more drift roses for calculation of the drift values. In most cases the drift roses do not make such "drastic" changes that a refinement becomes necessary.

To further clarify the method, drift rates are calculated for Ponce de Leon Inlet on the East Coast of Florida (see Figures 17, 18 and Table 4) as based on the shoreline segments of St. Augustine Inlet to Ponce de Leon Inlet, and Ponce de Leon Inlet to Cape Kennedy. Here the South side of the inlet has an azimuth of 59° and the North side

TABLE 3

AVERAGE ANNUAL LITTORAL DRIFT RATE GAIN OR LOSS IN INLET CONTROL SECTION

Location	Net Littoral Drift on Updrift Side of Inlet Minus Net Littoral Drift on Downdrift Side of Inlet in Cubic Yards Per Year
Atlantic Coast	
St. John's River	0
St. Augustine Inlet	-46,000
Ponce de Leon Inlet	47,000
Canaveral Harbor	0
Sebastian Inlet	0
Fort Pierce Inlet	0
St. Lucie Inlet	12,400
Lake Worth Inlet	0
Hillsboro Inlet	-20,000
Port Everglades	0
Miami Harbor Entrance	-55,000
Lower Gulf Coast	
Gordon Pass	11,000
Venice Inlet	- 5,400
New Pass	-35,600
Clearwater Pass	- 3,500
Upper Gulf Coast	
Perdido Pass (Ala.)	0
Pensacola Pass	-40,000
East Pass	33,000

Negative signs infer a net erosion from the control section.

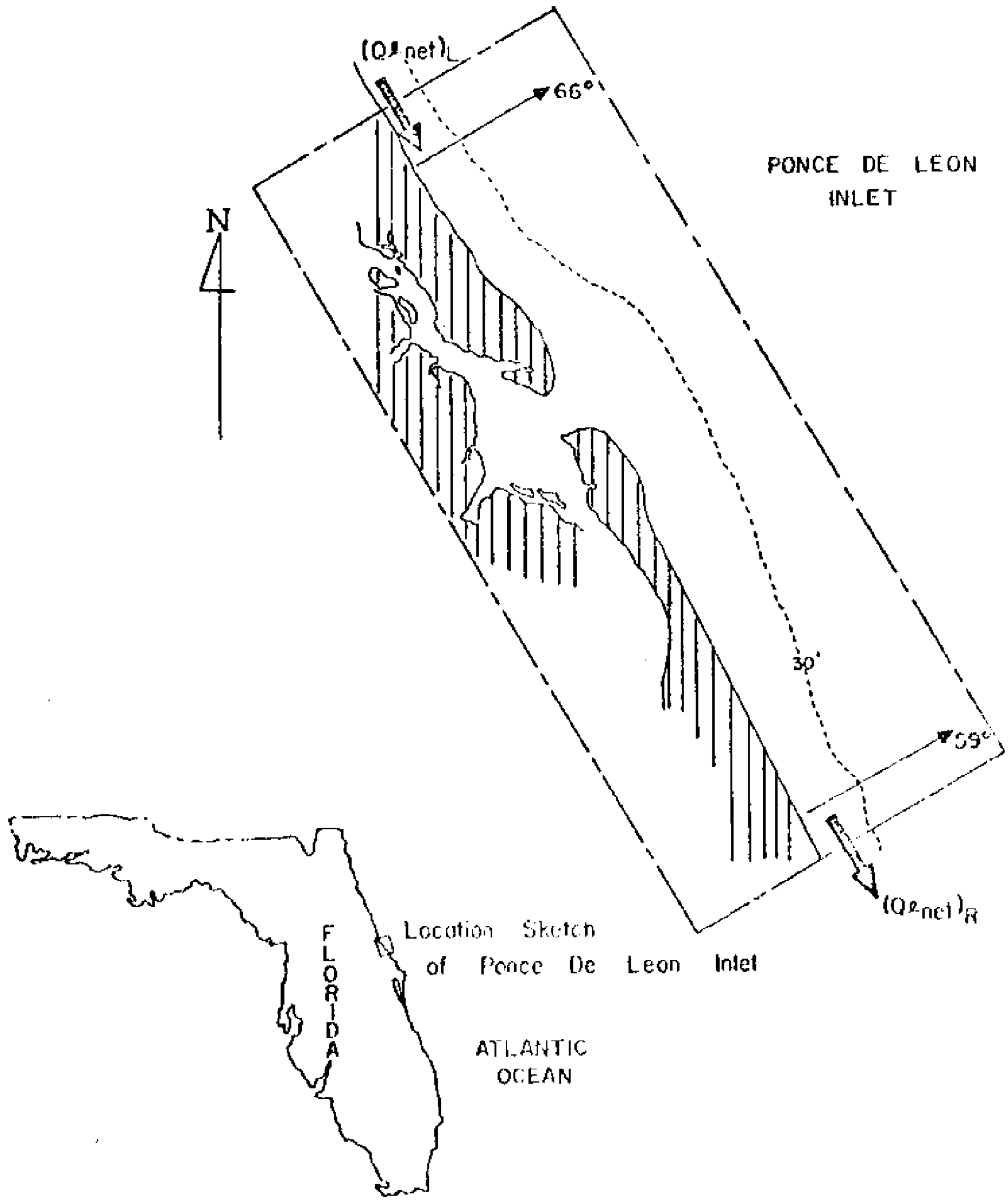

FIGURE 17. PONCE DE LEON INLET CONTROL SECTION

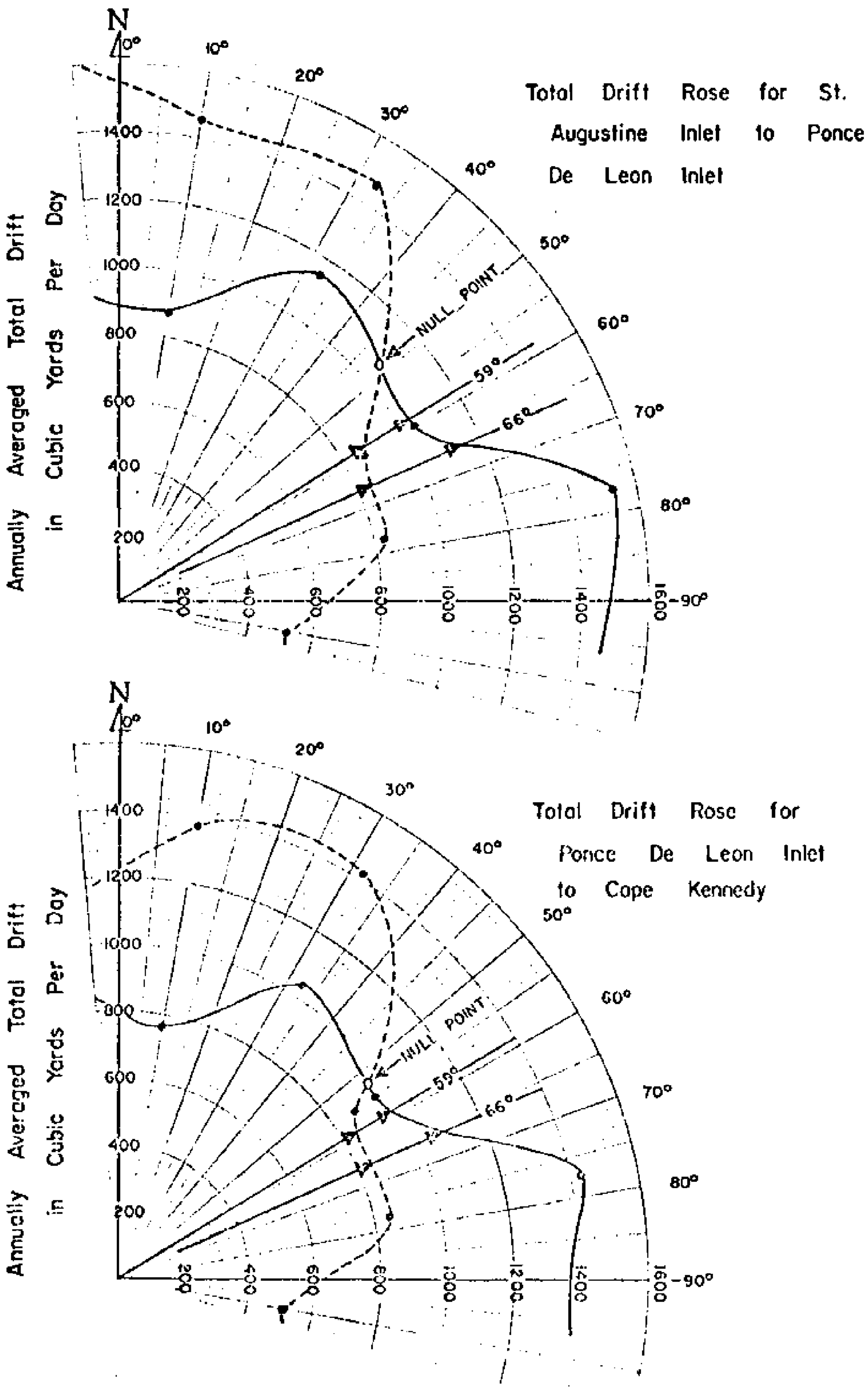

FIGURE 18. TOTAL DRIFT ROSES FOR SEGMENTS OF SHORE ADJACENT TO PONCE DE LEON INLET

TABLE 4

DRIFT COMPUTATIONS AT PONCE DE LEON INLET, FLORIDA

Net Drift Computations (in cubic yards per day)

Drift on Left Side of Inlet

		$\pm$ 11-1/4° Range	
$(Q_{\ell+})_L$	= 1150	1040 to 1520	St. Augustine Inlet to Ponce de Leon Inlet Rose
	1080	950 to 1430	Ponce de Leon Inlet to Cape Kennedy Rose
Average	1115	995 to 1475	
$(Q_{\ell-})_L$	= 840	840 to 920	St. Augustine Inlet to Ponce de Leon Inlet Rose
	840	840 to 860	Ponce de Leon Inlet to Cape Kennedy Rose
Average	840	840 to 890	
$(Q_{\ell\ net})_L$	= 1115		
	-840		
	275 South		

Drift on Right Side of Inlet

$(Q_{\ell+})_R$	= 1040	1040 to 1240	St. Augustine Inlet to Ponce de Leon Inlet Rose
	960	960 to 1160	Ponce de Leon Inlet to Cape Kennedy Rose
Average	1000	1000 to 1200	
$(Q_{\ell-})_R$	= 870	840 to 1080	St. Augustine Inlet to Ponce de Leon Inlet Rose
	840	840 to 1080	Ponce de Leon Inlet to Cape Kennedy Rose
Average	855	840 to 1080	
$(Q_{\ell\ net})_R$	= 1000		
	-855		
	145 South		

Net Drift

$$Q_{\ell\ net} = \frac{(Q_{\ell\ net})_R + (Q_{\ell\ net})_L}{2} = \frac{275 + 145}{2}$$

$= 210$ South ($= 76.7 \times 10^3$ cubic yards per year)

Total Drift Computations (in cubic yards per day)

Total Drift in Southerly Direction

$$Q_{\ell+} = \frac{(Q_{\ell+})_R + (Q_{\ell+})_L}{2} = \frac{1000 + 1115}{2}$$

$= 1058$ South ($= 386 \times 10^3$ cubic yards per year)

Total Drift in Northerly Direction

$$Q_{\ell-} = \frac{(Q_{\ell-})_R + (Q_{\ell-})_L}{2} = \frac{855 + 840}{2}$$

$= 848$ North ($= 309 \times 10^3$ cubic yards per year)

Gain (or Loss) to Inlet Control Section (in cubic yards per day)

$$\Delta Q_{\ell\ net} = (Q_{\ell\ net})_L - (Q_{\ell\ net})_R = 275 - 145$$

$= 130$ ($= 47 \times 10^3$ cubic yards per year)

a gain to the inlet control section and thus a corresponding loss to the entire littoral system an azimuth of 66°. Rates of $(Q_{\ell\ net})_R$ and $(Q_{\ell\ net})_L$ corresponding to the above azimuths are 53,000 cubic yards per year (South) and 100,000 cubic yards per year (South) respectively as averaged from the drift roses corresponding to the shore segments on each side of the inlet and shown in Figure 18. The net drift is thus the average of these two rates and is 76,700 cubic yards per year to the South. Considering a $\pm$ 11 1/4° range of azimuth angles to account for directional bias of wave data, the net drift would be in a range of rates from 4,000 cubic yards per year (South) to 181,000 cubic yards per year (South). The total positive drift would thus be 386,000 cubic yards per year as averaged from $Q_{\ell+}$ on each side of the inlet from each diagram. The total negative drift would thus be 309,000 cubic yards per year as averaged from $Q_{\ell-}$, the negative drift, in the same manner as above. Ranges of $Q_{\ell+}$ and $Q_{\ell-}$ are given in Table 2. These values are all calculated from the positive and negative drift roses for better interpolation accuracy. The amount of drift gained by the inlet control section and thus lost to the overall littoral system is $(Q_{\ell\ net})_L - (Q_{\ell\ net})_R$ which equals 100,000 - 53,000 = 47,000 cubic yards per year. The major reason for the large difference in the net drift at Ponce de Leon Inlet as compared to the inlets North of Ponce de Leon Inlet is in the orientation of the coastline, not the drift rose magnitudes, as can be seen by comparing net drift or positive-negative drift diagrams for the North Florida area (Atlantic side). The orientation of the coastline at Ponce de Leon Inlet as described by θ_n, the azimuth normal to shore, approaches a null point, that is, a point where the total Northerly drift is equal to the total Southerly drift.

The Corps of Engineers estimated value of net drift is 500,000 cubic yards per year (South), with total Southerly drift equal to 600,000 cubic yards per year and total Northerly drift equal to 100,000 cubic yards per year for a "gross" drift value of 700,000 cubic yards per year.

2. Littoral Drift Computations for Barrier Islands

For a barrier island, computation of littoral drift was based on the range of azimuth angles of the coastline perpendicular to the island. Values of drift were based on the particular drift rose corresponding to the section of coast containing the island. Often inlets or passes at the ends of an island act as littoral barriers and cause an accretion of sand at both ends of an island and erosion in the middle. This is typical of barrier islands and results in the island developing a concave shape on its seaward side. Thus, there will be a range of azimuth angles through which the island is exposed to offshore wave climate and there will be a corresponding range of possible drift values that would occur. As an example of the computational procedure, Treasure Island on the Gulf Coast is considered (see Figure 19). Azimuth angles, θ_n, range from 214° at the northern end of the island to 247° at the southern end of the island. For this range of angles, the values of $(Q_{\ell+}) - (Q_{\ell-})$ range from +40,200 cubic yards per year (Northerly) to -58,400 cubic yards per year (Southerly). If an additional range of ± 11 1/4° is considered to account for directional bias in wave data, the values of drift become +58,400 cubic yards per year (Northerly) to -73,000 cubic yards per year (Southerly).

(a)

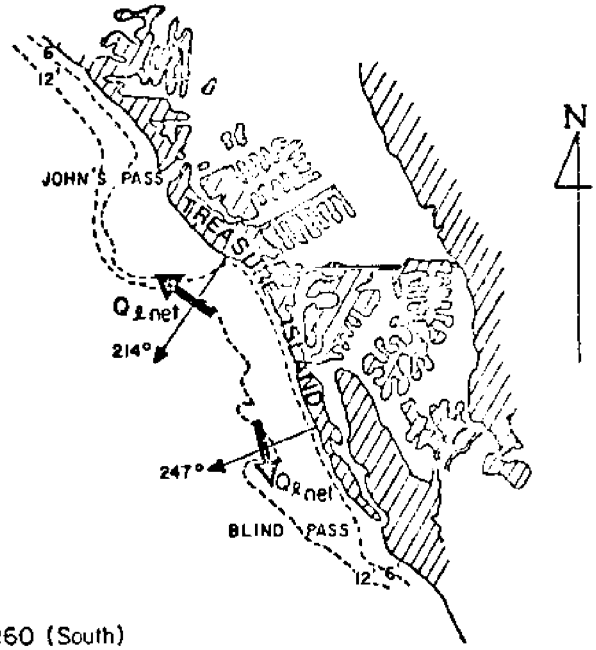

$$Q\ell_{net} = Q\ell_{+} - Q\ell_{-}$$

$= +110$ (North) to -160 (South)

(40.2×10^3 to -58.4×10^3 Cubic Yards Per Year)

or when considering a $\pm 11\frac{1}{4}°$ range of azimuths to coast

$= +160$ (North) to -200 (South)

(58.4×10^3 to -73.0×10^3 Cubic Yards Per Year)

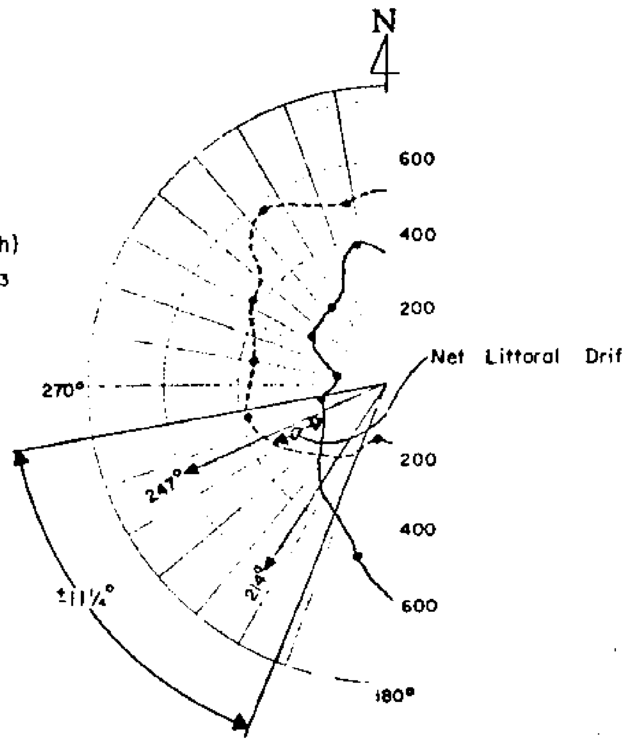

(b)

FIGURE 19. EXAMPLE DRIFT CALCULATIONS AT TREASURE ISLAND, FLORIDA

The estimated value of net drift by the Corps of Engineers is given as 50,000 cubic yards per year in a Southerly direction which lies within the computed range. The computed total Northerly drift is 73,000 to 124,000 cubic yards per year, and the total Southerly drift per year is -84,000 to -131,000 cubic yards per year.

Note that some of the comparisons presented in Table 1 and Table 2 may be misleading in that they are extremely close to Corps estimated values when the assumptions involved in the program to compute drift are possibly violated. A place in question is Fort Myers Beach on the Gulf Coast. The computed value of net drift is 21,900 cubic yards per year in a Northerly direction which is extremely close to the Corps estimated value of 22,000 cubic yards per year. The assumption of parallel offshore contours is violated here though, and, refraction of waves from a Northeasterly direction is undoubtedly much different from what the simplified analysis based on Snell's Law would compute it to be. Refraction of N W waves off Sanibel Island would tend to create a complex nearshore current situation with the probable direction of drift being North even if the wave climate and ideal bottom topography would normally tend to create a Southerly drift.

It is suggested that use of the results presented in the littoral drift roses be carried out with a knowledge of the assumptions present in the study such that one is not misled by the seemingly good comparisons as given above which may be fortuitous.

B. General Trends and Specific Cases of Littoral Drift

Along the Atlantic Coast, the SSMO data confirm the Corps estimates of net Southerly movement of sand, and on most of the lower

Gulf Coast the data confirm net sand movement in a Southerly direction. Along the Panhandle the net movement is in a Westerly direction which also agrees with other studies. Except for certain anomalies in drift directions due to coastline orientation, the overall trends confirm past observations with regard to direction, although magnitudes are different. Reason for the extremely high values of drift computed in Southeast Florida are not known at this time although the author speculates three possibilities:

(1) The effect of the Gulf Stream current on wave height observations as mentioned earlier.

(2) Effects of the Bahama Banks.

(3) Resolution of wave data into large data squares rather than smaller squares where overall offshore conditions are the same.

Specific cases of accretion or erosion patterns can be confirmed when viewed from the "closed system" type of approach as used in the inlet drift predictions. One such case is an accretion of sand at Cape San Blas on the Gulf Coast. From computing the net drift on the section of coast containing St. Joseph Spit, a small net Southward drift value is noted. East of Cape San Blas, a large net Westward drift value can be found from the corresponding drift diagram. Accretion is thus building Cape San Blas toward the Gulf from both directions which is confirmed by Corps studies. The Corps of Engineers states the net drift on St. Joseph Spit to be moving in a Northward direction from spit growth rates, but this is probably due to local refraction effects at the spit terminus rather than the overall ideal beach drift pattern.

In the same manner, Cape St. George can also be found accreting. Accretion of these two capes is linked to the overall erosion patterns experienced on the connecting barrier islands. Other isolated examples such as these will be investigated further in the future to confirm drift patterns.

An interesting observation was made in this study with regard to null points in net drift. By viewing either the net drift diagrams or the total positive and total negative drift diagrams, it can be seen that two types of null points exist in the drift regime. In Figure 20(a) a "Type 1" null point is shown for a portion of a typical total drift diagram. Assume first that an island exists such that its original orientation conforms to the null drift point (total positive drift = total negative drift), Figure 20(b). A perturbation in the system such as a storm, or the building of jetties at ends of the island could cause the sand to be shifted to a position shown in Figure 20(c). In this case the net drift on the right side of the island would now be to the right while the net drift on the left side of the island would be to the left. Thus the overall effect of the perturbation would produce instability in the island, with the net result that the perturbation would increase and eventually the island would experience a breakthrough as shown in Figure 20(d).

The orientation of the Gulf Coast shoreline in Lee County, Florida, is found to be approximately characterized by a Type 1 null point. It is noted that this section of coastline contains numerous inlets and has a history of inlet breakthroughs. Another area where

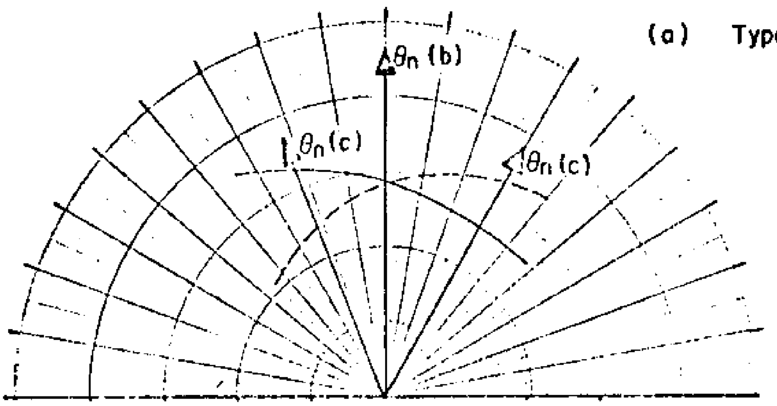

(a) Type I null point

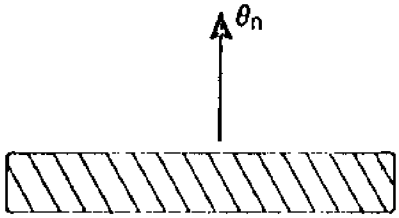

(b) Ideal Island oriented to null point – zero net drift

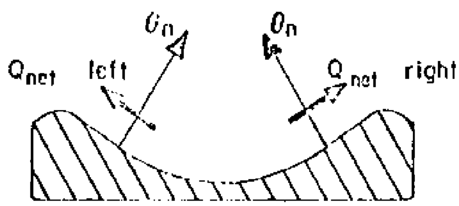

(c) Perturbation in system causes orientation of Island with associated drift pattern

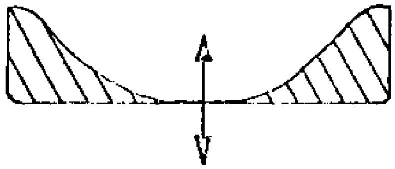

(d) Instability leads to eventual breakthrough

FIGURE 20. IDEAL CASE OF AN UNSTABLE NULL POINT

this type of null point is experienced is the Gulf Coast near St. Petersburg. Islands in this region tend to be extremely concave and would have probably broken through by now if not for the extensive groin fields hindering the transport of drift in the region. It should be noted that a perturbation in the convex sense would also be unstable and lead to an increasing convexity. No cases of this type system were noted, except as small scale features on offshore islands.

The second type of null point is shown in Figure 21(a). An ideal island when oriented to this type of null point has a tendency to stabilize itself once a perturbation in the system drives it from the ideal state. Figures 21(b), 21(c), and 21(d) show the series of events leading to stability. Part of the East Coast of Florida is near this type of null point where a predominant tendency for few inlets exists. Many of the inlets (such as Sebastian Inlet which occurs very near a "Type 2" null point) have had a record of numerous closures after being cut. Of course, many additional factors influence stability and instability in true physical systems such as the amount of drift supplied to an area, and the ocean tidal ranges. These additional effects may overshadow those discussed here. It is hoped that in the future this theory can be explored further.

C. Comparison of Estimated and Observed Wave Climates

To determine the reliability of the SSMO data and computed shoaling, refraction, etc. effects in the present study, a comparison was made using wave records obtained from shore-based gages. Data from step resistance wave gages operated by the Coastal Engineering

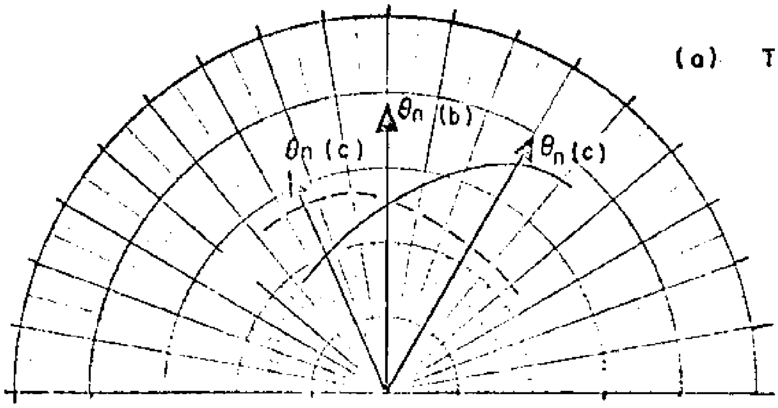

(a) Type II null point

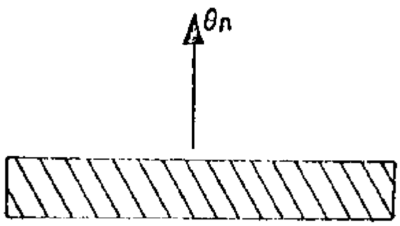

(b) Ideal Island oriented to null point – zero net drift

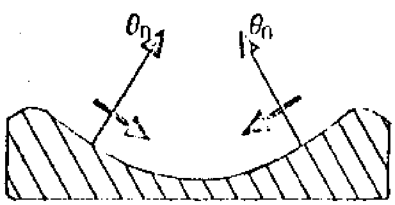

(c) Perturbation in system causes orientation of Island with associated drift pattern

(d) Self-stabilizing drift pattern leads to original island conditions

FIGURE 21. IDEAL CASE OF A STABLE NULL POINT

Research Center were made available for three wave gage stations: Daytona Beach (East Coast), Lake Worth-Palm Beach (East Coast), and Naples (Gulf Coast). Wave data were obtained intermittently during the years of operation of these stations due to various storms damaging equipment or structures on which the gages were mounted. To avoid a seasonal bias in the shore-based recordings, a sample of data best representing the average annual conditions was used in each comparison. Table 5 shows the observation periods used, the total number of observations, and the depths at these stations.

In regard to the SSMO data, certain assumptions had to be made with respect to the frequency of occurrence for wave heights and periods. Only the onshore directed waves were used for obvious reasons, which gave an extremely high frequency of "calm" conditions ($H \cong 0$) at shore. It was assumed for the plotting of cumulative height curves that the sea state at shore is best represented by wave heights of less than one foot when offshore directed waves were being recorded. Most likely, many waves greater than one foot would be recorded at shore during this time. This assumption gives a poor basis of comparison for recorded and observed low wave heights in which the majority of waves fall. In the cumulative distribution curves for wave period, the assumed frequency of occurrence of a specific wave period was assumed equal to the frequency of the onshore directed wave (of a specific period) times one (1.0), divided by the total fraction of onshore directed waves.

Cumulative curves of the plotted wave height and period distributions at these three stations are shown in Figures 22 through 27. The wave height cumulative curves show three sets of points with corresponding

TABLE 5

RECORDING PERIODS OF SHORE BASED CERC WAVE GAGES USED IN COMPARISON OF ACTUAL TO PREDICTED SHORE WAVE CLIMATE

Daytona Beach, Florida

(Depth of Wave Gage = 15 ft. MWL)

February-December	1954		1570 observations*
February-November	1955		1151 observations
February-March	1956		234 observations
January -April	1957		321 observations
November-December	1964		304 observations

Lake Worth-Palm Beach, Florida

(Depth of Wave Gage = 18.2 ft. MWL at Lake Worth and = 15.7 ft. MWL at Palm Beach)

January-April and June -December	1958	Palm Beach	1161 observations
January-December	1960	Palm Beach	2020 observations
January-December	1960	Palm Beach	1687 observations
January-April and June -December	1961	Palm Beach	1301 observations
January-December	1966	Lake Worth	1751 observations

Naples, Florida

(Depth of Wave Gage = 16.6 ft. MWL)

January-December	1958		1454 observations

*Each observation is the significant wave height and period as determined from a 7-minute recording of sea surface elevation measured using a step resistance type wave gage.

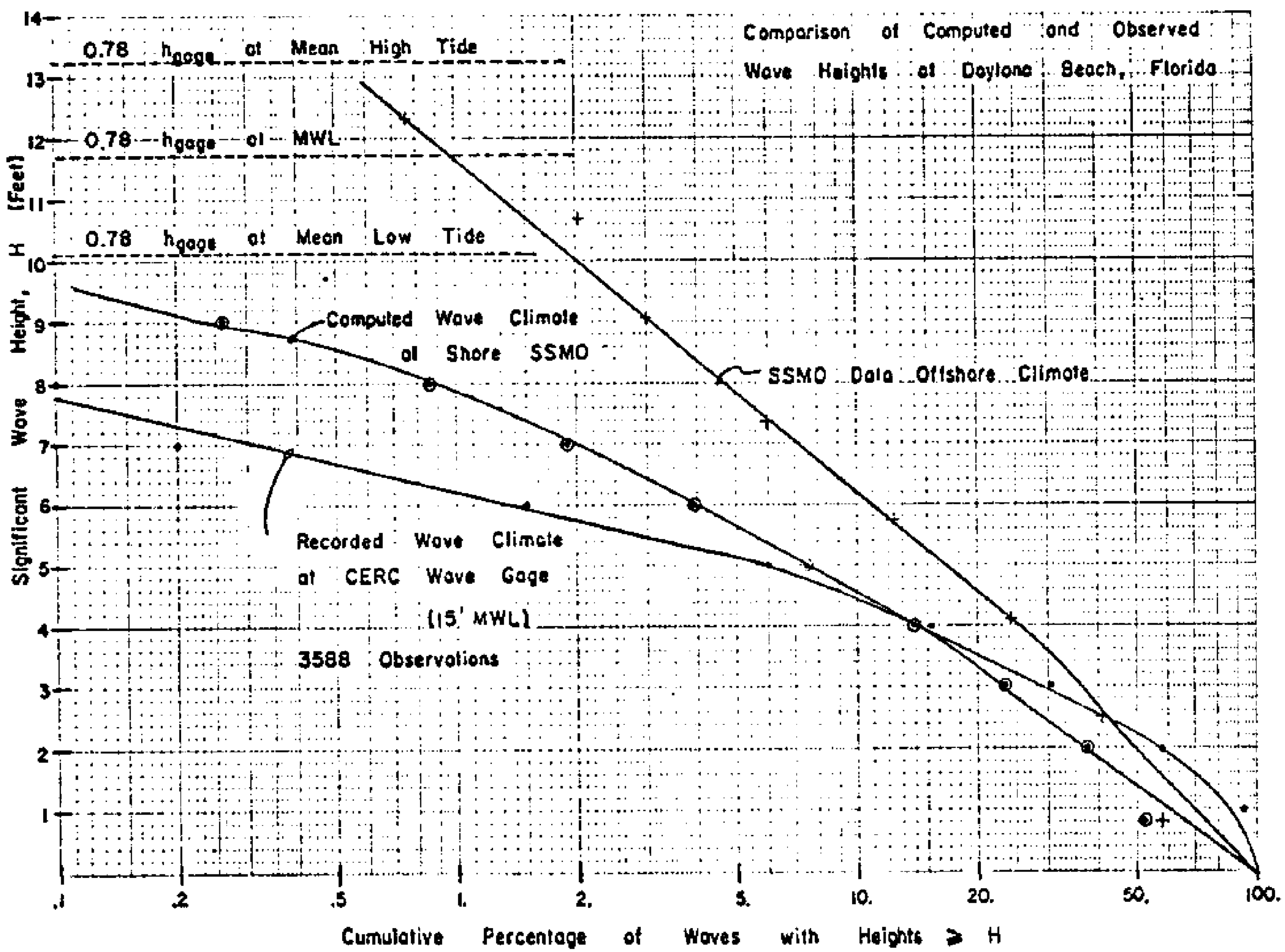

FIGURE 22. COMPARISON OF COMPUTED AND OBSERVED WAVE HEIGHTS AT DAYTONA BEACH, FLORIDA

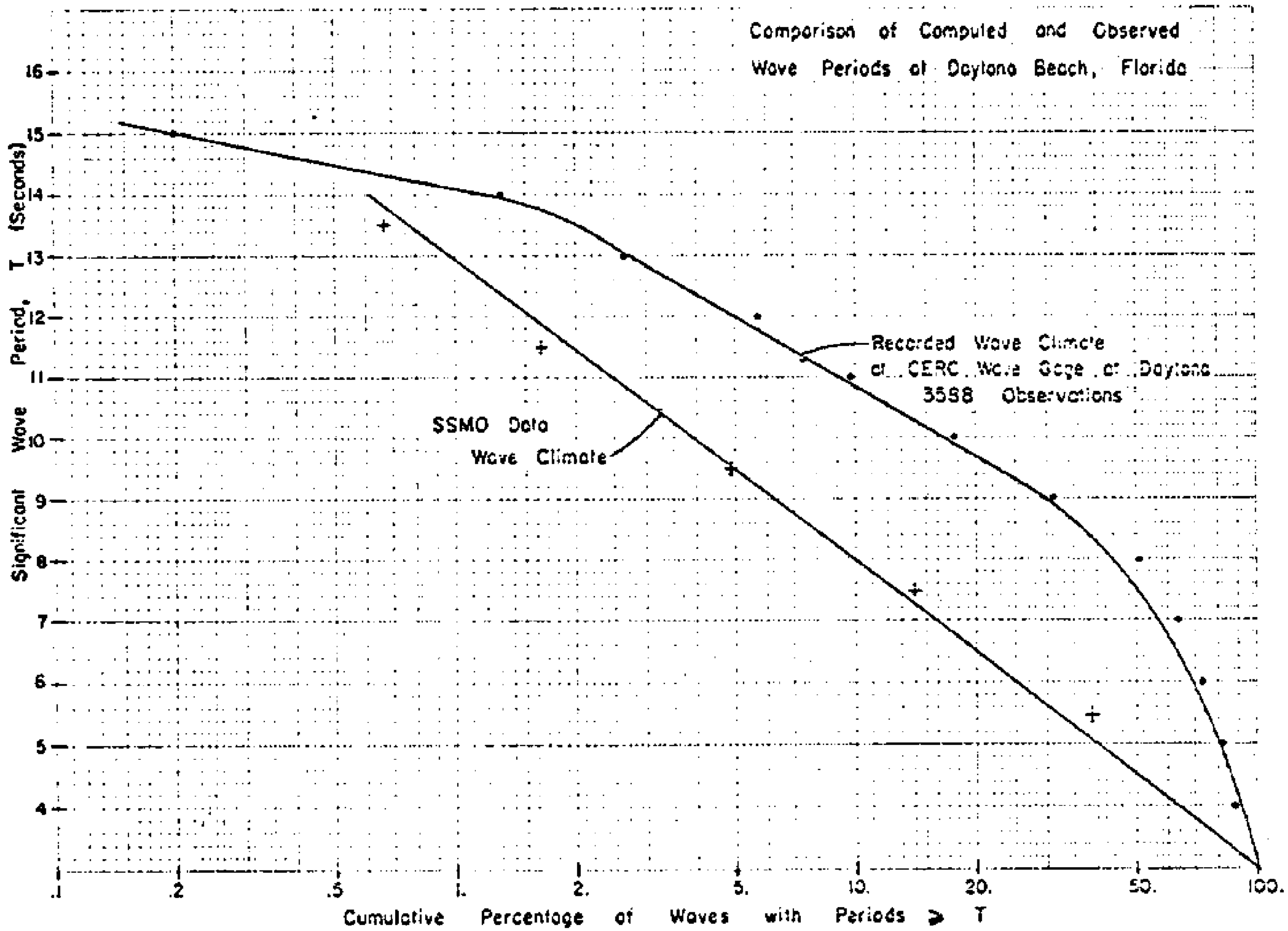

FIGURE 23. COMPARISON OF COMPUTED AND OBSERVED WAVE PERIODS AT DAYTONA BEACH, FLORIDA

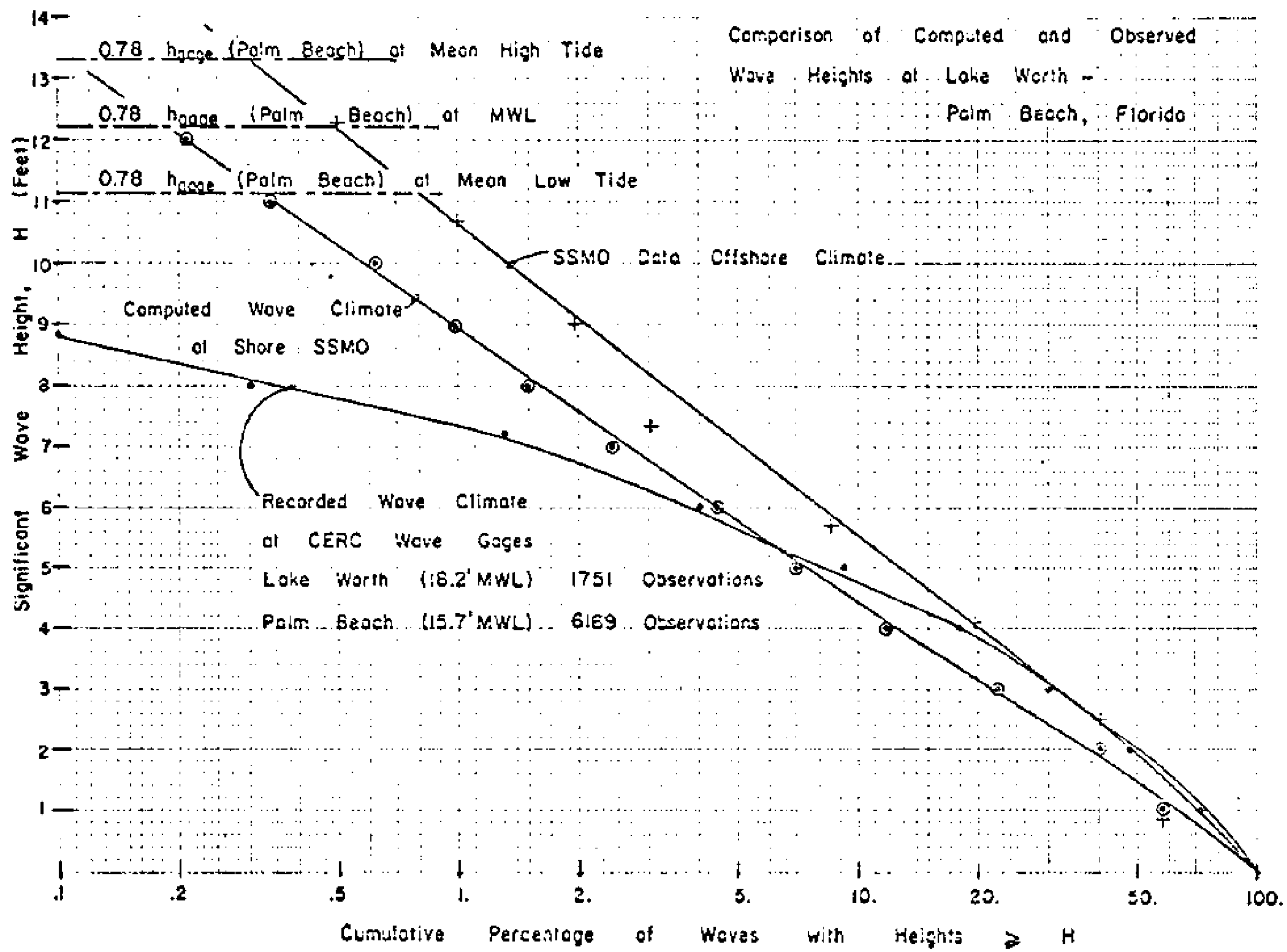

FIGURE 24. COMPARISON OF COMPUTED AND OBSERVED WAVE HEIGHTS AT LAKE WORTH - PALM BEACH, FLORIDA

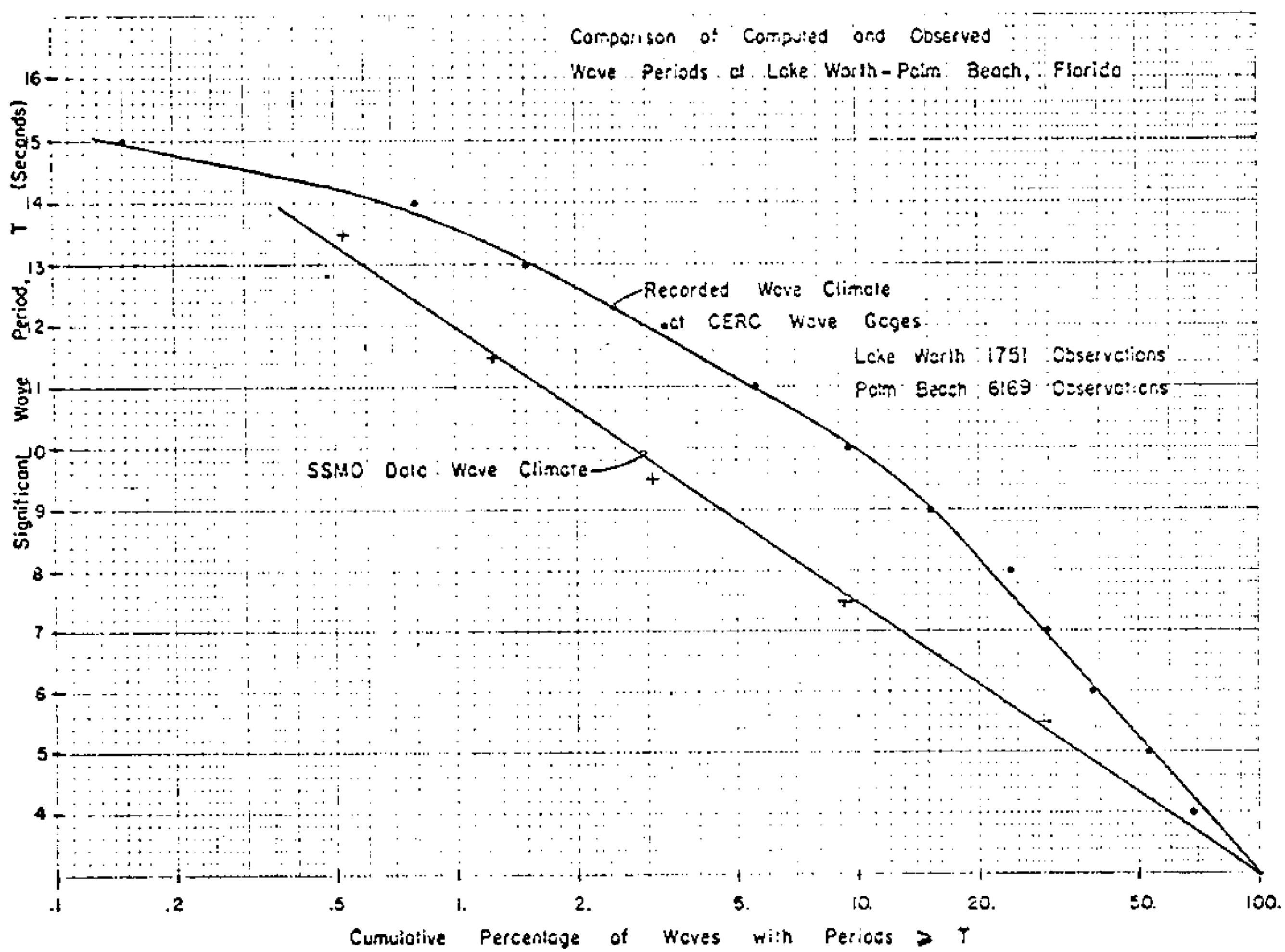

FIGURE 25. COMPARISON OF COMPUTED AND OBSERVED WAVE PERIODS AT LAKE WORTH - PALM BEACH, FLORIDA

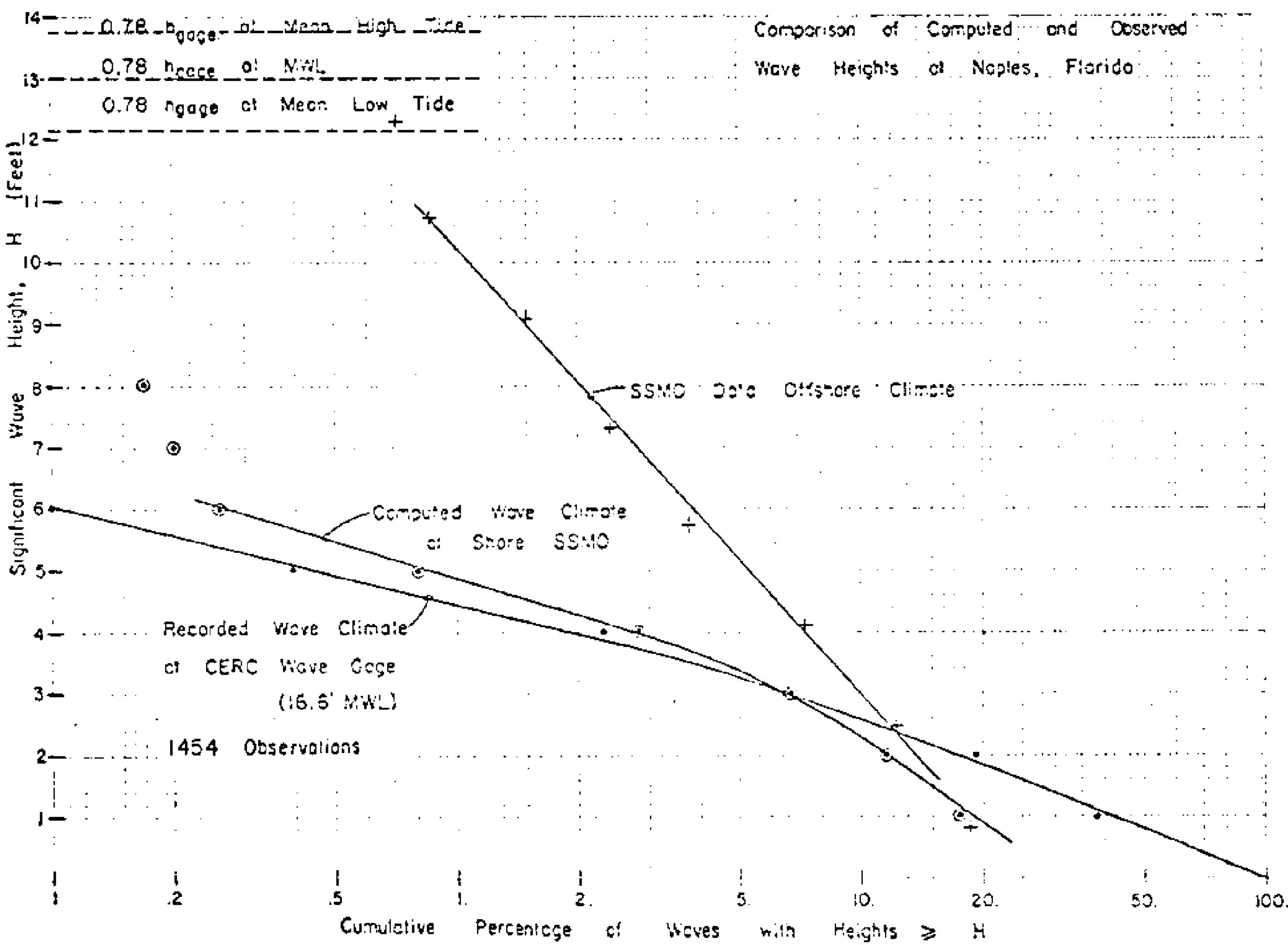

FIGURE 26. COMPARISON OF COMPUTED AND OBSERVED WAVE HEIGHTS AT NAPLES, FLORIDA

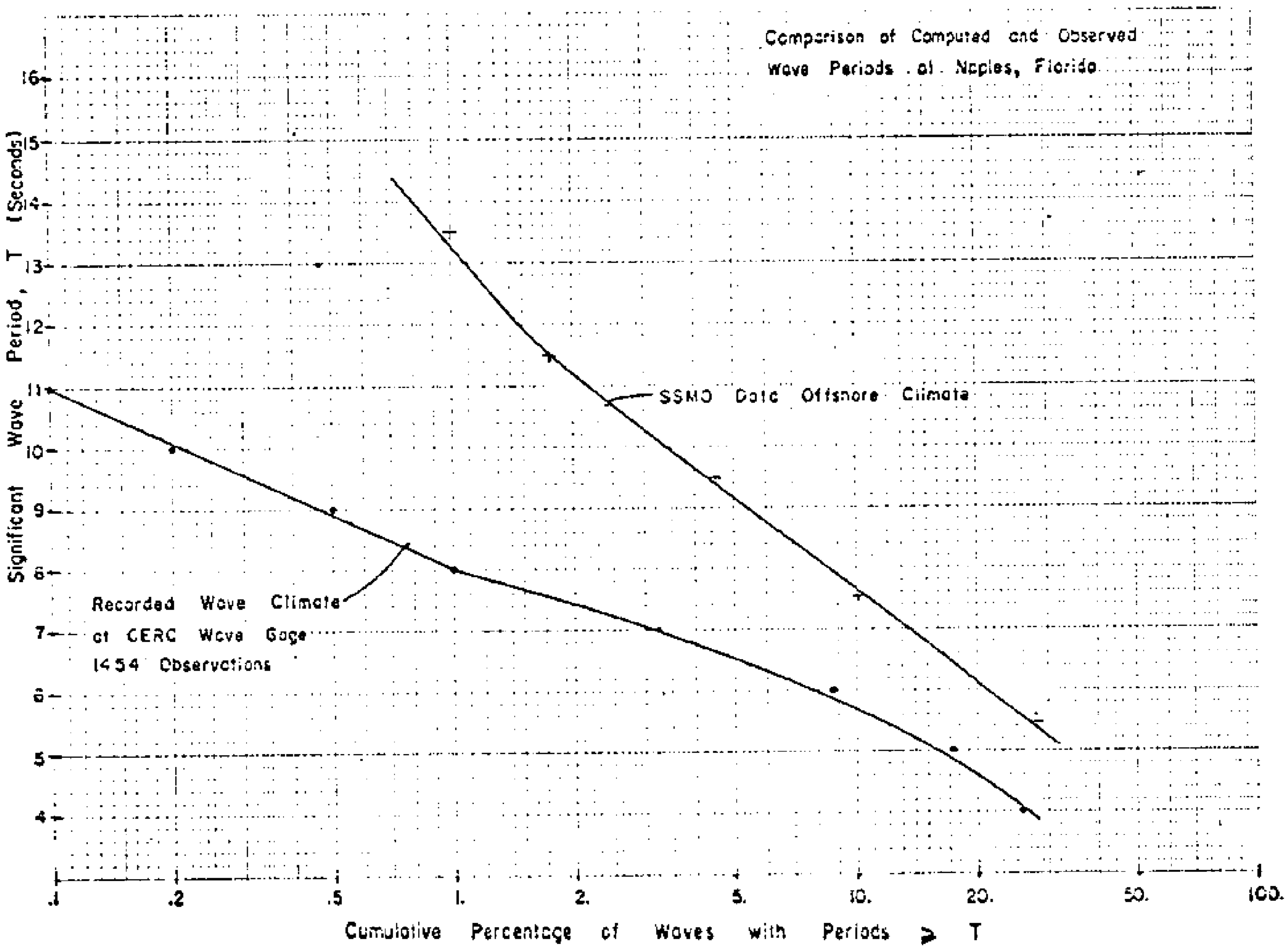

FIGURE 27. COMPARISON OF COMPUTED AND OBSERVED WAVE PERIODS AT NAPLES, FLORIDA

smooth curves drawn through them, one curve for the CERC gages, one curve for the deep water onshore wave climate as recorded by SSMO, and one curve for the SSMO wave climate as modified by the present study to the depth of the recording wave gage. Since it is assumed that periods are not modified by offshore topography, two curves are shown on the wave period cumulative distribution curves, one for CERC recorded wave climate, and one for SSMO recorded wave climate with inherent assumptions.

The curves show that wave heights of the higher energy waves are represented well by the modified SSMO data. Unfortunately though, periods are poorly defined by the data source. These findings are similar to other research efforts using this data source (see Reference [25]). Due to the large dependence of wave modification on wave periods, it is felt that an even closer correspondence to offshore observations might be obtained with improved period observations.

CHAPTER V

CONCLUSIONS

A method has been presented for computation of littoral drift along coastlines using existing ship wave observations as a data source. This method encompasses numerous assumptions which limit the final results to a beach with no significant anomalies in offshore topography.

The method was applied to portions of Florida's sandy shoreline, and results of drift calculations at many locations were compared to estimates of littoral drift by the U.S. Army Corps of Engineers. Except for a portion of the Southeast Florida Coast, the magnitudes of net drift computed are in reasonable agreement with previous estimates. Directions of net drift compare well in most cases although one notable exception occurs at East Pass on the Florida Panhandle. The cause of the extremely high values of computed drift in Southeast Florida is not known at this time although possible explanations have been mentioned. It is recommended that this study not be used for prediction of drift in the section of Florida south of Jupiter Inlet.

The simple analysis used is very powerful in that it can also be employed on a monthly basis to give the seasonal variation of drift in a specific area. Between Fort Pierce Inlet and St. Lucie Inlet, the orientation of the coast does not change appreciably and monthly averaged net littoral drift rates were computed for the average orientation of the shoreline and are shown in Figure 28 as an example of future possibilities for this type of analysis.

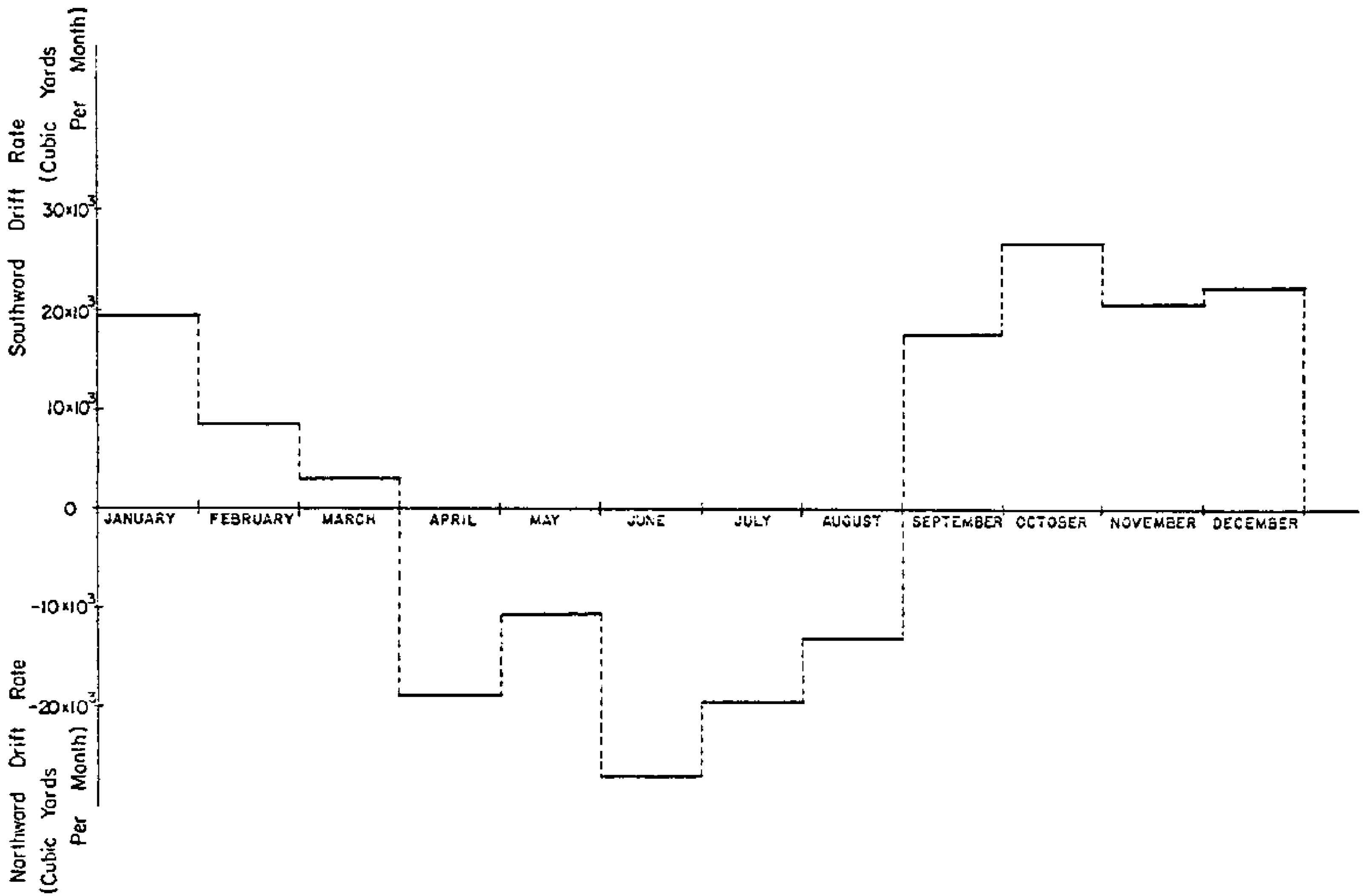

FIGURE 28. VARIATION OF NET LITTORAL DRIFT WITH SEASONAL WAVE CLIMATE BETWEEN FORT PIERCE INLET AND ST. LUCIE INLET

To substantiate the wave modifications used in this study, and to ascertain whether the data source observations are reasonable, a comparison was made of this modified (shore) wave climate predicted, and the wave climate measured by shore-based step resistance wave gages. The results showed that extreme wave heights compared well, but due to assumptions made in regard to "calms" in the data source, a reasonable comparison between the majority of smaller waves was impossible. Comparisons of wave periods indicated that the periods obtained from the ship data generally differed from those determined from the shore gage by two to three seconds.

If offshore topography is not appreciably different from ideal conditions, it is believed that littoral drift computations based on the results of this study should lead to more rational design standards and criteria for coastal works in Florida.

REFERENCES

1. U.S. Army Corps of Engineers, "National Shoreline Study, Regional Inventory Report; South Atlantic-Gulf Region," August 1971.

2. P. Bruun, W. H. Morgan, J. A. Purpura, "Review of Beach Erosion and Storm Tide Conditions in Florida 1961-1962," Technical Progress Report No. 13, University of Florida, November 1962.

3. P. Bruun, H. Skipnes, Tidal Inlets and Littoral Drift, Offsettrykkeri, Trondheim, Norway, 1966.

4. P. Bruun, "Sea Level Rise as a Cause of Shore Erosion," Proc. ASCE, Vol. 88, No. WW1, pp. 117-130.

5. U.S. Army Corps of Engineers, "Shore Protection Guidelines," Washington, 1971.

6. Estuary and Coastline Hydrodynamics, Chapters 1, 2, 3, and 9, edited by A. Ippen, McGraw-Hill, 1966.

7. D. L. Inman and J. D. Frautschy, "Littoral Processes and the Development of Shorelines," Santa Barbara Coastal Engineering Conference, October 1965.

8. J. C. Ingle, Jr., The Movement of Beach Sand, Elsevier Publishing Company, 1966.

9. V. P. Zenkovich, Processes of Coastal Development, John Wiley and Sons, New York, 1967.

10. P. D. Komar, "The Longshore Transport of Sand on Beaches," Ph.D. Thesis, University of California, 1969.

11. U.S. Army Corps of Engineers, "Shore Protection Planning and Design," Third Edition, Technical Report No. 4, Coastal Engineering Research Center, Washington, 1966.

12. J. M. Caldwell, "Wave Action and Sand Movement Near Anaheim Bay, California," Beach Erosion Board Technical Memorandum No. 68, Washington, 1956.

13. R. P. Savage, "Laboratory Study of the Effect of Groins on the Rate of Littoral Transport: Equipment Development and Initial Tests," Beach Erosion Board Technical Memorandum No. 114, Washington, 1959.

14. G. M. Watts, "A Study of Sand Movement at South Lake Worth Inlet, Florida," Beach Erosion Board Technical Memorandum No. 42, Washington, 1953.

15. M. G. Sauvage and M. G. Vincent, "Transport Littoral Formation de Fleches et de Tombolos," Proc. Fifth Conf. Coastal Engr., Grenoble, 1954.

16. Ning Chien, "Sediment Motion at the Vicinity of a Barrier," Wave Research Lab, Series 14, Issue 17, University of California, 1955.

17. T. Saville, Jr., "Scale Effects in Two Dimensional Beach Studies," Proc. Conf. IAHR, Lisbon, 1957.

18. W. C. Krumbein, "Shore Currents and Sand Movement on a Model Beach," Beach Erosion Board Technical Memorandum No. 7, Washington, 1944.

19. E. A. Shay and J. W. Johnson, "Model Studies on the Movement of Sand Transported by Wave Action Along a Straight Beach," Issue No. 7, Series 14, Inst. Eng. Res., University of California, 1951 (unpublished).

20. U.S. Army Corps of Engineers, "Correlation of Littoral Transport with Wave Climate Along the Shores of New York and New Jersey," Technical Memorandum No. 18, Washington, November 1966.

21. "Coastal Processes in the Vicinity of Cape Thompson, Alaska," Geologic Investigations in Support of Project Chariot in the Vicinity of Cape Thompson, Northwestern Alaska--Preliminary Report, U.S. Geological Survey Trace Elements Investigations Report 753.

22. M. M. Das, "Longshore Sediment Transport Rates: A Compilation of Data," U.S. Army Corps of Engineers, Coastal Engineering Research Center, Miscellaneous Paper No. 1-71, September, 1971.

23. U.S. Naval Weather Service Command, "Summary of Synoptic Meteorological Observations (SSMO) for North American Coastal Marine Areas," Vols. 4 and 5.

24. C. L. Bretschneider and R. O. Reid, "Modification of Wave Height Due to Bottom Friction, Percolation, and Refraction," Beach Erosion Board (CERC), U.S. Army Corps of Engineers, Technical Memorandum No. 45, 1954.

25. D. Lee Harris, "Characteristics of Wave Records in the Coastal Zone," to be published in "Advanced Seminar on Waves and Beaches," Academic Press, 1972.

26. M. A. Mason, "The Transformation of Waves in Shallow Water," Proceedings of the First Conference of Coastal Engineering, Chapter 3, Long Beach, California, 1950.

27. J. A. Putnam and J. W. Johnson, "The Dissipation of Wave Energy by Bottom Friction," Trans. Amer. Geophys. Union, Vol. 30, No. 1, February 1949.

28. J. A. Putnam, "Loss of Wave Energy Due to Percolation in a Permeable Sea Bottom," Trans. Amer. Geophys. Union, Vol. 30, No. 3, June 1949.

29. E. P. Meisburger and D. B. Duane, "Geomorphology and Sediments of the Inner Continental Shelf--Palm Beach to Cape Kennedy, Florida," Technical Memorandum No. 34, Coastal Engineering Research Center, Washington, 1971.

ADDITIONAL REFERENCES

1. E. B. Thornton, "Longshore Current and Sediment Transport," Ph.D. Thesis, Technical Report No. 5, Dept. of Coastal and Oceanographic Engr., University of Florida, December 1969.

2. F. D. Shepard and H. K. Wanless, Our Changing Coastlines, McGraw-Hill, 1970.

APPENDICES

APPENDIX I

DERIVATION OF THE LONGSHORE ENERGY FLUX EQUATION

The purpose of this appendix is to develop a relationship for the longshore component of energy flux in terms of the deep water wave parameters. As before, this relationship is strictly valid only for bathymetry represented by straight and parallel bottom contours (see Figure I-1).

Consider a wave system propagating from deep water to shallow water along the rays (paths) shown in Figure I-1. By definition, there is no flux of energy normal to the rays; conservation of energy therefore requires that, on the average, the energy flux past Station 1 must be equal to the sum of the energy flux past Station 2 and the energy losses between Stations 1 and 2,

Energy flux past Station 1 = Energy flux past Station 2
+ Energy losses between Stations 1 and 2

The energy flux for a ray separation of $\Delta \ell$ can be expressed in terms of the product of the energy density E and the group velocity, Cg; i.e.,

$$\text{Energy flux} = E\ Cg \cdot \Delta \ell \qquad \text{(I-1)}$$

where, for small amplitude wave theory, the energy density E and group velocity Cg are:

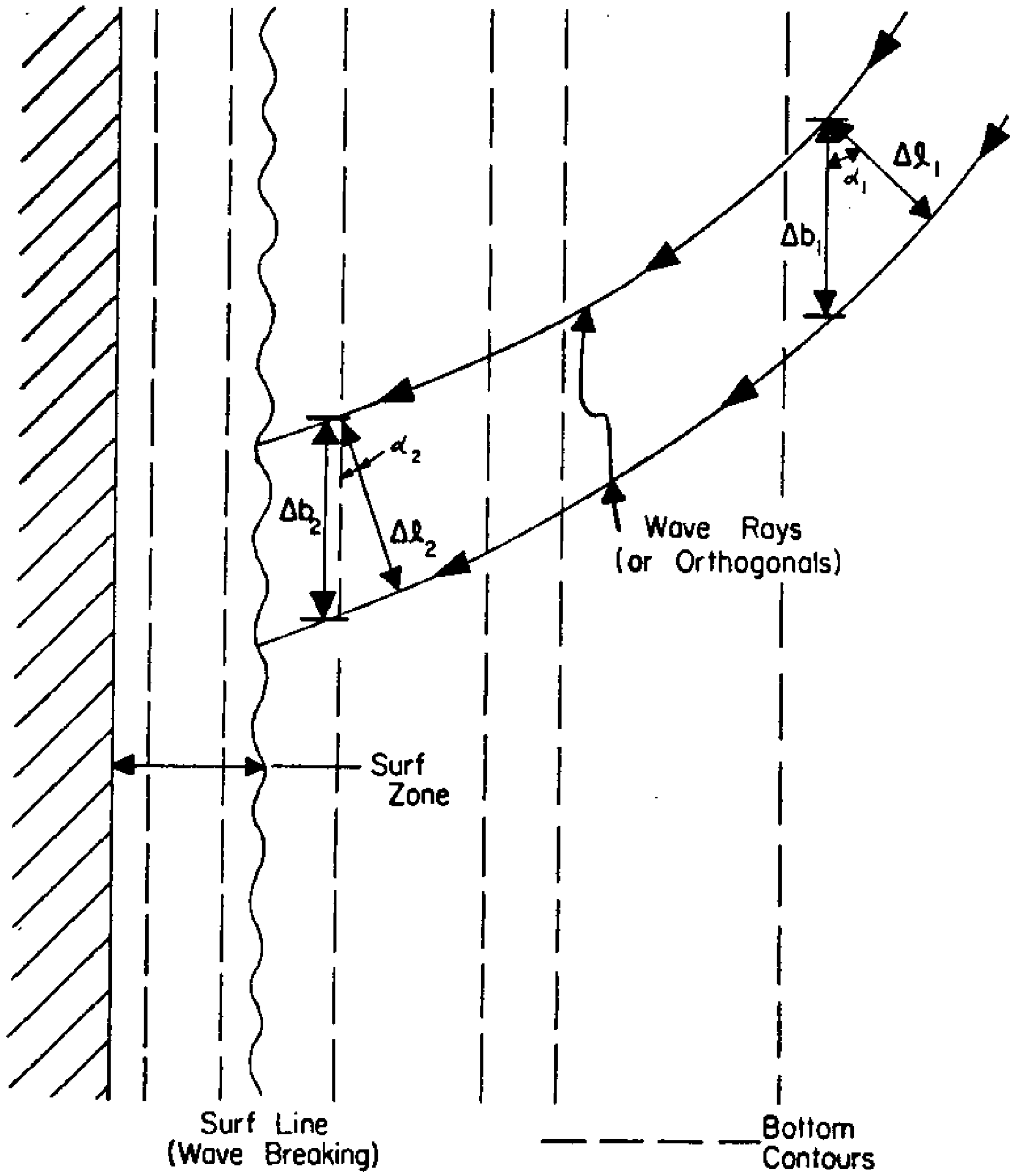

FIGURE I-1. PARAMETER DESCRIBING PROPAGATION OF WAVES FROM DEEP TO SHALLOW WATER

$$E = \frac{\gamma H^2}{8} \frac{\text{ft.-lbs.}}{\text{ft}^2} \tag{I-2}$$

$$Cg = nC = \frac{C}{2}\left[1 + \frac{2Kh}{\sinh\ 2Kh}\right] \frac{\text{ft.}}{\text{sec.}} \tag{I-3}$$

with H = wave height, feet

γ = specific weight at seawater, lbs./ft^3

C = wave celerity = $\frac{L}{T}$, feet/second

K = wave number, $\frac{2\pi}{L}$, (ft)$^{-1}$

h = depth of water below mean sea level

Reference to Figure I-1 will show that between any two adjacent rays, Δb is uniform and also that

$$\Delta \ell = \Delta b \cos \alpha \tag{I-4}$$

where the length Δb is oriented parallel to the bottom contours.

The energy flux is a vector quantity; at any location the onshore and longshore components of energy flux between adjacent wave rays per foot of beach length are given by

$$\text{Onshore Component of Energy Flux} = E\ Cg\ \Delta b \cos^2 \alpha \tag{I-5}$$

$$\text{Longshore Component of Energy Flux} = E\ Cg\ \Delta b \cos \alpha \sin \alpha \tag{I-6}$$

At any location, the wave height, H, is related to the wave height, H_o, in deep water by

$$H = H_o\ K_r\ K_s\ K_{fp} \tag{I-7}$$

where K_s = linear shoaling coefficient = $\left(\frac{n_o C_o}{nC}\right)^{1/2}$, with $n_o = 1/2$

K_r = refraction coefficient

K_{fp} = friction-percolation coefficient, a reduction factor accounting for the energy losses due to bottom friction and percolation occurring between deep water and the location of interest.

Because sand transport occurs primarily within the surf zone, the energy flux into the surf zone and the (breaking) conditions at the surf line are of primary interest. From Equation (I-6), the longshore energy flux per unit beach length at the surf line is

$$E_a = \frac{\gamma H_b^2}{8} Cg_b \sin \alpha_b \cos \alpha_b \tag{I-8}$$

which can be expressed in terms of deep water conditions as:

$$E_a = \frac{\gamma H_o^2}{8} (K_r\ K_s\ K_{fp})_b^2\ Cg_b \sin \alpha_b \cos \alpha_b \tag{I-9}$$

According to linear theory,

$$K_{s_b} = \sqrt{\frac{Cg_o}{Cg_b}} \tag{I-10}$$

$$K_{r_b} = \sqrt{\frac{\cos \alpha_o}{\cos \alpha_b}} \tag{I-11}$$

and

$$Cg_o = \frac{1}{2} \frac{Lo}{T} \tag{I-12}$$

Equation (I-8) therefore becomes:

$$E_a = \left(\frac{\gamma H_o^2}{8}\right)\left(\frac{Lo}{2T}\right) K_{r_b}^2 \; K_{fp_b}^2 \; \sin\alpha_b \cos\alpha_b \; \frac{\text{ft - lbs}}{\text{sec}} \text{ per foot of beach} \qquad \text{(I-13)}$$

The form of Equation (I-13) that is recommended in the literature (see Reference [11]) is obtained by considering a one-day period and re-writing in terms of millions of ft-lbs of longshore energy per day per foot of beach as:

$$E_a = \frac{E_o^*}{2} \text{ (number of waves per day) } \sin\alpha_b \cos\alpha_b \; K_r^2 \; \frac{\text{ft - lbs}}{\text{day}} \text{ per foot of beach} \qquad \text{(I-14)}$$

in which $$E_o^* = \frac{\gamma H_o^2 L}{8}$$

and $$\text{(number of waves per day)} = \frac{24(3600)}{T}$$

It can be seen by comparing Equations (I-13) and (I-14), that the above equation embodies the assumption of $K_{fp} = 1$, i.e., no energy losses. This assumption can be considerably in error in coastal areas with broad shallow continental shelves.

By substitution of Equation (I-11) into Equation (I-13), another form of the longshore energy flux equation is derived as:

$$E_a = \left(\frac{\gamma H_o^2}{8}\right) Cg_o \cos\alpha_o \sin\alpha_b \; K_{fp_b}^2 \; \frac{\text{ft - lbs}}{\text{sec}} \text{ per foot of beach} \qquad \text{(I-15)}$$

or

$$E_a = \left(\frac{\gamma H_o^2}{8}\right) Cg_o \cos\alpha_o \sin\alpha_b \; K_{fp_b}^2 \; \frac{(24)(3600)}{106} \text{ million } \frac{\text{ft - lbs}}{\text{day}} \text{ per foot of beach} \qquad \text{(I-16)}$$

Note that in the above equations, the effects of bottom friction and percolation were retained. Equation (I-16) is the form of the longshore energy flux equation used in the computations of this report.

APPENDIX II

ANALYSIS OF SSMO WAVE HEIGHT, PERIOD, AND DIRECTION RANGES

The purpose of this appendix is to describe the manner in which the groupings of wave data listed in the SSMO volumes were handled for computations of longshore energy flux.

Wave Height

For the SSMO data, a representative value of H_o must be chosen for each interval of wave heights contained in SSMO Tables 18 and 19. Since energy is a function of wave height squared (in linear theory), a representative value of H_o for a given range of H_o values should be based on the mean square root value of the wave height over the range.

Consider the probability of occurrence of a wave with specific height H as equal to p(H) in the range H_1 to H_2. The energy represented in this band of wave heights is proportional to H_r^2 the mean value of a representative wave height squared where:

$$H_r^2 = \frac{\int_{H_1}^{H_2} p(H)\ H^2\ dH}{\int_{H_1}^{H_2} p(H)\ dH} \tag{II-1}$$

Since p(H) is not known, it is considered uniform, which is reasonable if the wave height range $H_1 < H < H_2$ is small. The equation then becomes:

$$H_r^2 = \frac{\int_{H_1}^{H_2} H^2 dH}{\int_{H_1}^{H_2} dH} = \frac{1(H_2^3 - H_1^3)}{3(H_2 - H_1)} \tag{II-2}$$

Taking the square root of this value,

$$H_r = \left[\frac{1(H_2^3 - H_1^3)}{3(H_2 - H_1)}\right]^{1/2} \tag{II-3}$$

Using Equation (II-3), representative values of H_o were found for the corresponding ranges of H_o given in SSMO data, and are summarized in Table II-1.

<u>Wave Period</u>

Representative values of T were assumed to be the average of the SSMO period ranges, and are given in Table II-2. For T > 13.5 seconds a representative value of T = 16 seconds was assumed.

<u>Wave Direction</u>

Directional observations as recorded in the SSMO volumes are given on eight points of the compass and thus correspond to eight 45° sectors of the compass. In the computation of the longshore energy flux, the midpoint of the sectors, as given in the SSMO data by the eight points of the compass, were used as the representative values of θ for direction of wave approach. When a representative wave having a given frequency was parallel to the coastline, the corresponding

TABLE II-1

REPRESENTATIVE VALUES OF WAVE HEIGHT USED IN COMPUTATION OF LONGSHORE ENERGY FLUX

SSMO Coded Height	Actual SSMO Range of Heights (feet)			Height Used in Computation (feet)
<1	0	$\leq H_{o1/3} <$	0.82	0.47
1-2	.82		2.46	1.71
3-4	2.46		4.10	3.31
5-6	4.10		5.74	4.94
7	5.74		7.38	6.58
8-9	7.38		9.04	8.22
10-11	9.04		10.70	9.85
12	10.70		12.30	11.49
13-16	12.30		15.60	13.98
17-19	15.60		18.90	17.25
20-22	18.90		22.15	20.53
23-25	22.15		22.43	23.81

TABLE II-2

REPRESENTATIVE VALUES OF WAVE PERIOD USED IN COMPUTATION OF LONGSHORE ENERGY FLUX

SSMO Coded Period	Actual SSMO Range of Periods			Period Used in Computation of Longshore Energy Flux
<6	0	$\leq T <$	5.5	3.0
6-7	5.5		7.5	6.5
8-9	7.5		9.5	8.5
10-11	9.5		11.5	10.5
12-13	11.5		13.5	12.5
>13	13.5		∞	16.

sector of waves was divided into two parts, one being deleted from the computation and the other approaching the coastline from the midpoint of its half sector with the corresponding frequency halved (see Figure II-1). Wave data in octants with midpoints in the offshore direction ($> \theta_n \pm 90°$) for a given coastline orientation have been deleted from the drift computations.

In the SSMO data it was ascertained that a considerable number of the original observations were taken on the 36 points of the compass, and, when reduced to the eight points of the compass in the SSMO tables, a skew of the wave direction was introduced. This skew amounts to a ten degree shift clockwise, and has been accounted for in the results of the littoral drift computations.

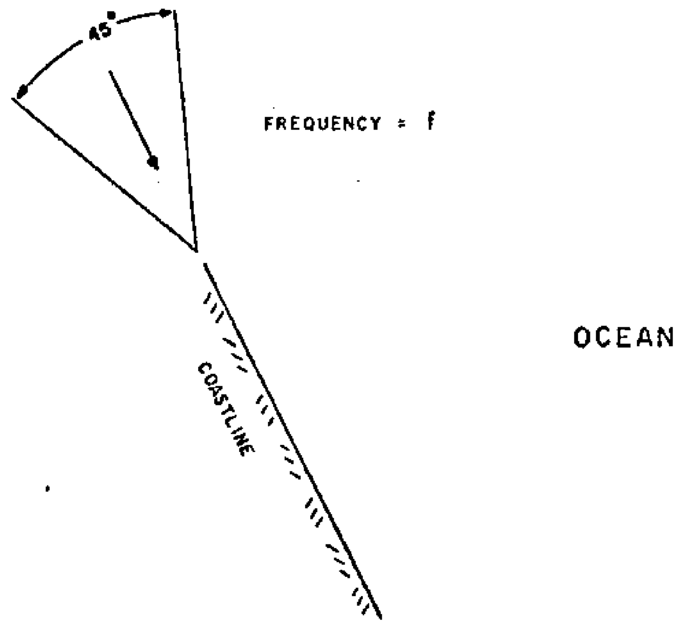

(a) Wave data before modification is converted to (b)

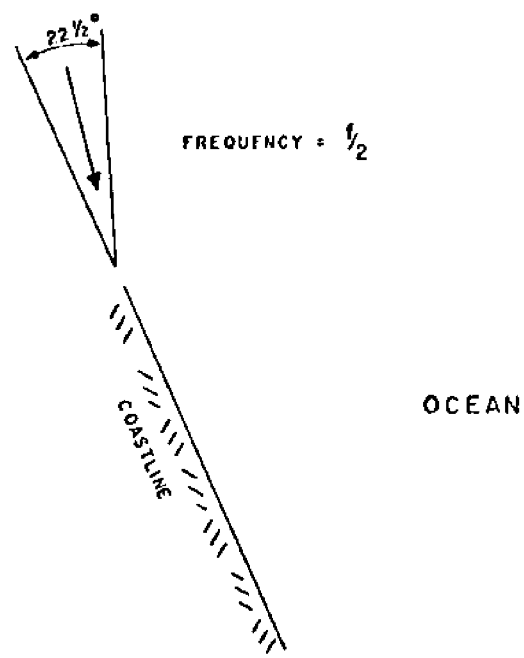

(b) Wave data after modification

FIGURE II-1. MODIFICATION OF WAVE DATA FOR WAVES PARALLEL TO COASTLINE

APPENDIX III

CALCULATION OF BREAKING WAVE HEIGHT, DEPTH, AND BREAKING ANGLE

This appendix presents the basis for calculating the breaking wave height and depth of breaking, by either linear or solitary wave theory. Also, the method for calculation of breaking wave angle necessary for computation of longshore energy flux is given.

The major factor in determining the breaking characteristics of a wave is the deep water wave steepness, equal to $\frac{H_o}{L_o}$ (or if refraction is considered $\frac{H'_o}{L_o}$). In the present analysis a judgement was made as to whether the waves break according to linear or solitary theory (see Figure 10, Page 30, Reference [26]) depending on whether $\frac{H'_o}{L_o}$ is greater than or less than the value 0.02.

Breaking According to Linear Theory

Iverson has shown that if $\frac{H'_o}{L_o} > 0.02$, a linear wave theory approximation to breaking depth is most reasonable. In this approach $H_b = H_o K_s K_r K_{fp}$ from linear wave theory where K_{fp}, K_r and K_s are the friction-percolation, refraction, and shoaling coefficients, respectively. Assuming K_r and K_{fp} are not further altered beyond a depth h_s, then $H_b = H'_o K_s$ where $H'_o = H_o K_r K_{fp}$ at the depth h_s (assumed 10 feet). Making the shallow water approximation:

$$K_s = \left(\frac{Kh}{K_o h}\right)^{1/2} (2)^{-1/2} \qquad \text{(III-1)}$$

and

$$\left(\frac{Kh}{K_o h}\right) = \frac{1}{\tanh Kh} \cong \frac{1}{Kh} \qquad \text{(III-2)}$$

Then,

$$K_o h = (Kh)^2 \qquad \text{(III-3)}$$

and

$$K_s \cong \frac{1}{(K_o h)^{1/4} \ (2)^{1/2}} \qquad \text{(III-4)}$$

At breaking,

$$h_b = 1.28 \ H_b \qquad \text{(III-5)}$$

and on substitution of this relationship into Equation (III-4), the following relationship is obtained:

$$K_s \cong \frac{1}{(2)^{1/2}(1.28)^{1/4}(K_o)^{1/4}(H_b)^{1/4}} \qquad \text{(III-6)}$$

Recalling that $H_b \cong H_o' K_s$ at breaking, the following equation for breaking height is found:

$$H_b = 0.692 \ H_o'^{4/5} \ T^{2/5} \qquad \text{(III-7)}$$

with H_o' and H_b in feet and T in seconds. Values of $\frac{H_b}{H_o'}$ versus $\frac{H_o'}{L_o}$ are plotted on Figure III-1 (from Reference [11]) which shows good correlation between this approximation and other theoretical and empirical formulas.

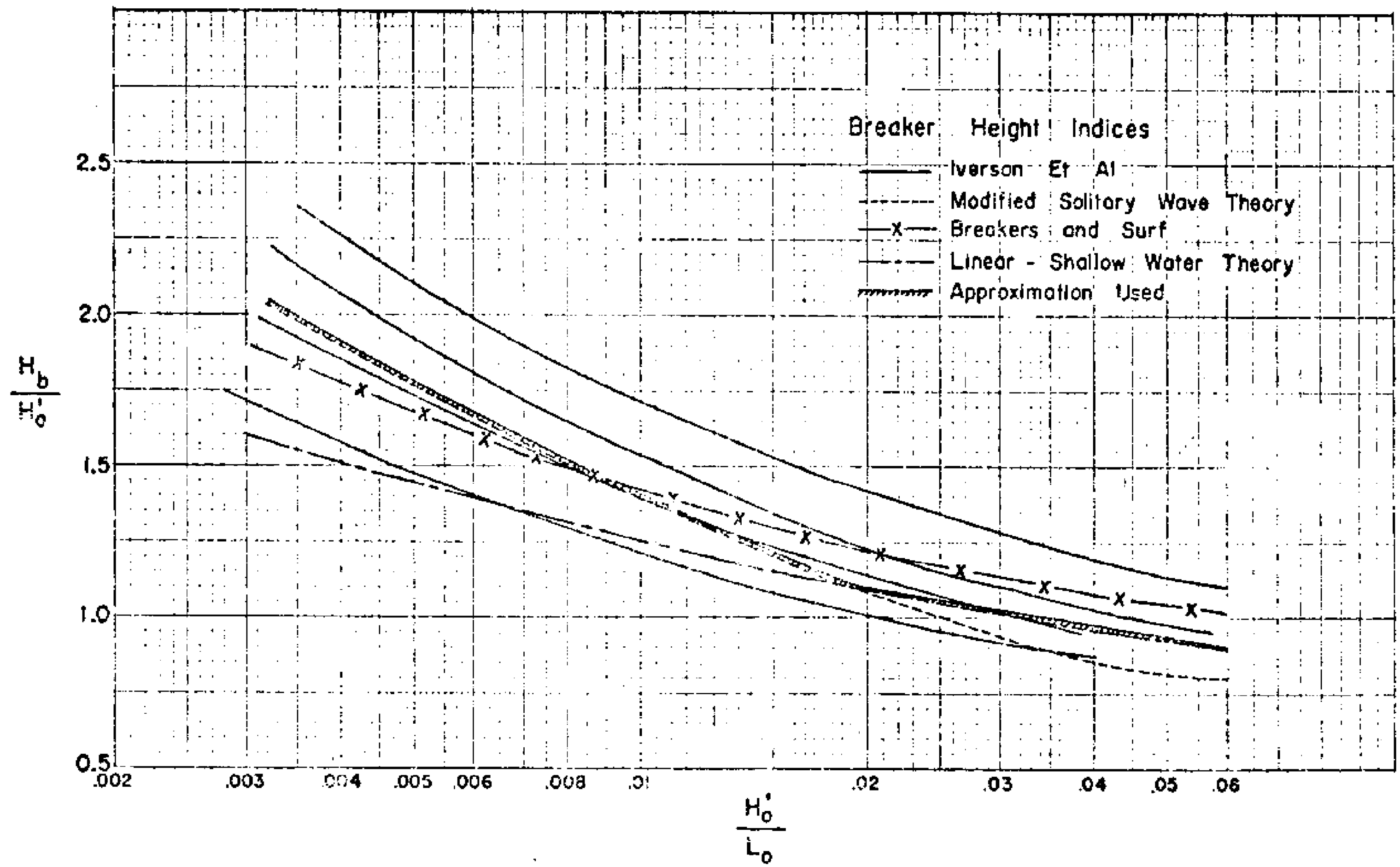

FIGURE III - 1. APPROXIMATION FOR BREAKER HEIGHT (FROM REFERENCE [11])

Using linear wave theory with the shallow water approximation, and a breaking criterion $h_b = 1.28\ H_b$, the sin α_b term becomes:

$$\sin \alpha_b = \left(\frac{C_b}{C_o}\right) \sin \alpha_o \qquad \text{(III-8)}$$

where $$C_b = (gh_b)^{1/2} = (1.28\ gH_b)^{1/2} \qquad \text{(III-9)}$$

$$C_o = 5.12T$$

$$\alpha_o = \text{deep water wave angle}$$

Breaking According to Solitary Theory

For $\frac{H_o'}{L_o} \leq 0.02$, solitary wave theory was used. The equation for breaking waves is given by Equation (1-34) in Reference [11].

$$H_b = \frac{H_o'}{3.3(H_o'/L_o)^{1/3}} \qquad \text{(III-10)}$$

The relationship between this equation and results of other studies can also be seen in Figure III-1. The term sin α_b is again calculated from Snell's law with C_b being the solitary wave celerity:

$$C_b = [g(h_b + H_b)]^{1/2} \qquad \text{(III-11)}$$

$$C_b = [g(2.28\ H_b)]^{1/2} \qquad \text{(III-12)}$$

where again Snell's law of refraction states

$$\sin \alpha_b = \left(\frac{C_b}{C_o}\right) \sin \alpha_o \qquad \text{(III-8)}$$

Figures A1 Through A50

Average Annual Net and Average Annual Total Littoral Drift

Diagrams Along the Florida Peninsula

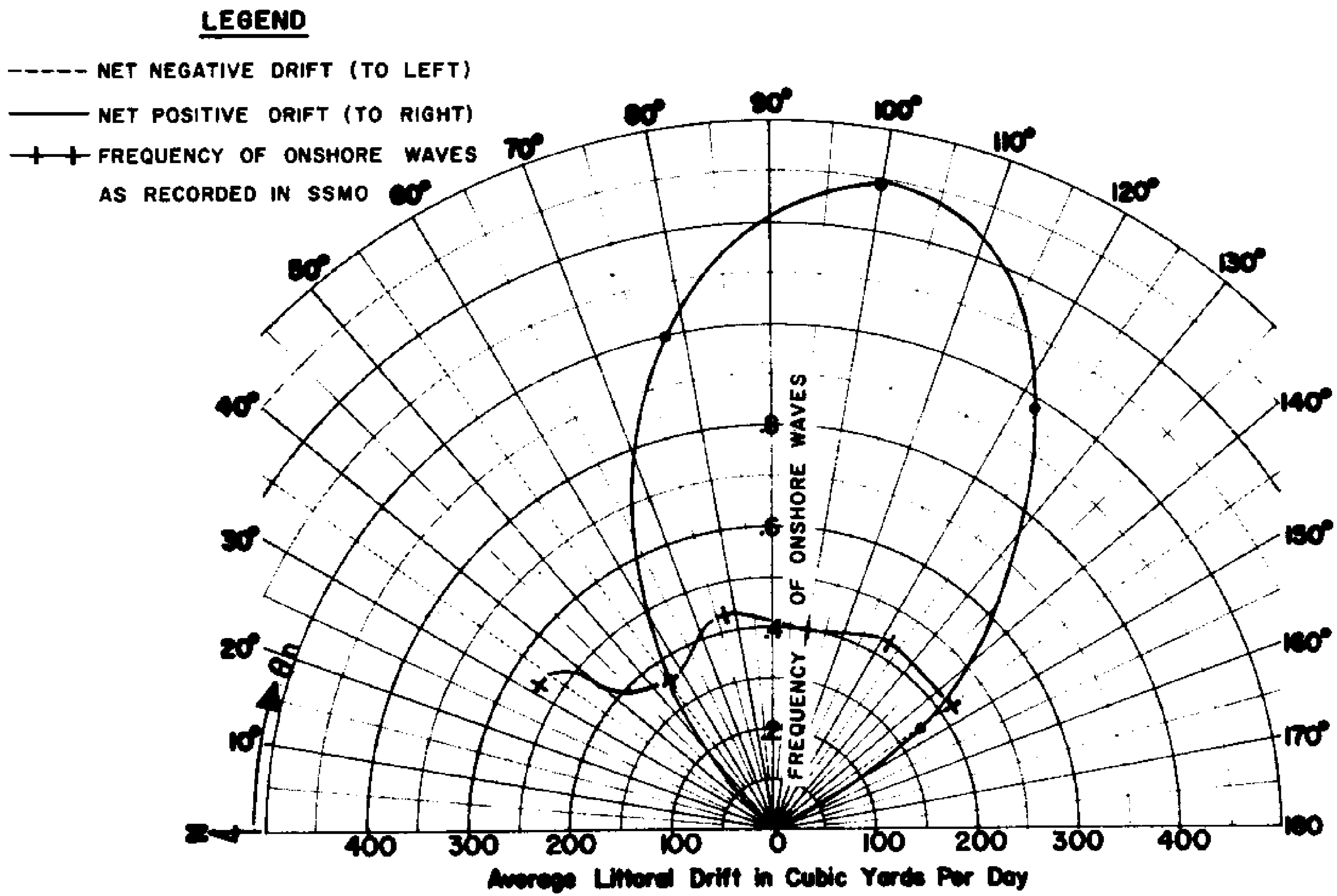

FIGURE A1. VARIATION OF AVERAGE ANNUAL NET LITTORAL DRIFT WITH BEACH ORIENTATION - FERNANDINA BEACH TO ST. JOHN'S RIVER, FLORIDA

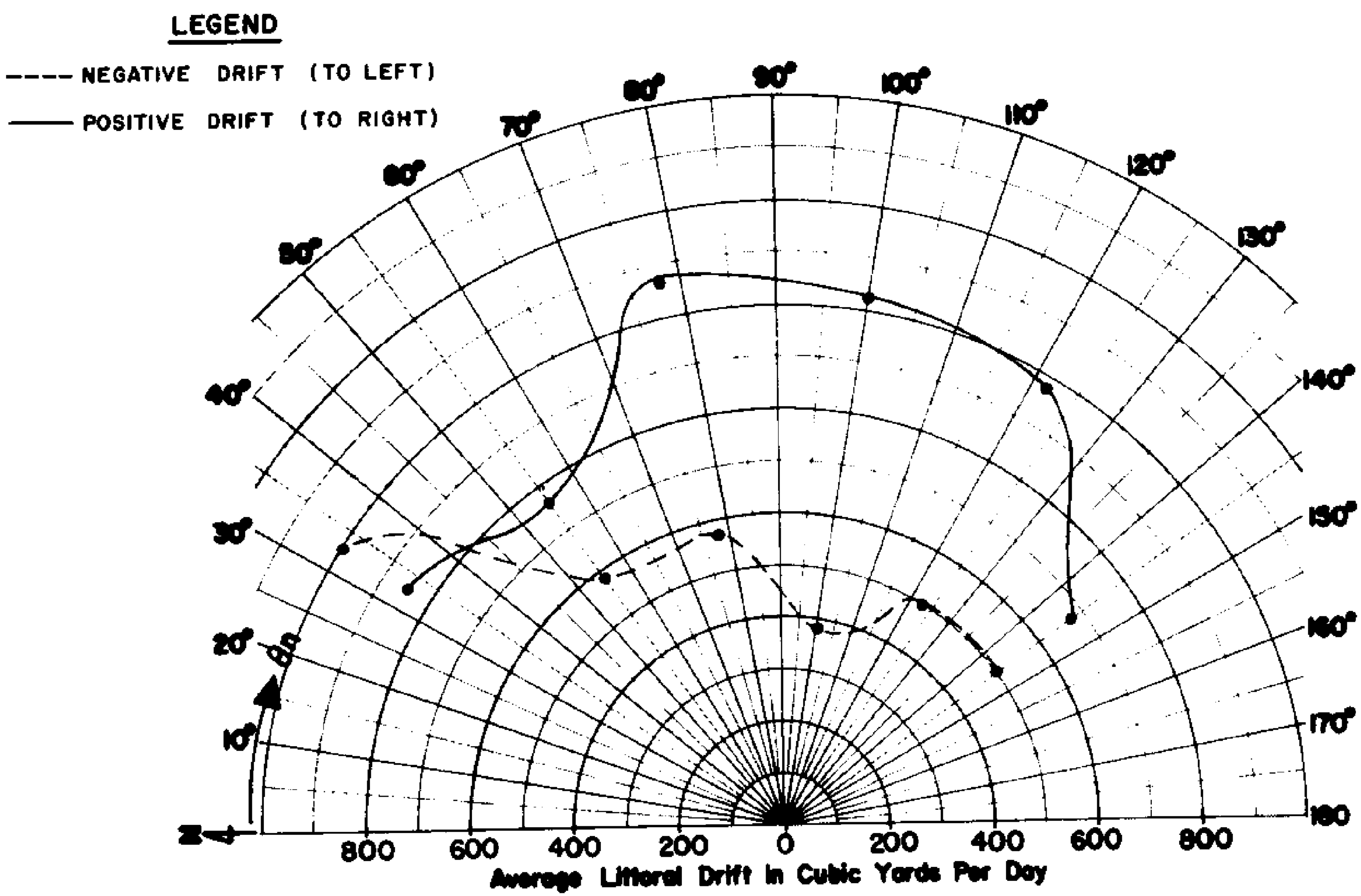

FIGURE A2. VARIATION OF AVERAGE ANNUAL TOTAL LITTORAL DRIFT WITH BEACH ORIENTATION - FERNANDINA BEACH TO ST. JOHN'S RIVER, FLORIDA

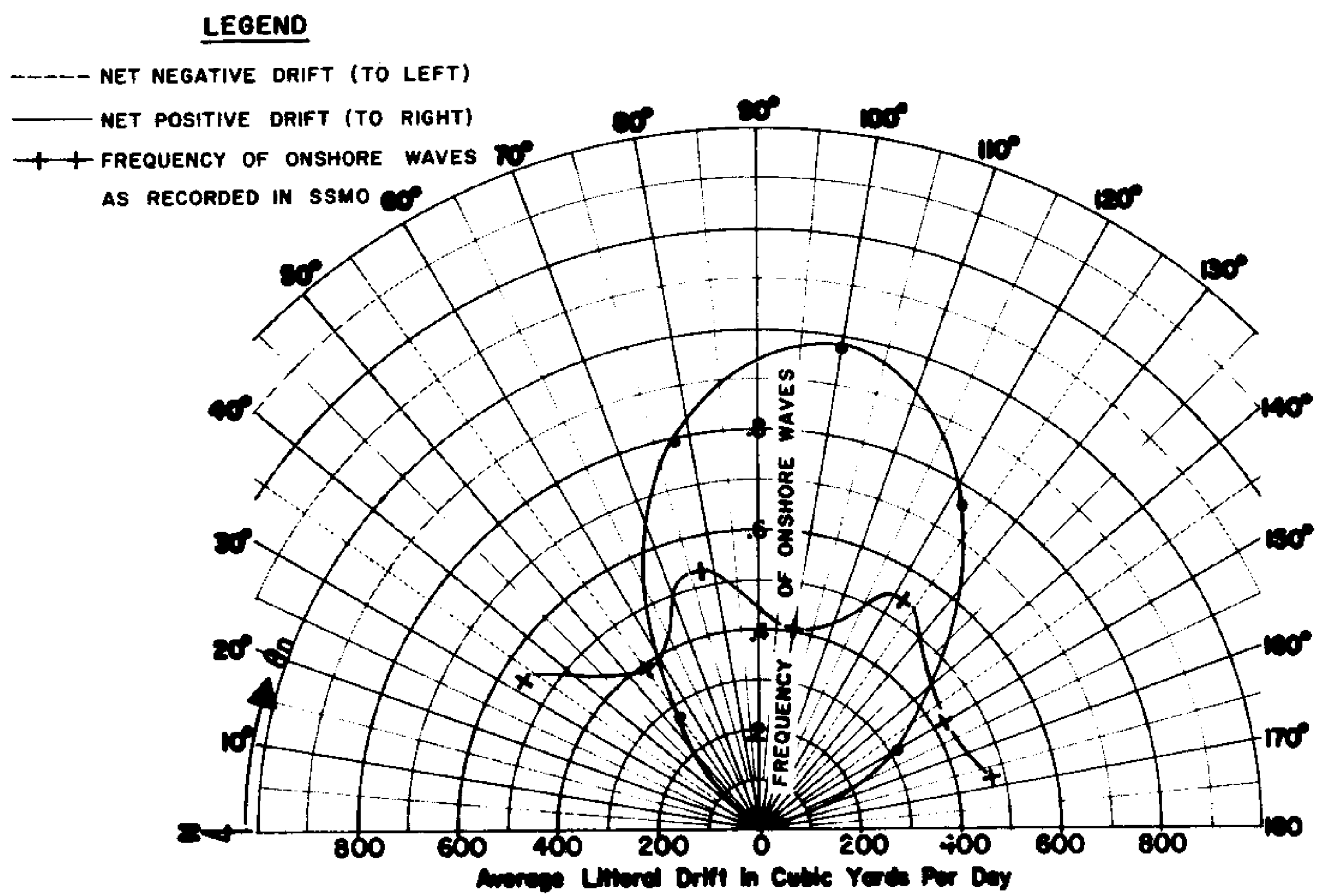

FIGURE A3. VARIATION OF AVERAGE ANNUAL NET LITTORAL DRIFT WITH BEACH ORIENTATION - ST. JOHN'S RIVER TO ST. AUGUSTINE INLET, FLORIDA

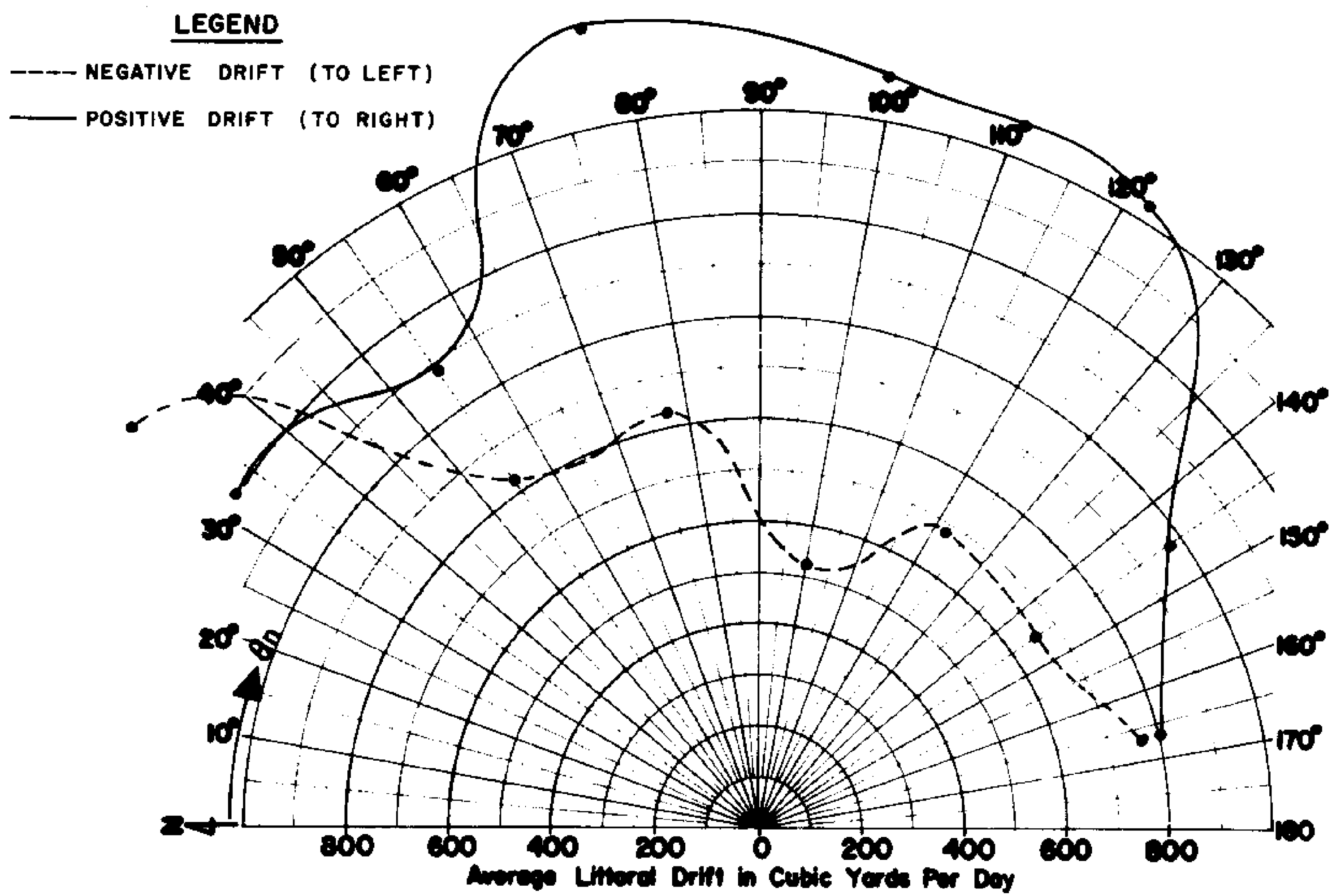

FIGURE A4. VARIATION OF AVERAGE ANNUAL TOTAL LITTORAL DRIFT WITH BEACH ORIENTATION - ST. JOHN'S RIVER TO ST. AUGUSTINE INLET, FLORIDA

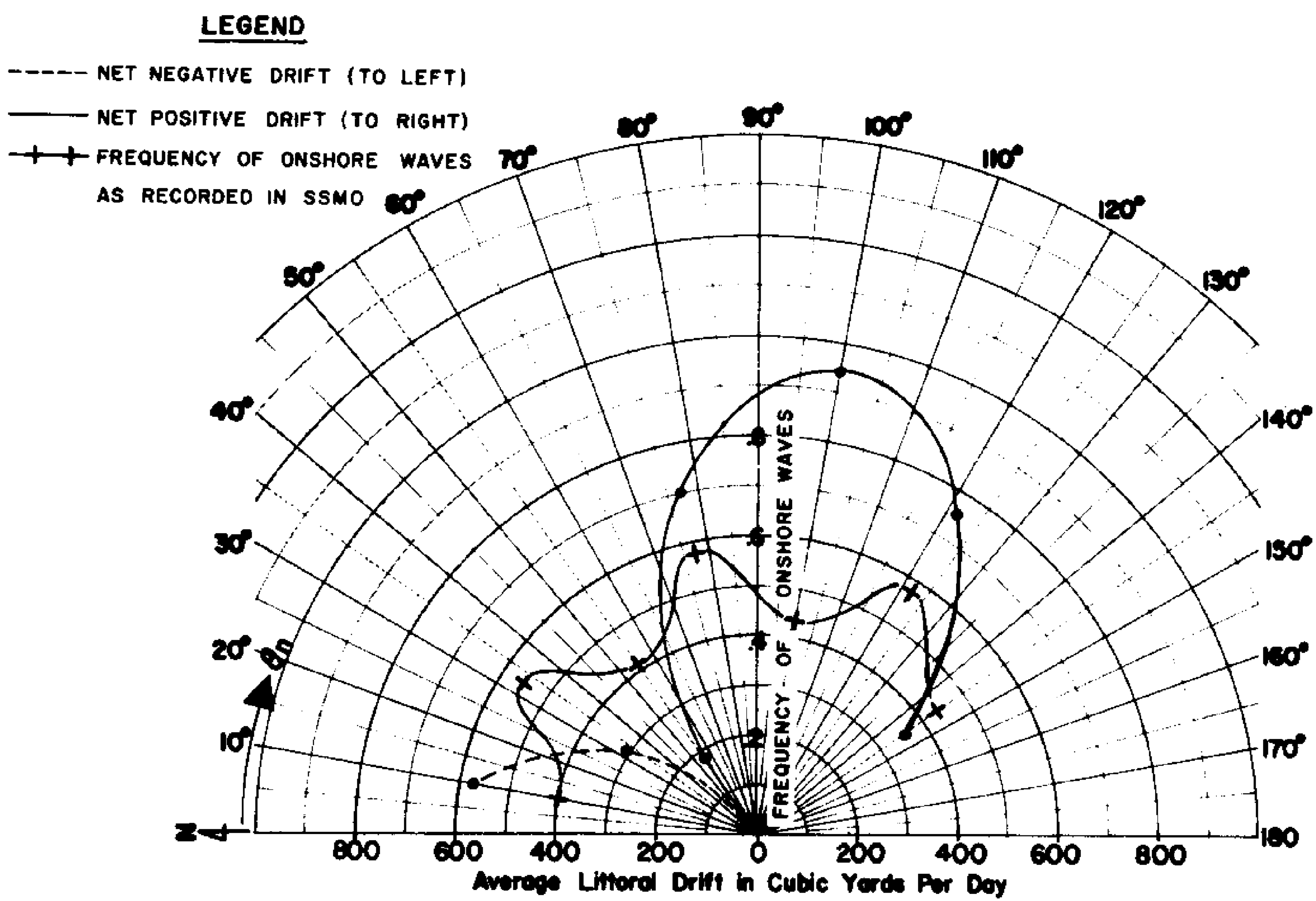

FIGURE A5. VARIATION OF AVERAGE ANNUAL NET LITTORAL DRIFT WITH BEACH ORIENTATION - ST. AUGUSTINE INLET TO PONCE DE LEON INLET, FLORIDA

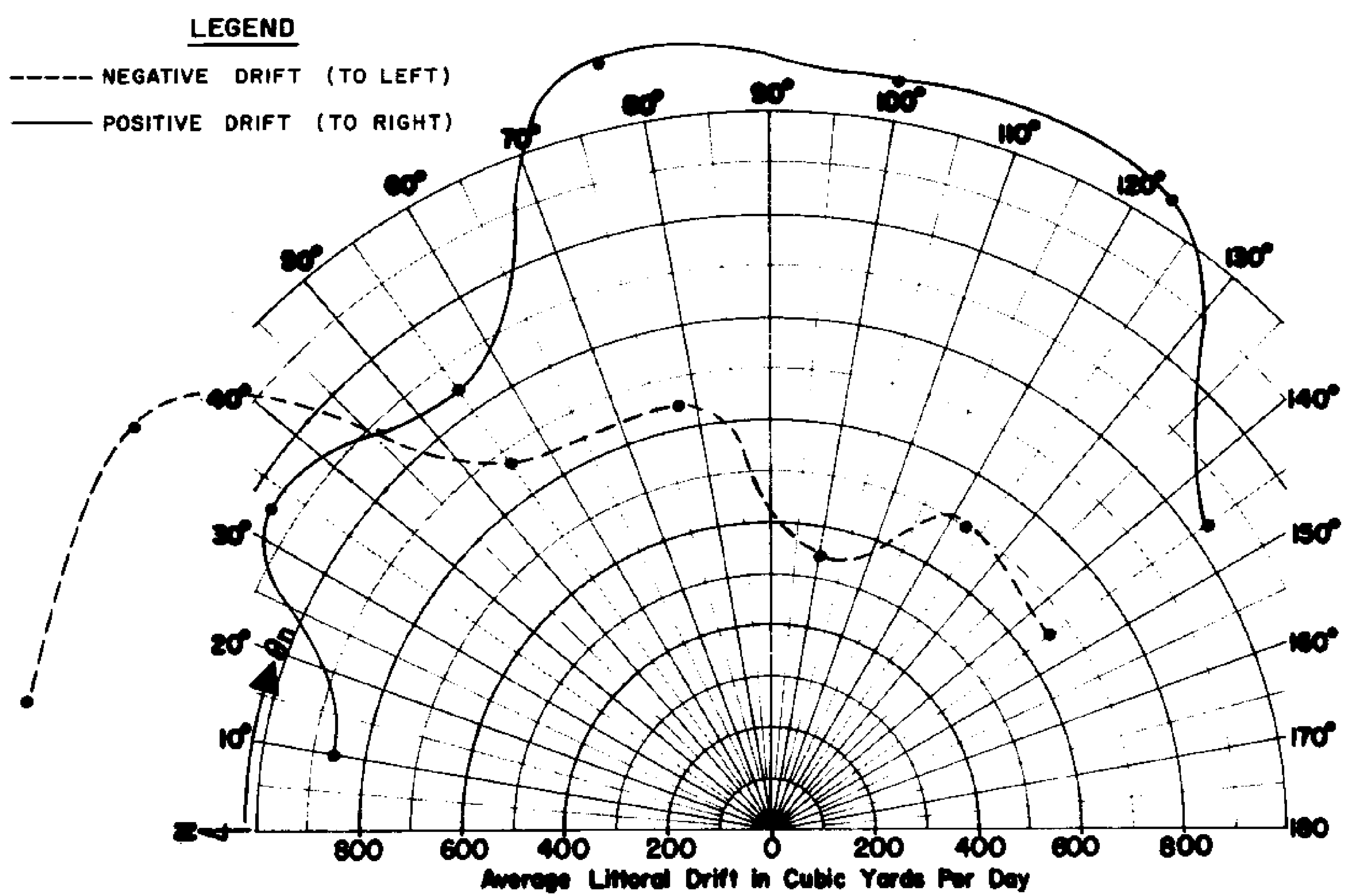

FIGURE A6. VARIATION OF AVERAGE ANNUAL TOTAL LITTORAL DRIFT WITH BEACH ORIENTATION - ST. AUGUSTINE INLET TO PONCE DE LEON INLET, FLORIDA

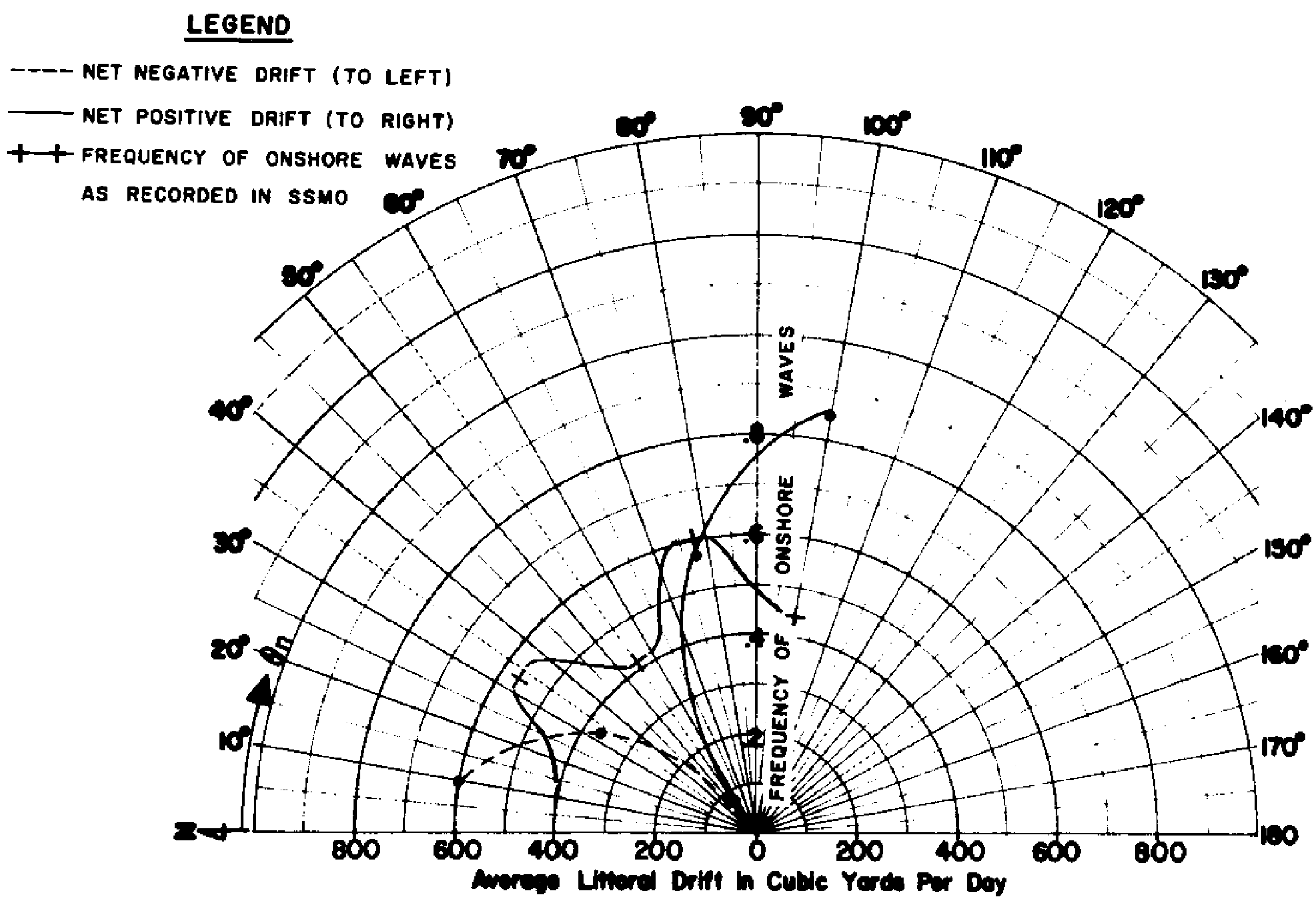

FIGURE A7. VARIATION OF AVERAGE ANNUAL NET LITTORAL DRIFT WITH BEACH ORIENTATION - PONCE DE LEON INLET TO CAPE KENNEDY, FLORIDA

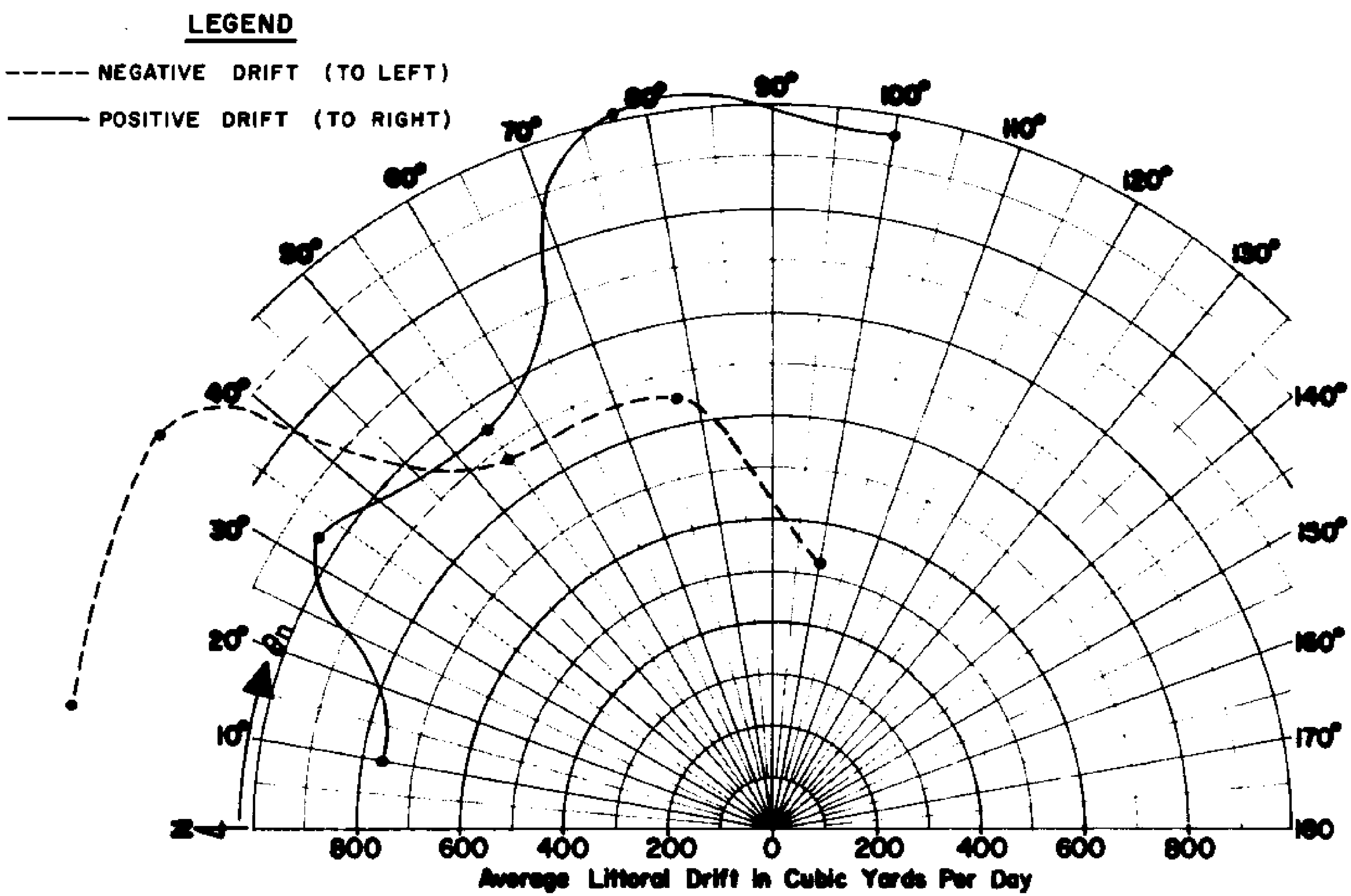

FIGURE A8. VARIATION OF AVERAGE ANNUAL TOTAL LITTORAL DRIFT WITH BEACH ORIENTATION - PONCE DE LEON INLET TO CAPE KENNEDY, FLORIDA

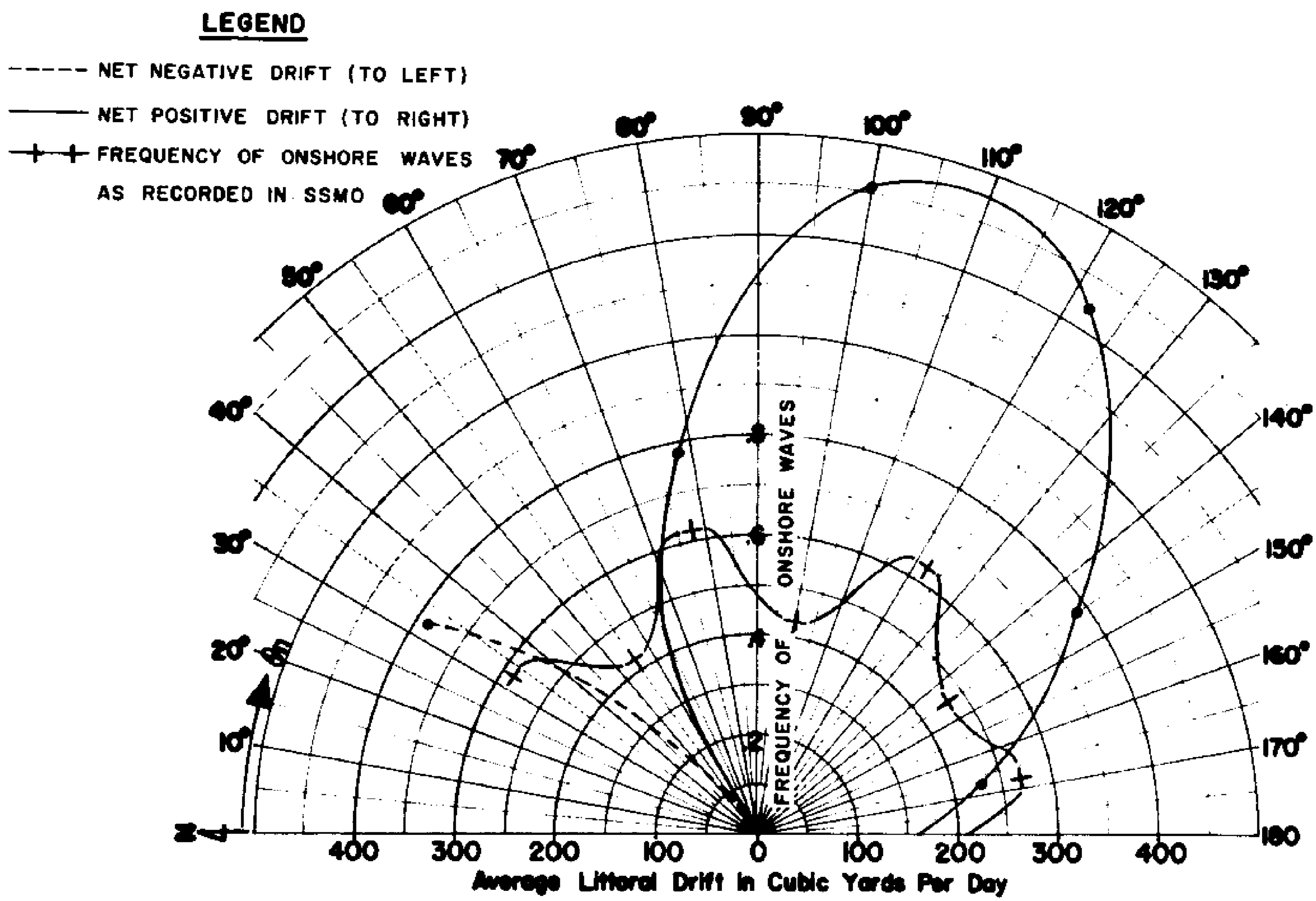

FIGURE A9. VARIATION OF AVERAGE ANNUAL NET LITTORAL DRIFT WITH BEACH ORIENTATION - CAPE KENNEDY TO SEBASTION INLET, FLORIDA

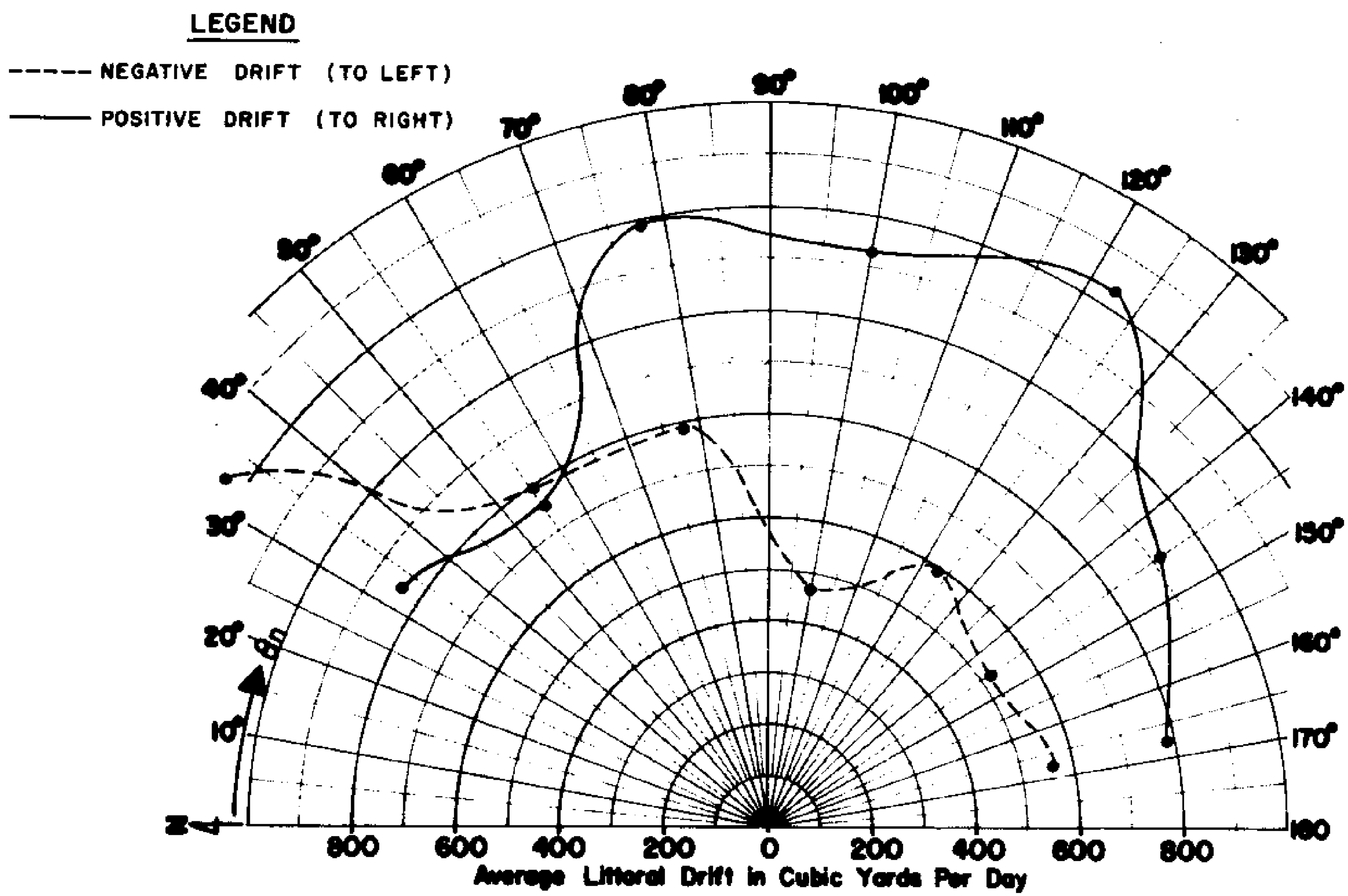

FIGURE A10. VARIATION OF AVERAGE ANNUAL TOTAL LITTORAL DRIFT WITH BEACH ORIENTATION - CAPE KENNEDY TO SEBASTION INLET, FLORIDA

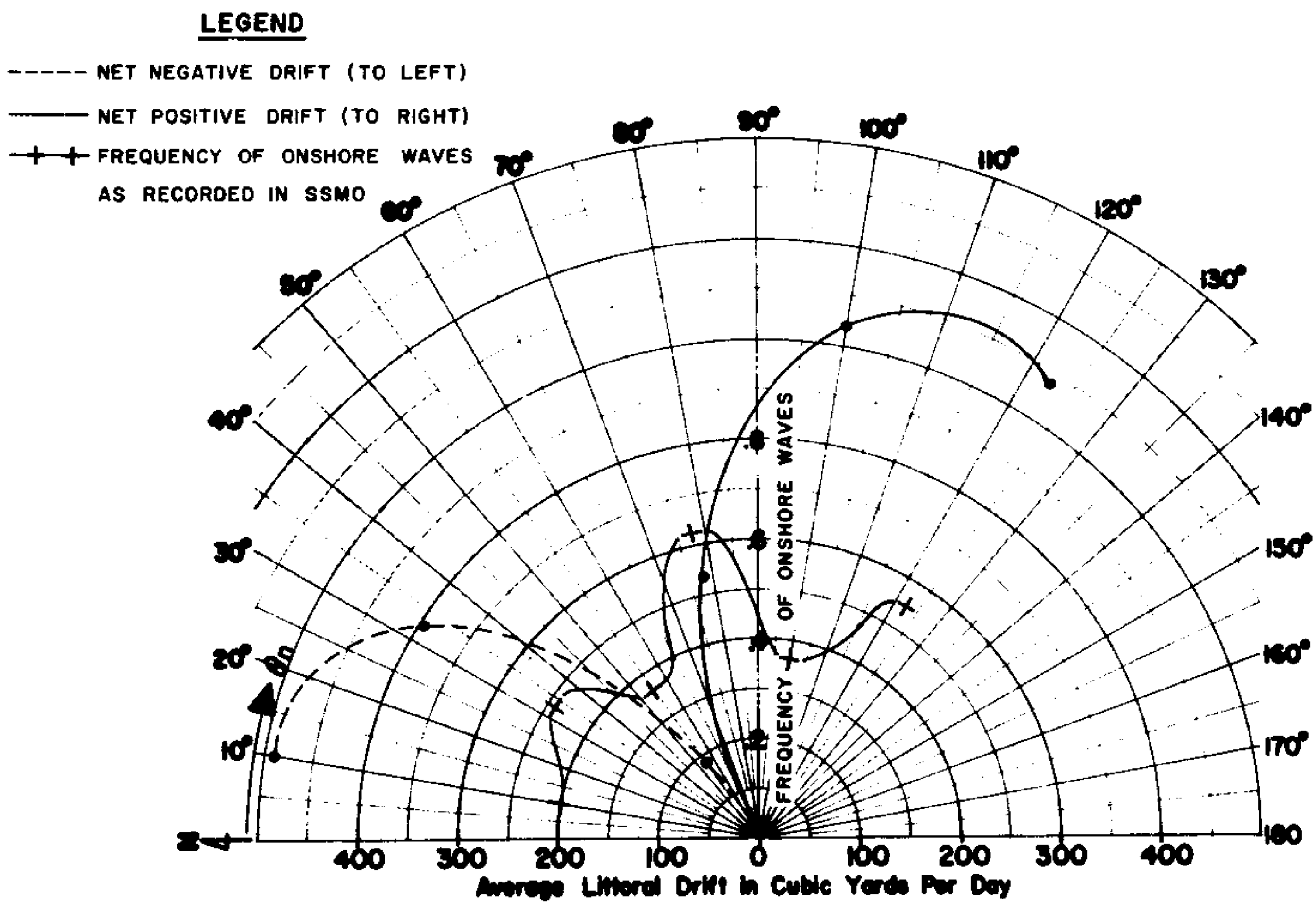

FIGURE A11. VARIATION OF AVERAGE ANNUAL NET LITTORAL DRIFT WITH BEACH ORIENTATION - SEBASTION INLET TO FORT PIERCE INLET, FLORIDA

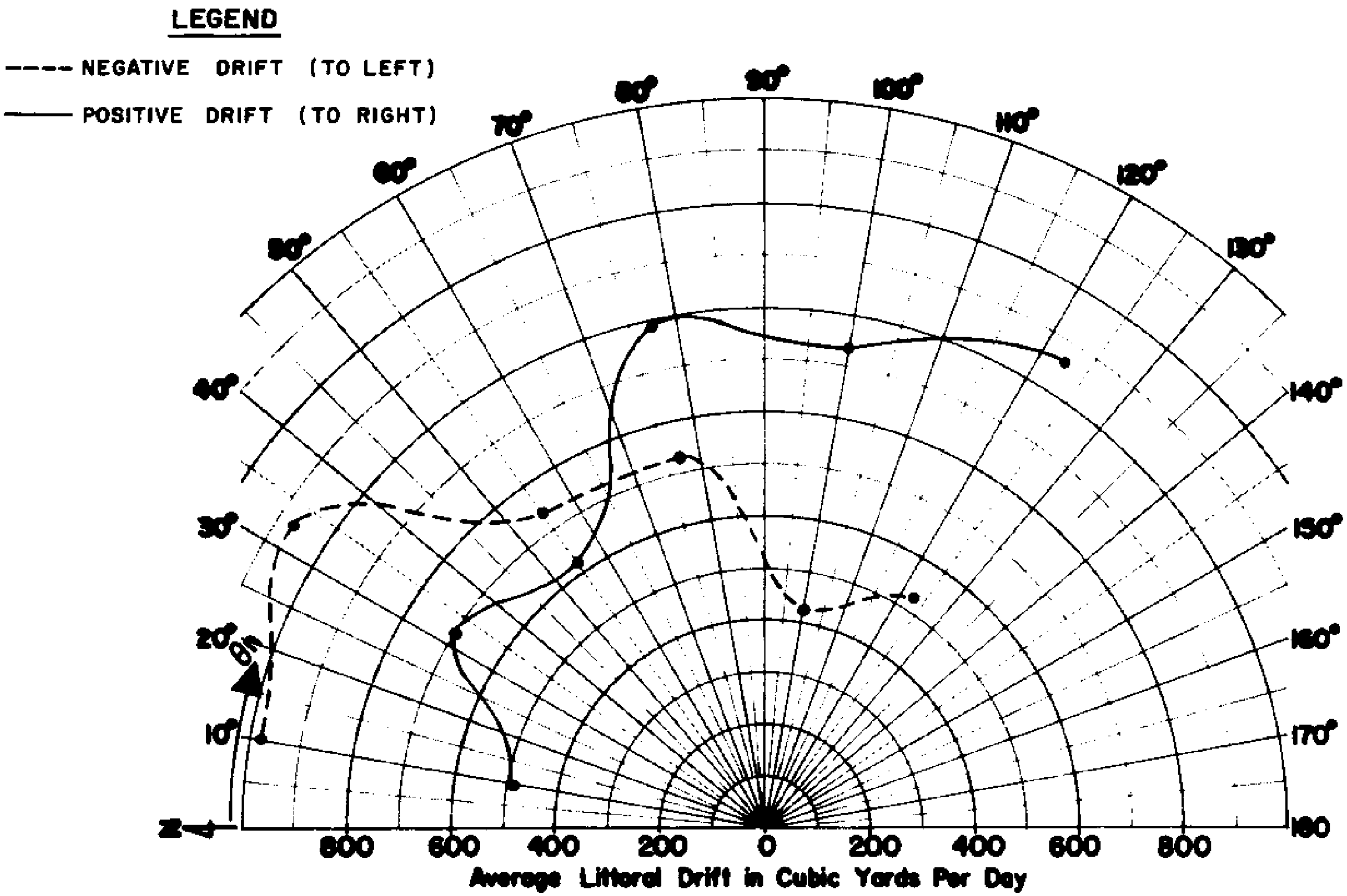

FIGURE A12. VARIATION OF AVERAGE ANNUAL TOTAL LITTORAL DRIFT WITH BEACH ORIENTATION - SEBASTION INLET TO FORT PIERCE INLET, FLORIDA

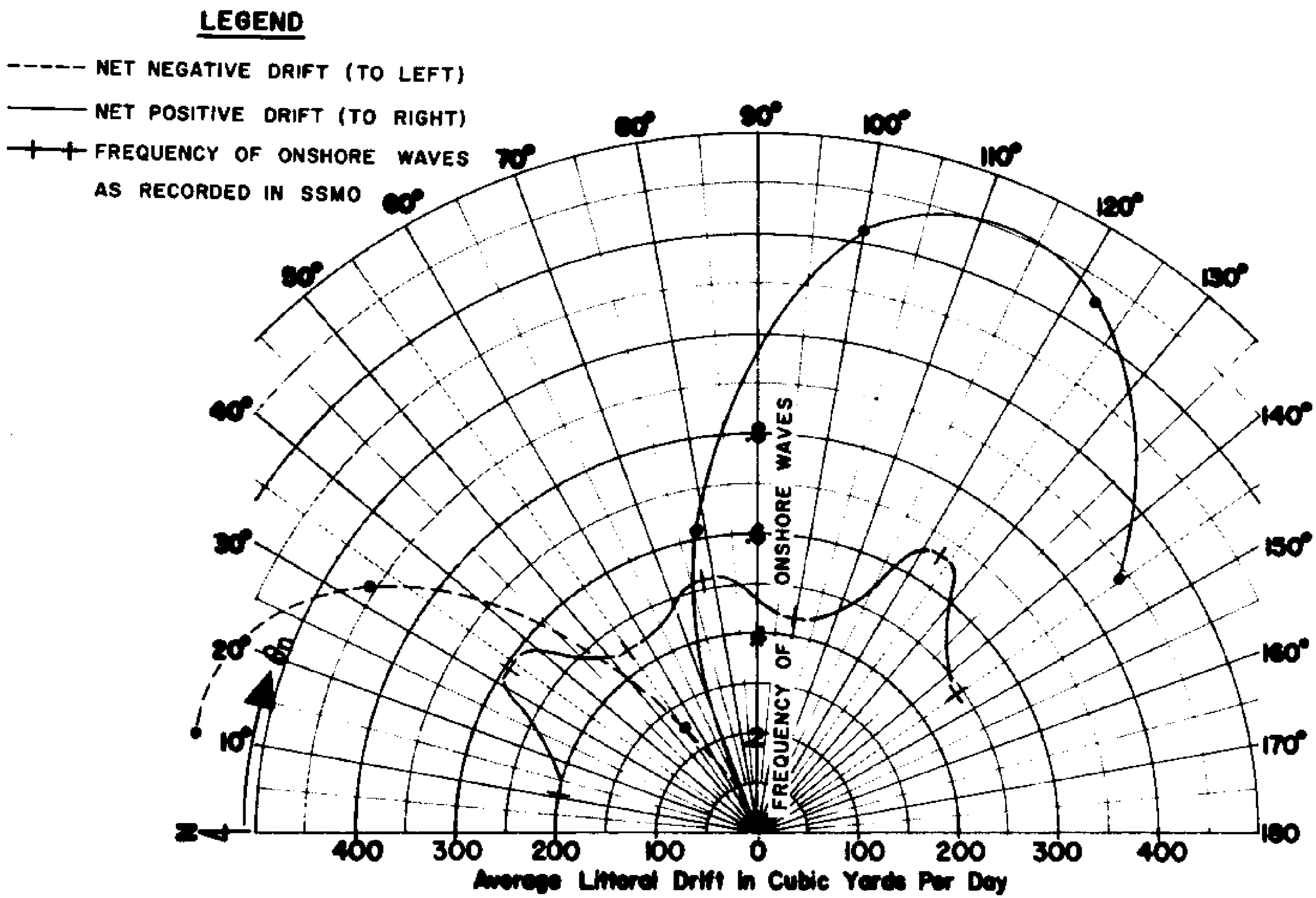

FIGURE A13. VARIATION OF AVERAGE ANNUAL NET LITTORAL DRIFT WITH BEACH ORIENTATION FORT PIERCE INLET TO ST. LUCIE INLET, FLORIDA

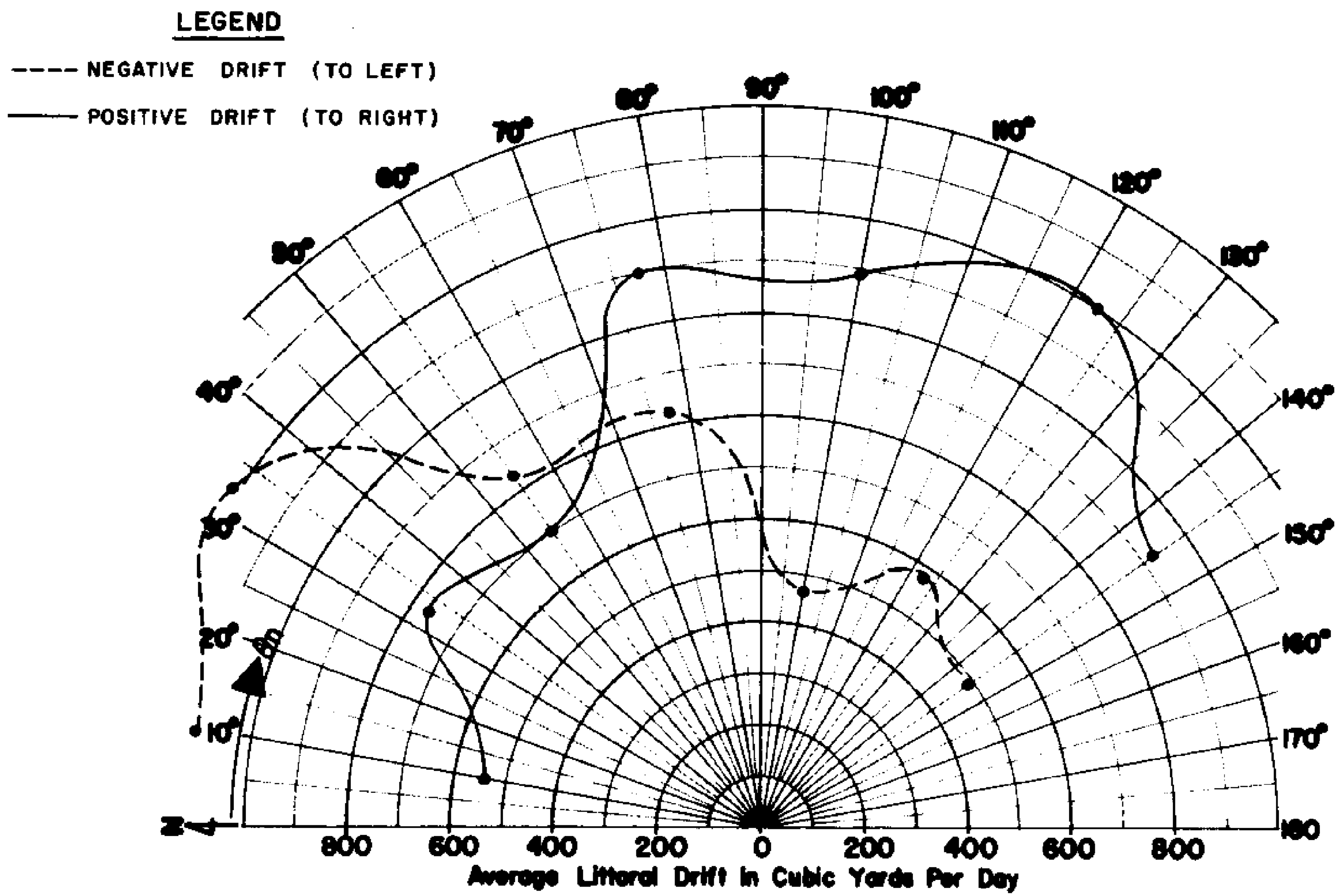

FIGURE A14. VARIATION OF AVERAGE ANNUAL TOTAL LITTORAL DRIFT WITH BEACH ORIENTATION - FORT PIERCE INLET TO ST. LUCIE INLET, FLORIDA

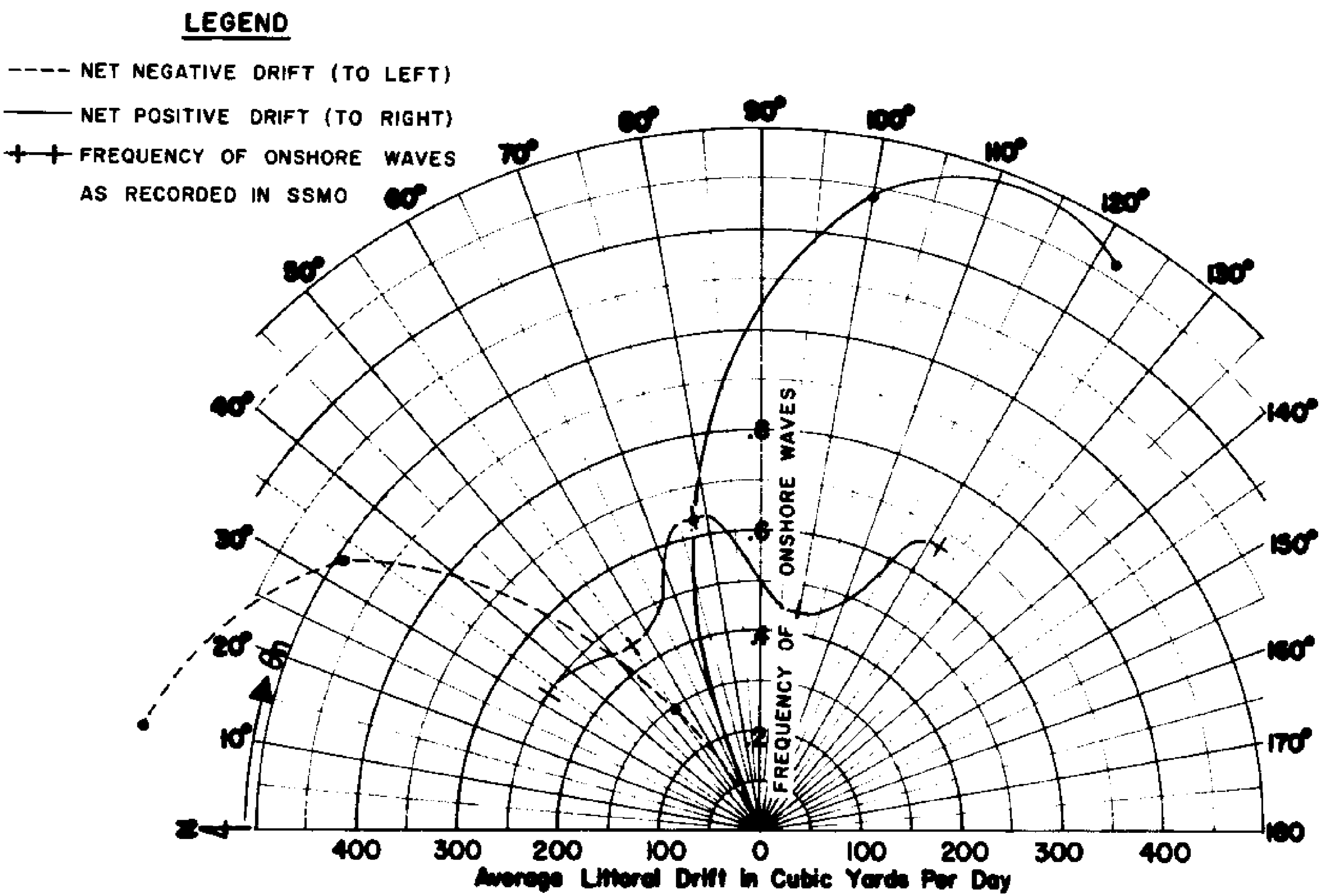

FIGURE A15. VARIATION OF AVERAGE ANNUAL NET LITTORAL DRIFT WITH BEACH ORIENTATION - ST. LUCIE INLET TO JUPITER INLET, FLORIDA

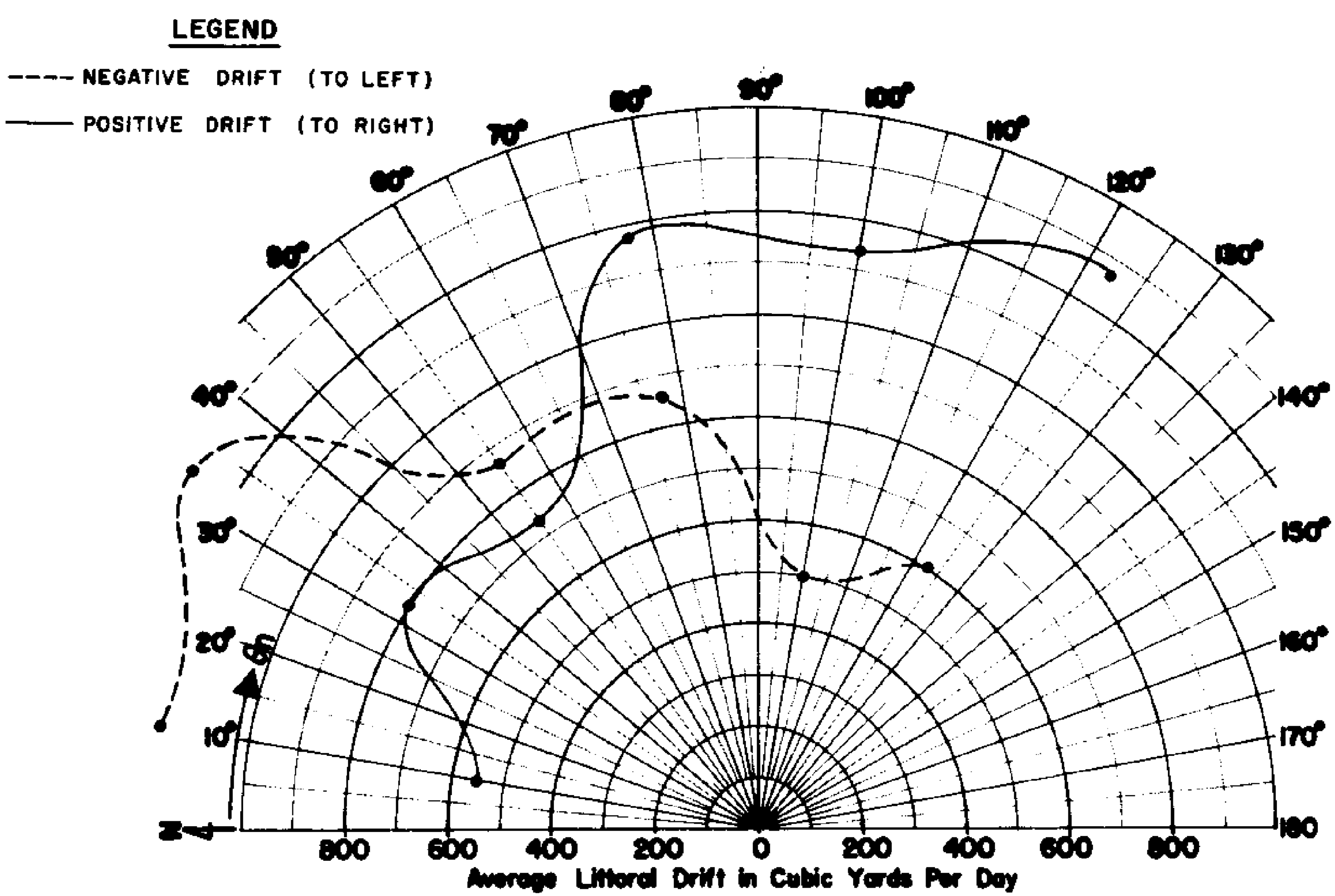

FIGURE A16. VARIATION OF AVERAGE ANNUAL TOTAL LITTORAL DRIFT WITH BEACH ORIENTATION ST. LUCIE INLET TO JUPITER INLET, FLORIDA

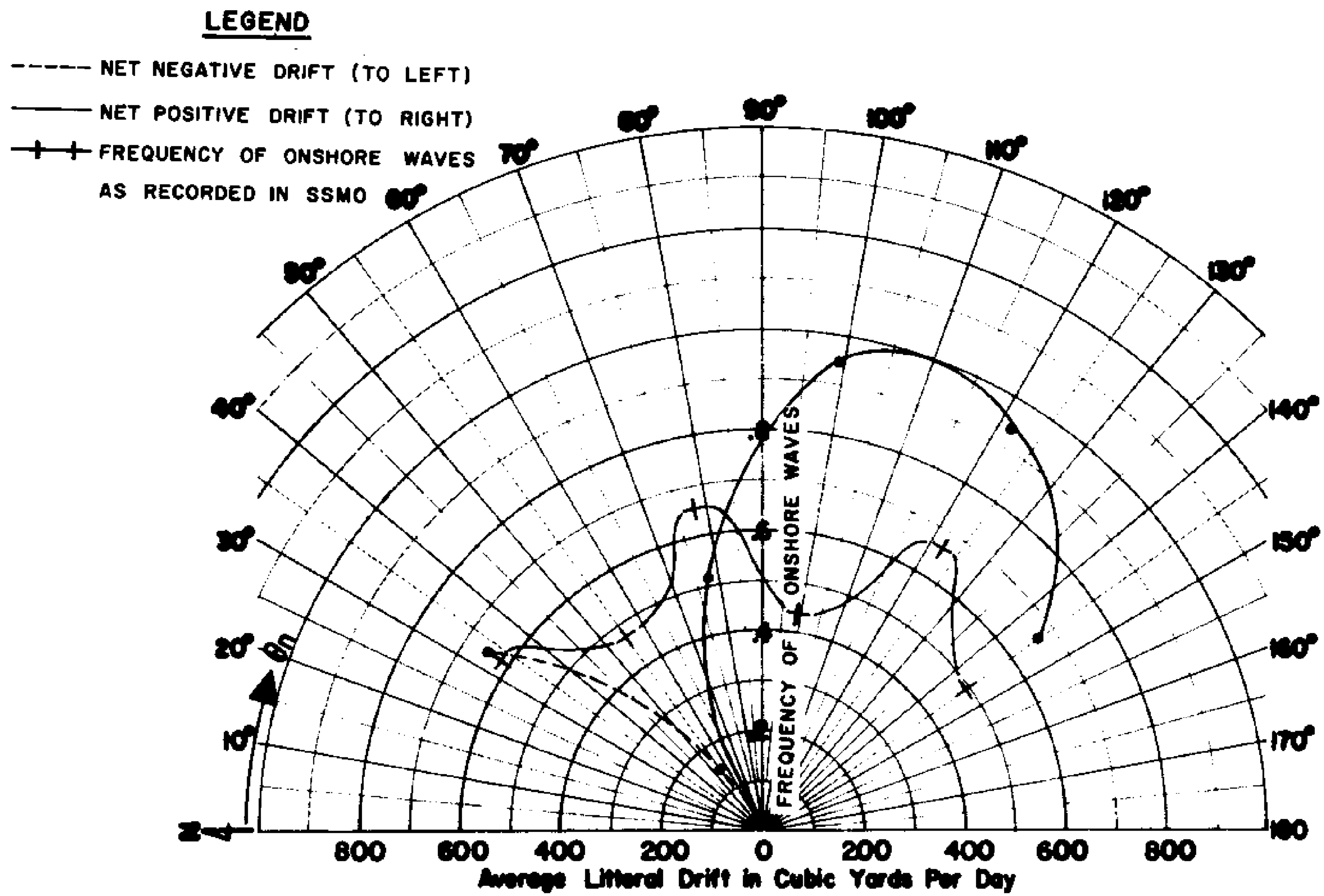

FIGURE A17. VARIATION OF AVERAGE ANNUAL NET LITTORAL DRIFT WITH BEACH ORIENTATION - JUPITER INLET TO LAKE WORTH INLET, FLORIDA

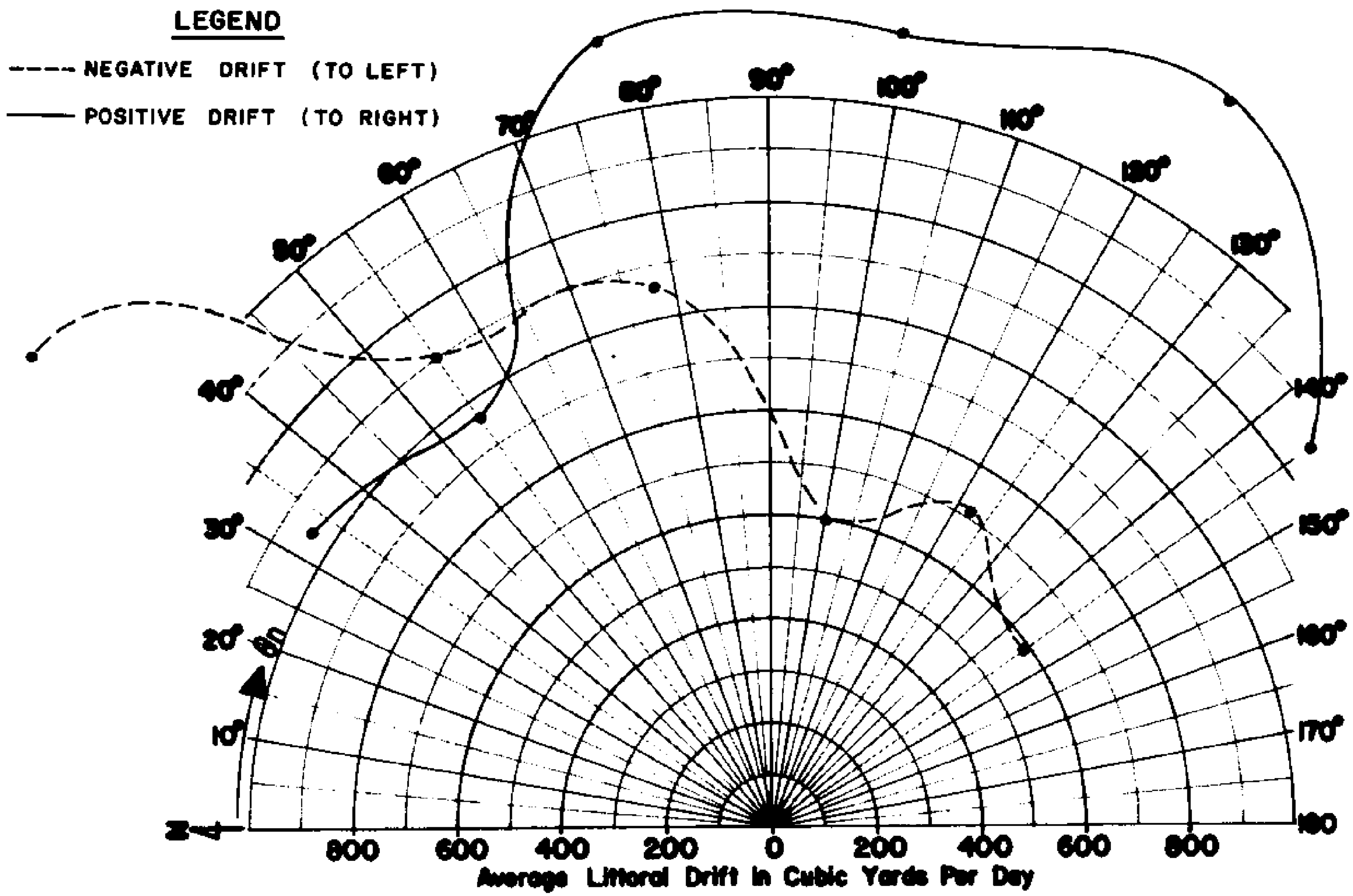

FIGURE A18. VARIATION OF AVERAGE ANNUAL TOTAL LITTORAL DRIFT WITH BEACH ORIENTATION JUPITER INLET TO LAKE WORTH INLET, FLORIDA

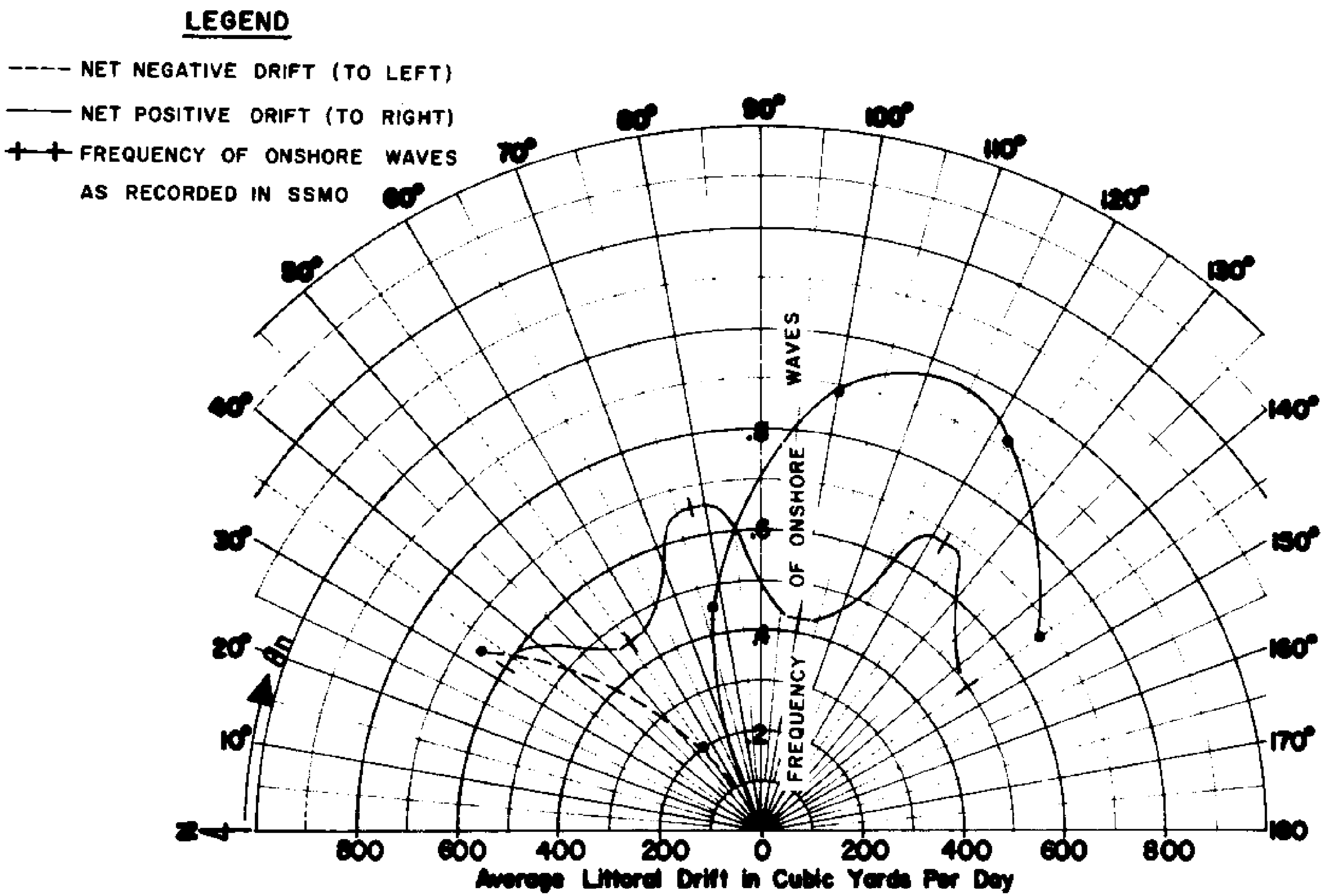

FIGURE A19. VARIATION OF AVERAGE ANNUAL NET LITTORAL DRIFT WITH BEACH ORIENTATION - LAKE WORTH INLET TO HILLSBORO INLET, FLORIDA

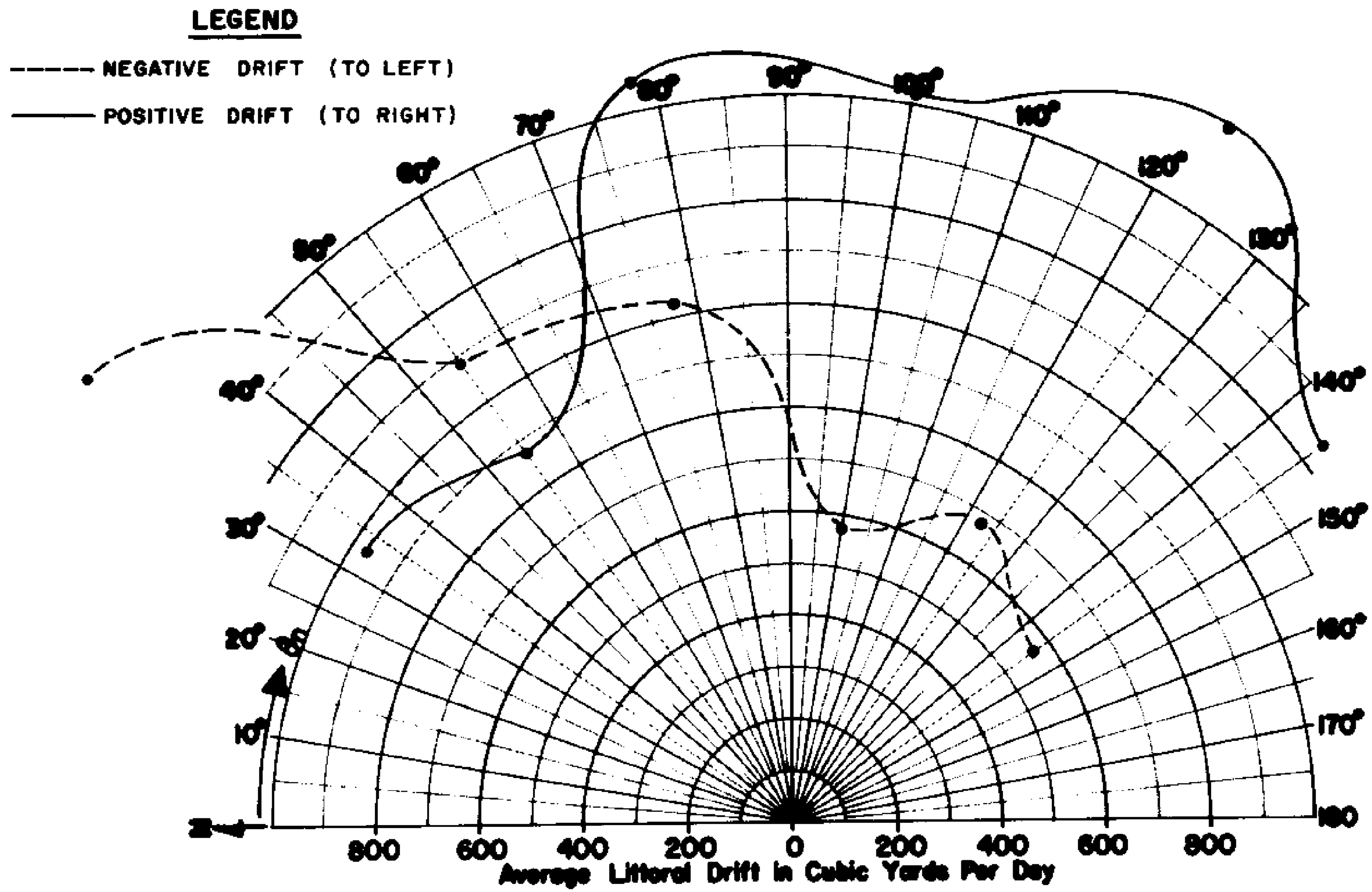

FIGURE A20. VARIATION OF AVERAGE ANNUAL TOTAL LITTORAL DRIFT WITH BEACH ORIENTATION LAKE WORTH INLET TO HILLSBORO INLET, FLORIDA

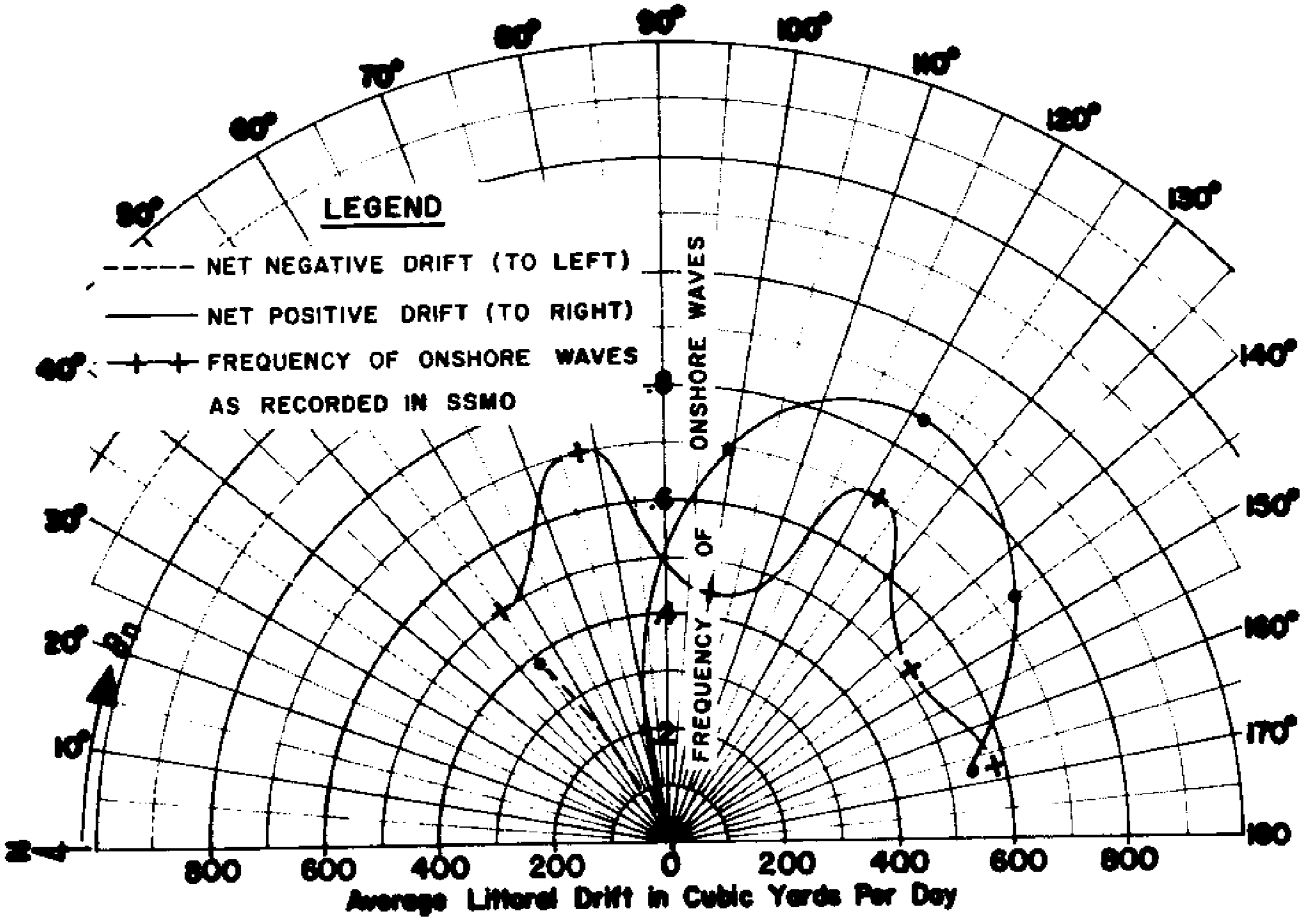

FIGURE A21. VARIATION OF AVERAGE ANNUAL NET LITTORAL DRIFT WITH BEACH ORIENTATION - HILLSBORO INLET TO CAPE FLORIDA, FLORIDA

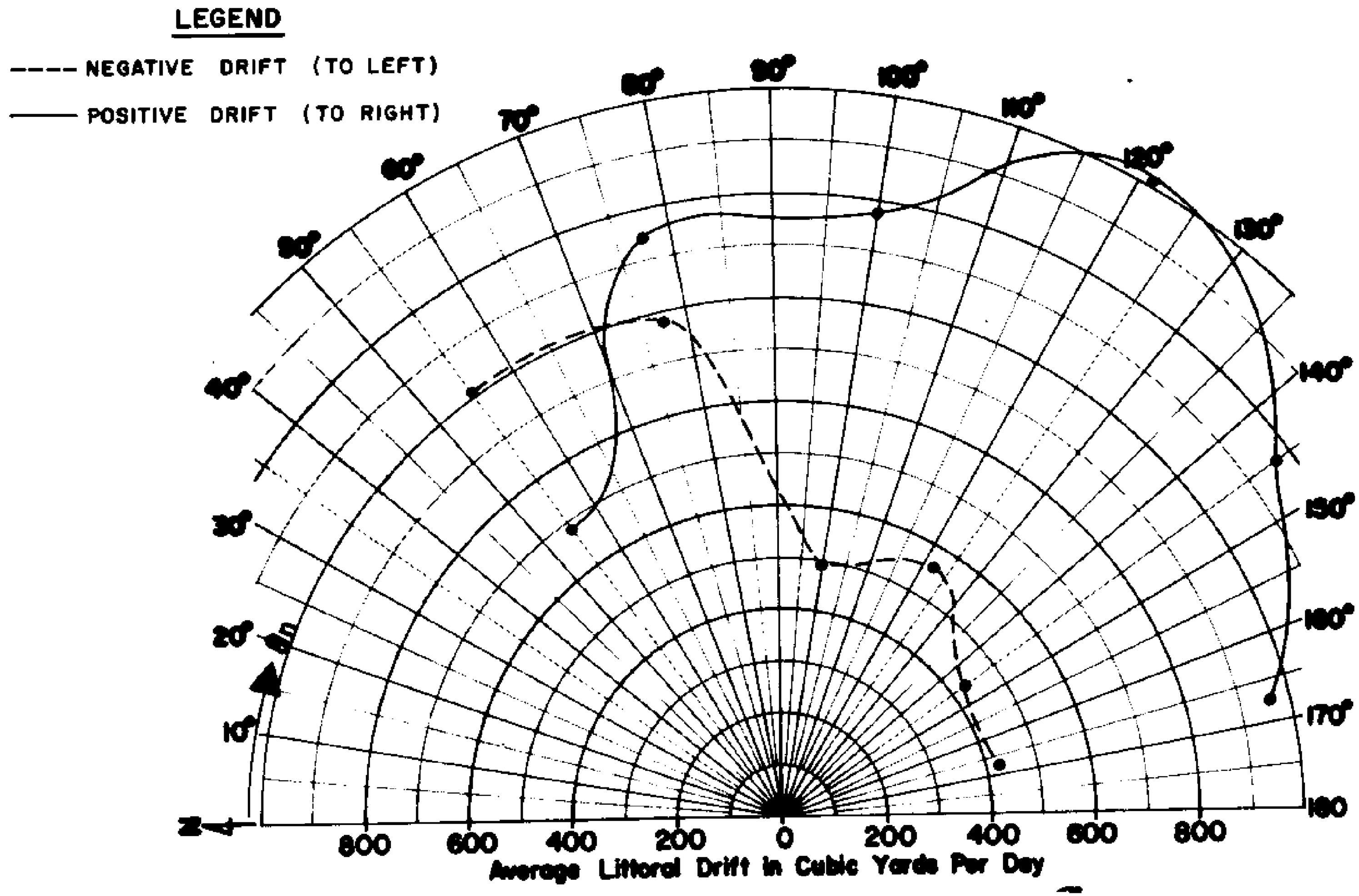

FIGURE A22. VARIATION OF AVERAGE ANNUAL TOTAL LITTORAL DRIFT WITH BEACH ORIENTATION - HILLSBORO INLET TO CAPE FLORIDA, FLORIDA

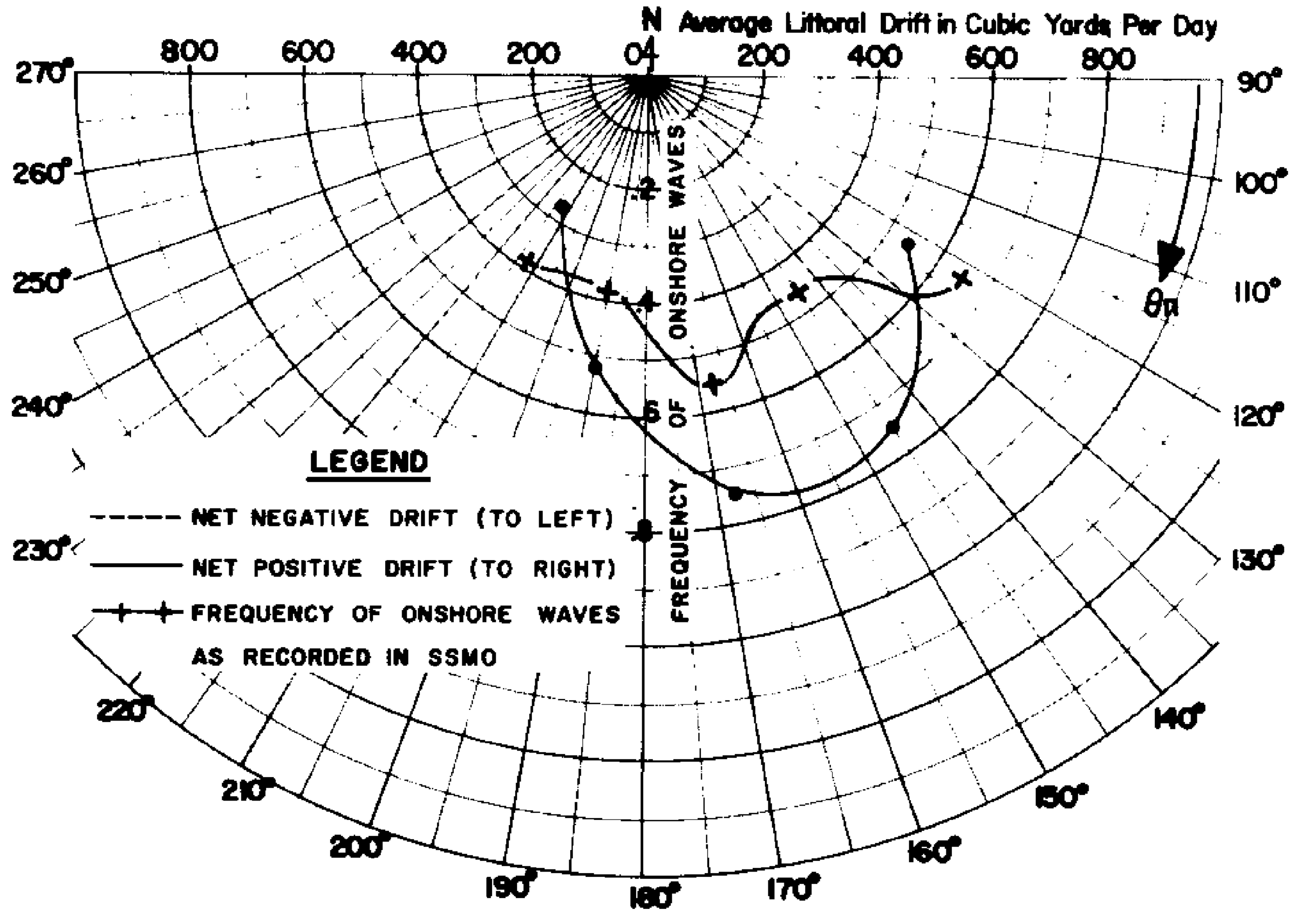

FIGURE A23. VARIATION OF AVERAGE ANNUAL NET LITTORAL DRIFT WITH BEACH ORIENTATION - PERDIDO PASS TO PENSACOLA BAY ENTRANCE, FLORIDA

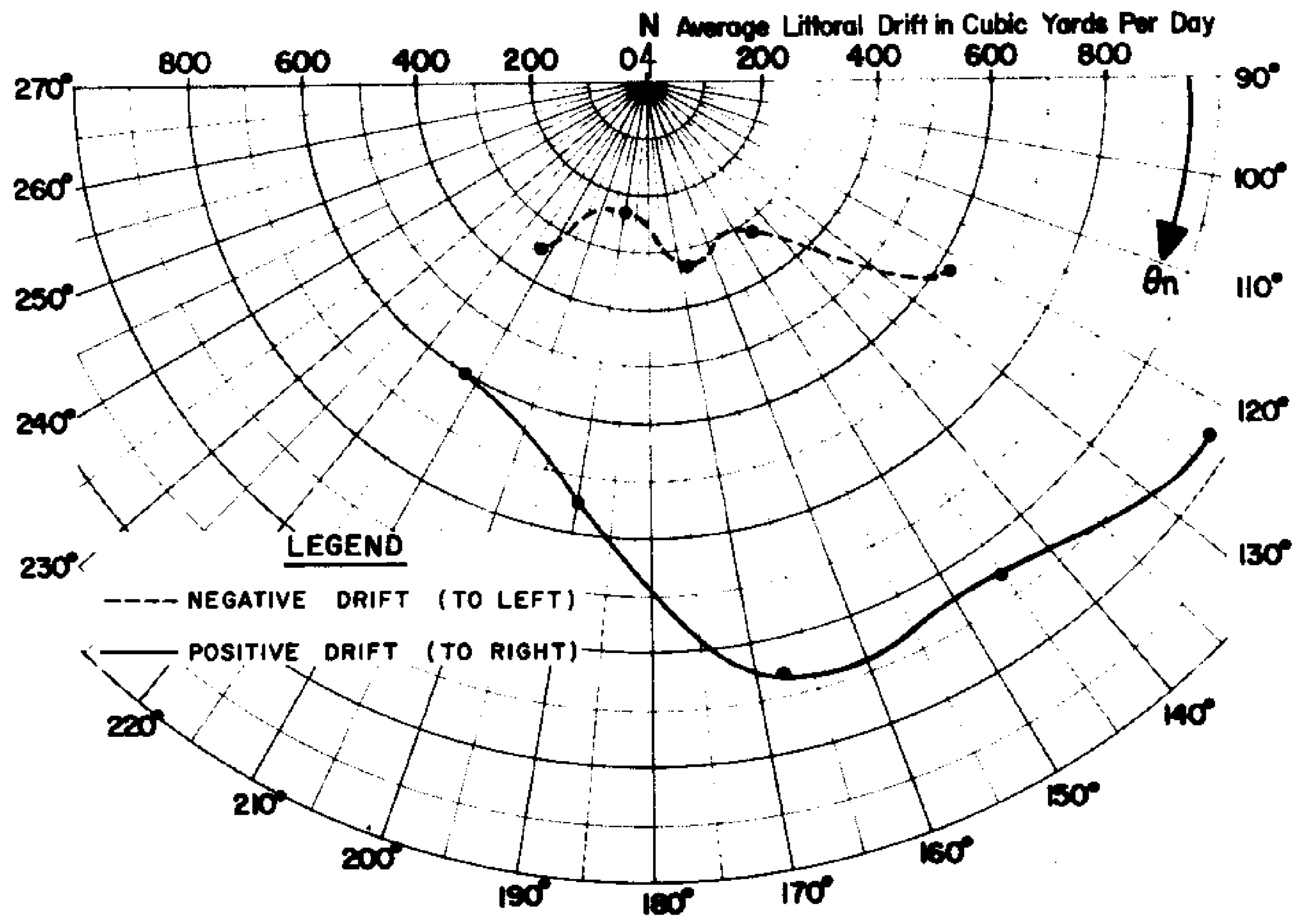

FIGURE A24. VARIATION OF AVERAGE ANNUAL TOTAL LITTORAL DRIFT WITH BEACH ORIENTATION - PERDIDO PASS TO PENSACOLA BAY ENTRANCE, FLORIDA

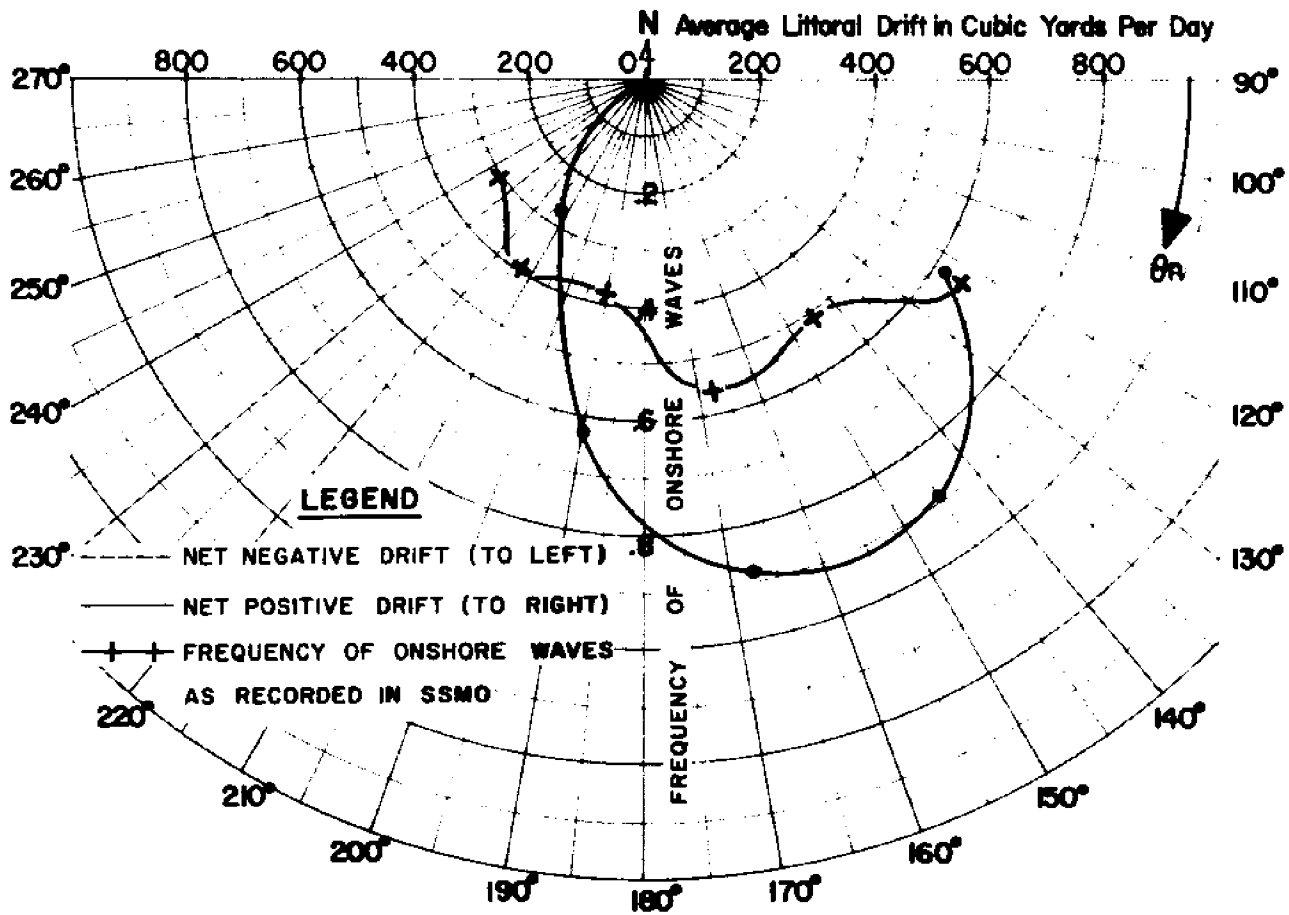

FIGURE A25. VARIATION OF AVERAGE ANNUAL NET LITTORAL DRIFT WITH BEACH ORIENTATION – PENSACOLA BAY ENTRANCE TO CHOTAWHATCHEE BAY ENTRANCE, FLORIDA

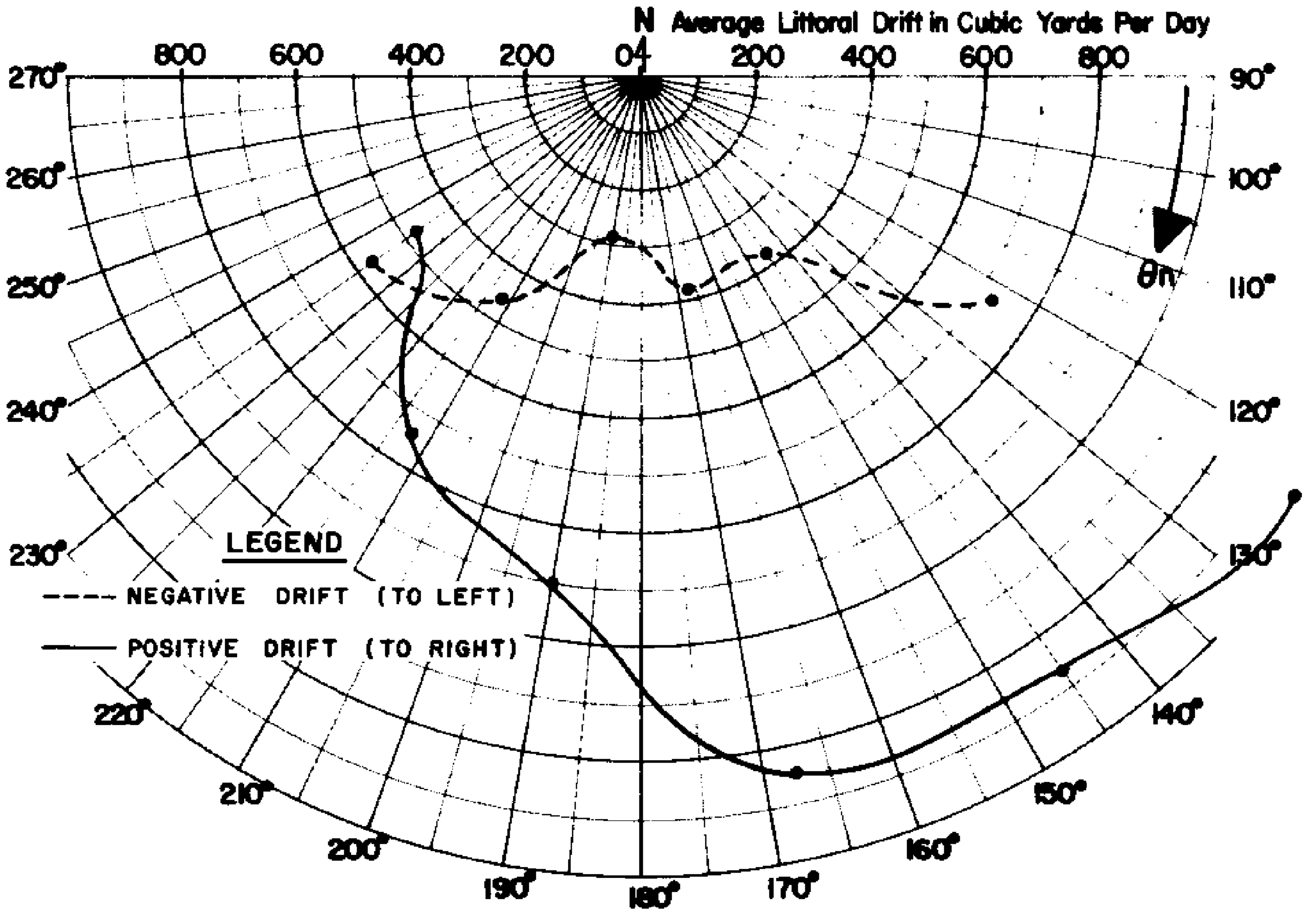

FIGURE A26. VARIATION OF AVERAGE ANNUAL TOTAL LITTORAL DRIFT WITH BEACH ORIENTATION - PENSACOLA BAY ENTRANCE TO CHOCTAWHATCHEE BAY ENTRANCE, FLORIDA

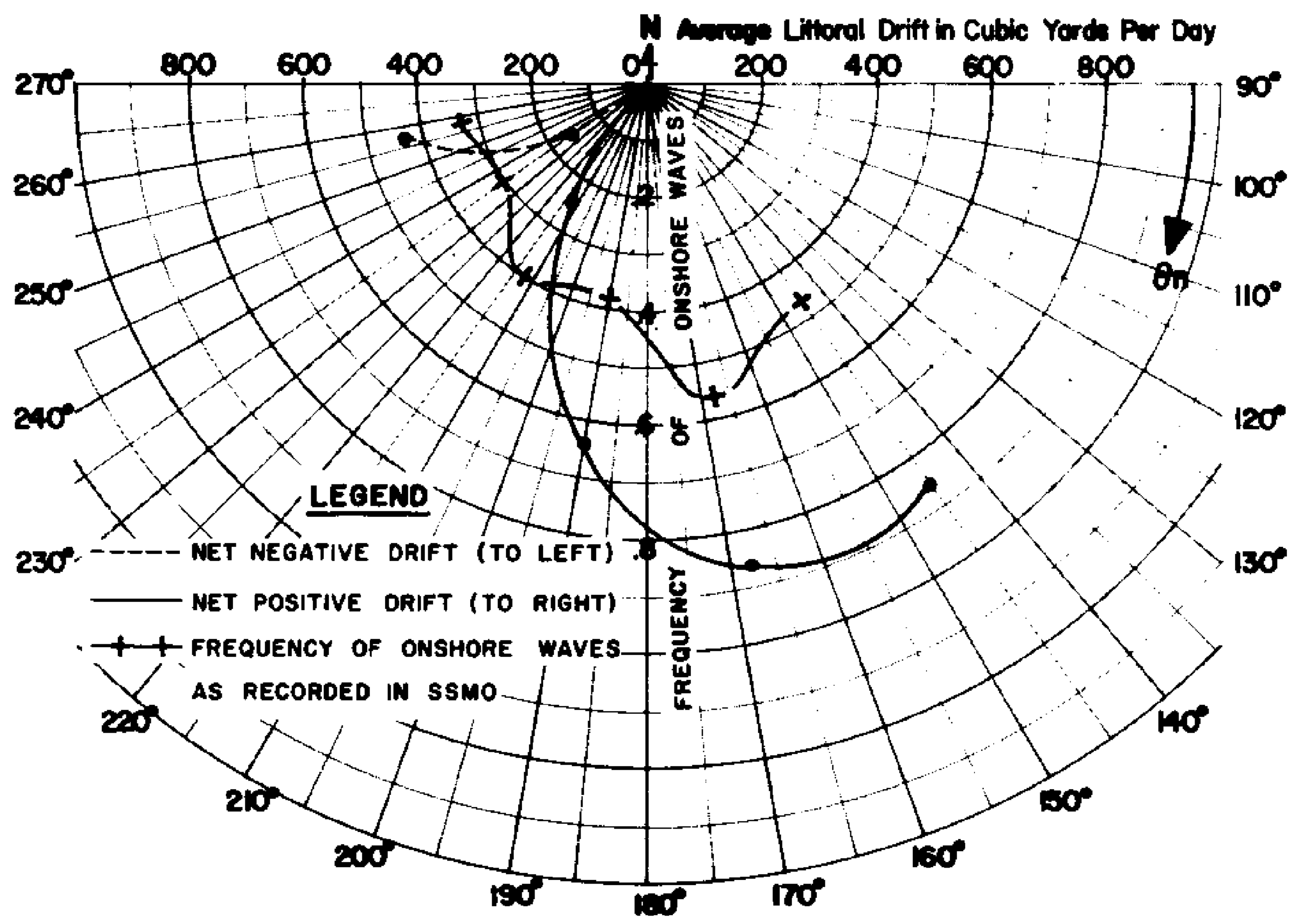

FIGURE A27. VARIATION OF AVERAGE ANNUAL NET LITTORAL DRIFT WITH BEACH ORIENTATION - CHOCTAWHATCHEE BAY ENTRANCE TO ST. ANDREW BAY ENTRANCE, FLORIDA

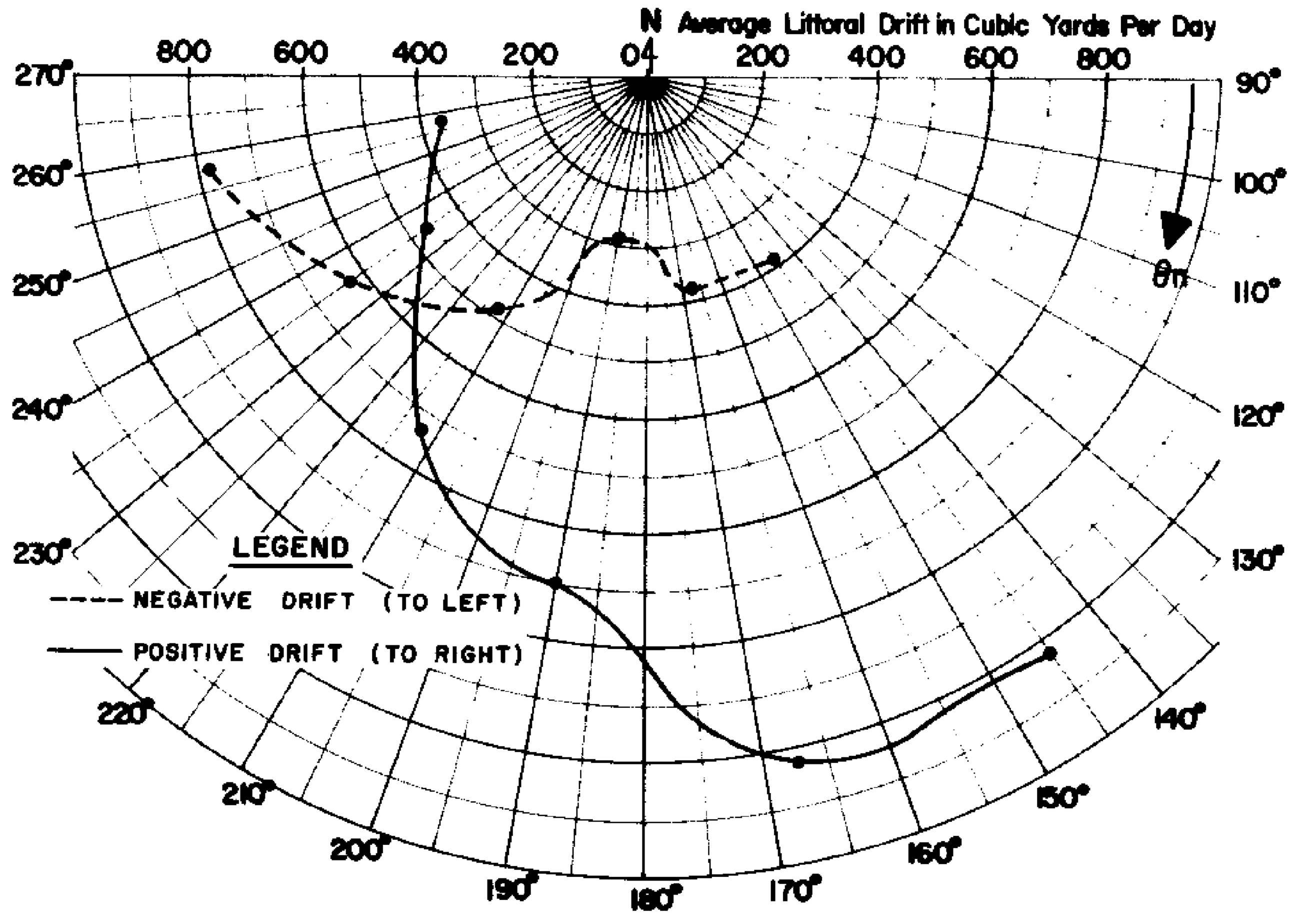

FIGURE A28. VARIATION OF AVERAGE ANNUAL TOTAL LITTORAL DRIFT WITH BEACH ORIENTATION – CHOCTAWHATCHEE BAY ENTRANCE TO ST. ANDREW BAY ENTRANCE, FLORIDA

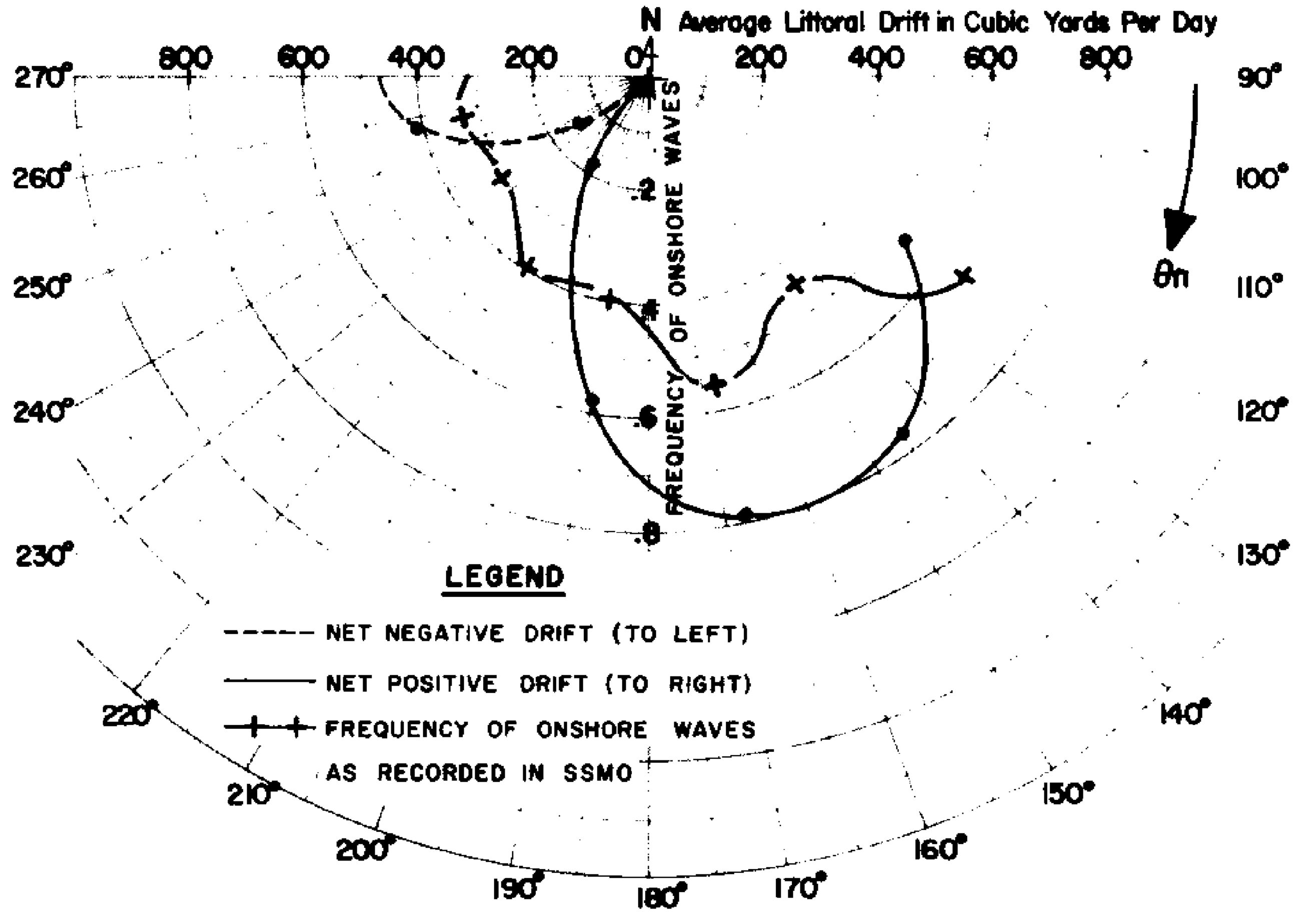

FIGURE A29. VARIATION OF AVERAGE ANNUAL NET LITTORAL DRIFT WITH BEACH ORIENTATION - ST. ANDREW BAY ENTRANCE TO ST. JOSEPH BAY ENTRANCE, FLORIDA

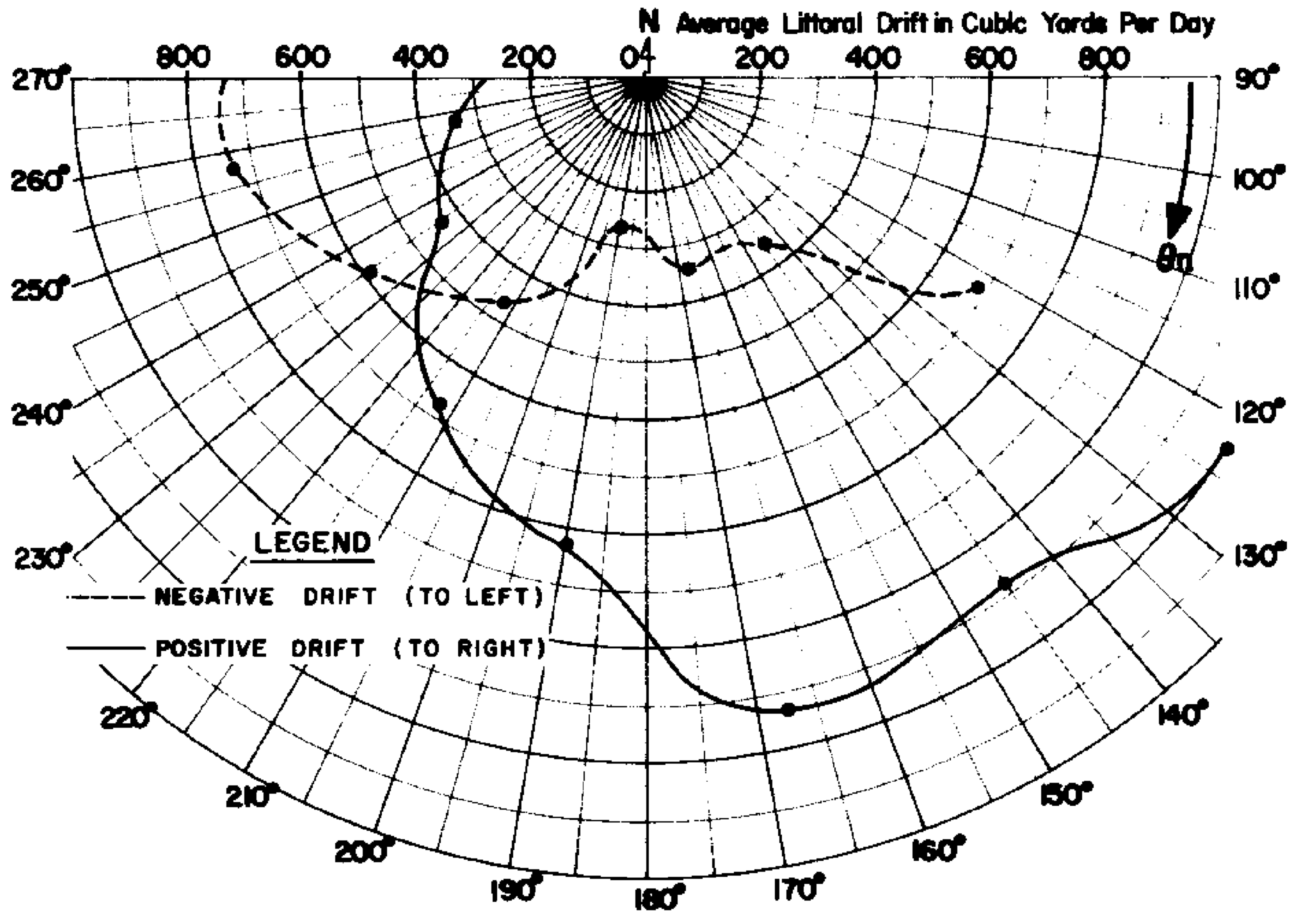

FIGURE A30. VARIATION OF AVERAGE ANNUAL TOTAL LITTORAL DRIFT WITH BEACH ORIENTATION – ST. ANDREW BAY ENTRANCE TO ST. JOSEPH BAY ENTRANCE, FLORIDA

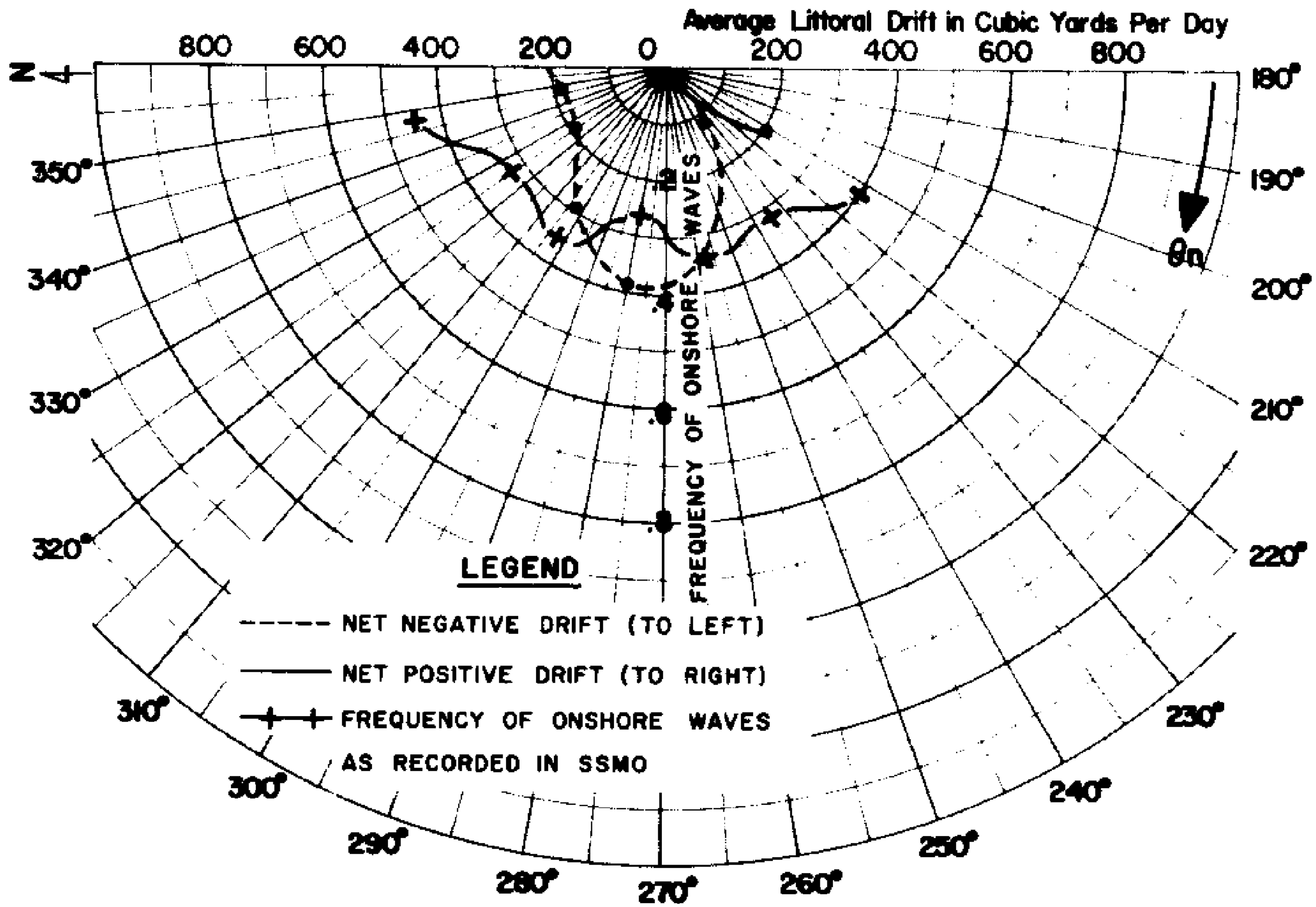

FIGURE A31. VARIATION OF AVERAGE ANNUAL NET LITTORAL DRIFT WITH BEACH ORIENTATION – ST. JOSEPH BAY ENTRANCE TO CAPE SAN BLAS, FLORIDA

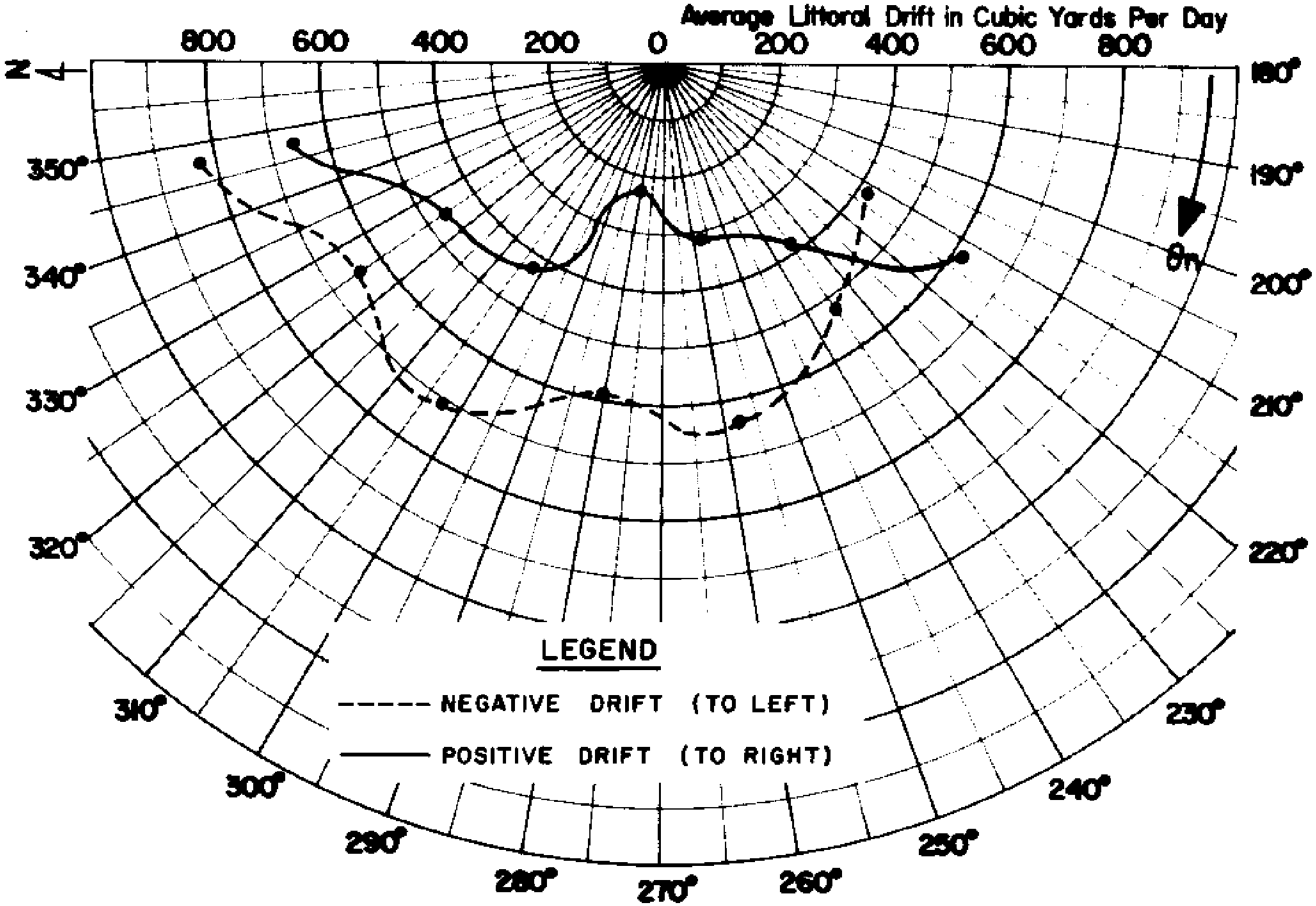

FIGURE A32. VARIATION OF AVERAGE ANNUAL TOTAL LITTORAL DRIFT WITH BEACH ORIENTATION - ST. JOSEPH BAY ENTRANCE TO CAPE SAN BLAS, FLORIDA

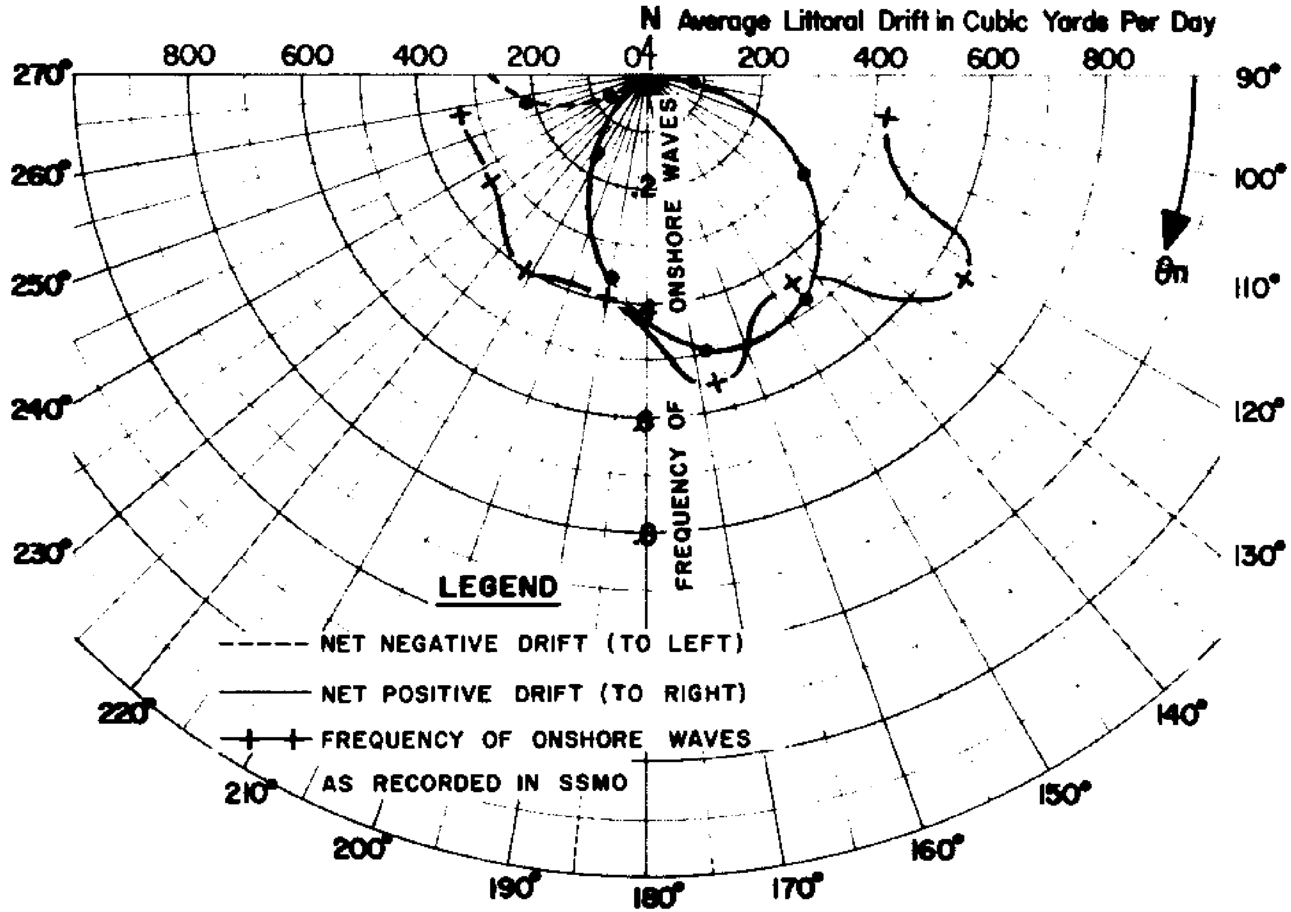

FIGURE A33. VARIATION OF AVERAGE ANNUAL NET LITTORAL DRIFT WITH BEACH ORIENTATION – CAPE SAN BLAS TO CAPE ST. GEORGE, FLORIDA

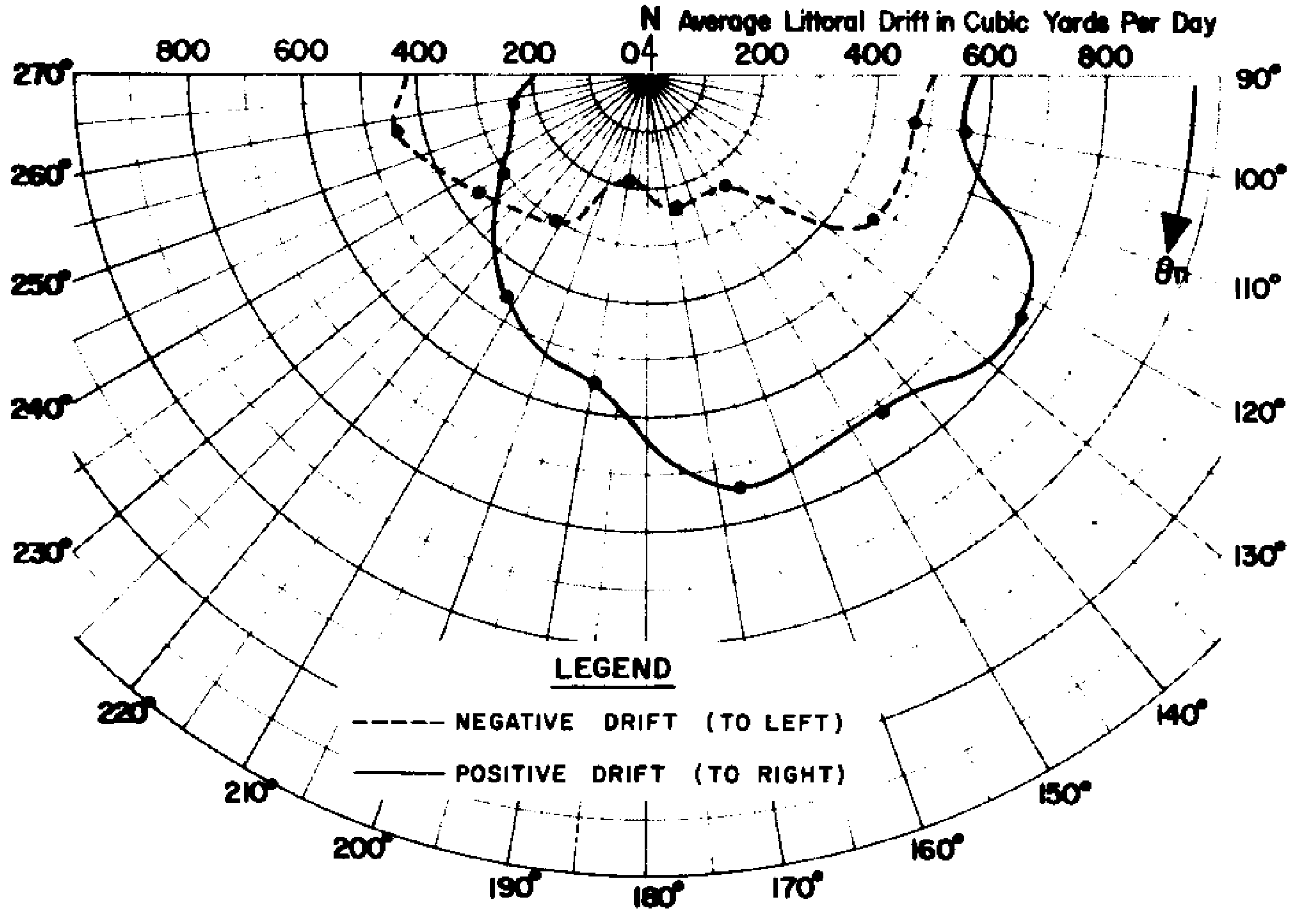

FIGURE A34. VARIATION OF AVERAGE ANNUAL TOTAL LITTORAL DRIFT WITH BEACH ORIENTATION – CAPE SAN BLAS TO CAPE ST. GEORGE, FLORIDA

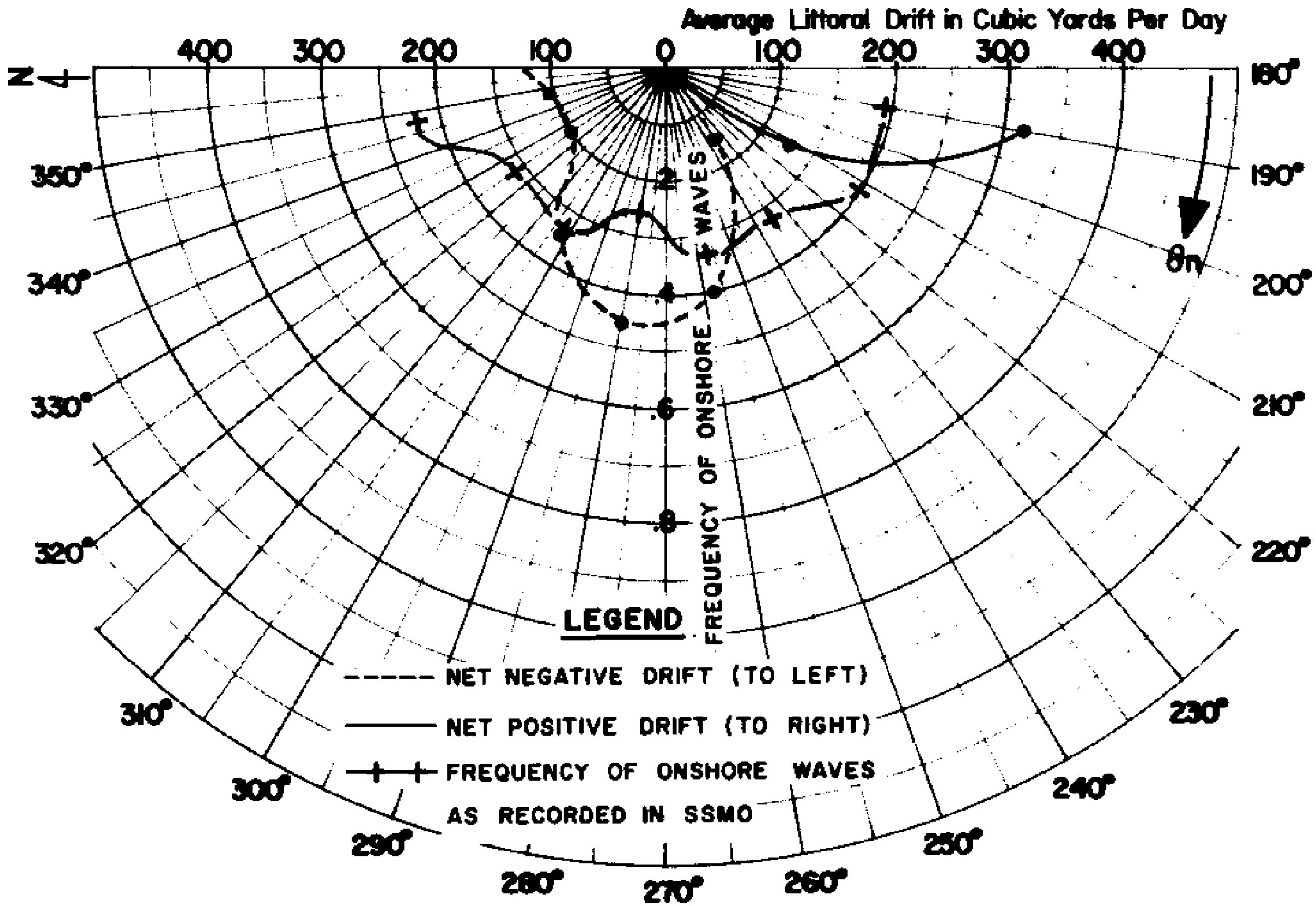

FIGURE A35. VARIATION OF AVERAGE ANNUAL NET LITTORAL DRIFT WITH BEACH ORIENTATION - ANCLOTE KEYS TO CLEARWATER PASS, FLORIDA

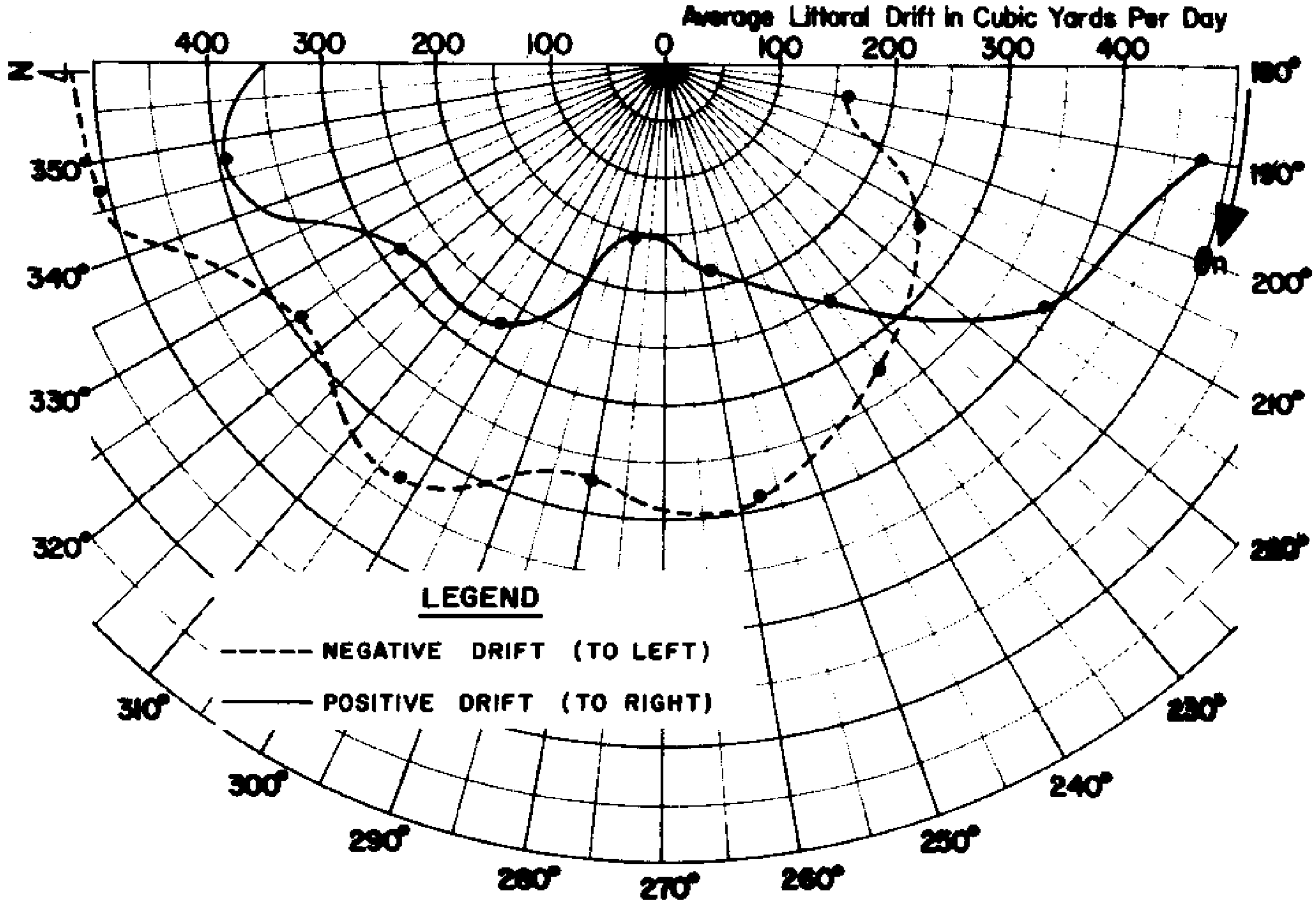

FIGURE A36. VARIATION OF AVERAGE ANNUAL TOTAL LITTORAL DRIFT WITH BEACH ORIENTATION - ANCLOTE KEYS TO CLEARWATER PASS, FLORIDA

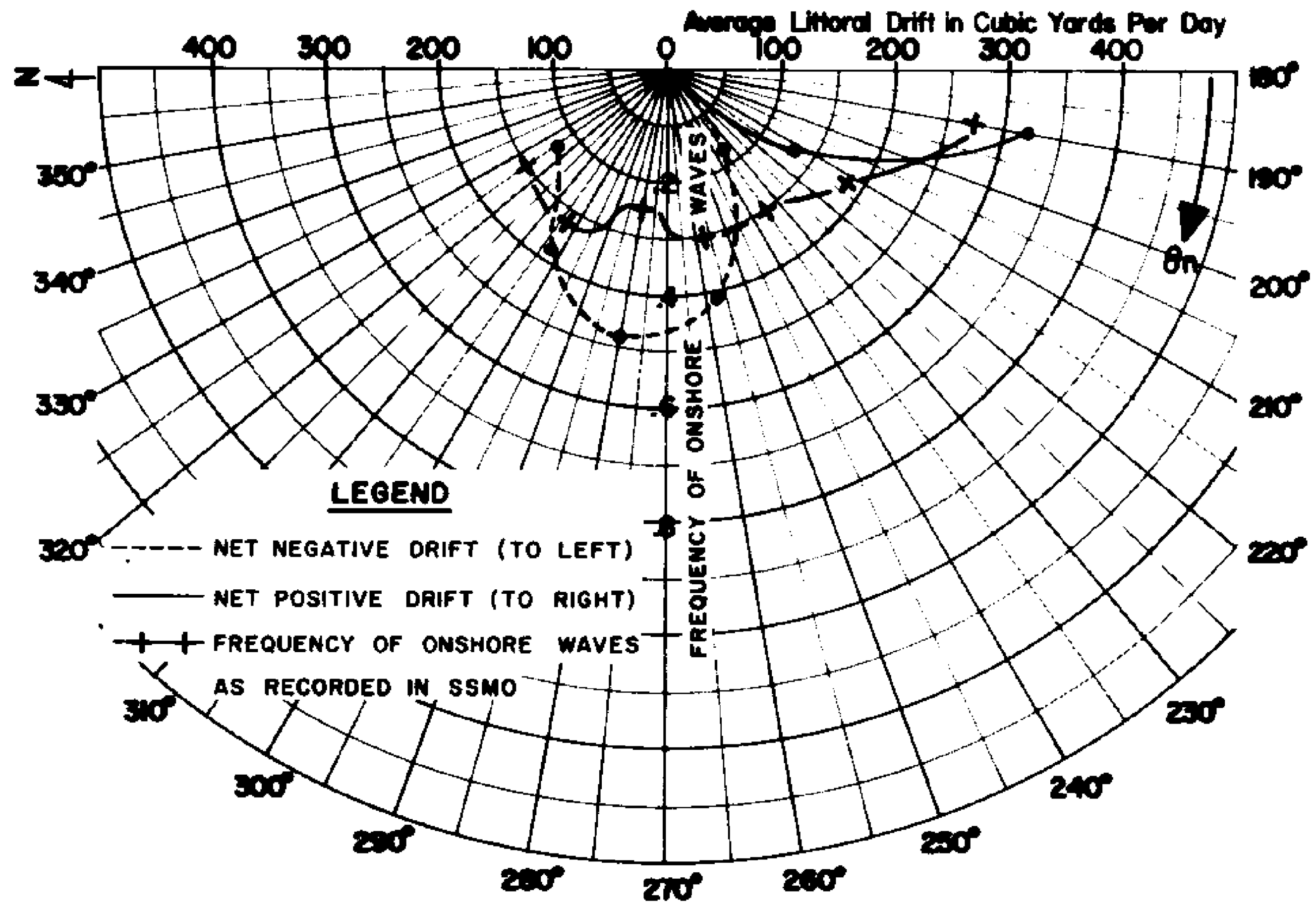

FIGURE A37. VARIATION OF AVERAGE ANNUAL NET LITTORAL DRIFT WITH BEACH ORIENTATION - CLEARWATER PASS TO TAMPA BAY ENTRANCE, FLORIDA

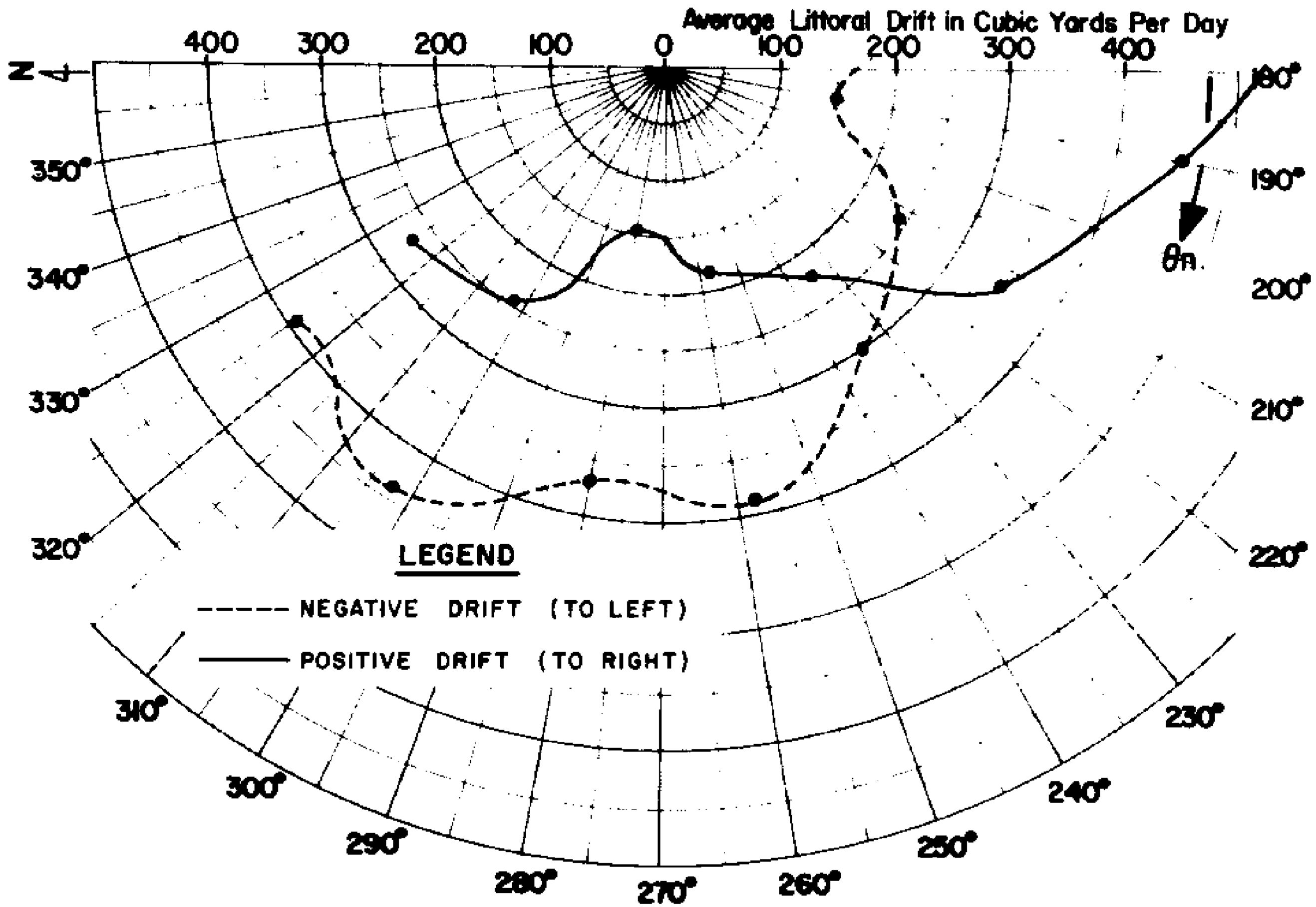

FIGURE A38. VARIATION OF AVERAGE ANNUAL TOTAL LITTORAL DRIFT WITH BEACH ORIENTATION - CLEARWATER PASS TO TAMPA BAY ENTRANCE, FLORIDA

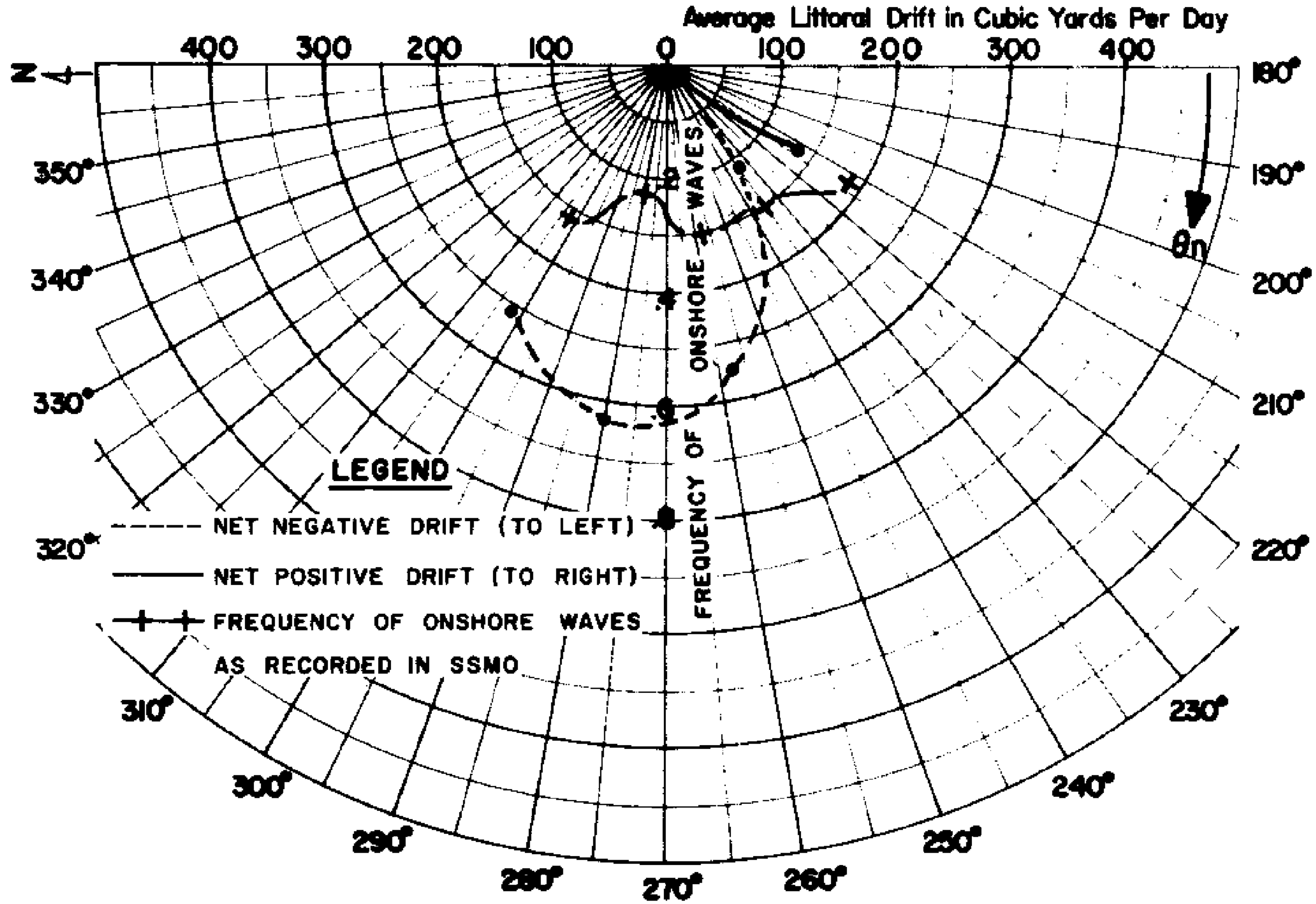

FIGURE A39. VARIATION OF AVERAGE ANNUAL NET LITTORAL DRIFT WITH BEACH ORIENTATION – TAMPA BAY ENTRANCE TO BIG SARASOTA PASS, FLORIDA

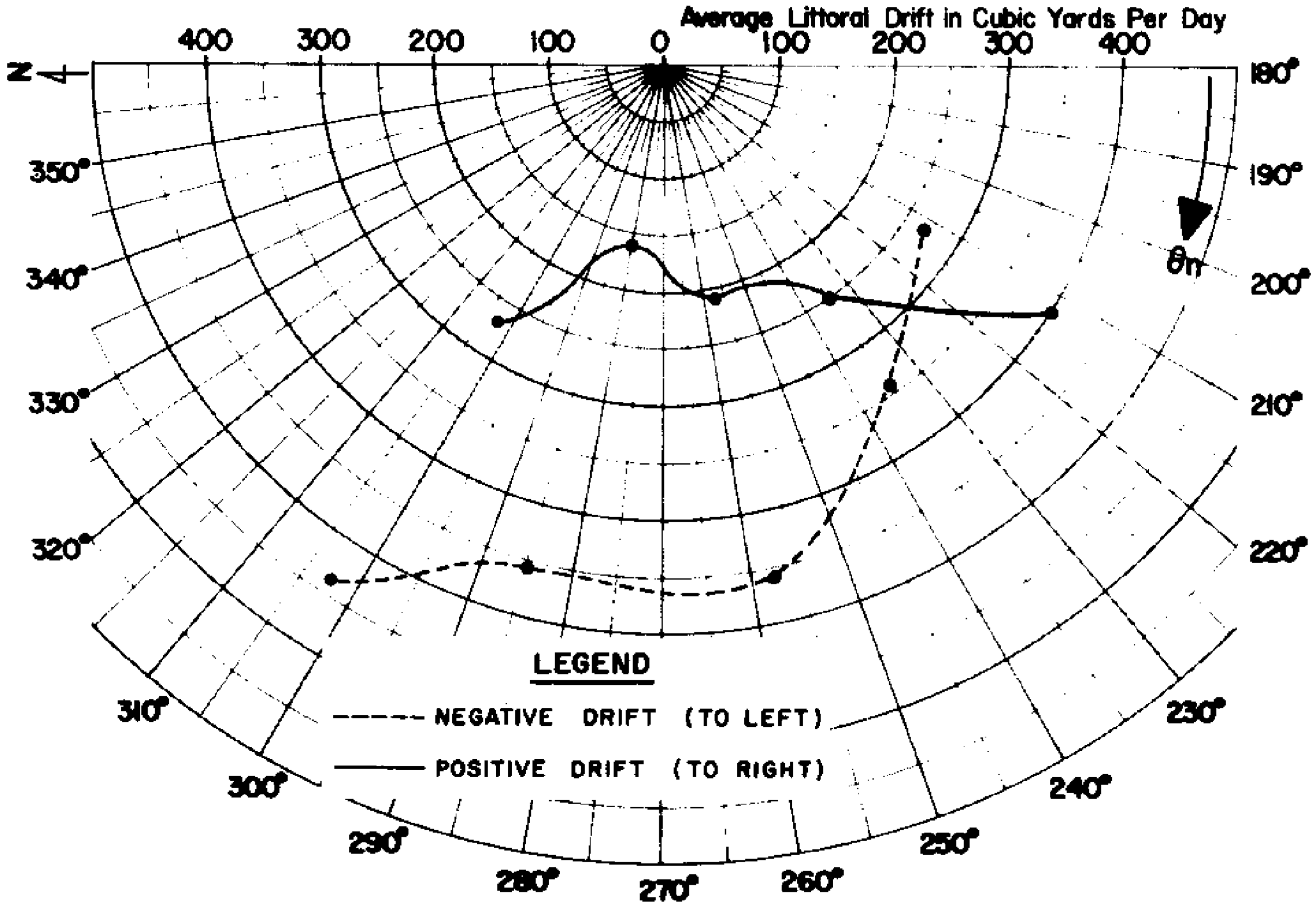

FIGURE A40. VARIATION OF AVERAGE ANNUAL TOTAL LITTORAL DRIFT WITH BEACH ORIENTATION - TAMPA BAY ENTRANCE TO BIG SARASOTA PASS, FLORIDA

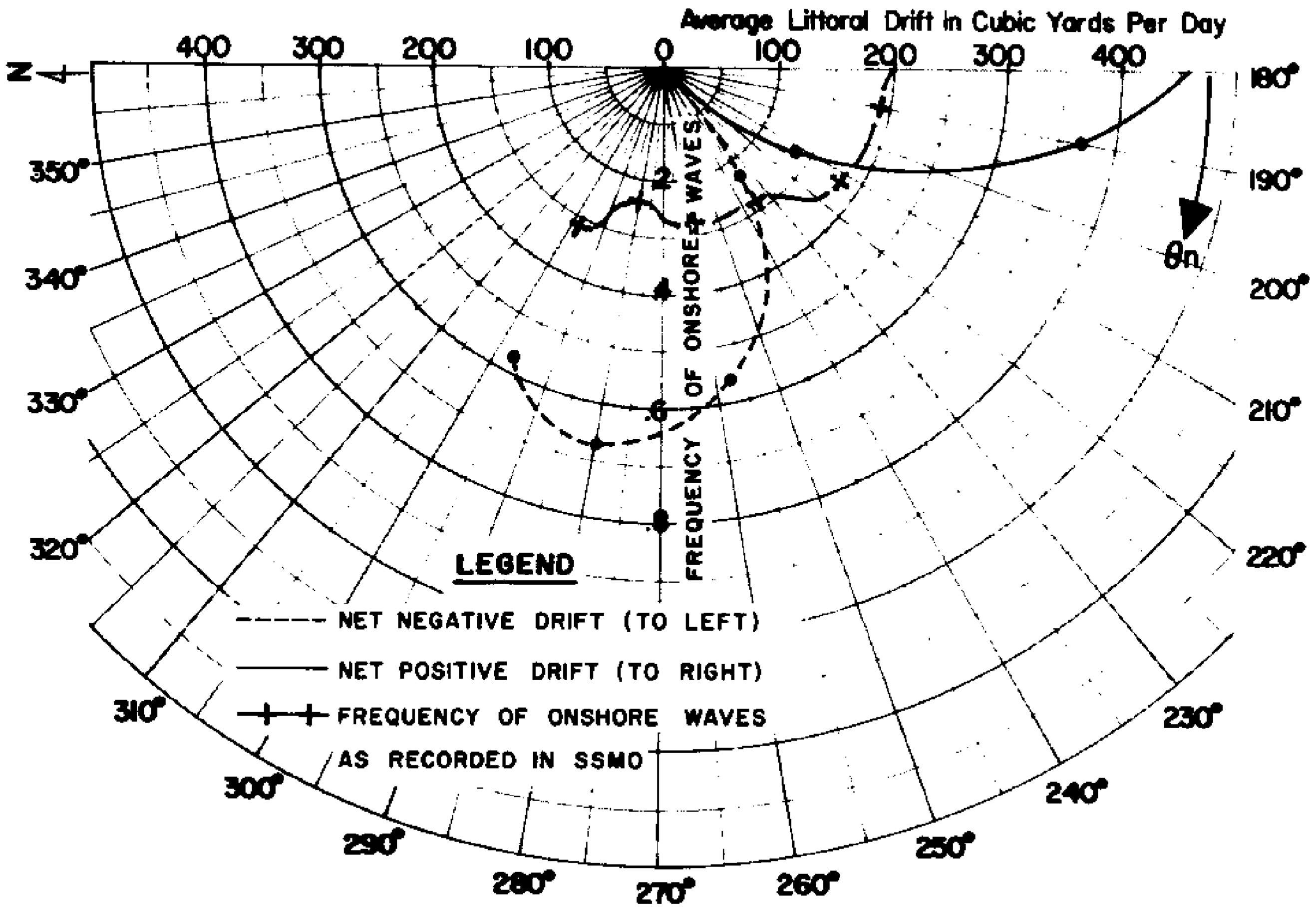

FIGURE A41. VARIATION OF AVERAGE ANNUAL NET LITTORAL DRIFT WITH BEACH ORIENTATION – BIG SARASOTA PASS TO VENICE INLET, FLORIDA

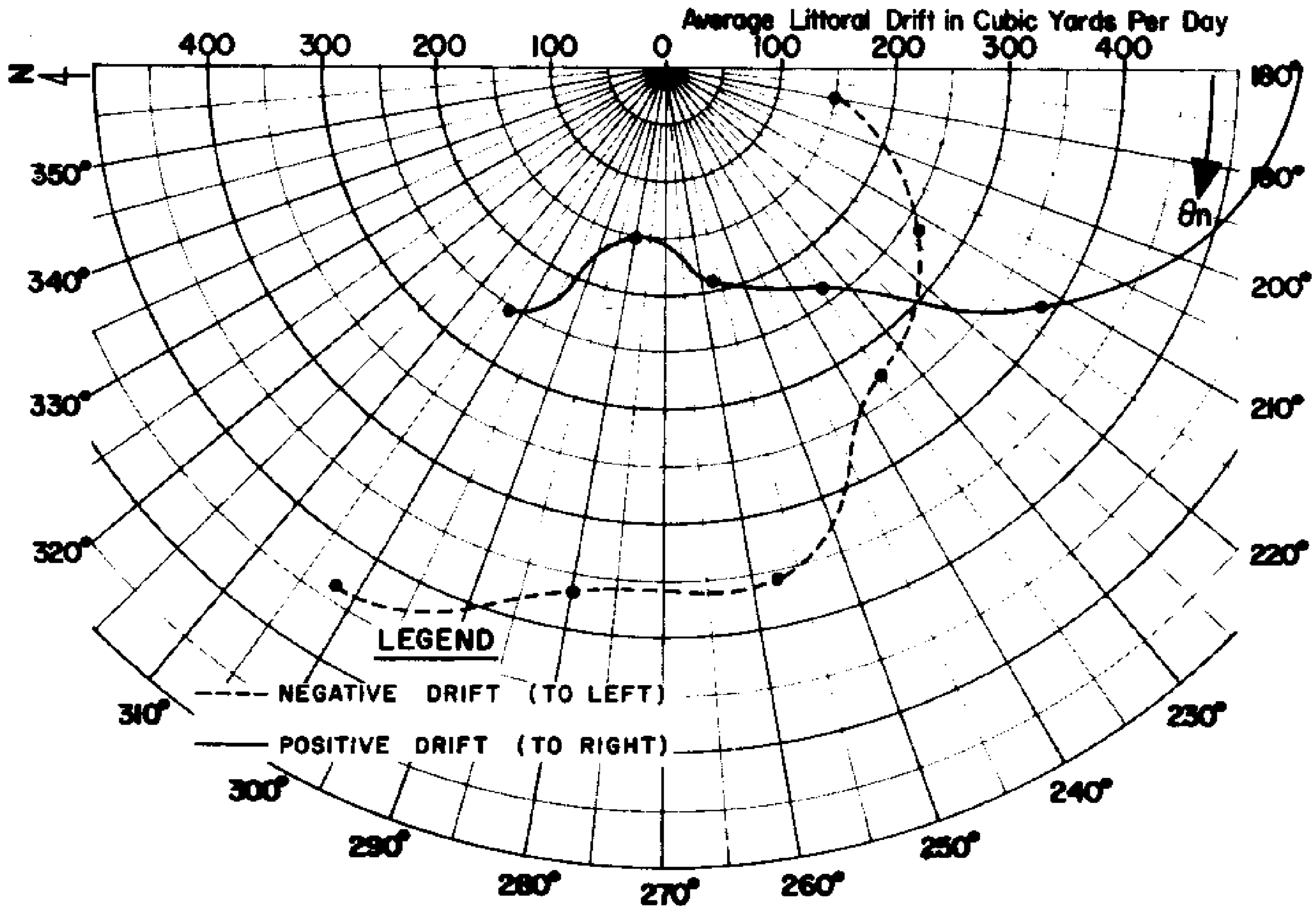

FIGURE A42. VARIATION OF AVERAGE ANNUAL TOTAL LITTORAL DRIFT WITH BEACH ORIENTATION – BIG SARASOTA PASS TO VENICE INLET, FLORIDA

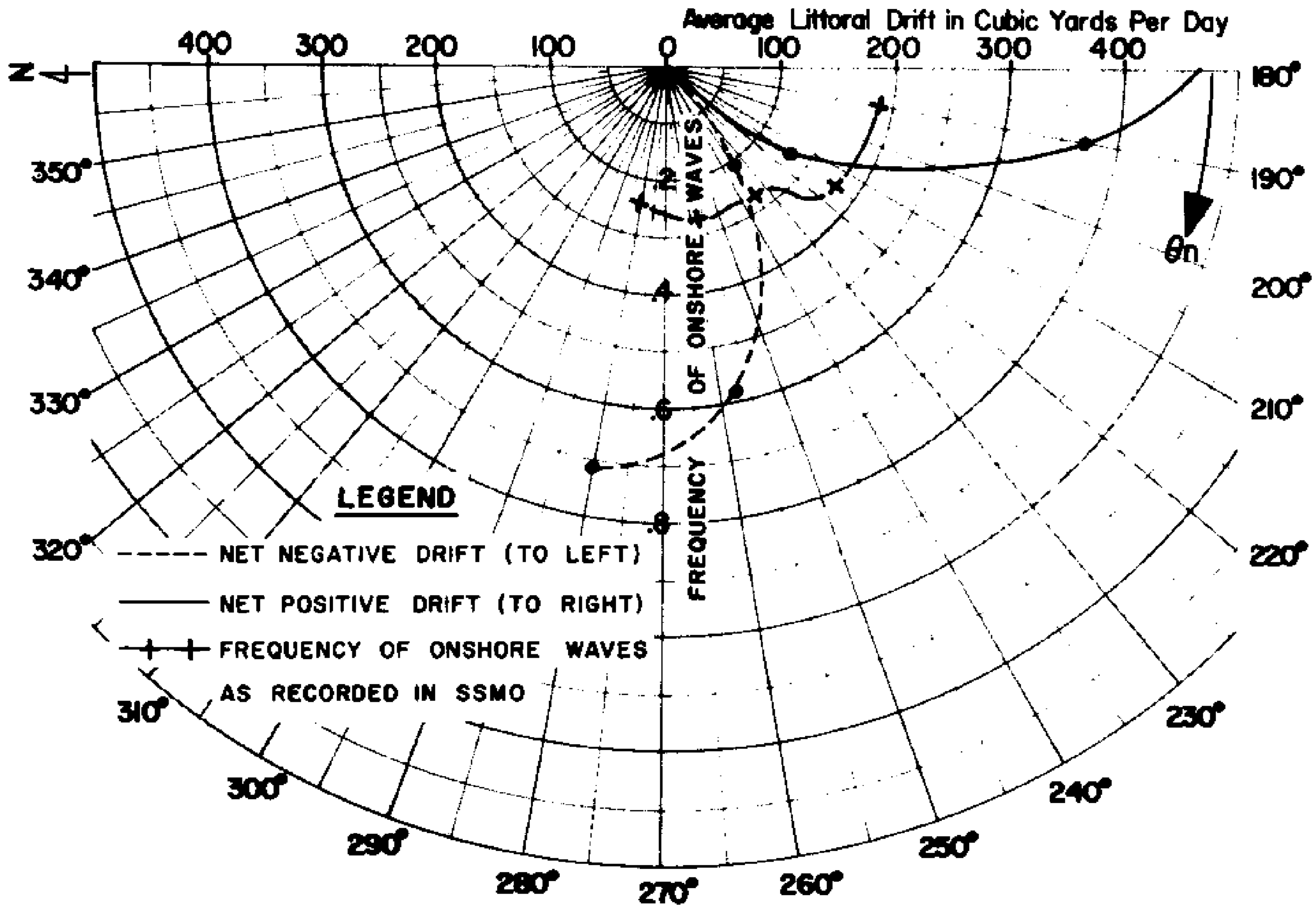

FIGURE A43. VARIATION OF AVERAGE ANNUAL NET LITTORAL DRIFT WITH BEACH ORIENTATION - VENICE INLET TO BOCA GRANDE INLET, FLORIDA

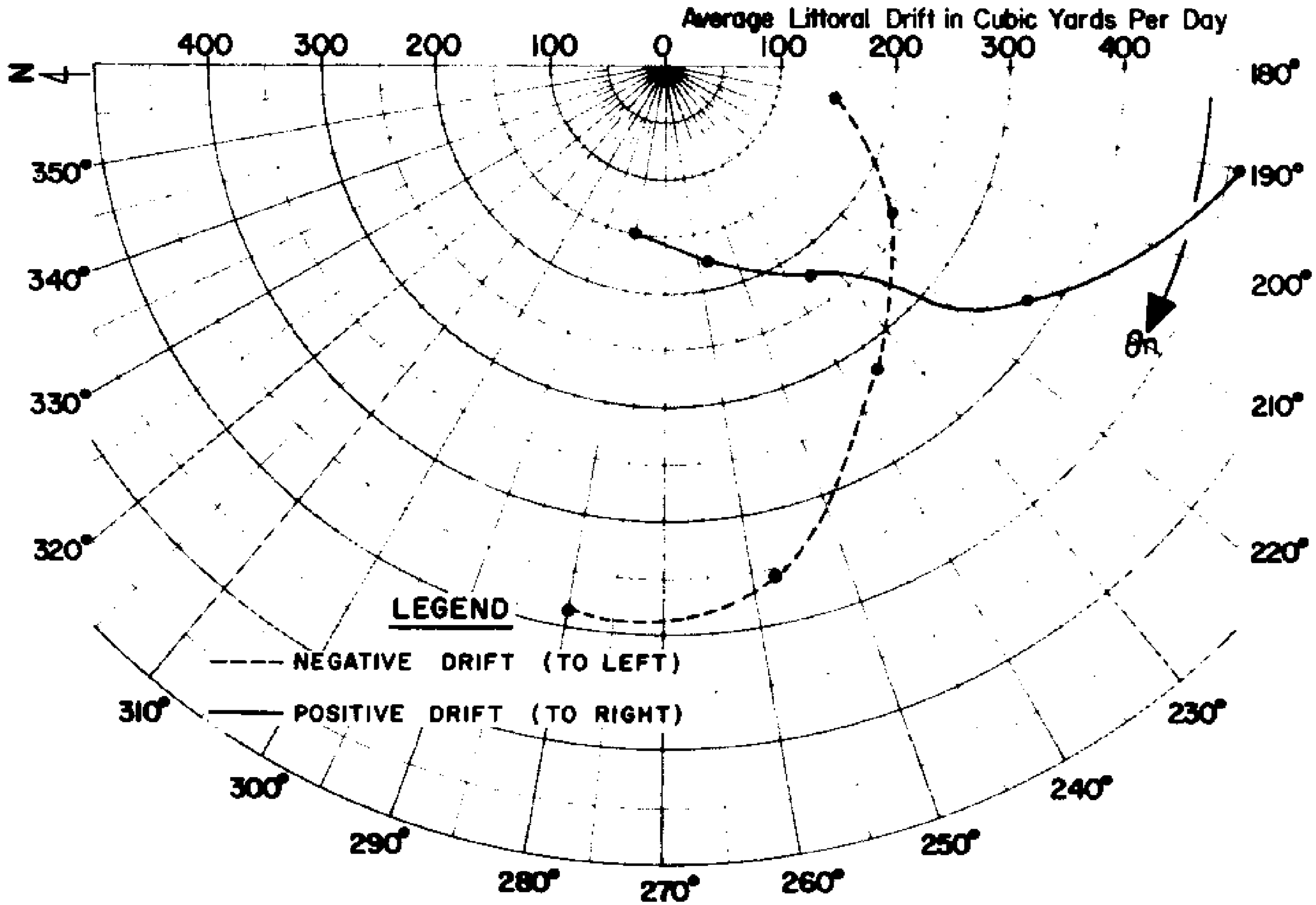

FIGURE A44. VARIATION OF AVERAGE ANNUAL TOTAL LITTORAL DRIFT WITH BEACH ORIENTATION – VENICE INLET TO BOCA GRANDE INLET, FLORIDA

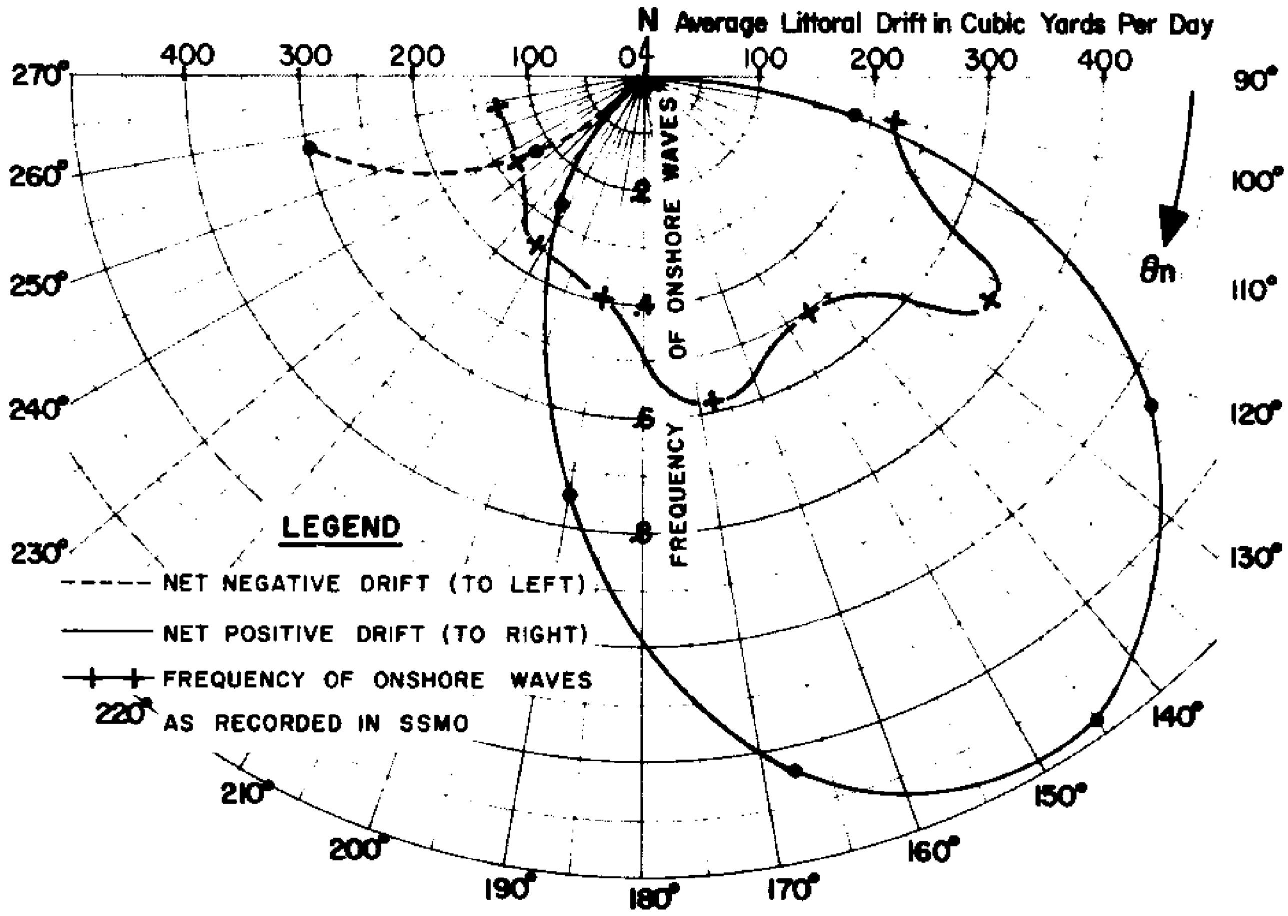

FIGURE A45(a). VARIATION OF AVERAGE ANNUAL NET LITTORAL DRIFT WITH BEACH ORIENTATION - BOCA GRANDE INLET TO SAN CARLOS BAY, FLORIDA

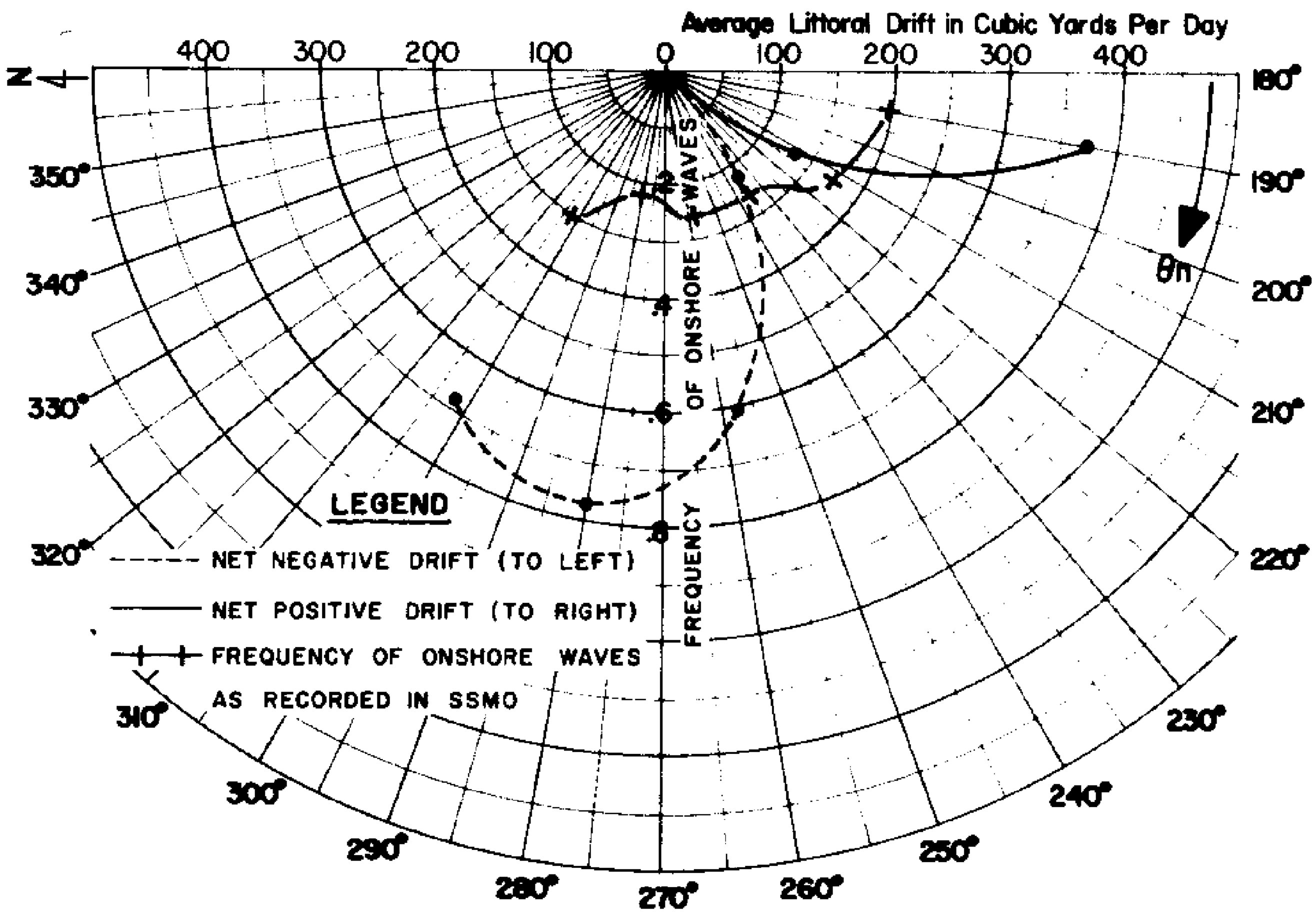

FIGURE A45(b). VARIATION OF AVERAGE ANNUAL NET LITTORAL DRIFT WITH BEACH ORIENTATION — BOCA GRANDE INLET TO SAN CARLOS BAY, FLORIDA

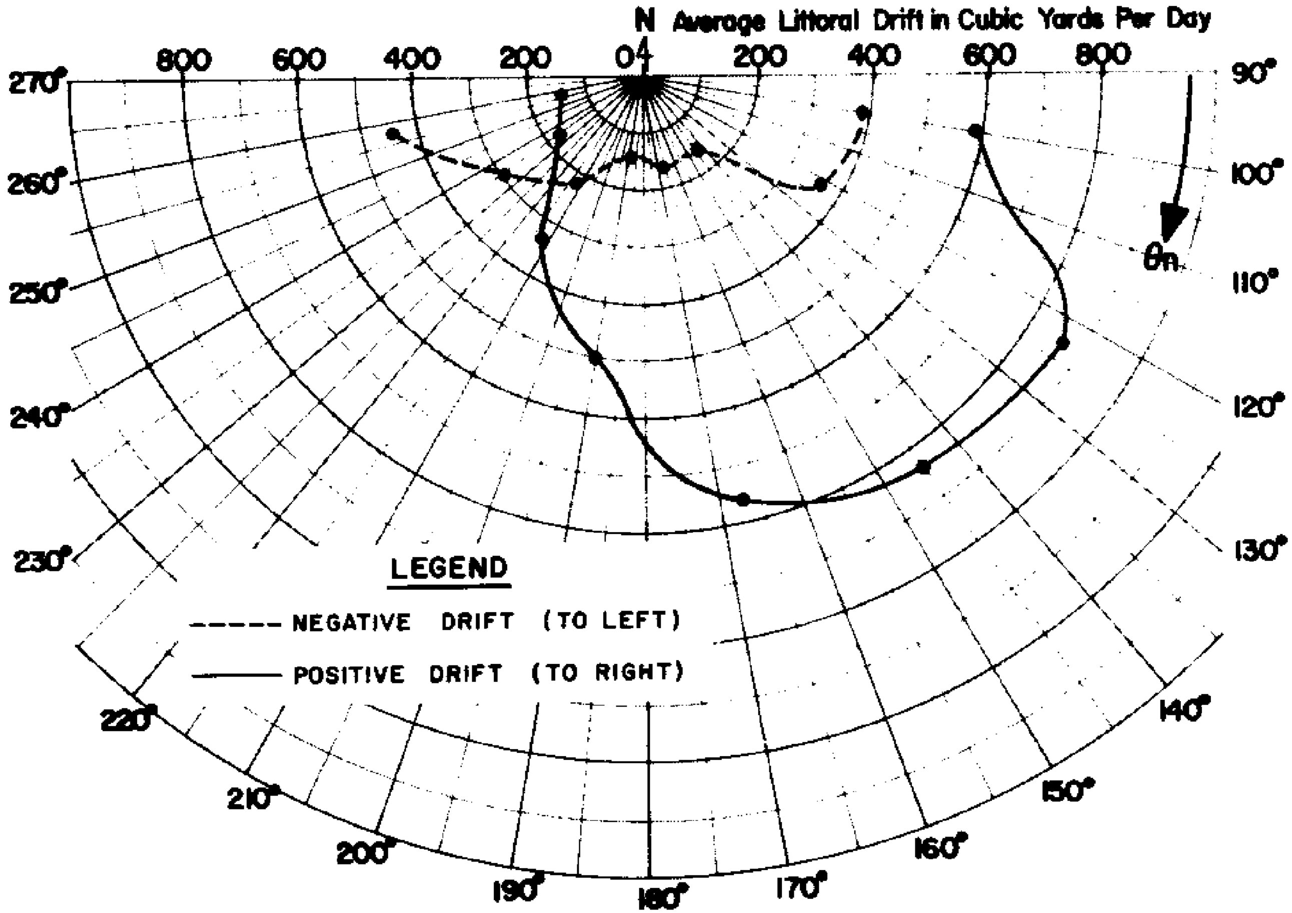

FIGURE A46(a). VARIATION OF AVERAGE ANNUAL TOTAL LITTORAL DRIFT WITH BEACH ORIENTATION – BOCA GRANDE INLET TO SAN CARLOS BAY, FLORIDA

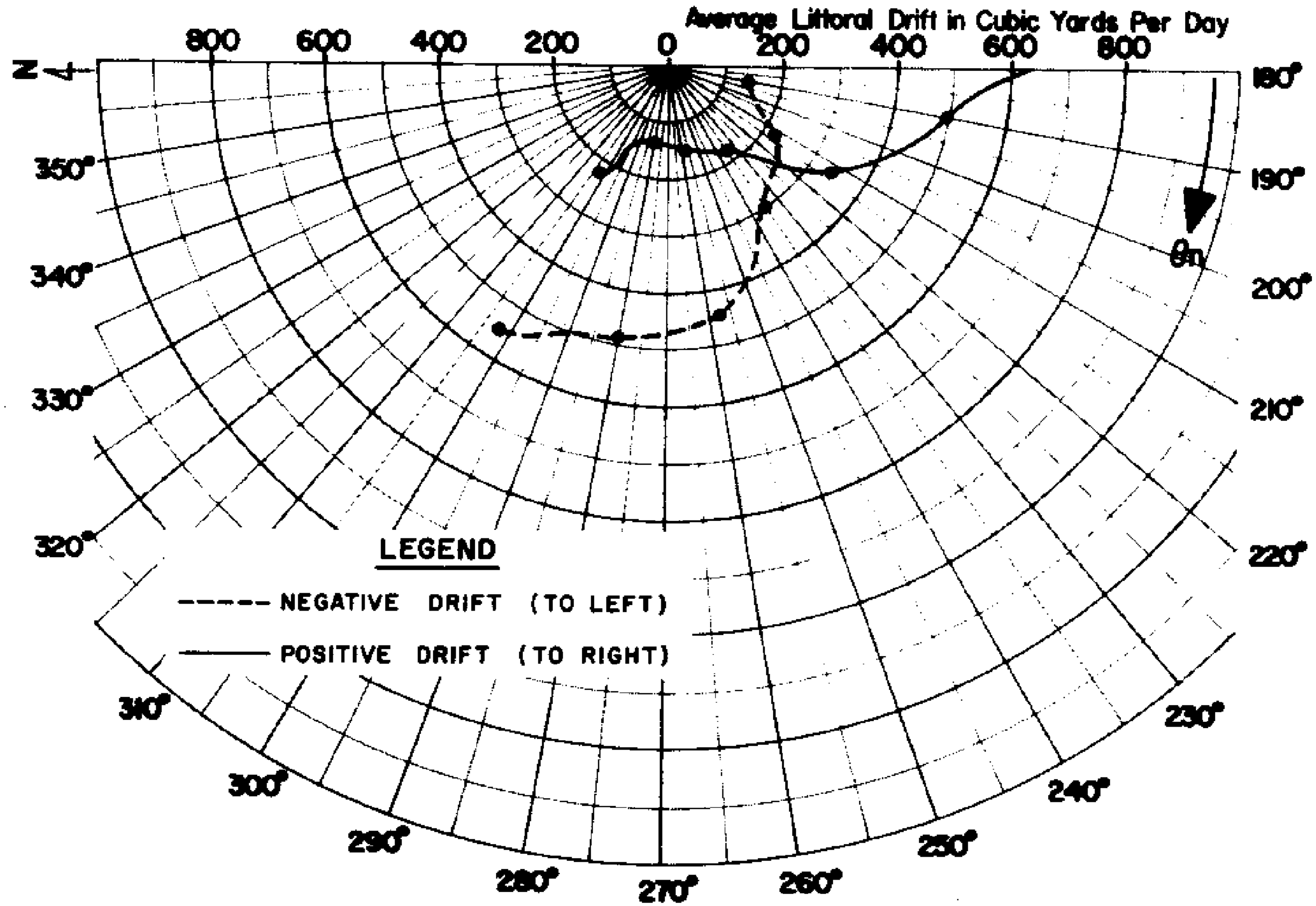

FIGURE A46(b). VARIATION OF AVERAGE ANNUAL TOTAL LITTORAL DRIFT WITH BEACH ORIENTATION – BOCA GRANDE INLET TO SAN CARLOS BAY, FLORIDA

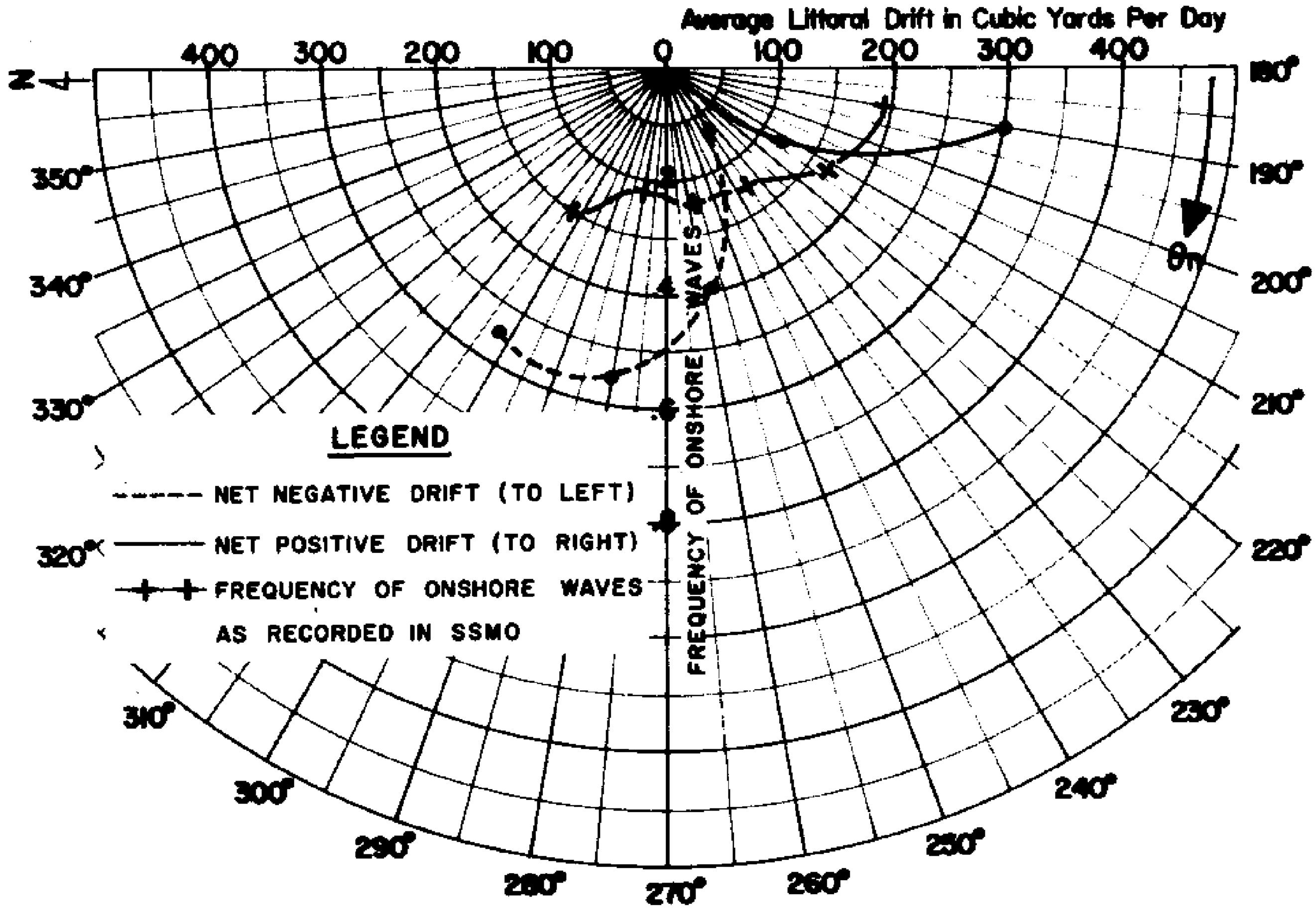

FIGURE A47. VARIATION OF AVERAGE ANNUAL NET LITTORAL DRIFT WITH BEACH ORIENTATION – SAN CARLOS BAY TO WIGGINS PASS, FLORIDA

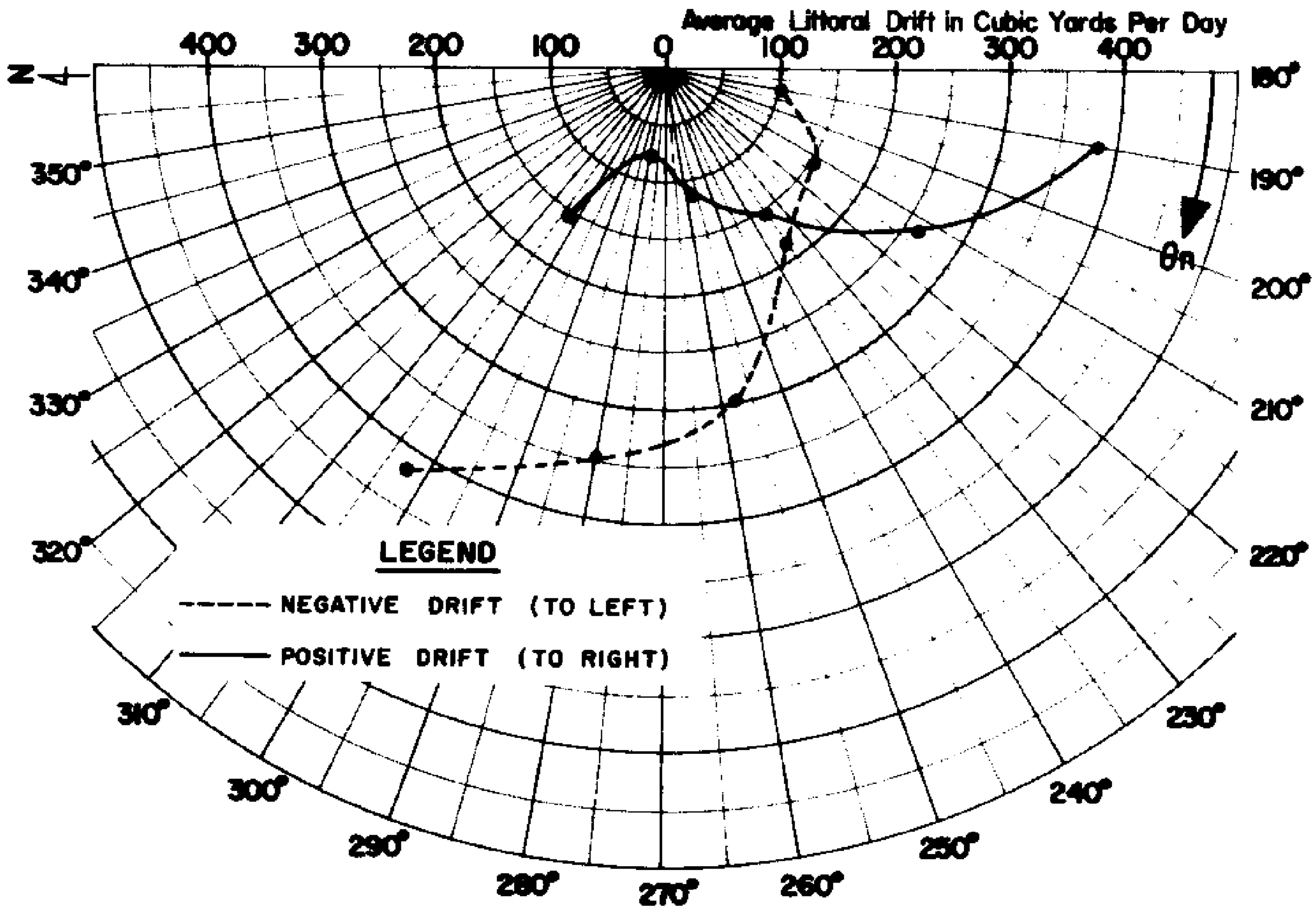

FIGURE A48. VARIATION OF AVERAGE ANNUAL TOTAL LITTORAL DRIFT WITH BEACH ORIENTATION – SAN CARLOS BAY TO WIGGINS PASS, FLORIDA

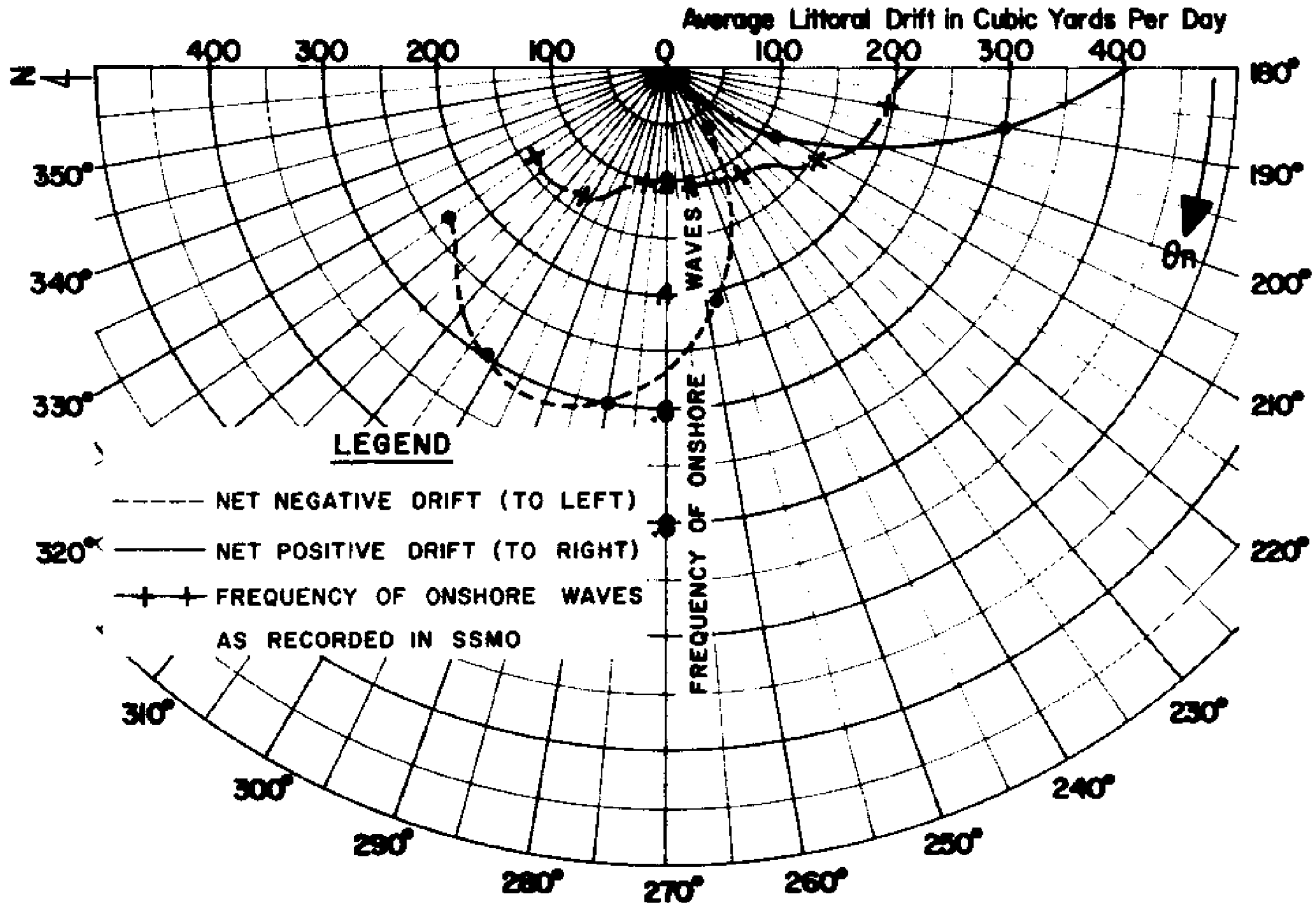

FIGURE A49. VARIATION OF AVERAGE ANNUAL NET LITTORAL DRIFT WITH BEACH ORIENTATION - WIGGINS PASS TO CAPE ROMANO, FLORIDA

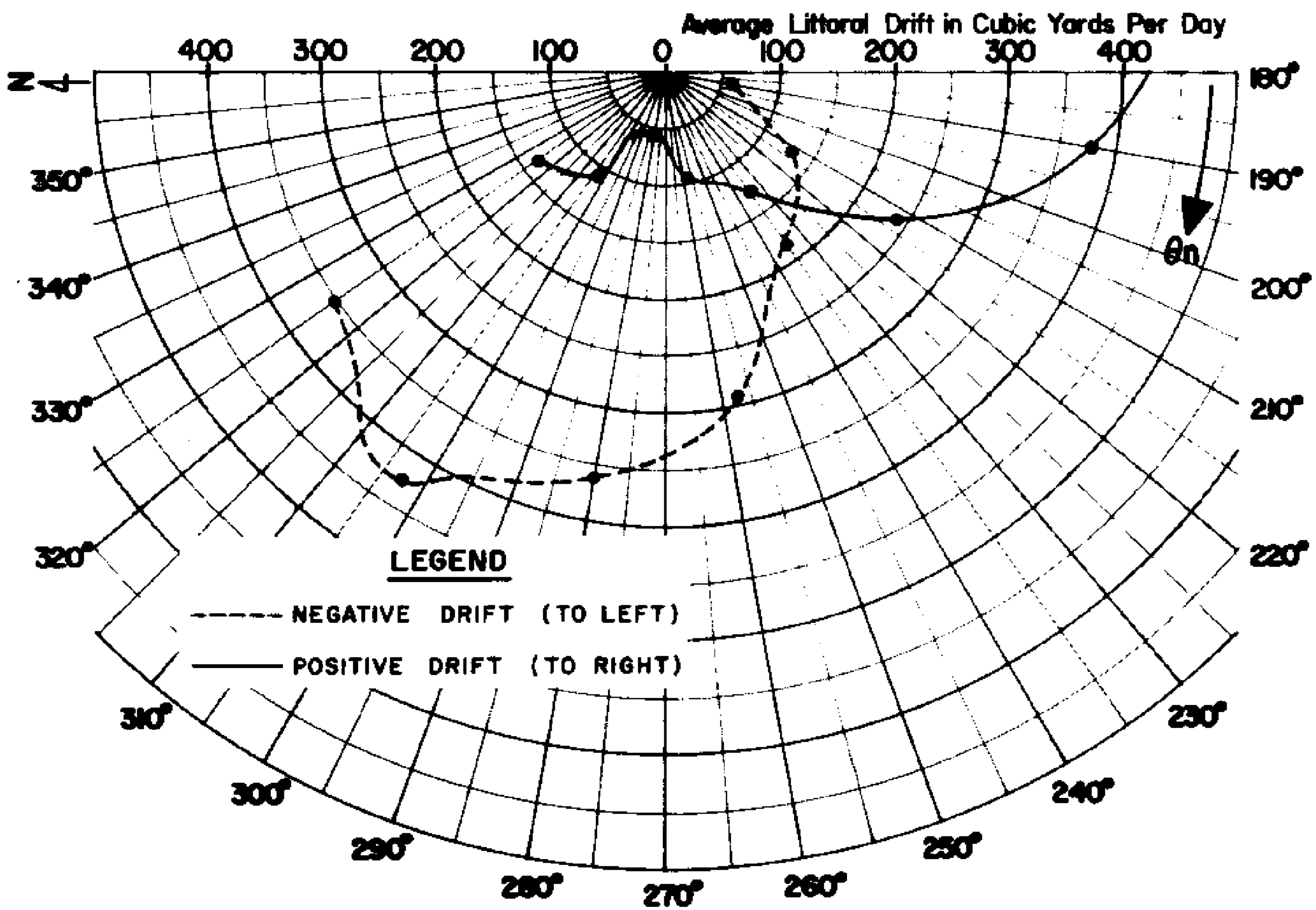

FIGURE A50. VARIATION OF AVERAGE ANNUAL TOTAL LITTORAL DRIFT WITH BEACH ORIENTATION – WIGGINS PASS TO CAPE ROMANO, FLORIDA

Figures B1 Through B12

Wave Height and Wave Period Roses for Offshore Wave

Climate Along the Florida Peninsula

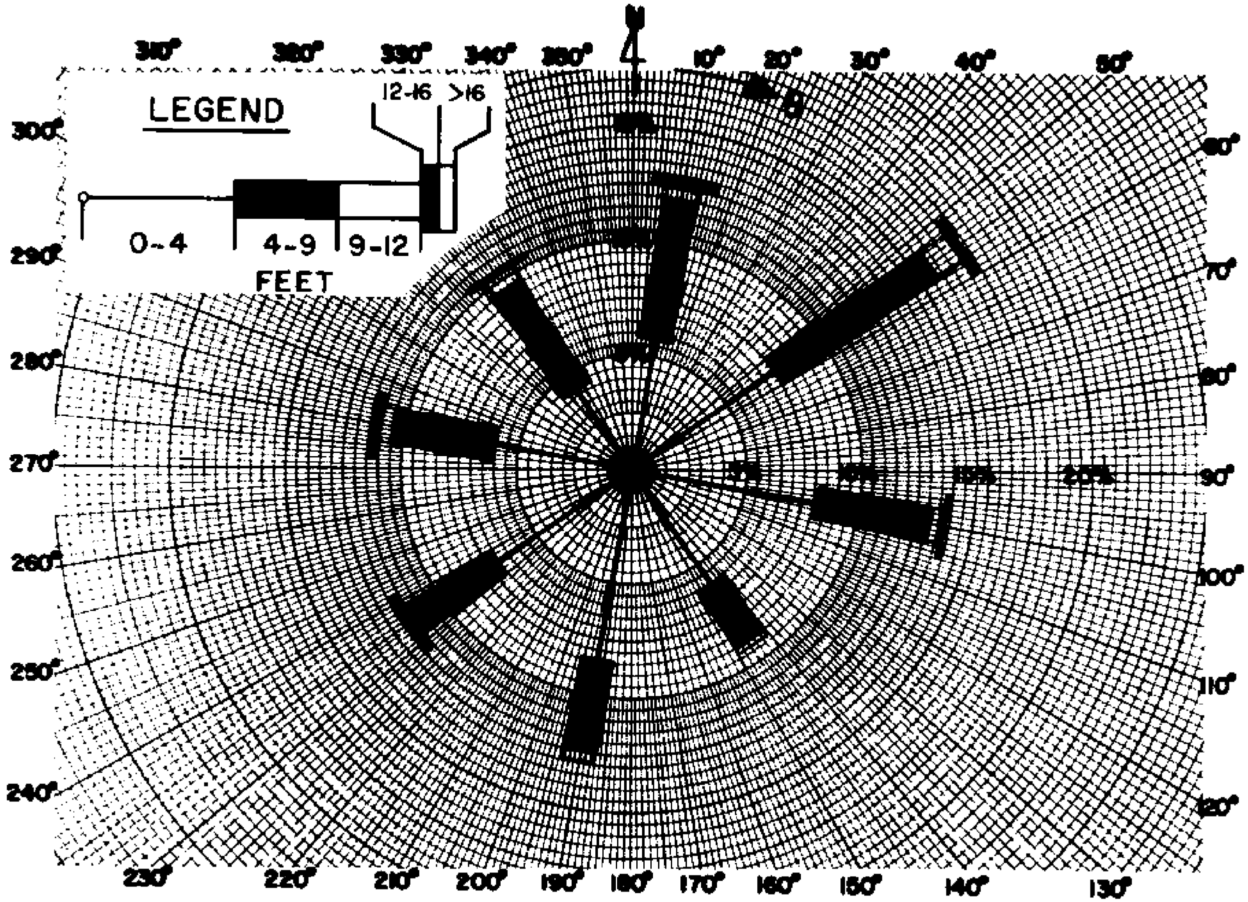

FIGURE B1. WAVE HEIGHT ROSE FOR OFFSHORE WAVE CLIMATE SSMO DATA SQUARE NO. 11 - ANNUAL

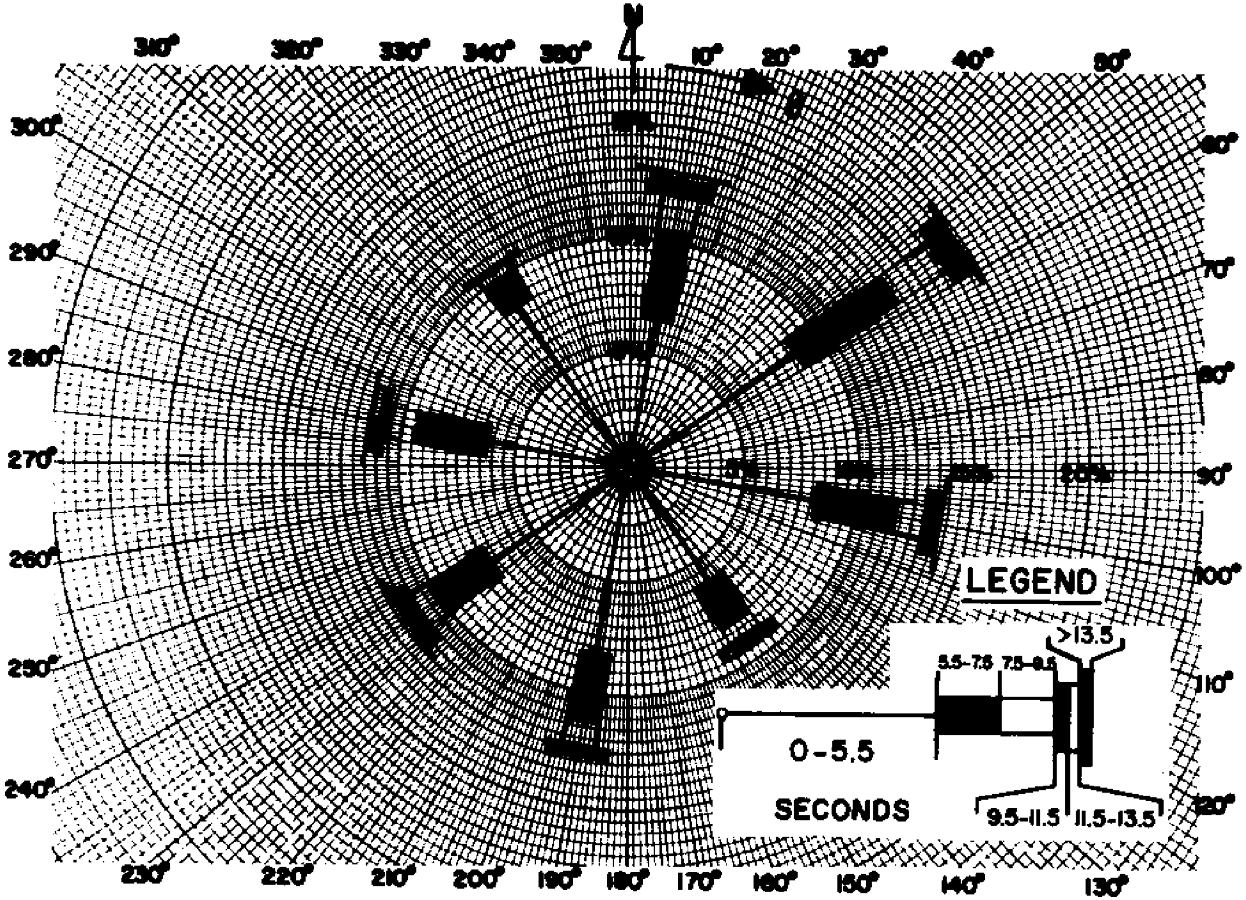

FIGURE B2. WAVE PERIOD ROSE FOR OFFSHORE WAVE CLIMATE
SSMO DATA SQUARE NO. 11 - ANNUAL

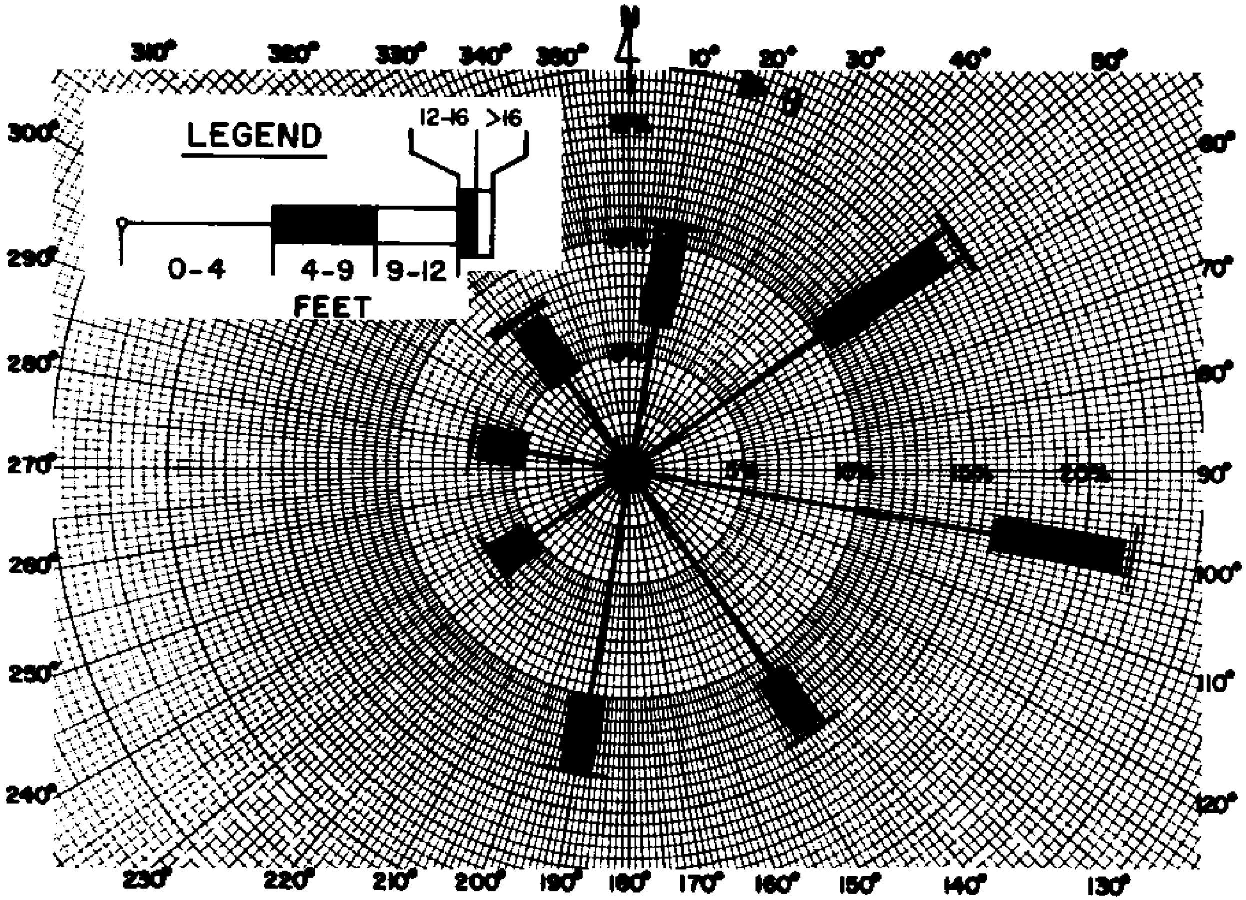

FIGURE B3. WAVE HEIGHT ROSE FOR OFFSHORE WAVE CLIMATE SSMO DATA SQUARE NO. 12 - ANNUAL

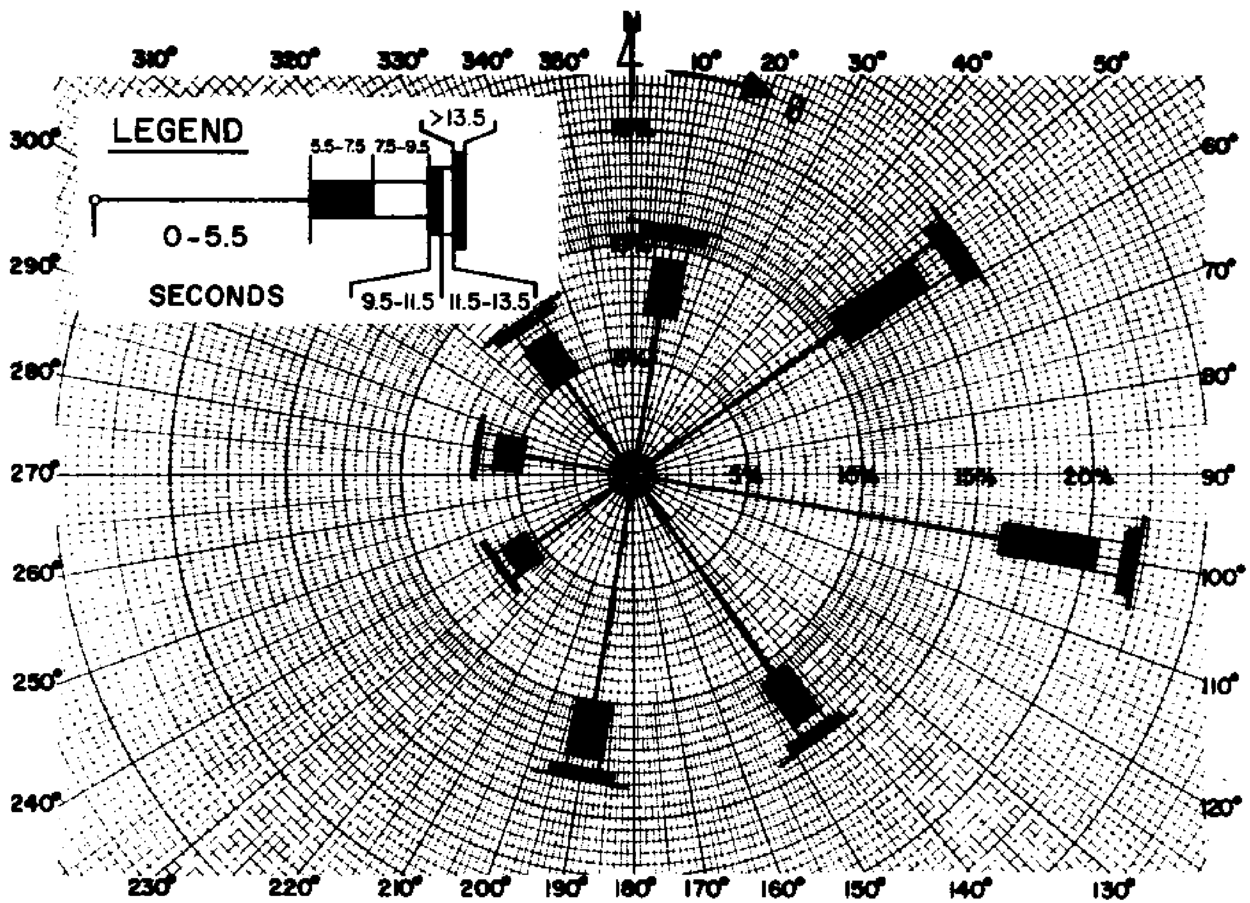

FIGURE B4. WAVE PERIOD ROSE FOR OFFSHORE WAVE CLIMATE
SSMO DATA SQUARE NO. 12 - ANNUAL

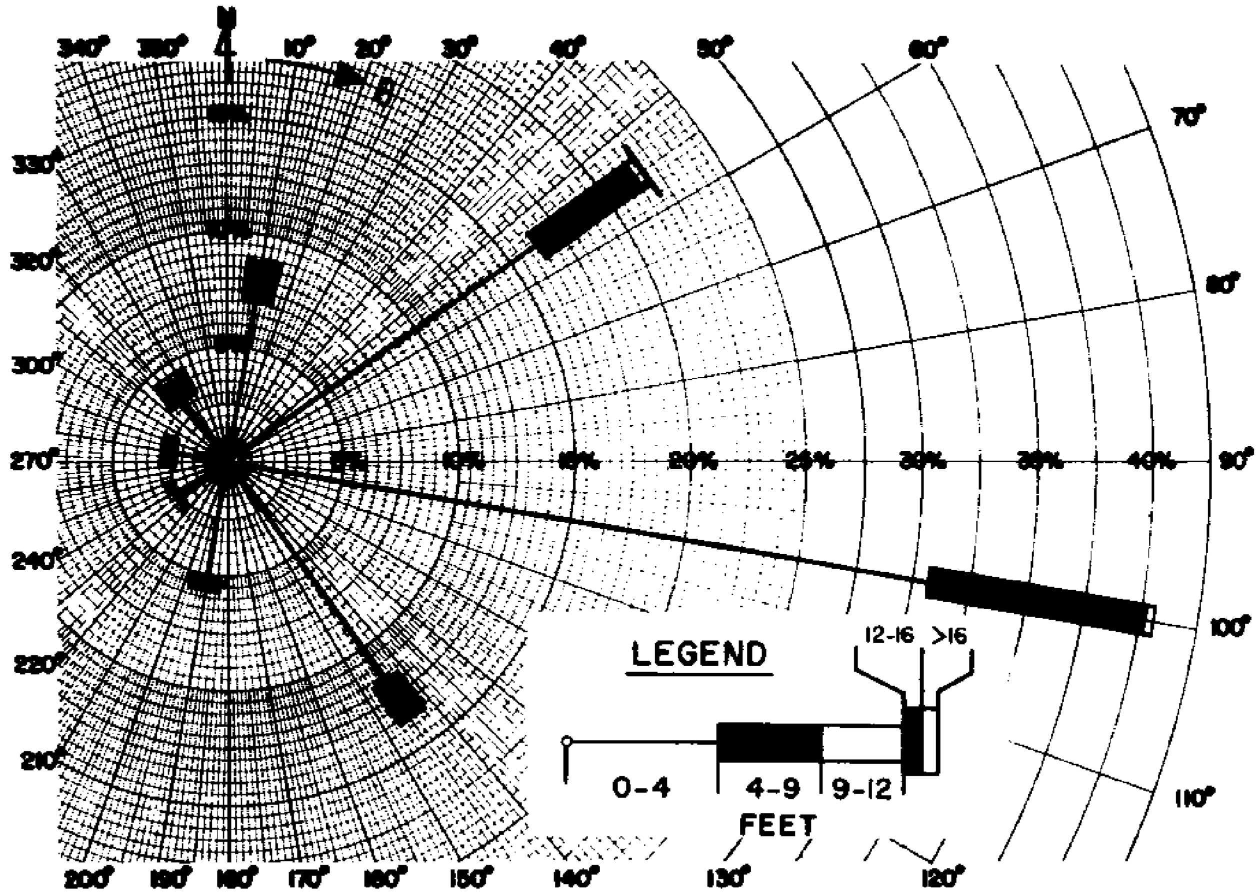

FIGURE B5. WAVE HEIGHT ROSE FOR OFFSHORE WAVE CLIMATE SSMO DATA SQUARE NO. 13 - ANNUAL

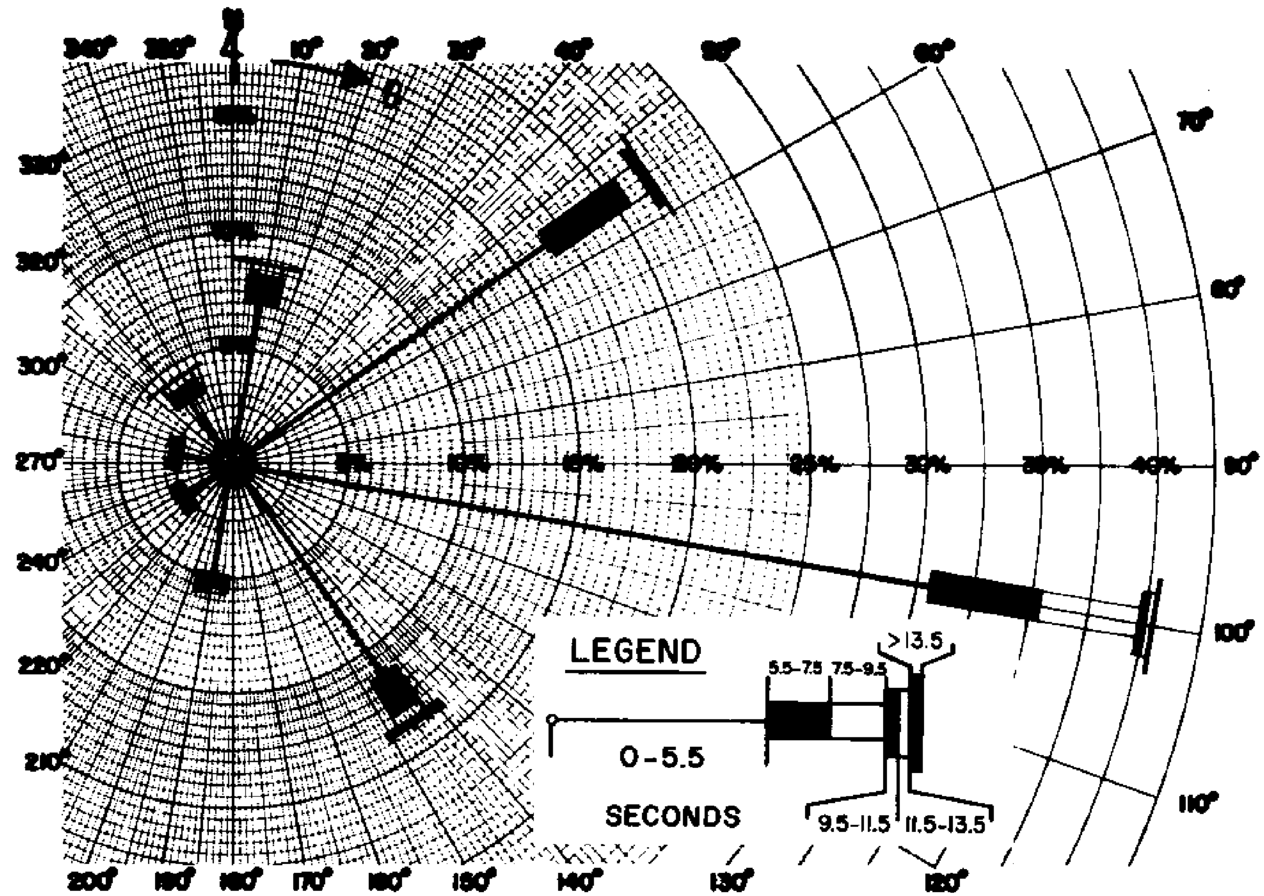

FIGURE B6. WAVE PERIOD ROSE FOR OFFSHORE WAVE CLIMATE
SSMO DATA SQUARE NO. 13 - ANNUAL

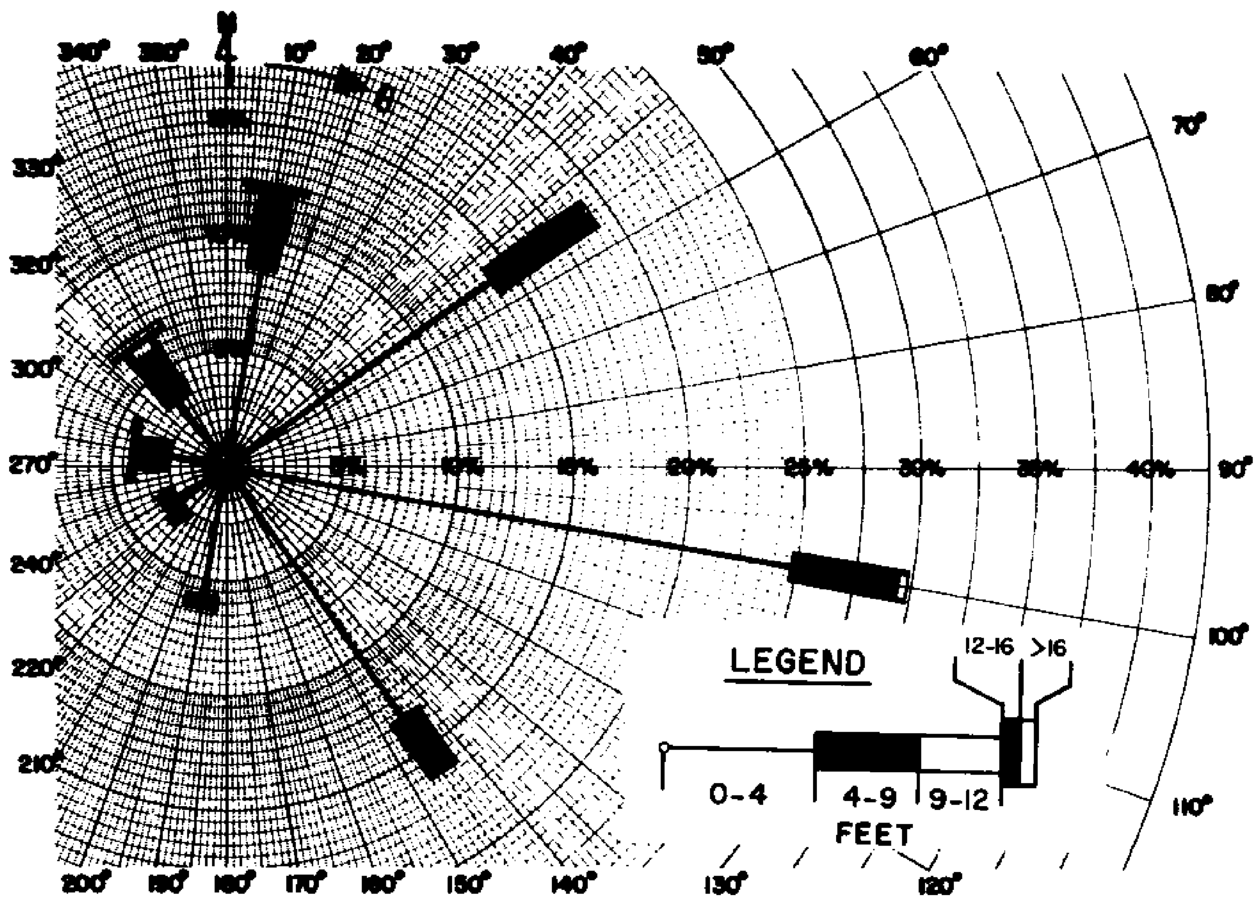

FIGURE B7. WAVE HEIGHT ROSE FOR OFFSHORE WAVE CLIMATE SSMO DATA SQUARE NO. 14 - ANNUAL

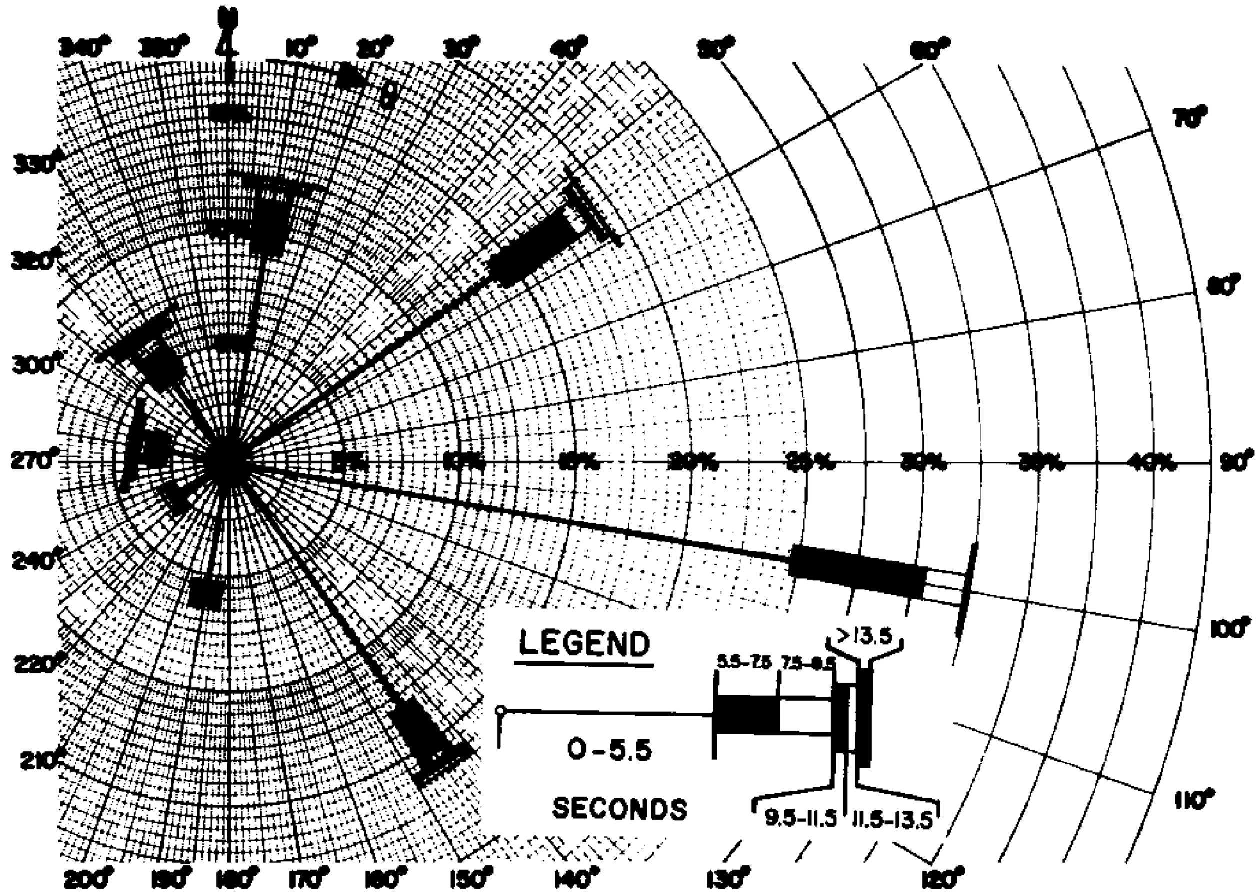

FIGURE B 8. WAVE PERIOD ROSE FOR OFFSHORE WAVE CLIMATE SSMO DATA SQUARE NO. 14 - ANNUAL

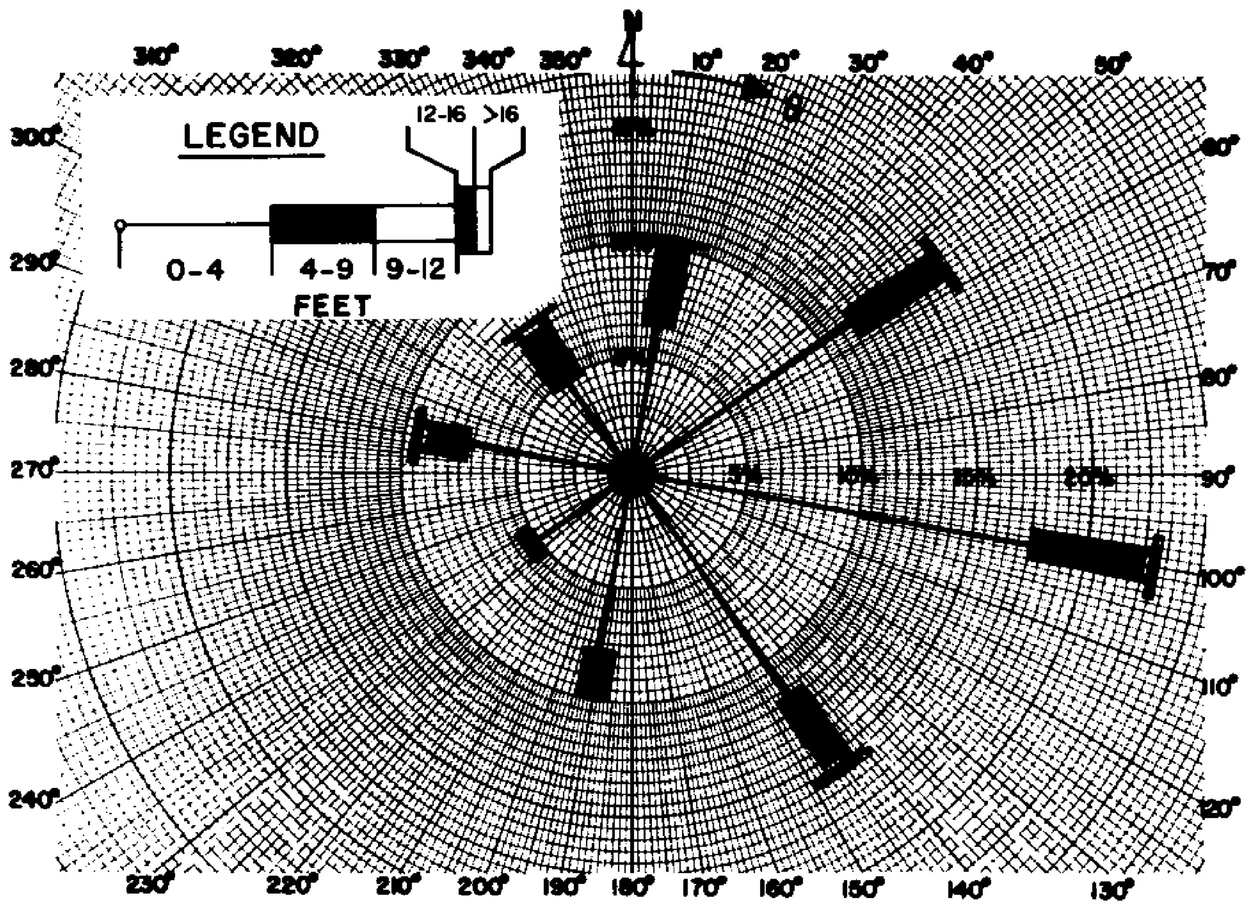

FIGURE B9. WAVE HEIGHT ROSE FOR OFFSHORE WAVE CLIMATE SSMO DATA SQUARE NO. 15 - ANNUAL

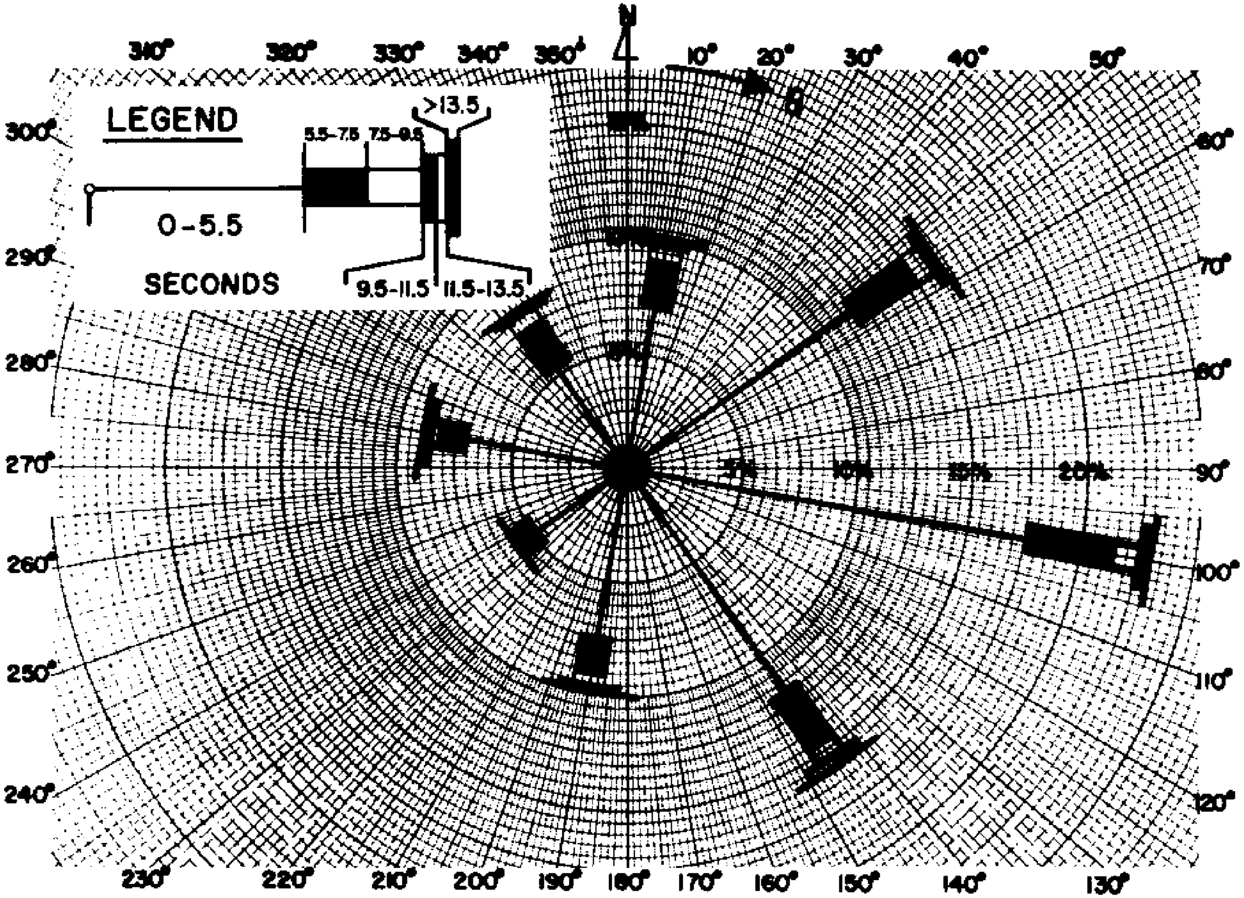

FIGURE B10. WAVE PERIOD ROSE FOR OFFSHORE WAVE CLIMATE SSMO DATA SQUARE NO. 15 - ANNUAL

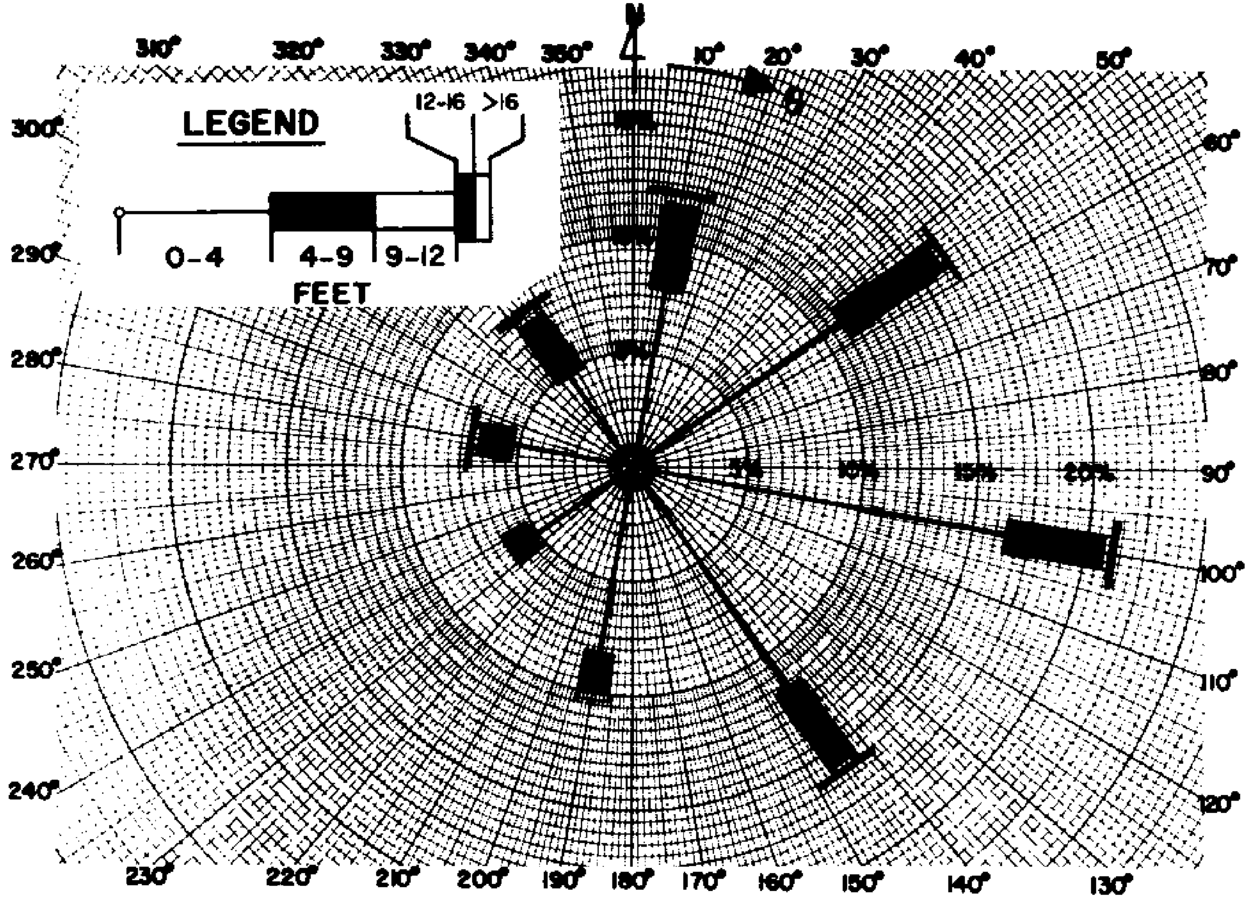

FIGURE B11. WAVE HEIGHT ROSE FOR OFFSHORE WAVE CLIMATE SSMO DATA SQUARE NO. 16 - ANNUAL

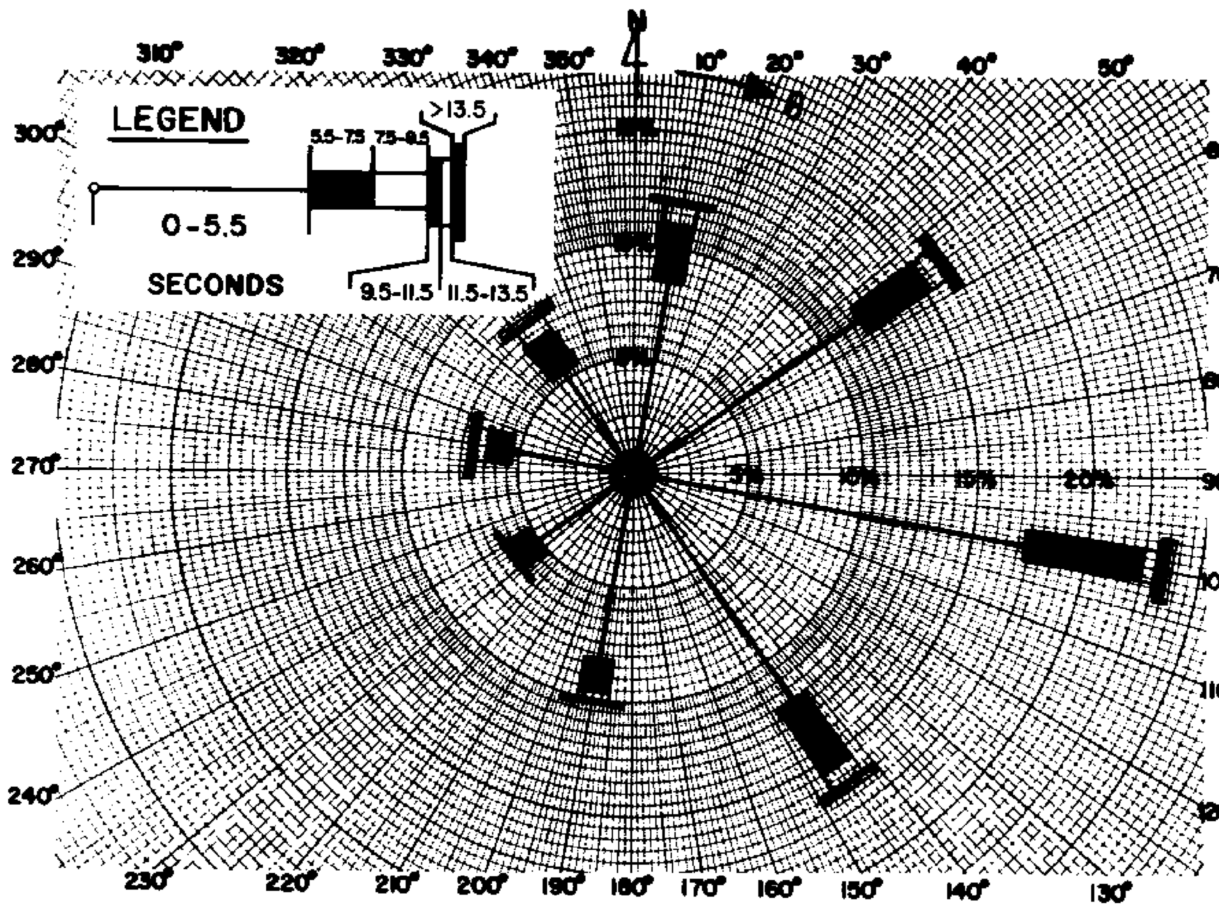

FIGURE B12. WAVE PERIOD ROSE FOR OFFSHORE WAVE CLIMATE
SSMO DATA SQUARE NO. 16 - ANNUAL

Figures C1 Through C24

Average Monthly Net and Average Monthly Total Littoral Drift Diagrams

for the Segment of Shore from Fort Pierce Inlet

to St. Lucie Inlet, Florida

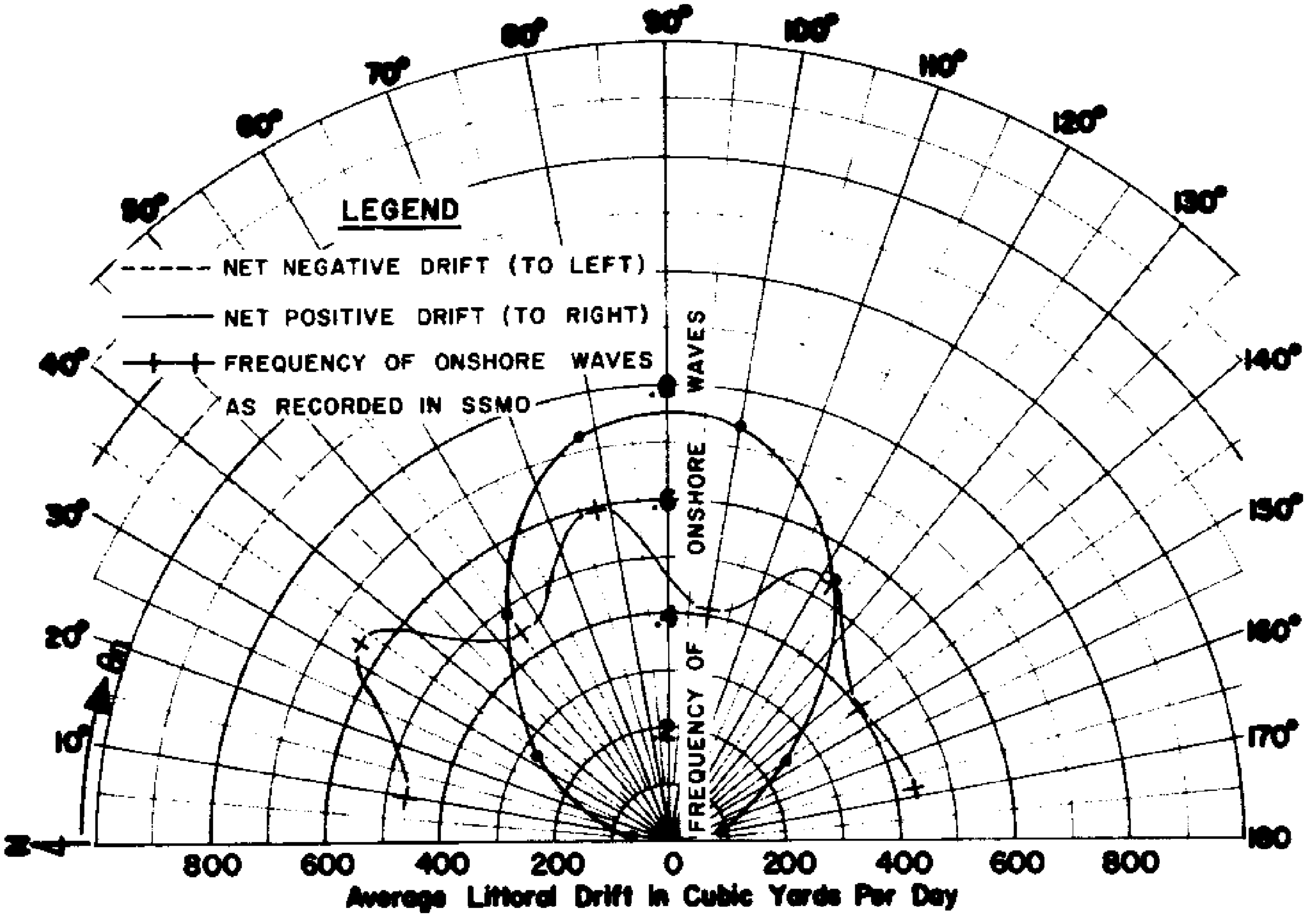

FIGURE CI. VARIATION OF AVERAGE MONTHLY NET LITTORAL DRIFT WITH BEACH ORIENTATION – JANUARY
FORT PIERCE INLET TO ST. LUCIE INLET, FLORIDA

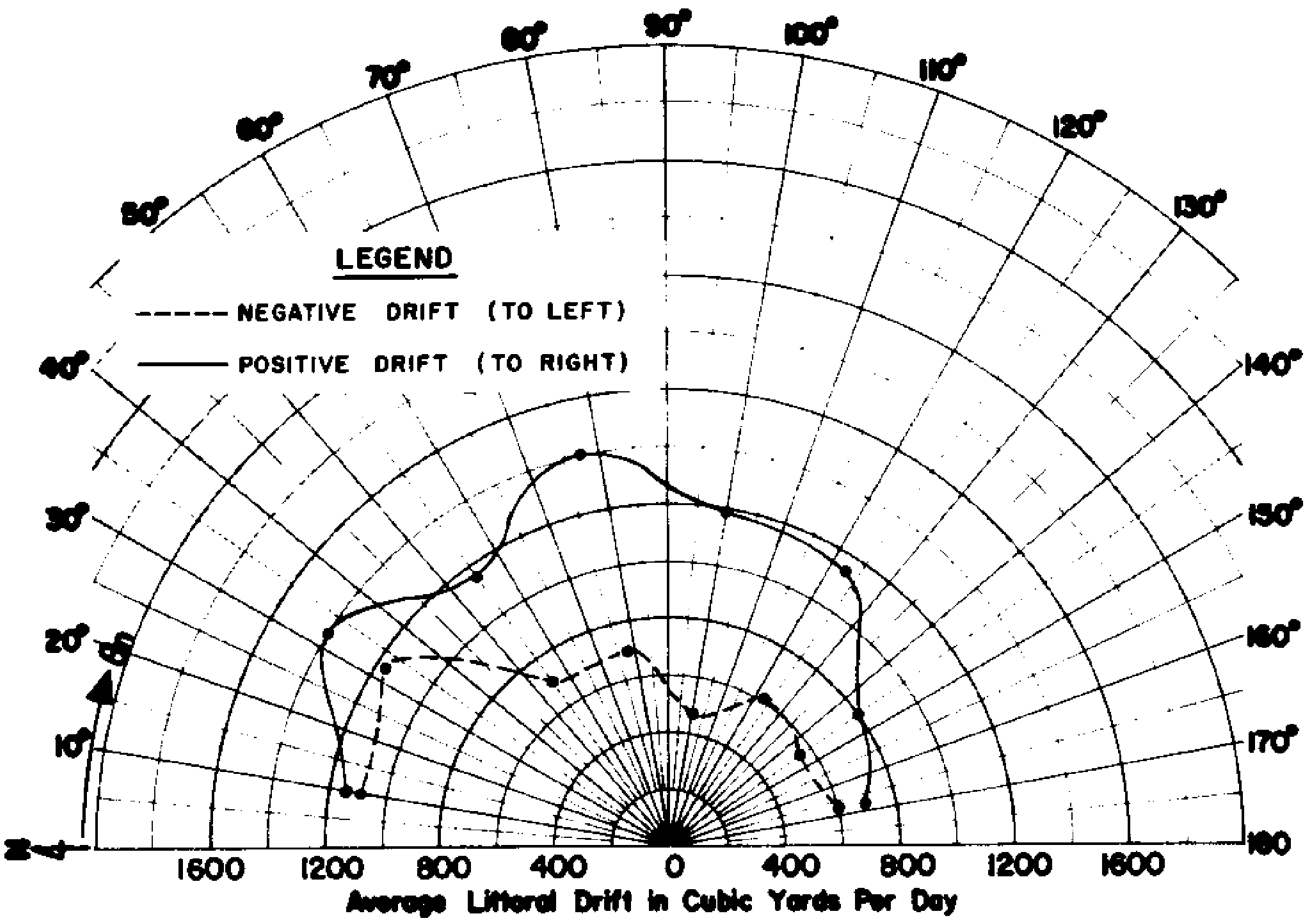

FIGURE C2. VARIATION OF AVERAGE MONTHLY TOTAL LITTORAL DRIFT WITH BEACH ORIENTATION - JANUARY
FORT PIERCE INLET TO ST. LUCIE INLET, FLORIDA

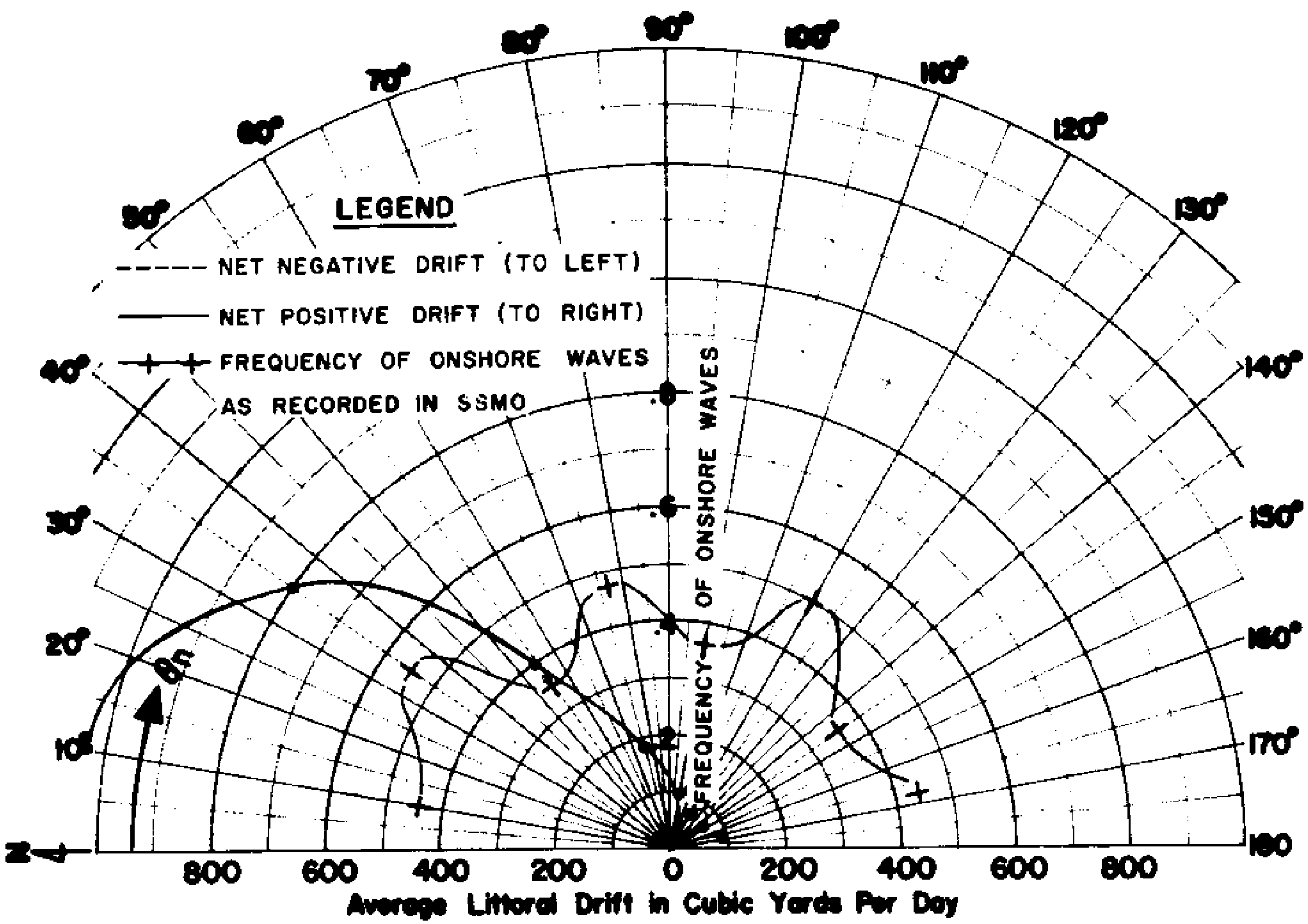

FIGURE C3. VARIATION OF AVERAGE MONTHLY NET LITTORAL DRIFT WITH BEACH ORIENTATION – FEBRUARY
FORT PIERCE INLET TO ST. LUCIE INLET, FLORIDA

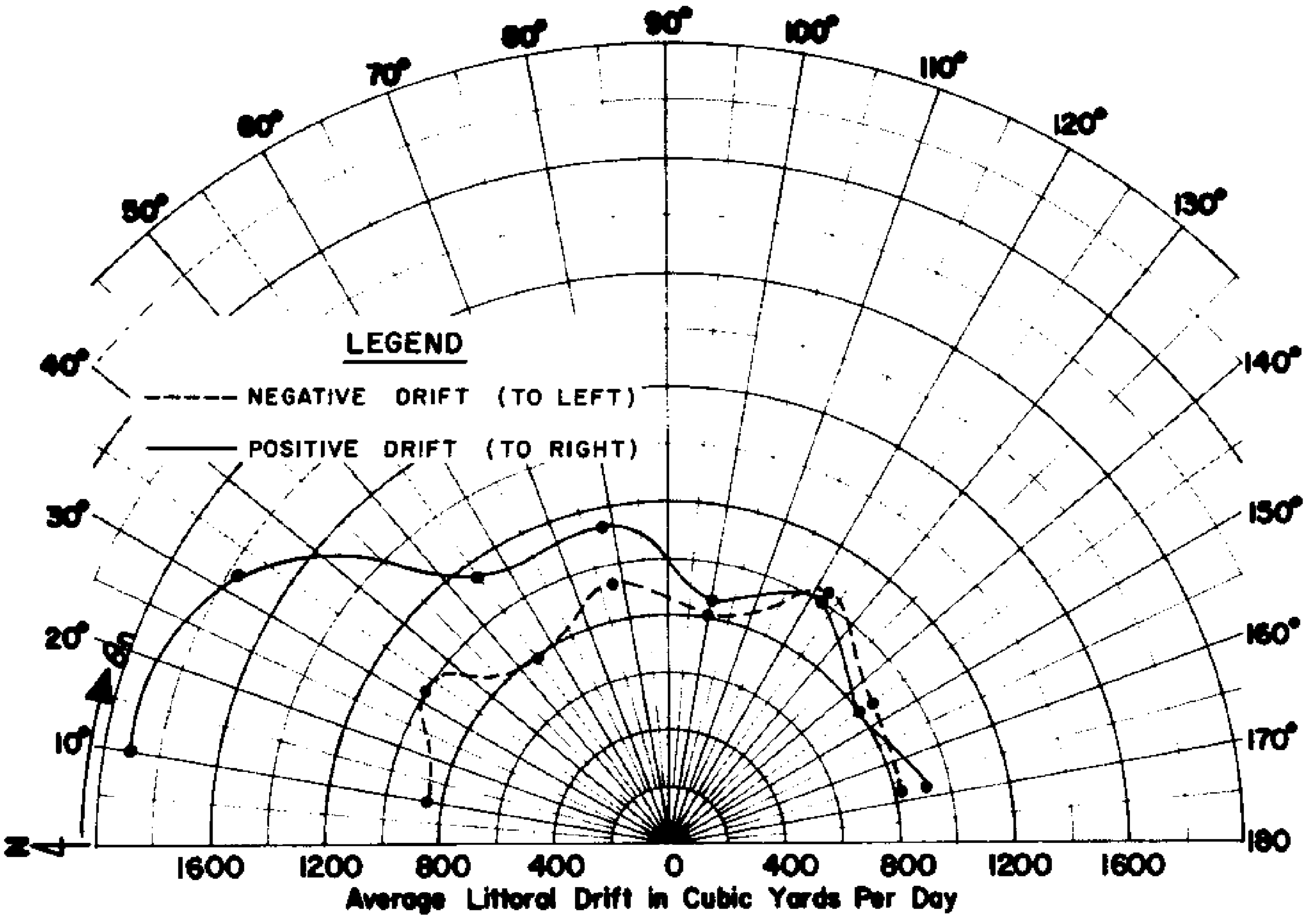

FIGURE C4. VARIATION OF AVERAGE MONTHLY TOTAL LITTORAL DRIFT WITH BEACH ORIENTATION - FEBRUARY
FORT PIERCE INLET TO ST. LUCIE INLET, FLORIDA

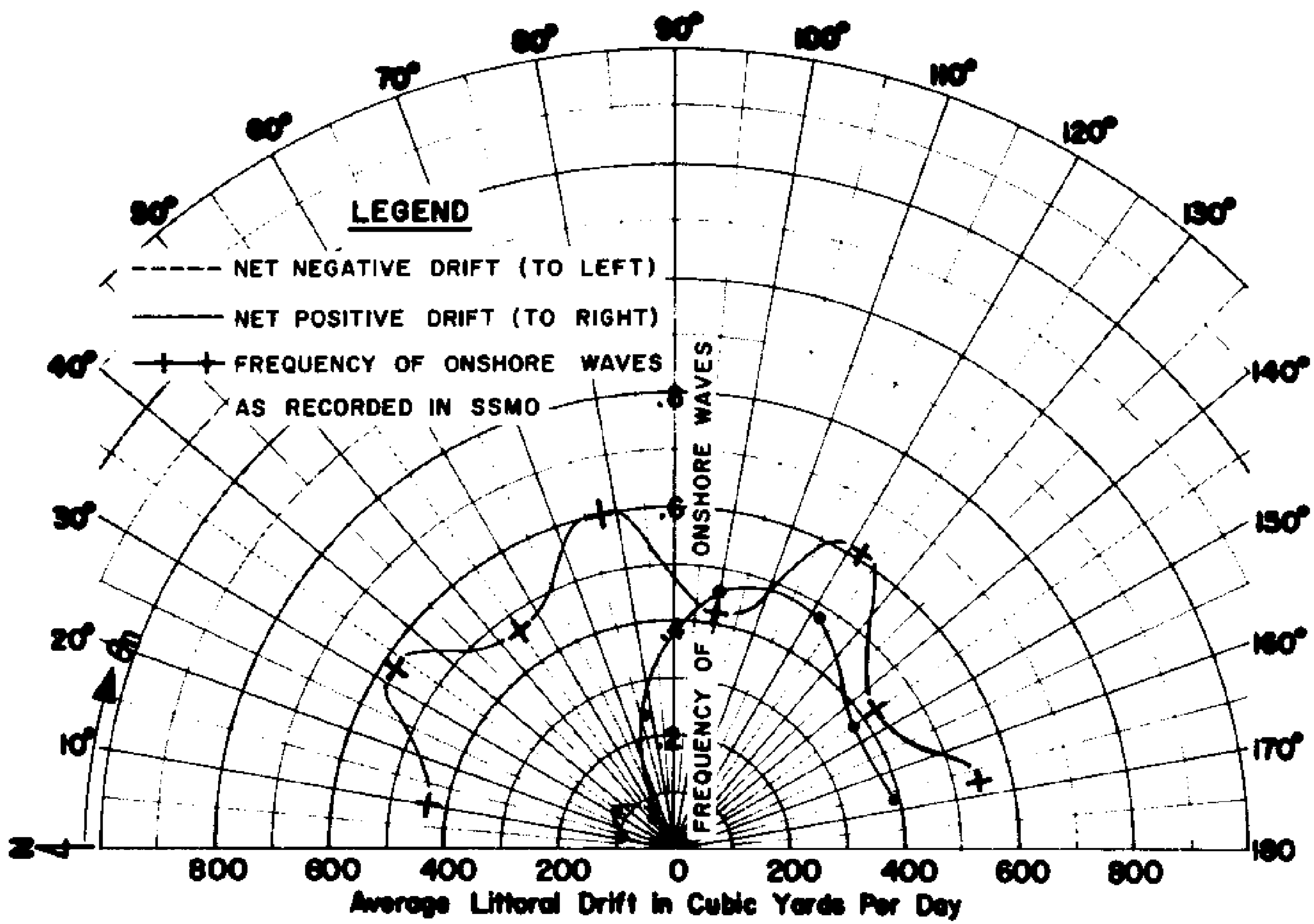

FIGURE C5. VARIATION OF AVERAGE MONTHLY NET LITTORAL DRIFT WITH BEACH ORIENTATION - MARCH
FORT PIERCE INLET TO ST. LUCIE INLET, FLORIDA

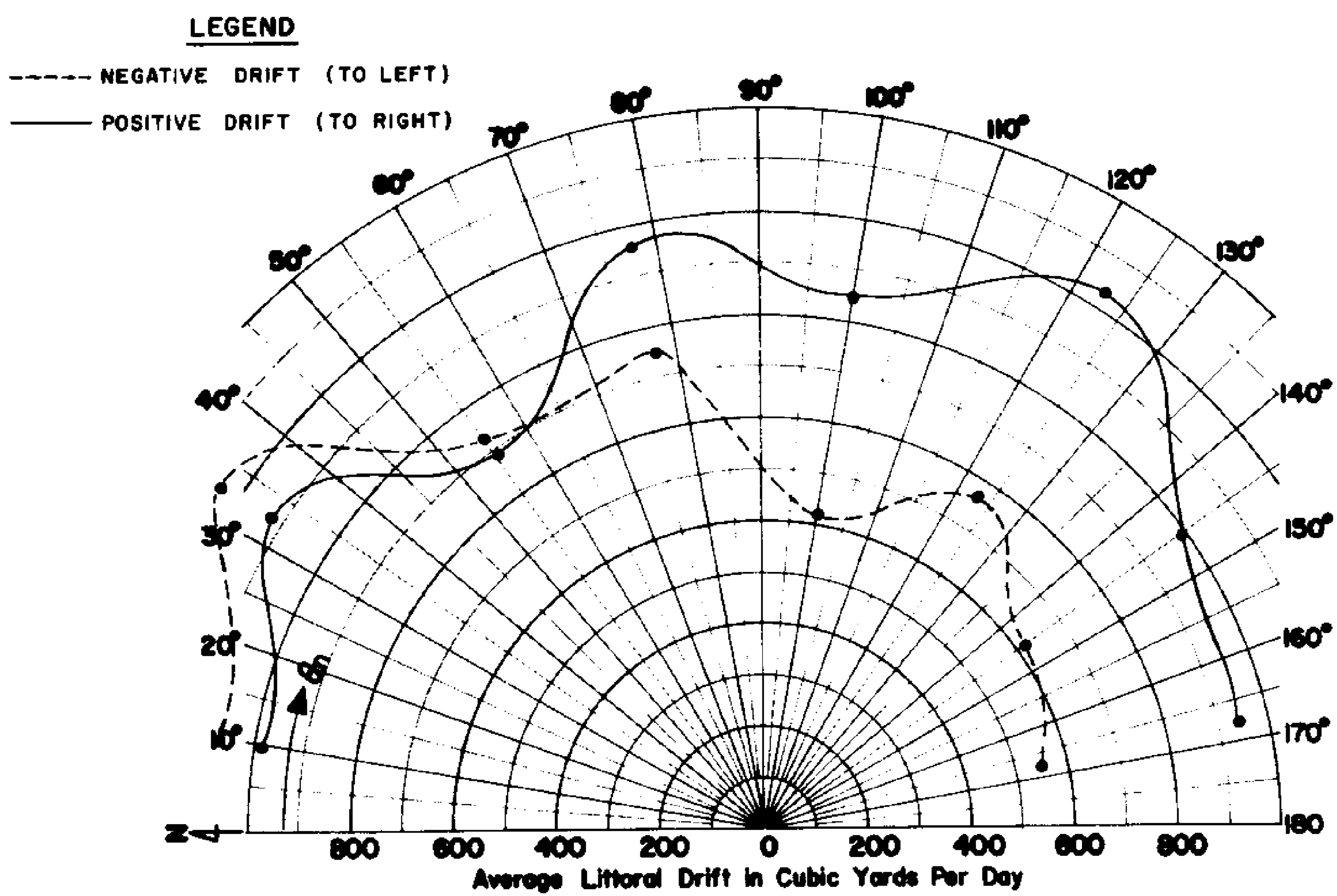

FIGURE C6. VARIATION OF AVERAGE MONTHLY TOTAL LITTORAL DRIFT WITH BEACH ORIENTATION — MARCH
FORT PIERCE INLET TO ST. LUCIE INLET, FLORIDA

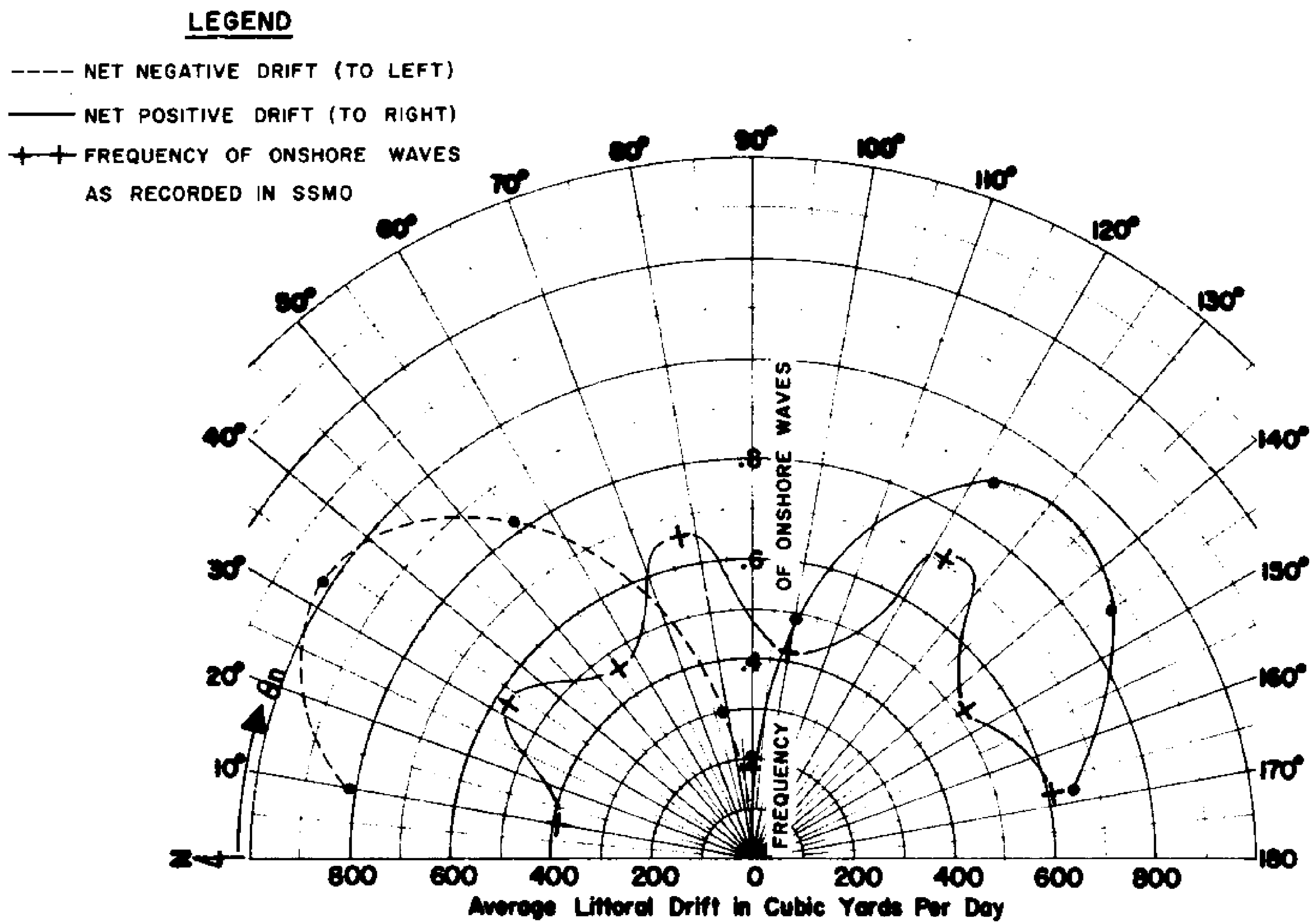

FIGURE C7. VARIATION OF AVERAGE MONTHLY NET LITTORAL DRIFT WITH BEACH ORIENTATION - APRIL
FORT PIERCE INLET TO ST. LUCIE INLET, FLORIDA

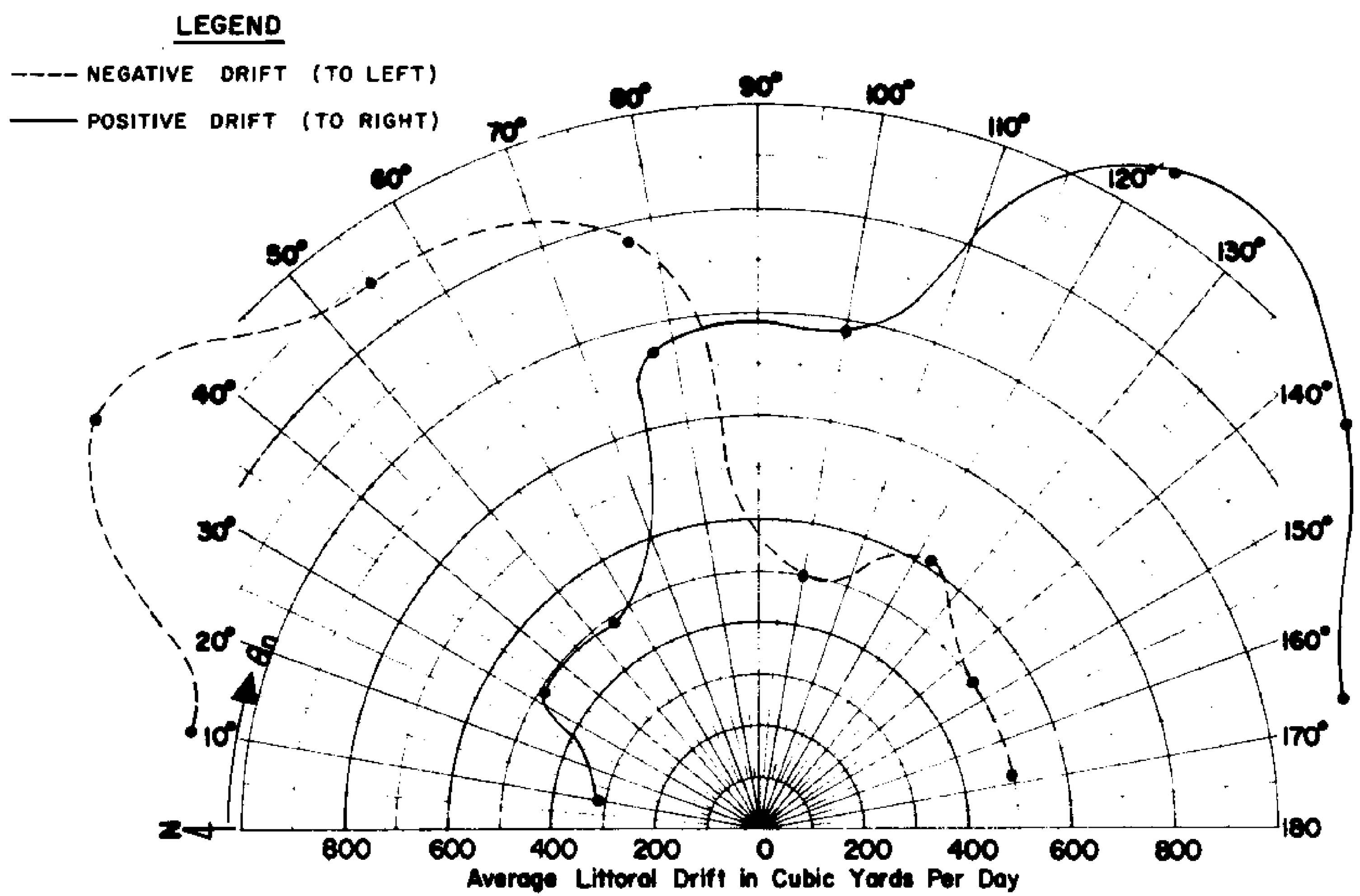

FIGURE C8. VARIATION OF AVERAGE MONTHLY TOTAL LITTORAL DRIFT WITH BEACH ORIENTATION - APRIL
FORT PIERCE INLET TO ST. LUCIE INLET, FLORIDA

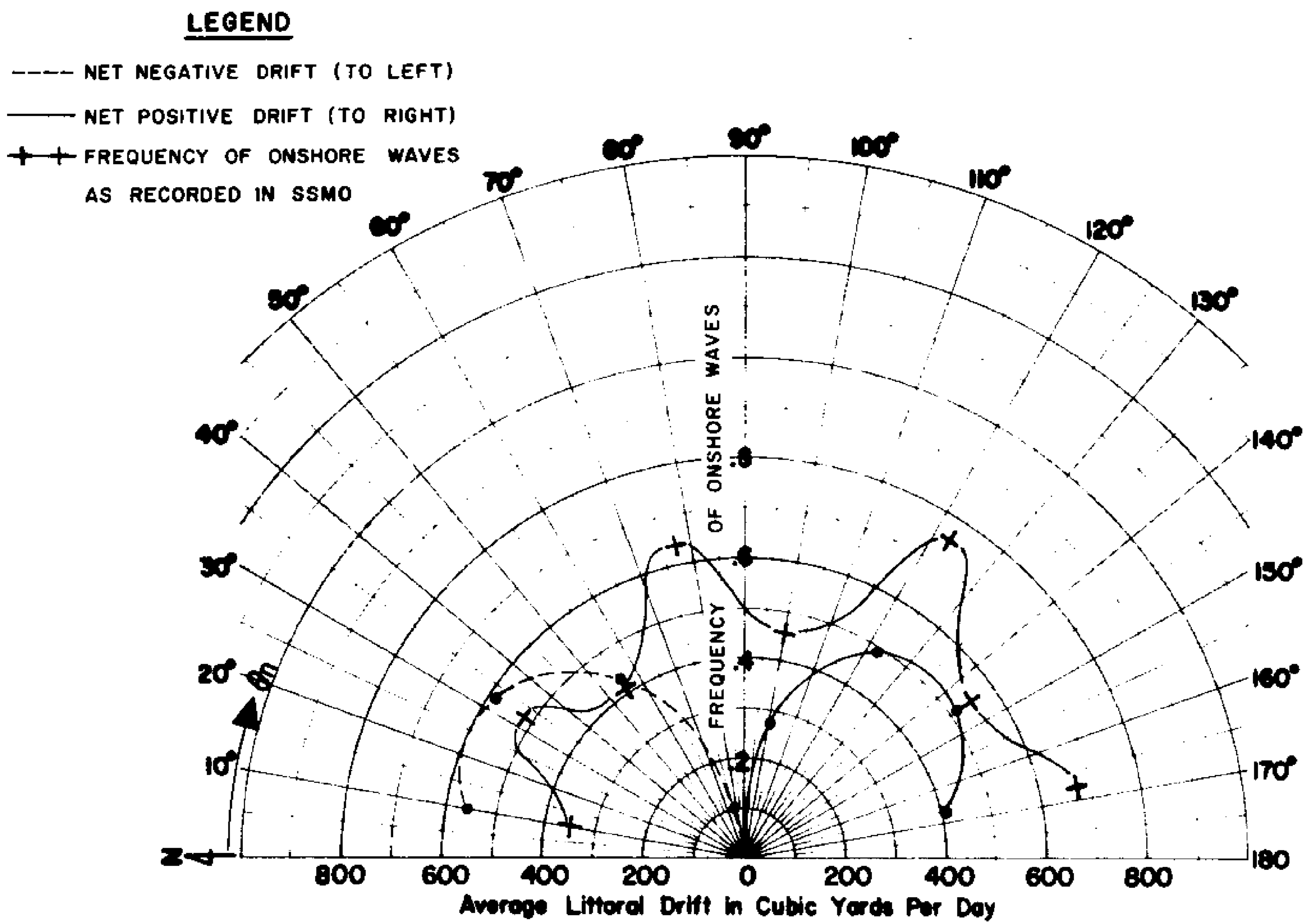

FIGURE C9. VARIATION OF AVERAGE MONTHLY NET LITTORAL DRIFT WITH BEACH ORIENTATION - MAY
FORT PIERCE INLET TO ST. LUCIE INLET, FLORIDA

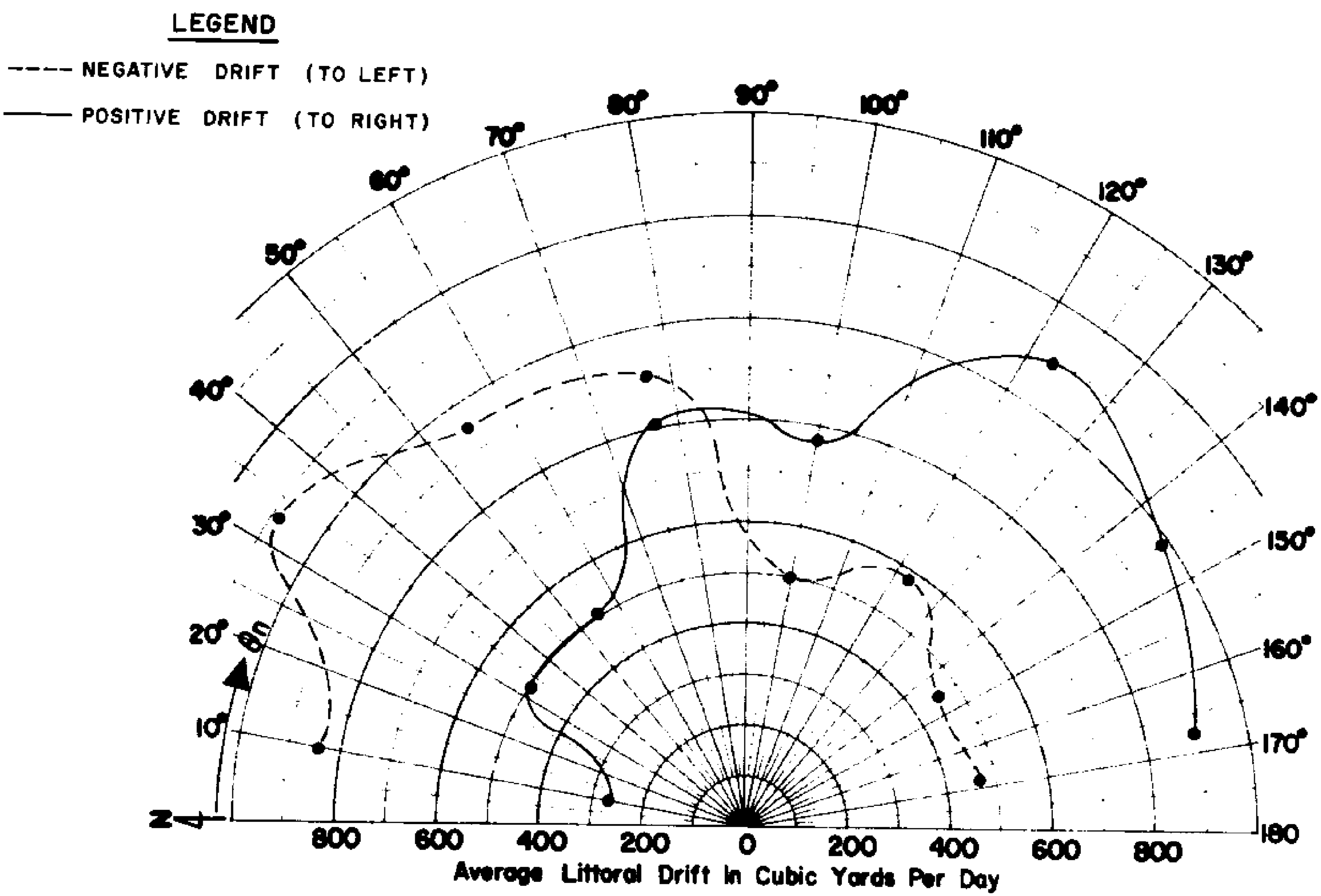

FIGURE C10. VARIATION OF AVERAGE MONTHLY TOTAL LITTORAL DRIFT WITH BEACH ORIENTATION – MAY
FORT PIERCE INLET TO ST. LUCIE INLET, FLORIDA

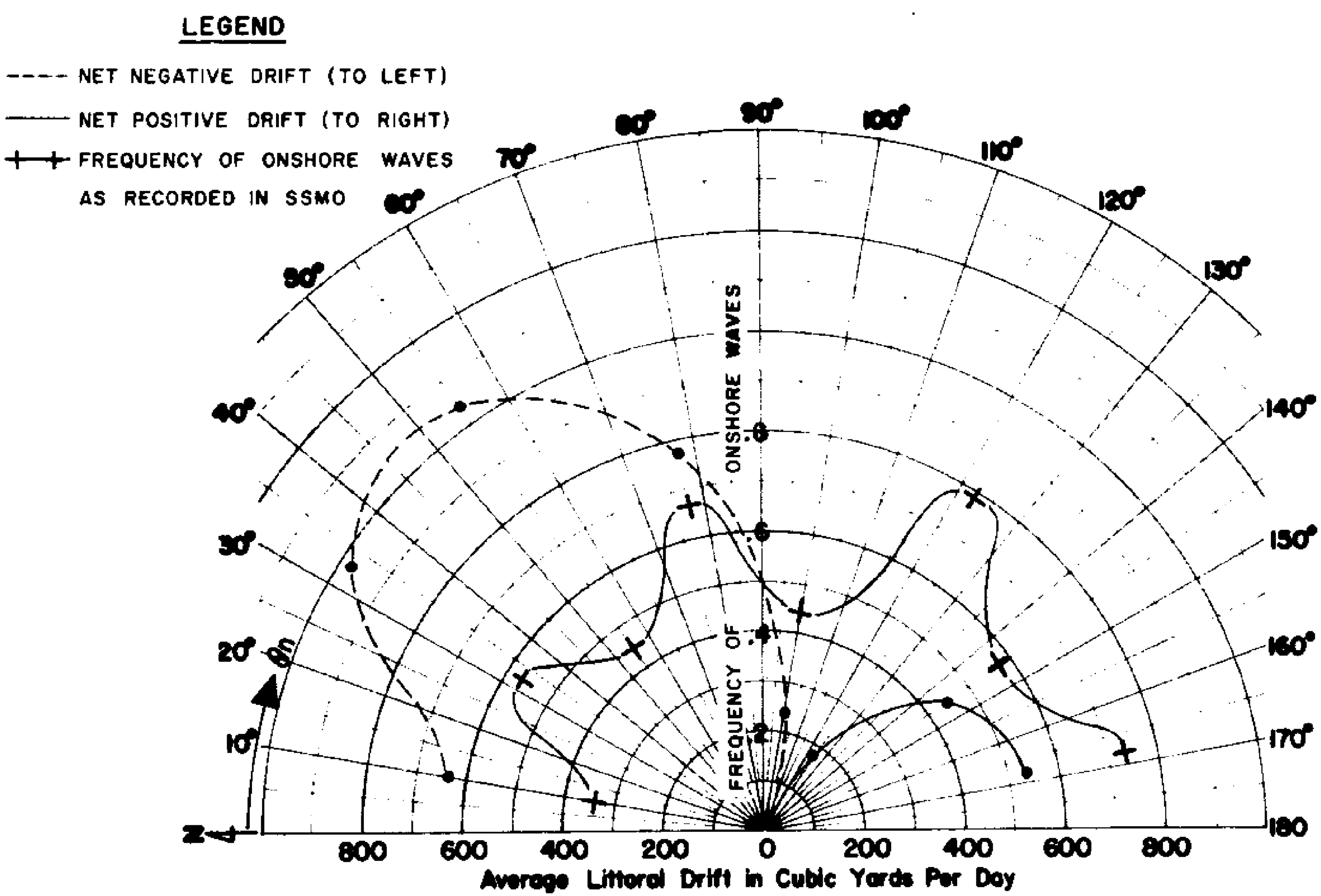

FIGURE CII. VARIATION OF AVERAGE MONTHLY NET LITTORAL DRIFT WITH BEACH ORIENTATION - JUNE
FORT PIERCE INLET TO ST. LUCIE INLET, FLORIDA

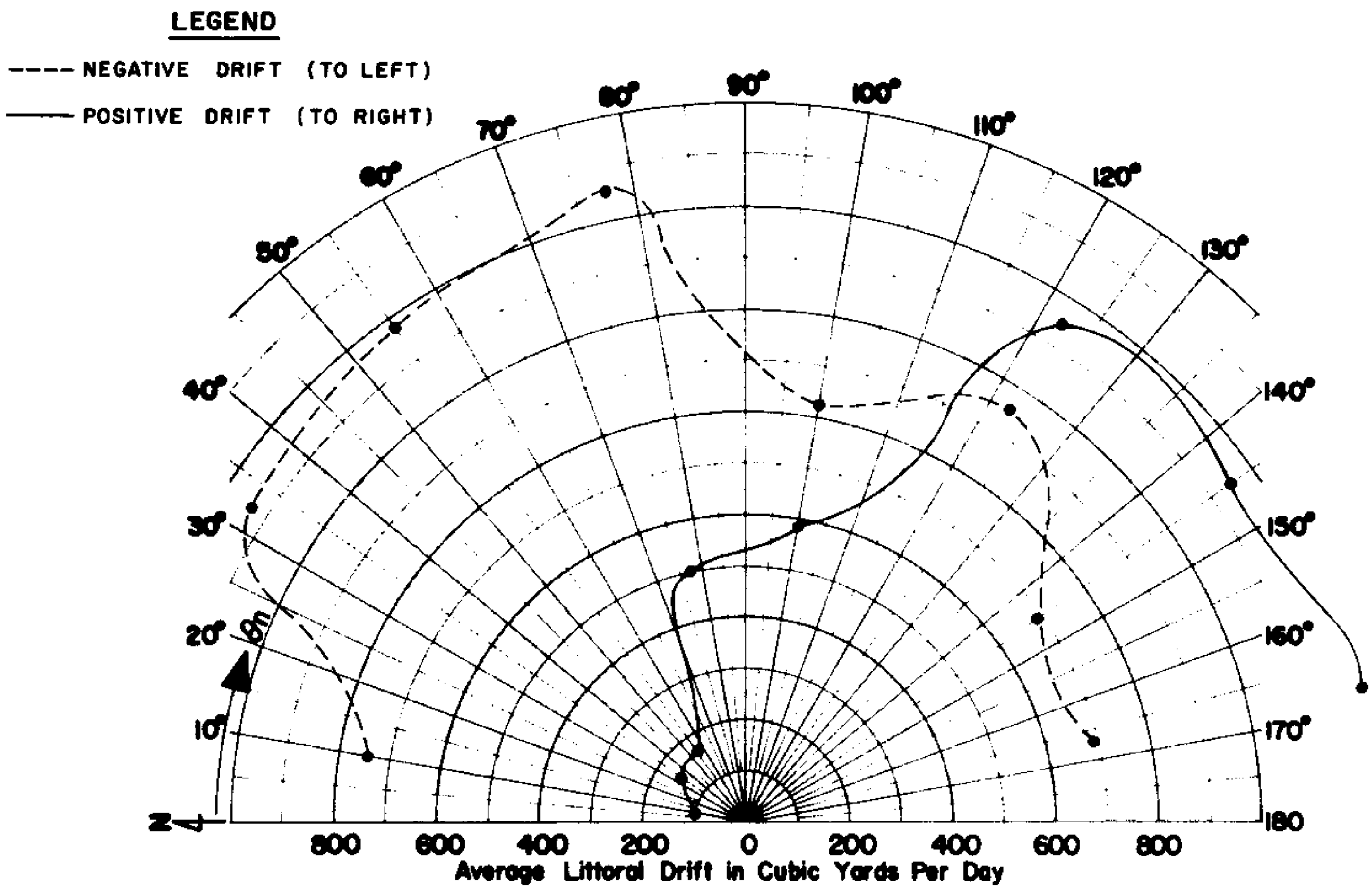

FIGURE C12. VARIATION OF AVERAGE MONTHLY TOTAL LITTORAL DRIFT WITH BEACH ORIENTATION - JUNE
FORT PIERCE INLET TO ST. LUCIE INLET, FLORIDA

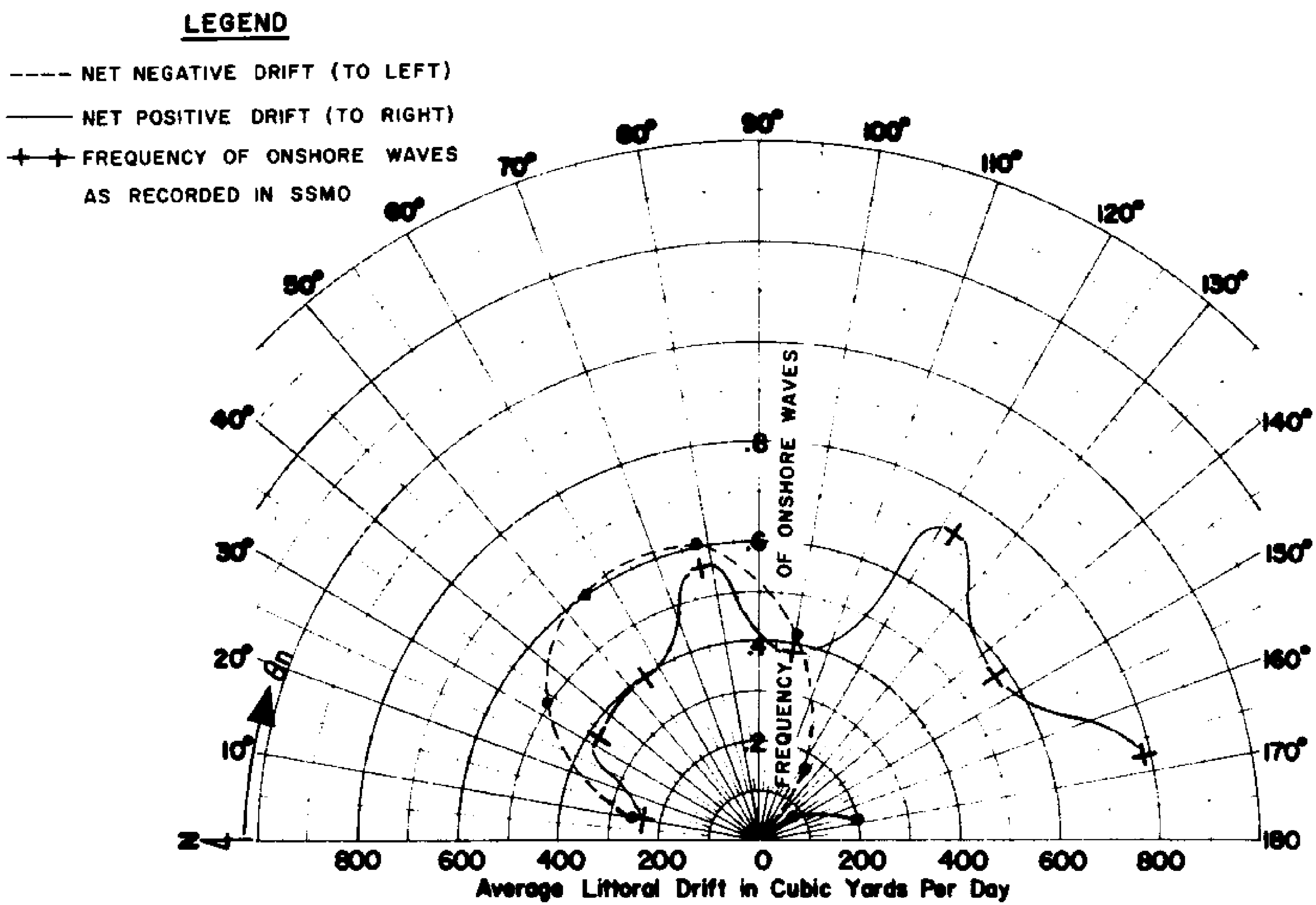

FIGURE C13. VARIATION OF AVERAGE MONTHLY NET LITTORAL DRIFT WITH BEACH ORIENTATION - JULY
FORT PIERCE INLET TO ST. LUCIE INLET, FLORIDA

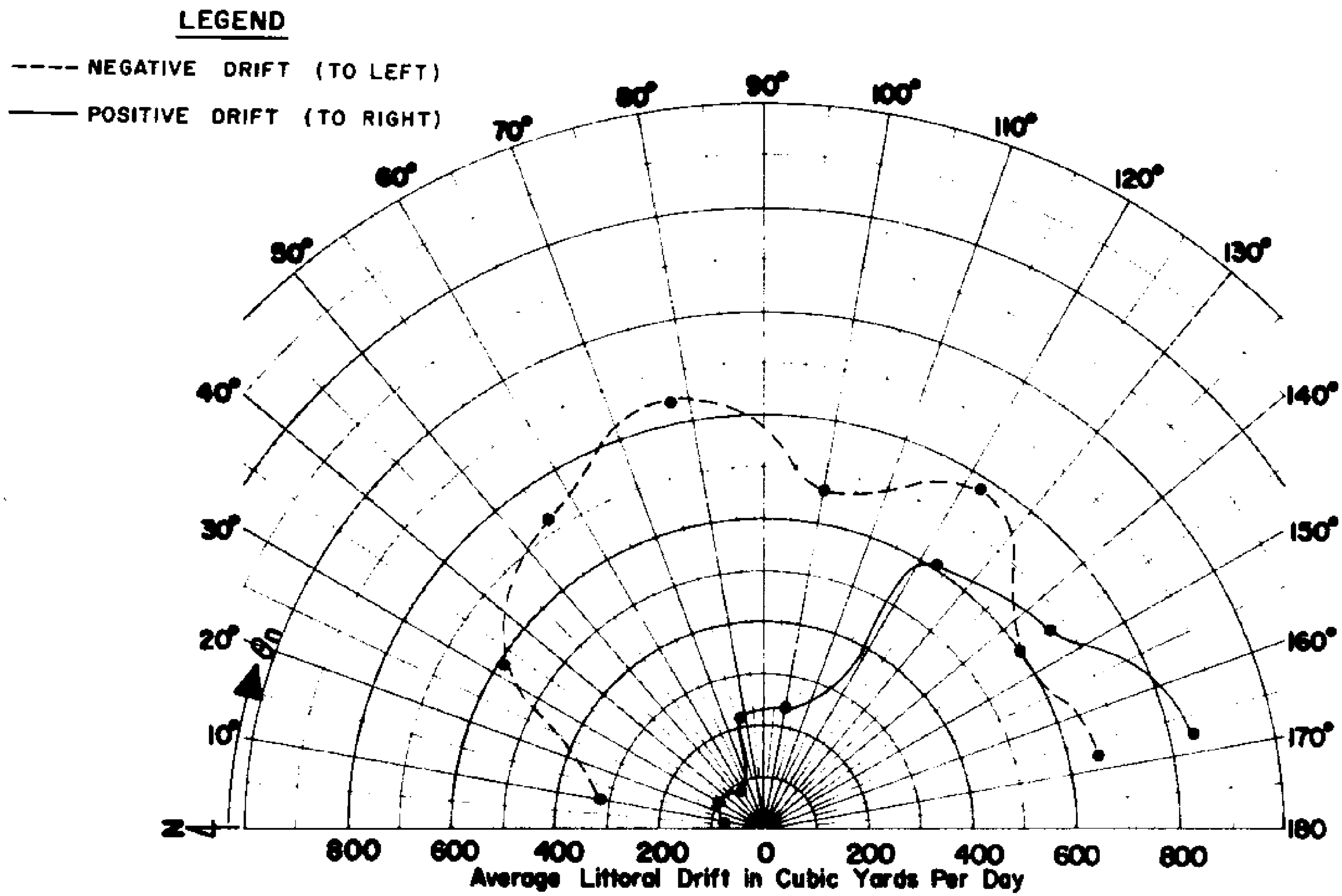

FIGURE C14. VARIATION OF AVERAGE MONTHLY TOTAL LITTORAL DRIFT WITH BEACH ORIENTATION - JULY
FORT PIERCE INLET TO ST. LUCIE INLET, FLORIDA

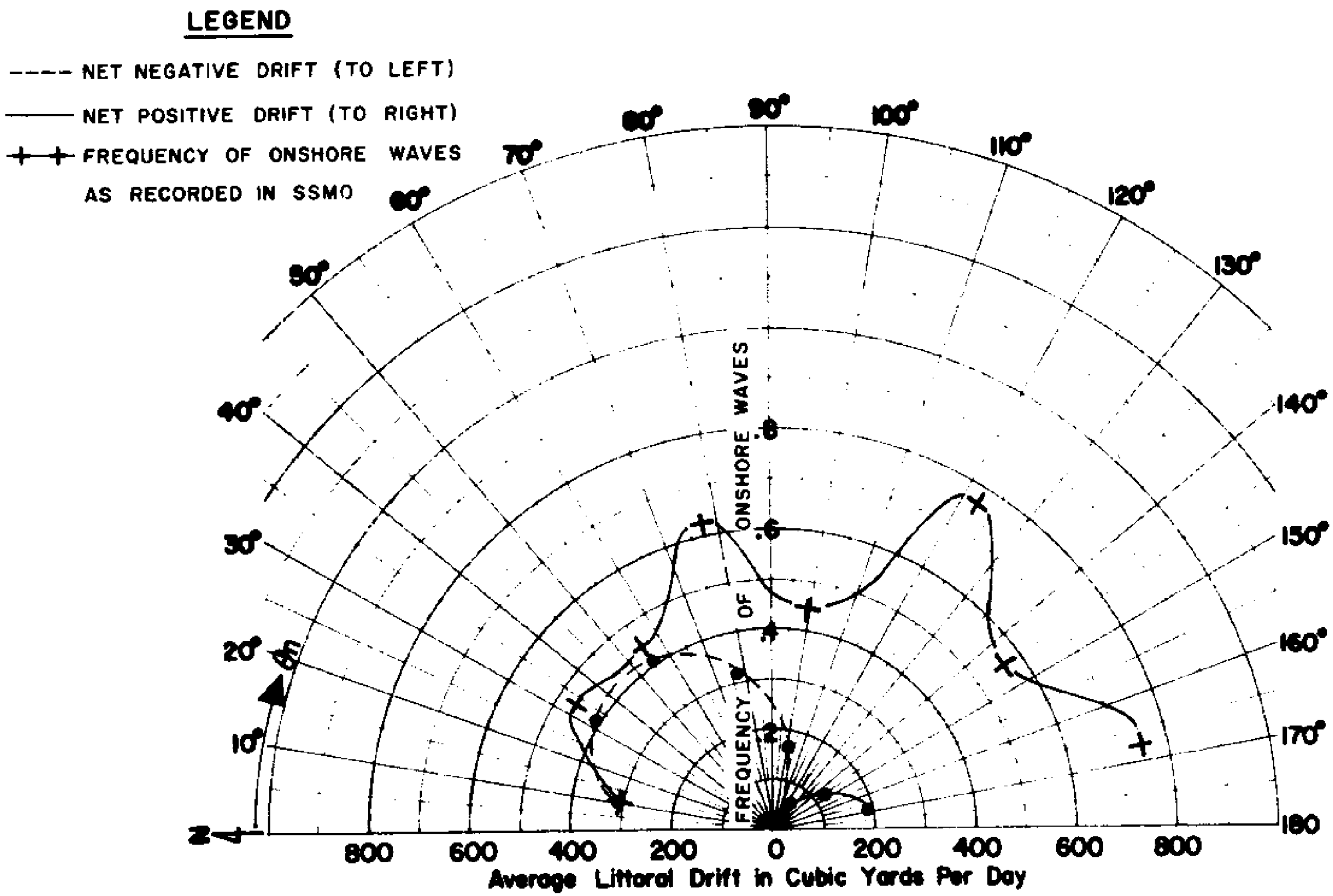

FIGURE C15. VARIATION OF AVERAGE MONTHLY NET LITTORAL DRIFT WITH BEACH ORIENTATION - AUGUST
FORT PIERCE INLET TO ST. LUCIE INLET, FLORIDA

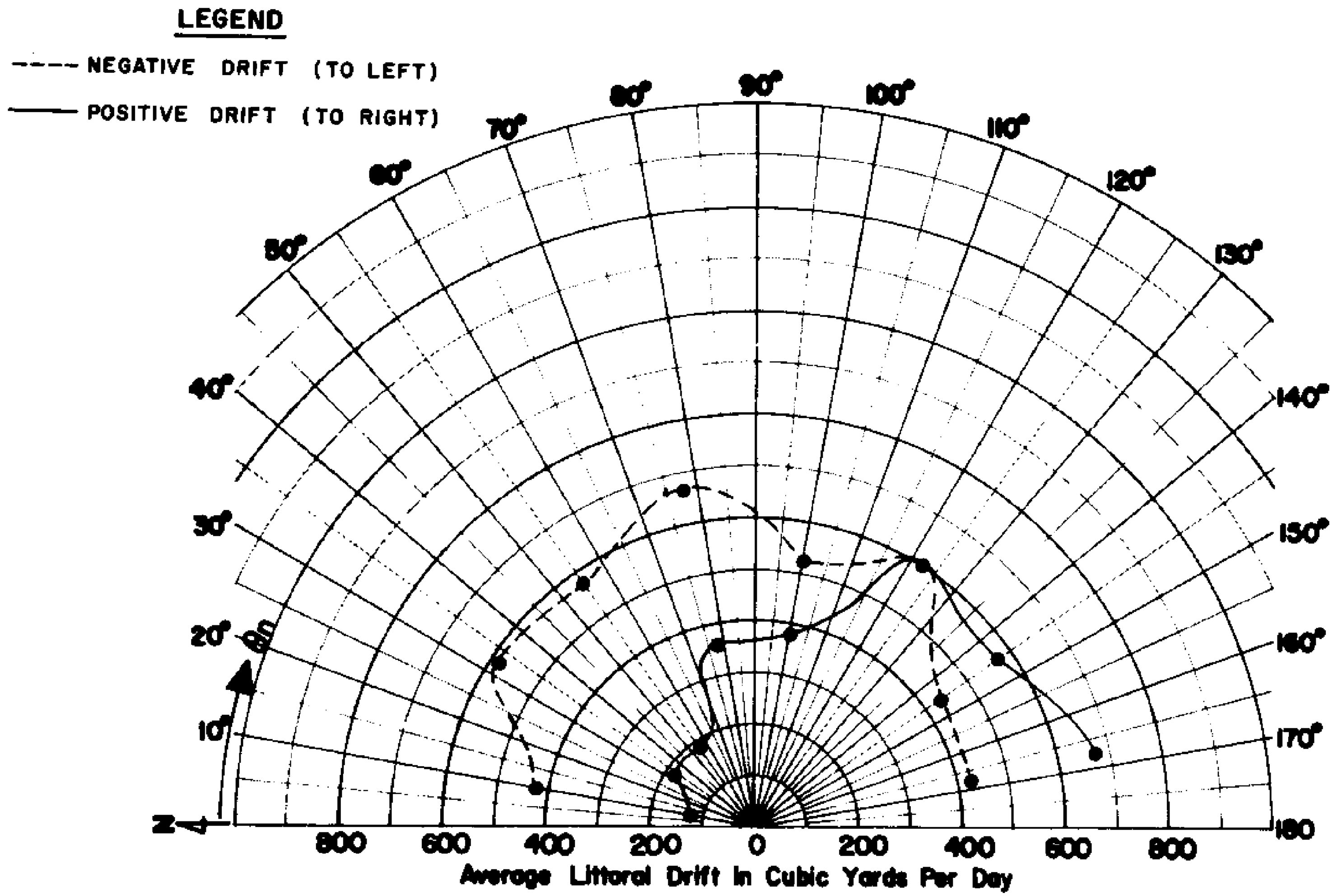

FIGURE C16. VARIATION OF AVERAGE MONTHLY TOTAL LITTORAL DRIFT WITH BEACH ORIENTATION - AUGUST
FORT PIERCE INLET TO ST. LUCIE INLET, FLORIDA

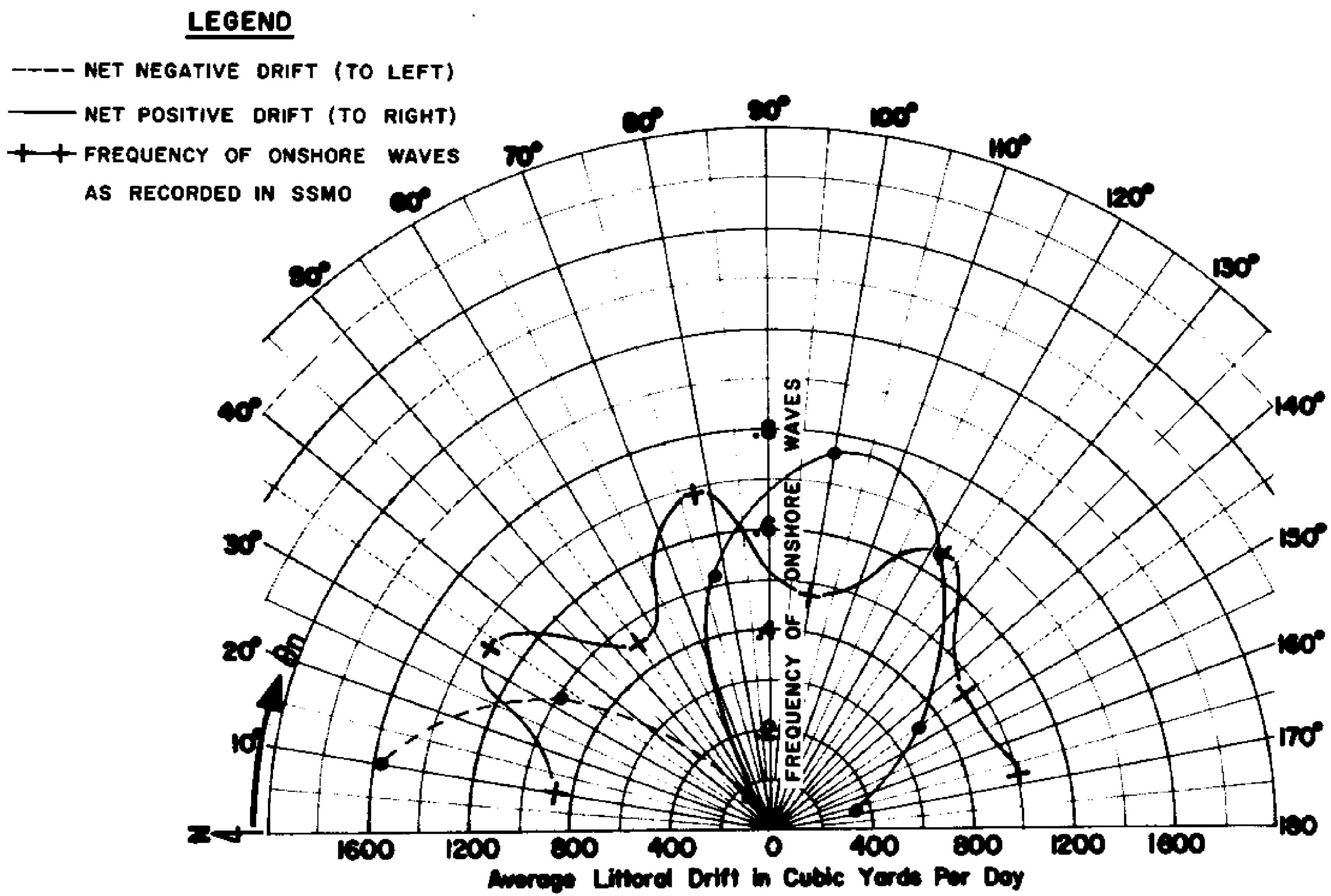

FIGURE C17. VARIATION OF AVERAGE MONTHLY NET LITTORAL DRIFT WITH BEACH ORIENTATION - SEPTEMBER
FORT PIERCE INLET TO ST. LUCIE INLET, FLORIDA

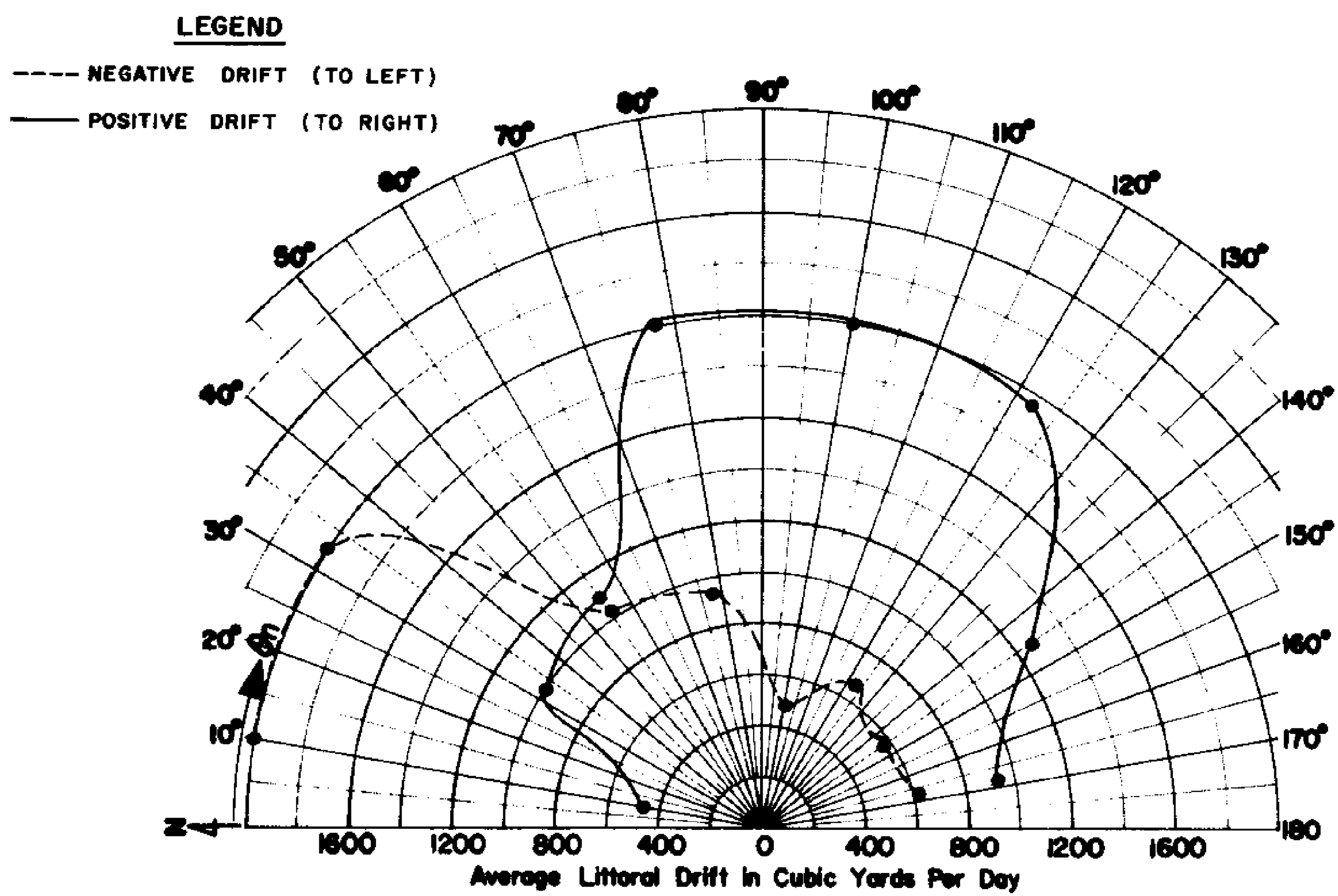

FIGURE C18. VARIATION OF AVERAGE MONTHLY TOTAL LITTORAL DRIFT WITH BEACH ORIENTATION - SEPTEMBER
FORT PIERCE INLET TO ST. LUCIE INLET, FLORIDA

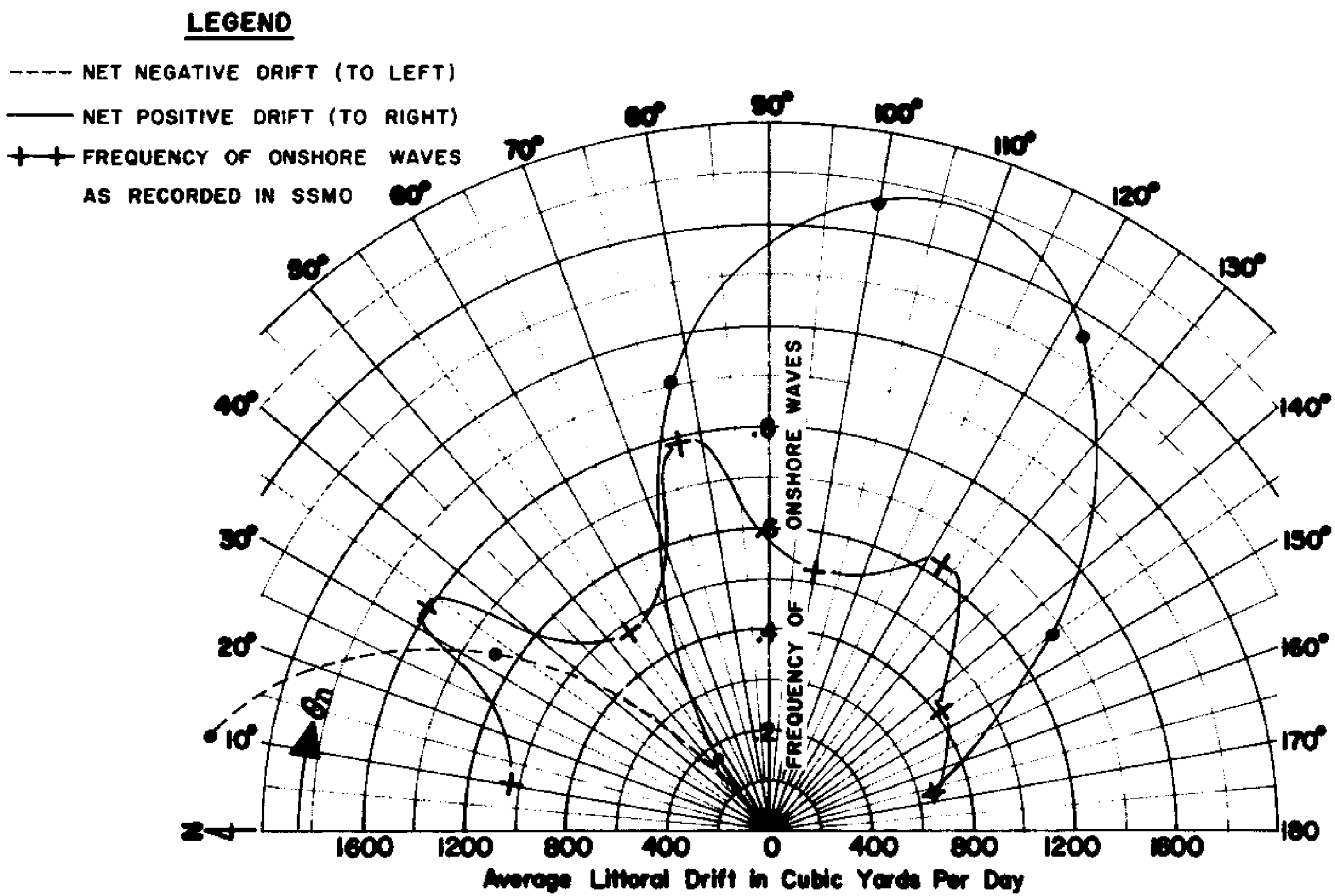

FIGURE C19. VARIATION OF AVERAGE MONTHLY NET LITTORAL DRIFT WITH BEACH ORIENTATION – OCTOBER
FORT PIERCE INLET TO ST. LUCIE INLET, FLORIDA

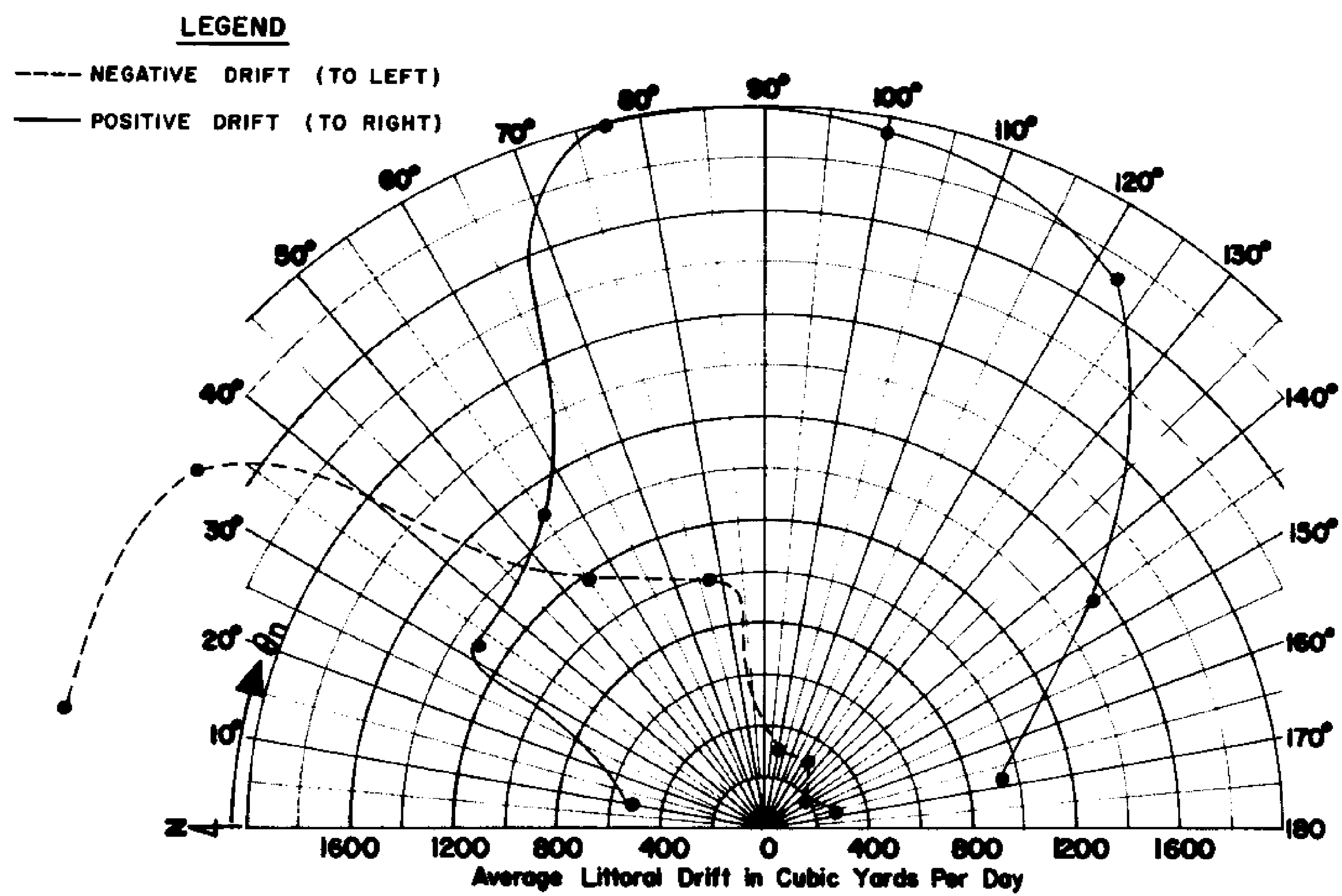

FIGURE C20. VARIATION OF AVERAGE MONTHLY TOTAL LITTORAL DRIFT WITH BEACH ORIENTATION - OCTOBER
FORT PIERCE INLET TO ST. LUCIE INLET, FLORIDA

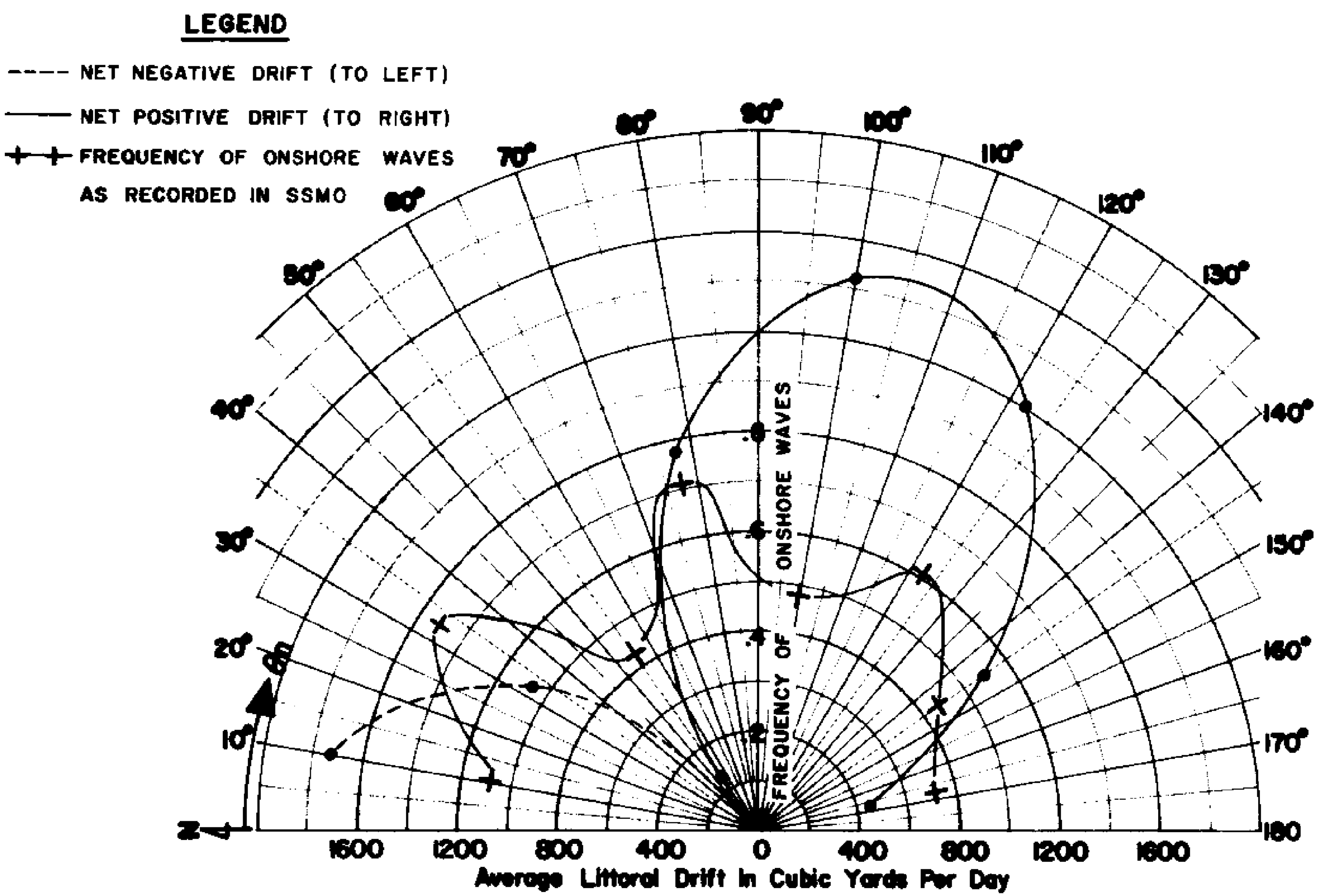

FIGURE C21. VARIATION OF AVERAGE MONTHLY NET LITTORAL DRIFT WITH BEACH ORIENTATION - NOVEMBER
FORT PIERCE INLET TO ST. LUCIE INLET, FLORIDA

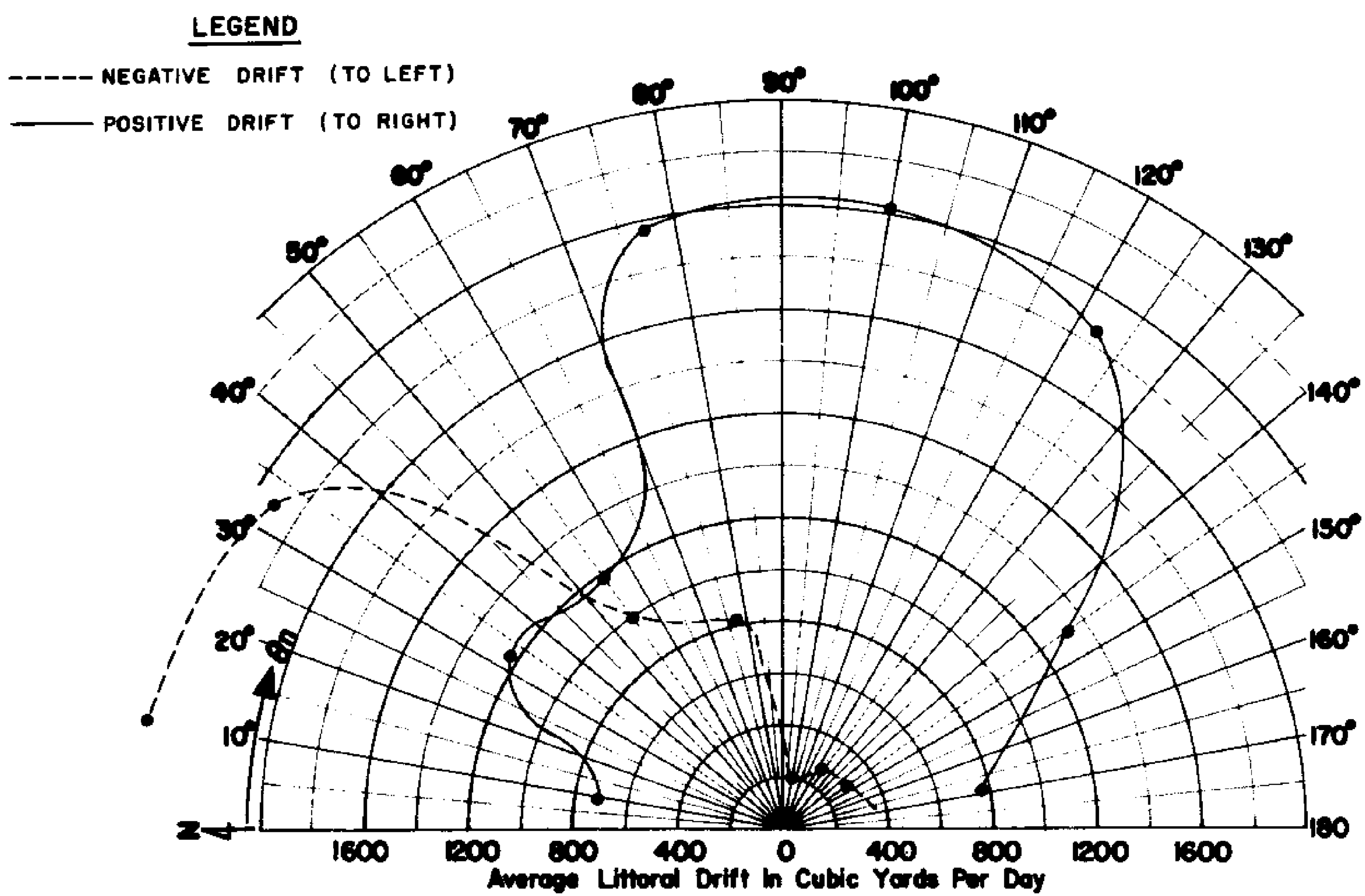

FIGURE C22. VARIATION OF AVERAGE MONTHLY TOTAL LITTORAL DRIFT WITH BEACH ORIENTATION - NOVEMBER FORT PIERCE INLET TO ST. LUCIE INLET, FLORIDA

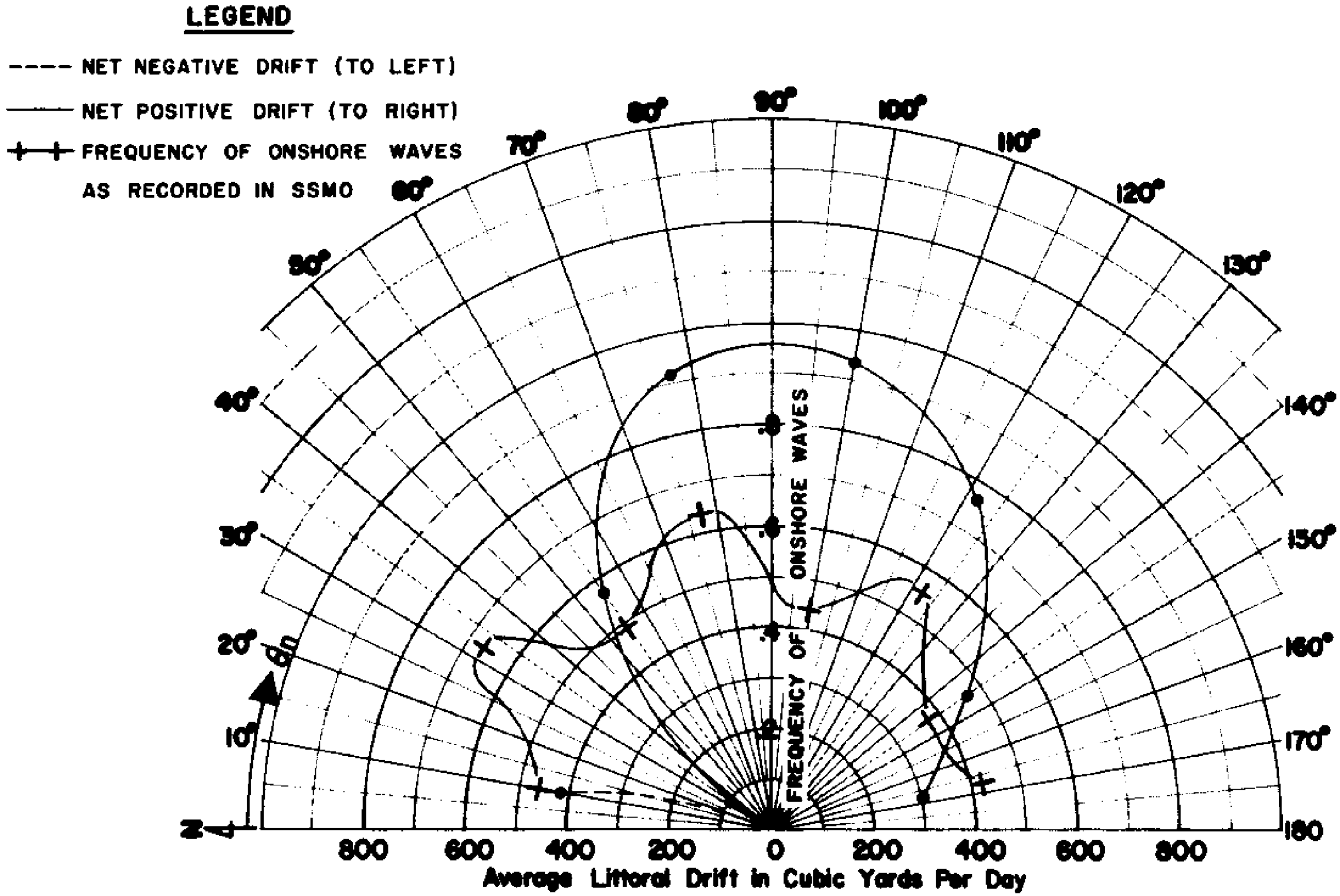

FIGURE C23. VARIATION OF AVERAGE MONTHLY NET LITTORAL DRIFT WITH BEACH ORIENTATION - DECEMBER
FORT PIERCE INLET TO ST. LUCIE INLET, FLORIDA

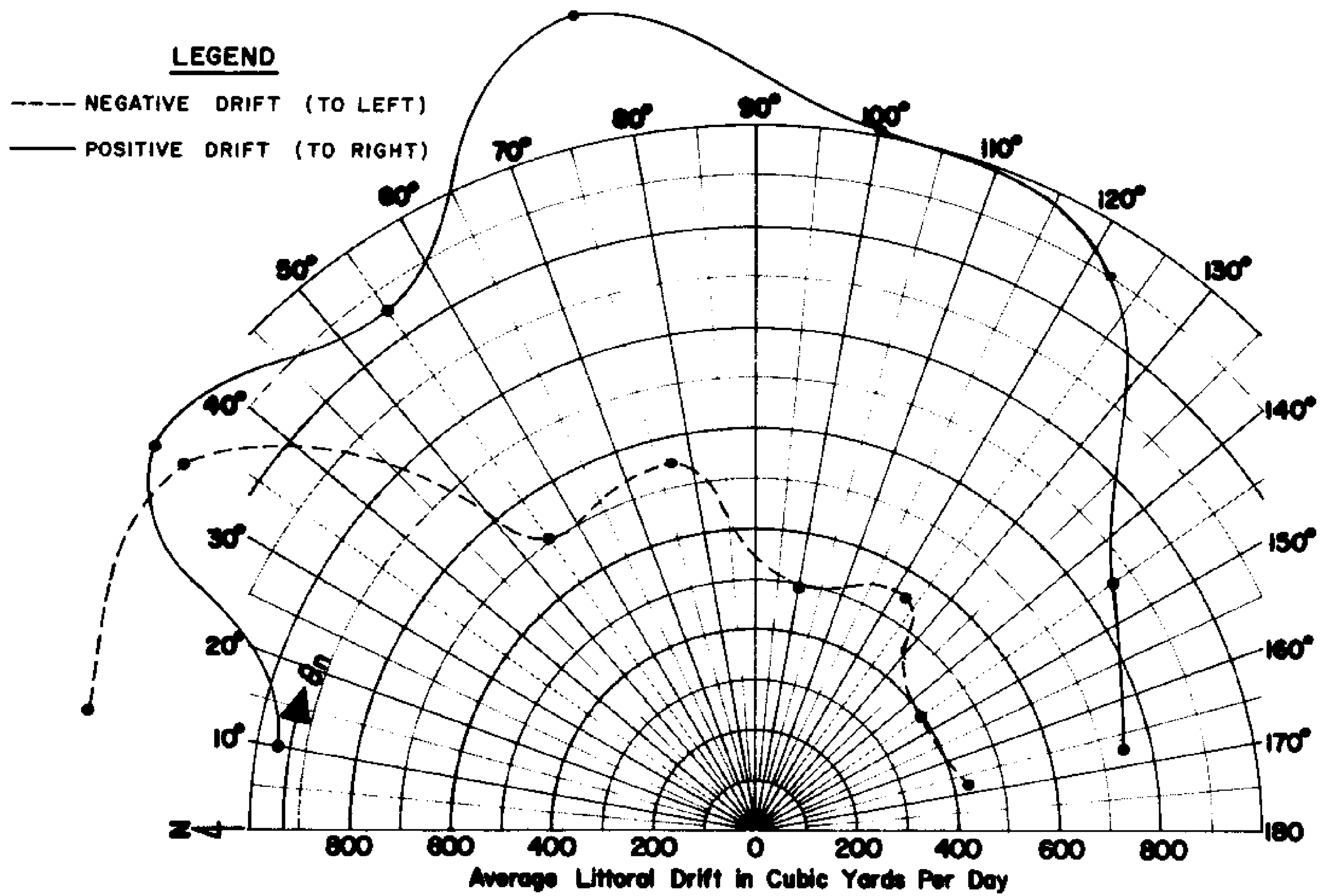

FIGURE C24. VARIATION OF AVERAGE MONTHLY TOTAL LITTORAL DRIFT WITH BEACH ORIENTATION - DECEMBER
FORT PIERCE INLET TO ST. LUCIE INLET, FLORIDA

Figures D1 Through D48

Monthly Wave Height and Wave Period Roses for Offshore

Wave Climate in SSMO Data Blocks 11 and 12

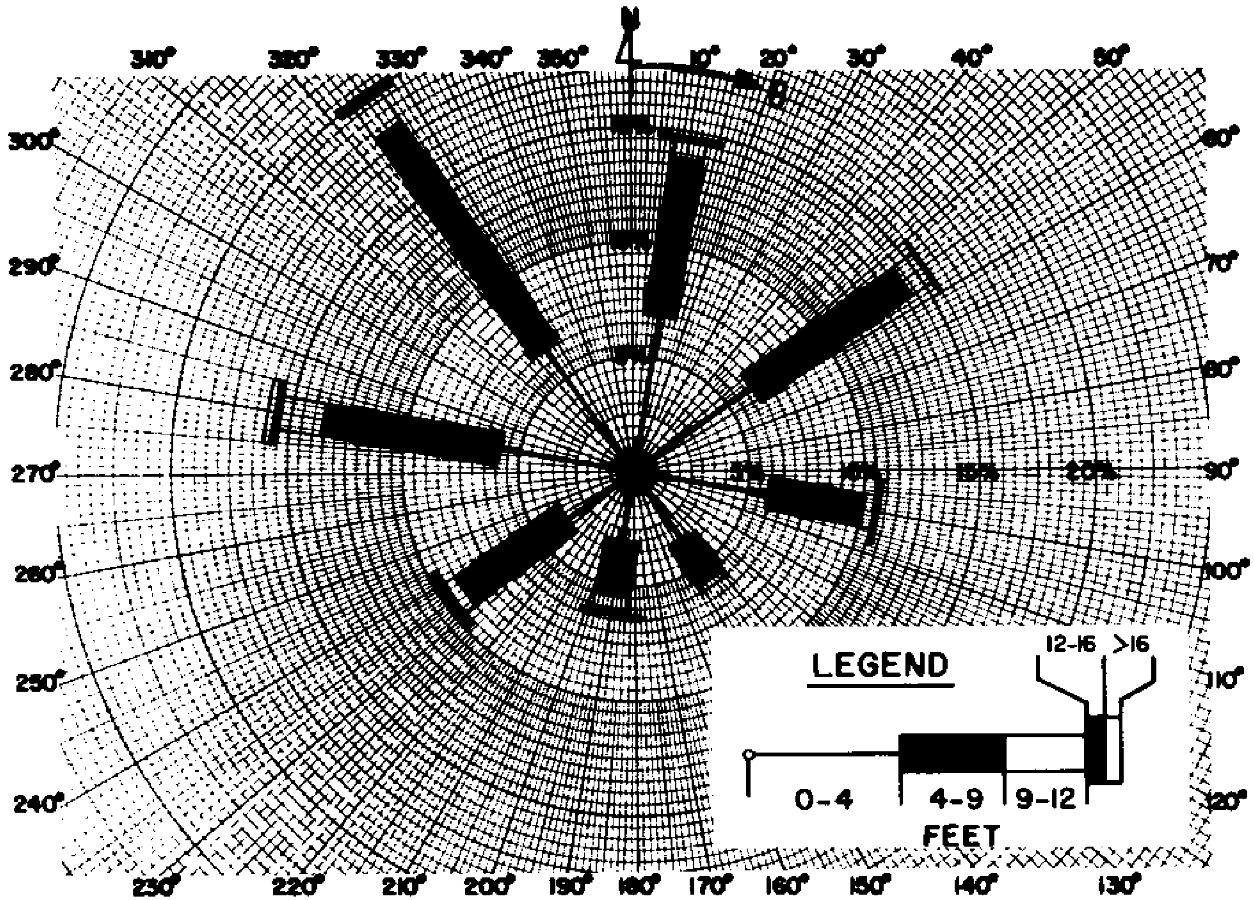

FIGURE D1. WAVE HEIGHT ROSE FOR OFFSHORE WAVE CLIMATE
SSMO DATA SQUARE NO. 11 - JANUARY

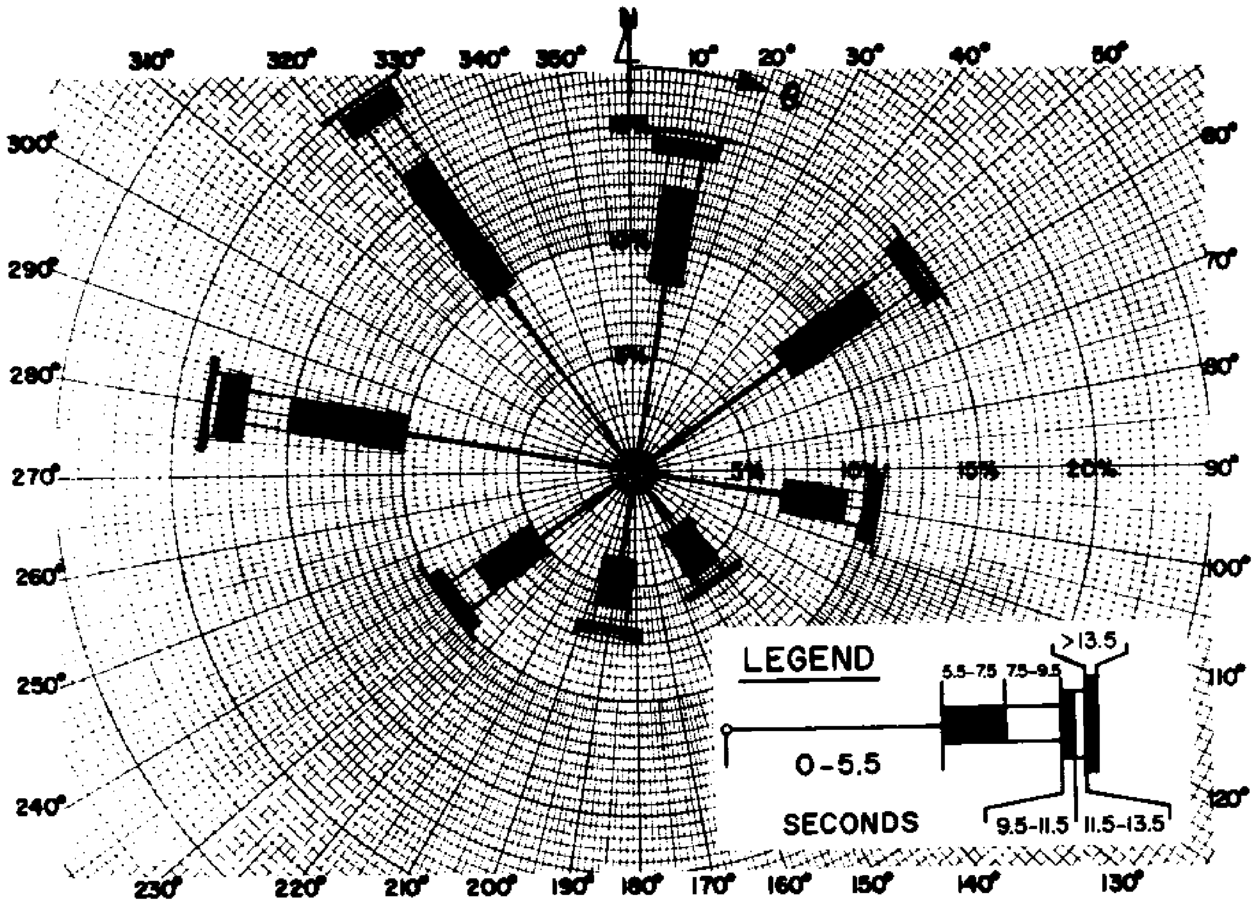

FIGURE D2. WAVE PERIOD ROSE FOR OFFSHORE WAVE CLIMATE
SSMO DATA SQUARE NO. 11 - JANUARY

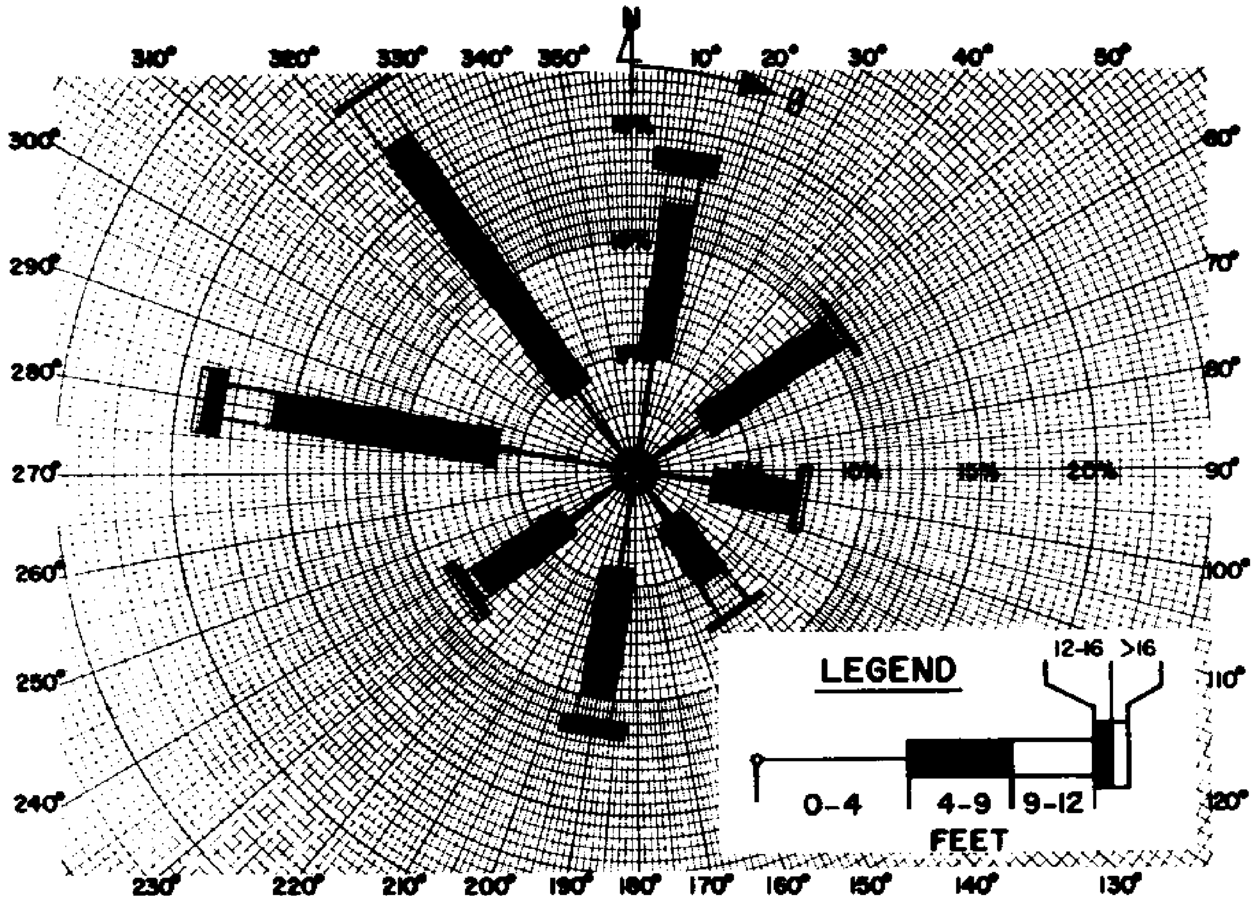

FIGURE D3. WAVE HEIGHT ROSE FOR OFFSHORE WAVE CLIMATE
SSMO DATA SQUARE NO. 11 - FEBRUARY

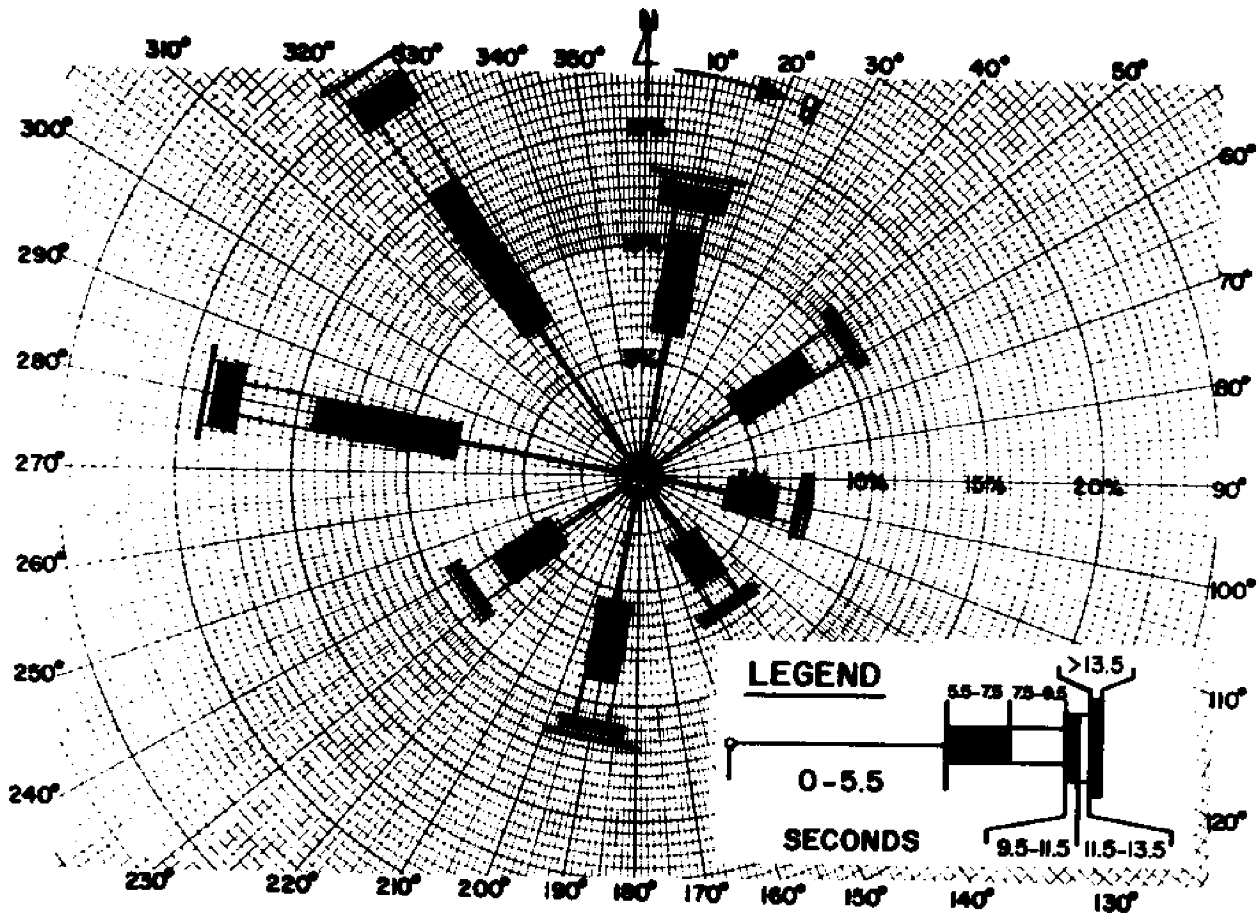

FIGURE D4. WAVE PERIOD ROSE FOR OFFSHORE WAVE CLIMATE SSMO DATA SQUARE NO. 11 - FEBRUARY

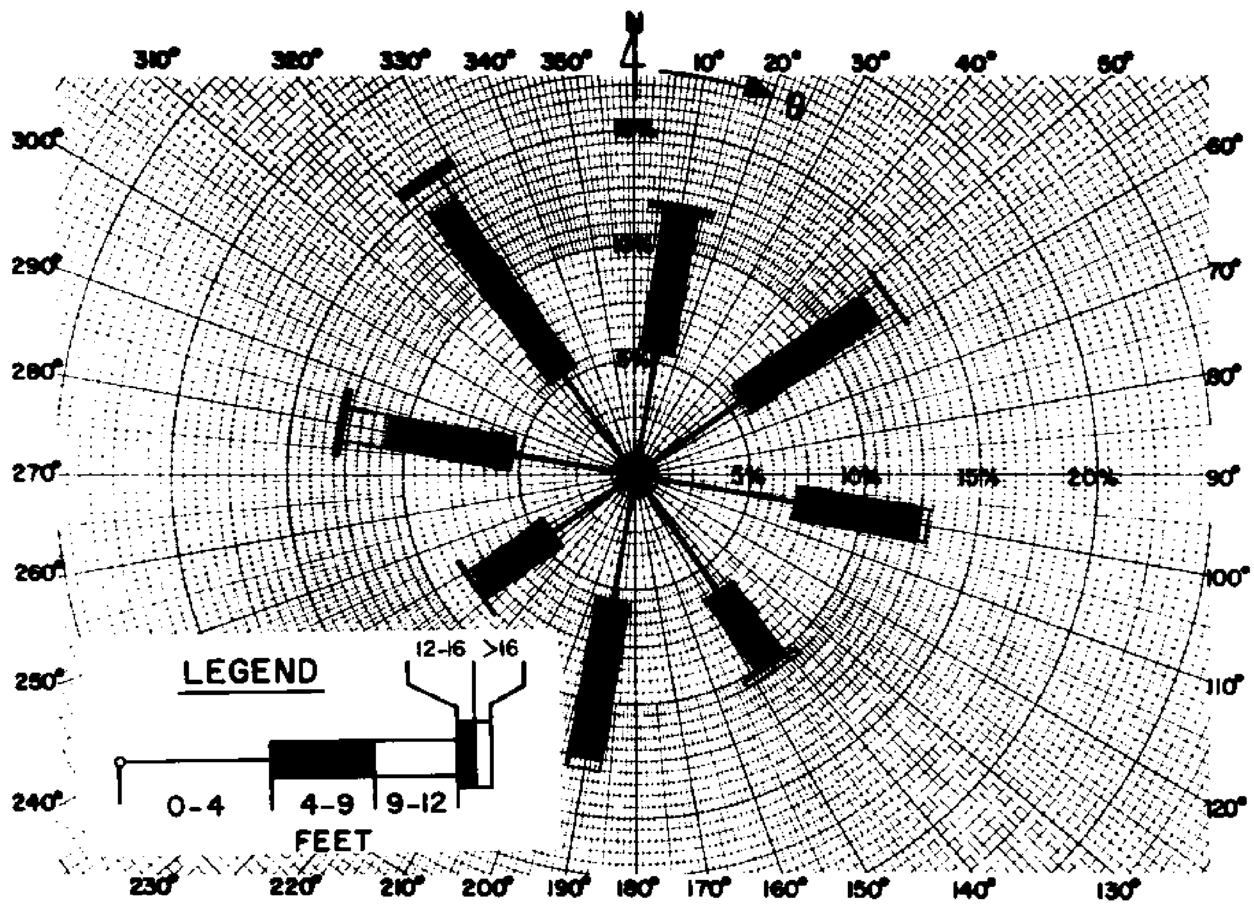

FIGURE D5. WAVE HEIGHT ROSE FOR OFFSHORE WAVE CLIMATE SSMO DATA SQUARE NO. 11 - MARCH

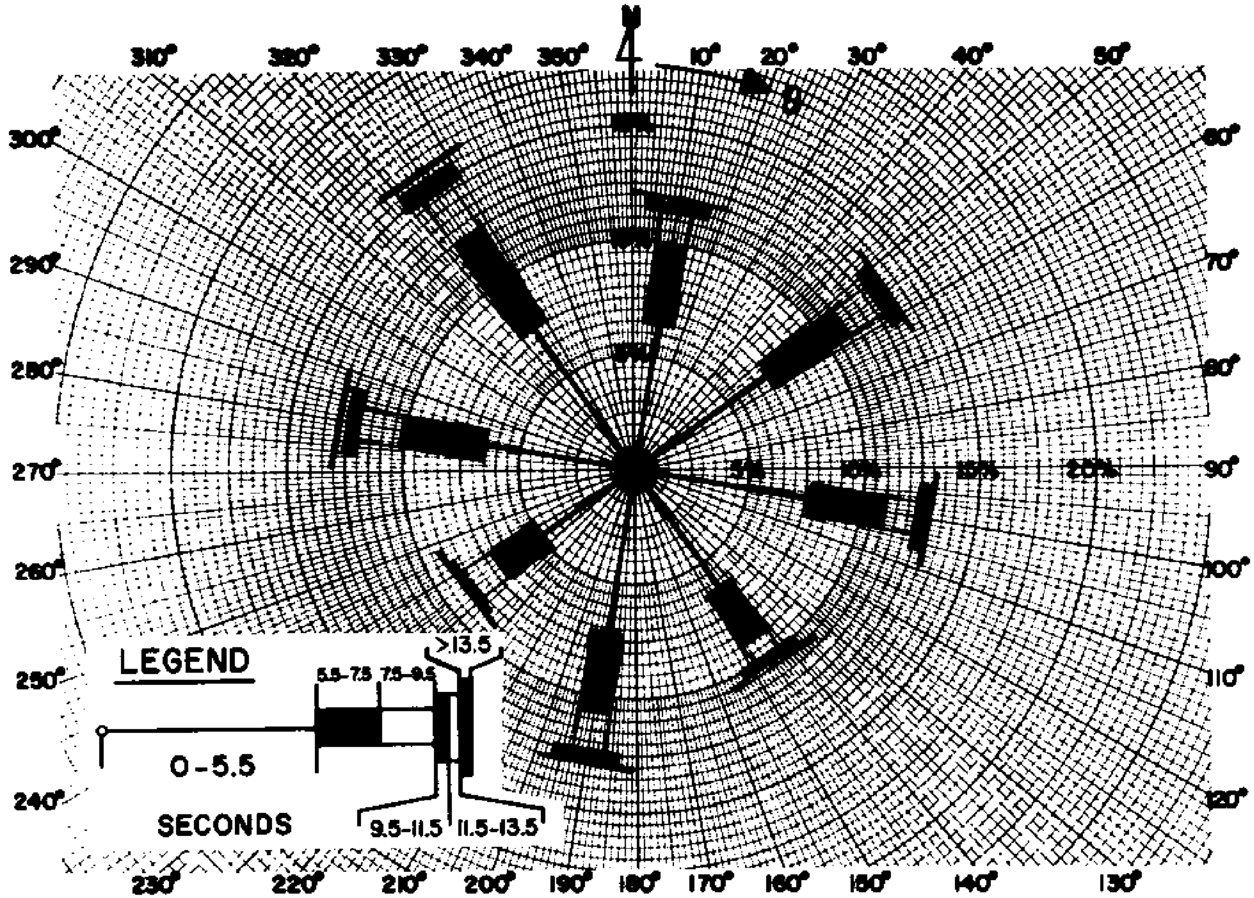

FIGURE D6. WAVE PERIOD ROSE FOR OFFSHORE WAVE CLIMATE SSMO DATA SQUARE NO. 11 - MARCH

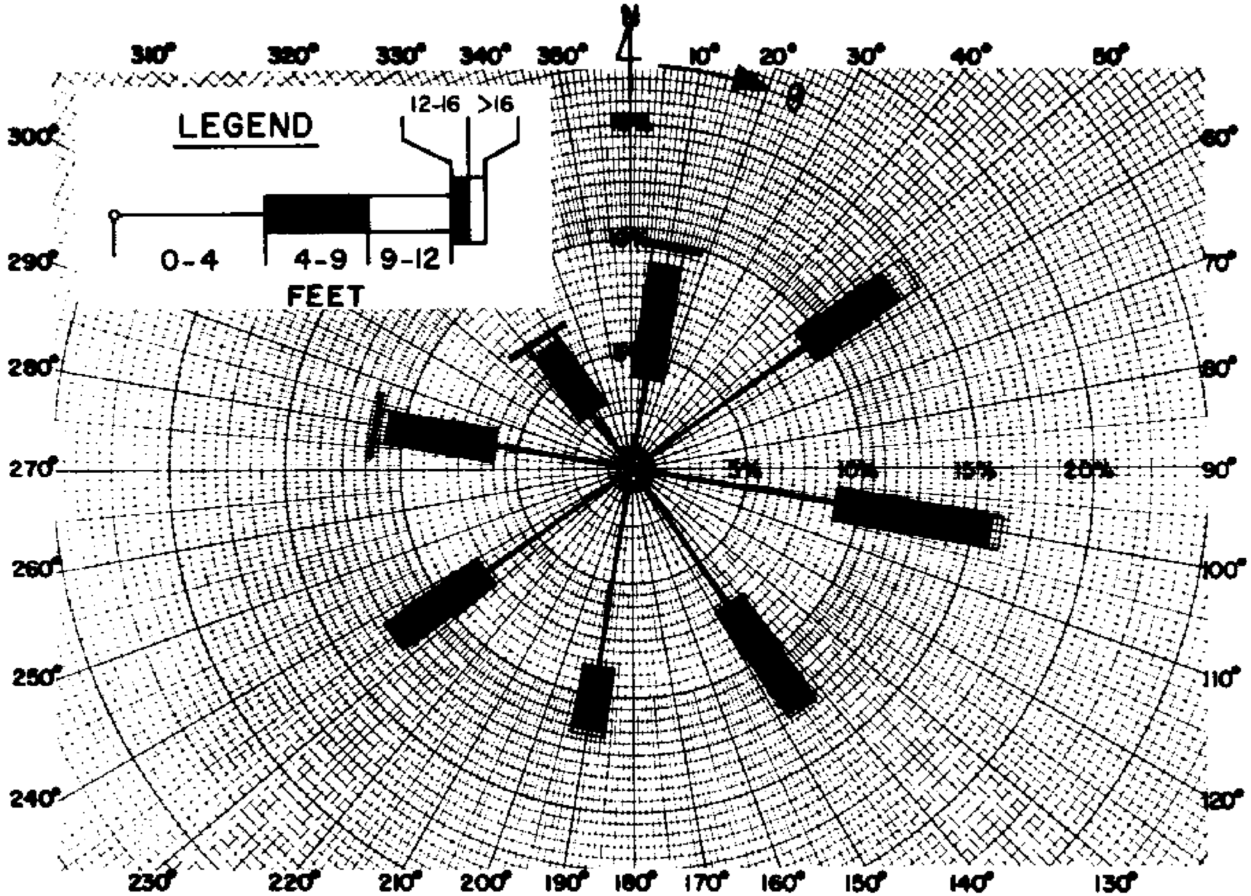

FIGURE D7. WAVE HEIGHT ROSE FOR OFFSHORE WAVE CLIMATE
SSMO DATA SQUARE NO. 11 - APRIL

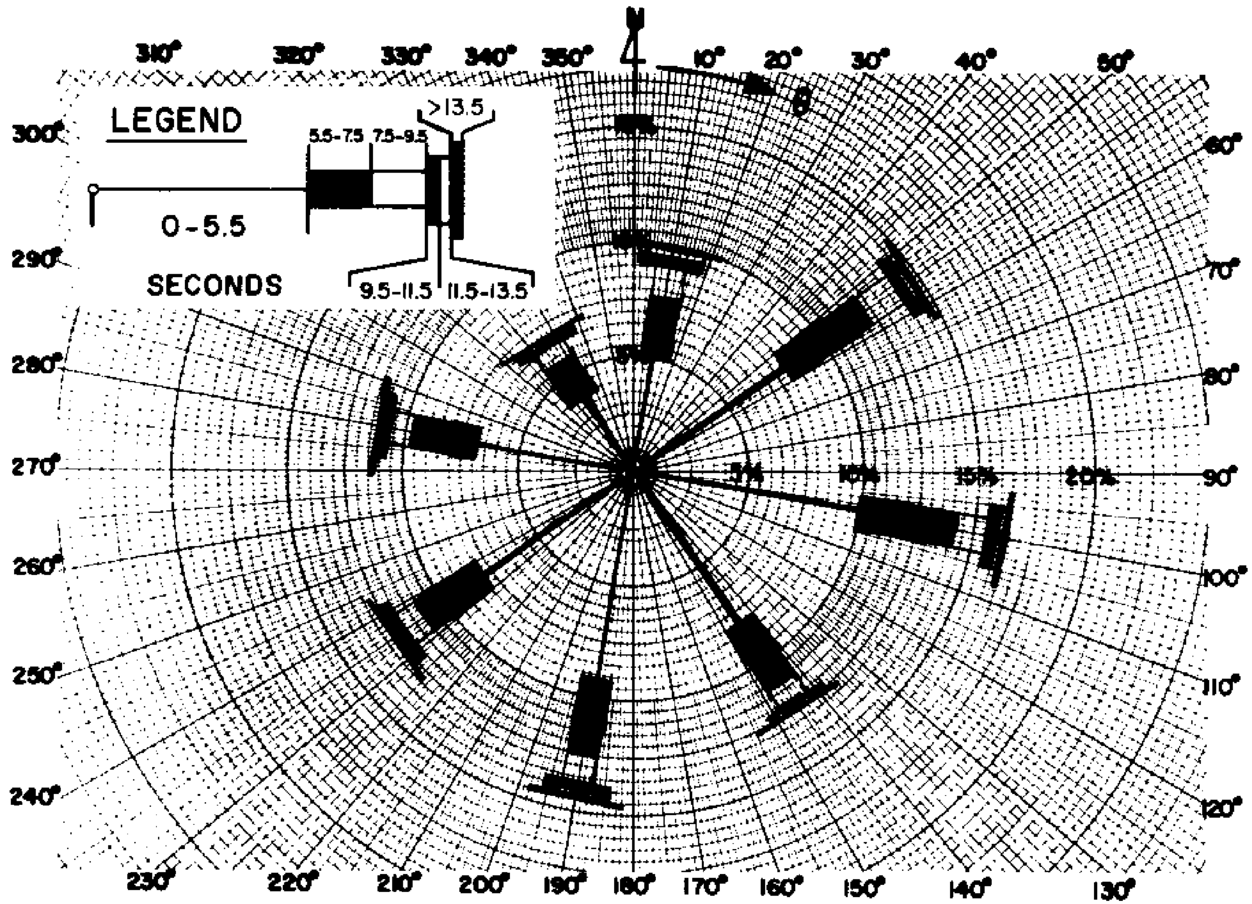

FIGURE D8. WAVE PERIOD ROSE FOR OFFSHORE WAVE CLIMATE
SSMO DATA SQUARE NO. 11 - APRIL

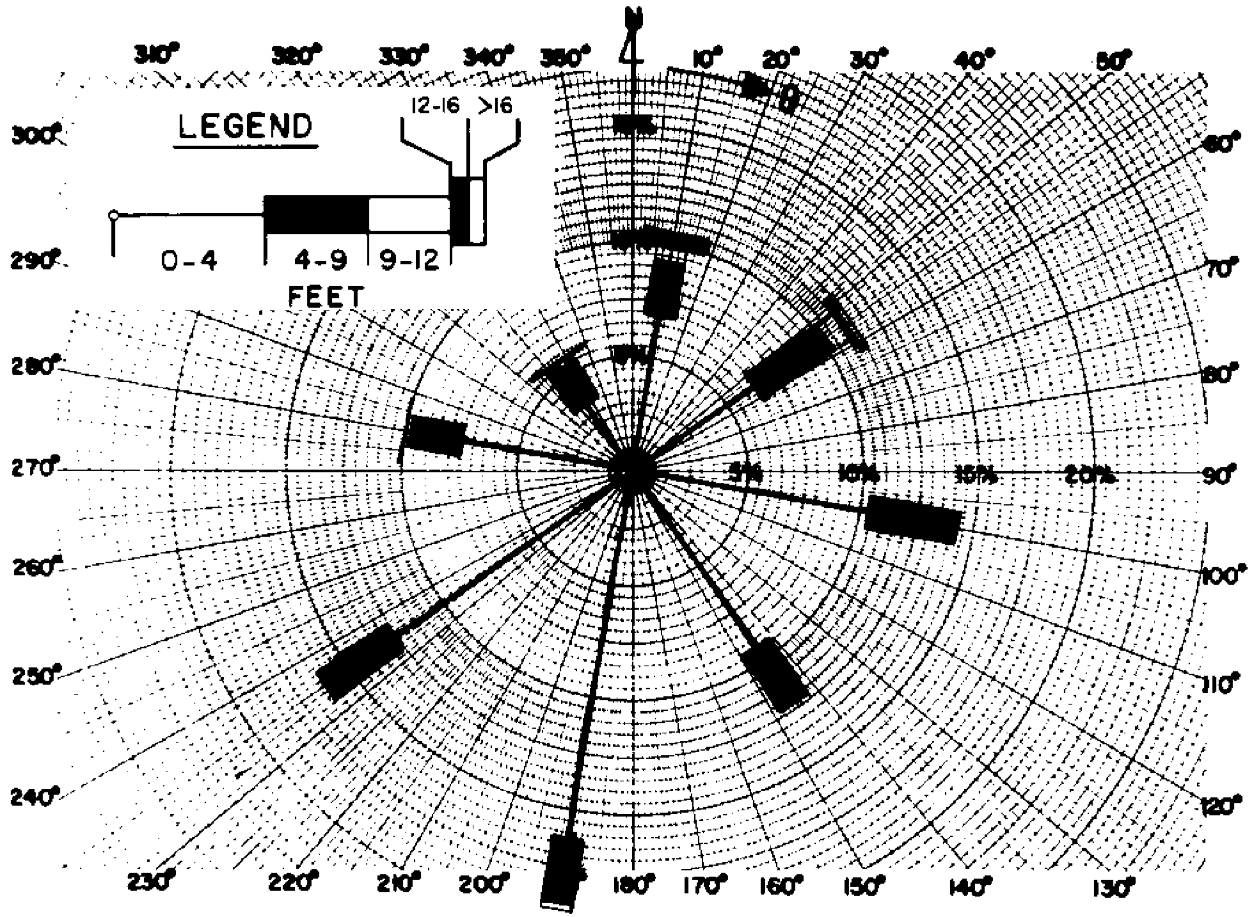

FIGURE D9. WAVE HEIGHT ROSE FOR OFFSHORE WAVE CLIMATE SSMO DATA SQUARE NO. 11 - MAY

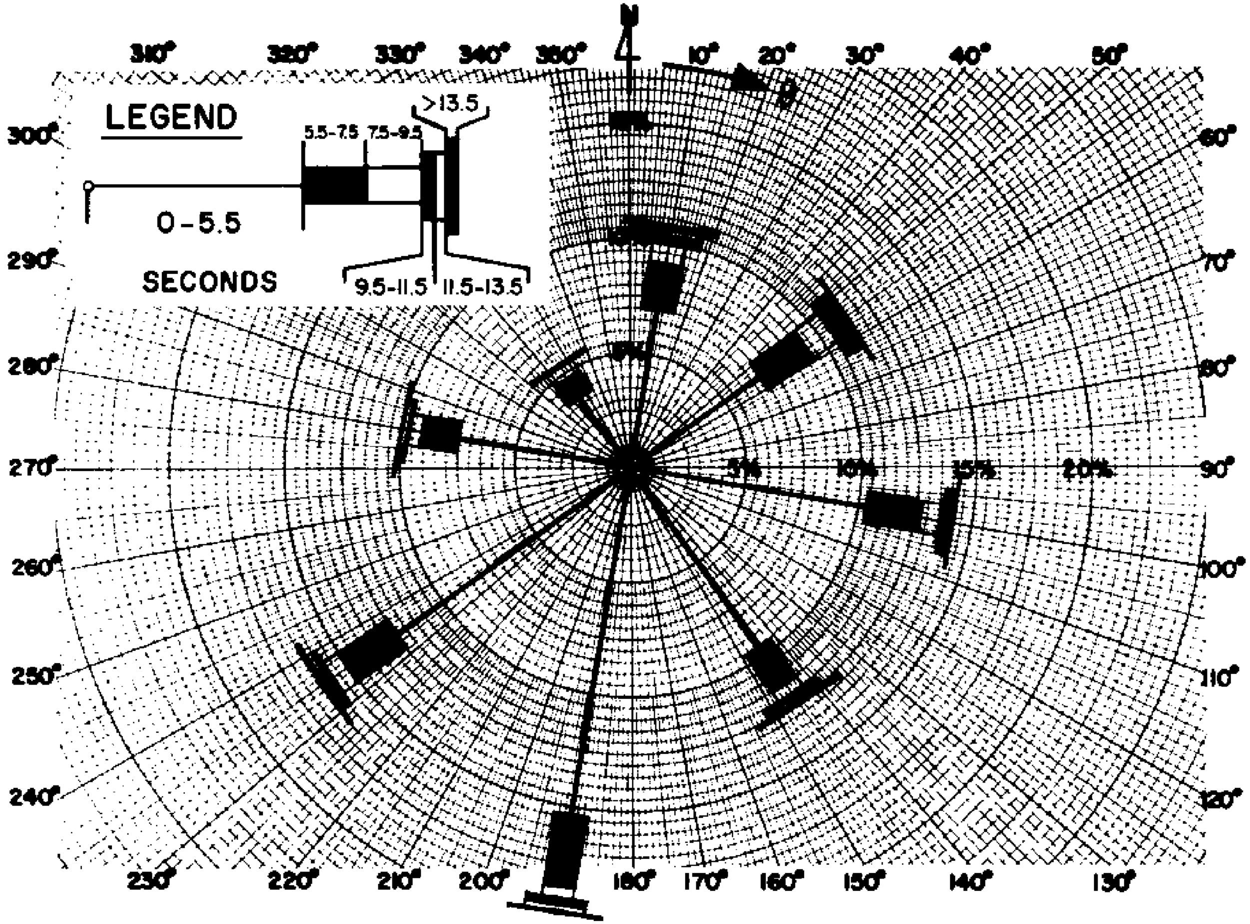

FIGURE D10. WAVE PERIOD ROSE FOR OFFSHORE WAVE CLIMATE
SSMO DATA SQUARE NO. 11 - MAY

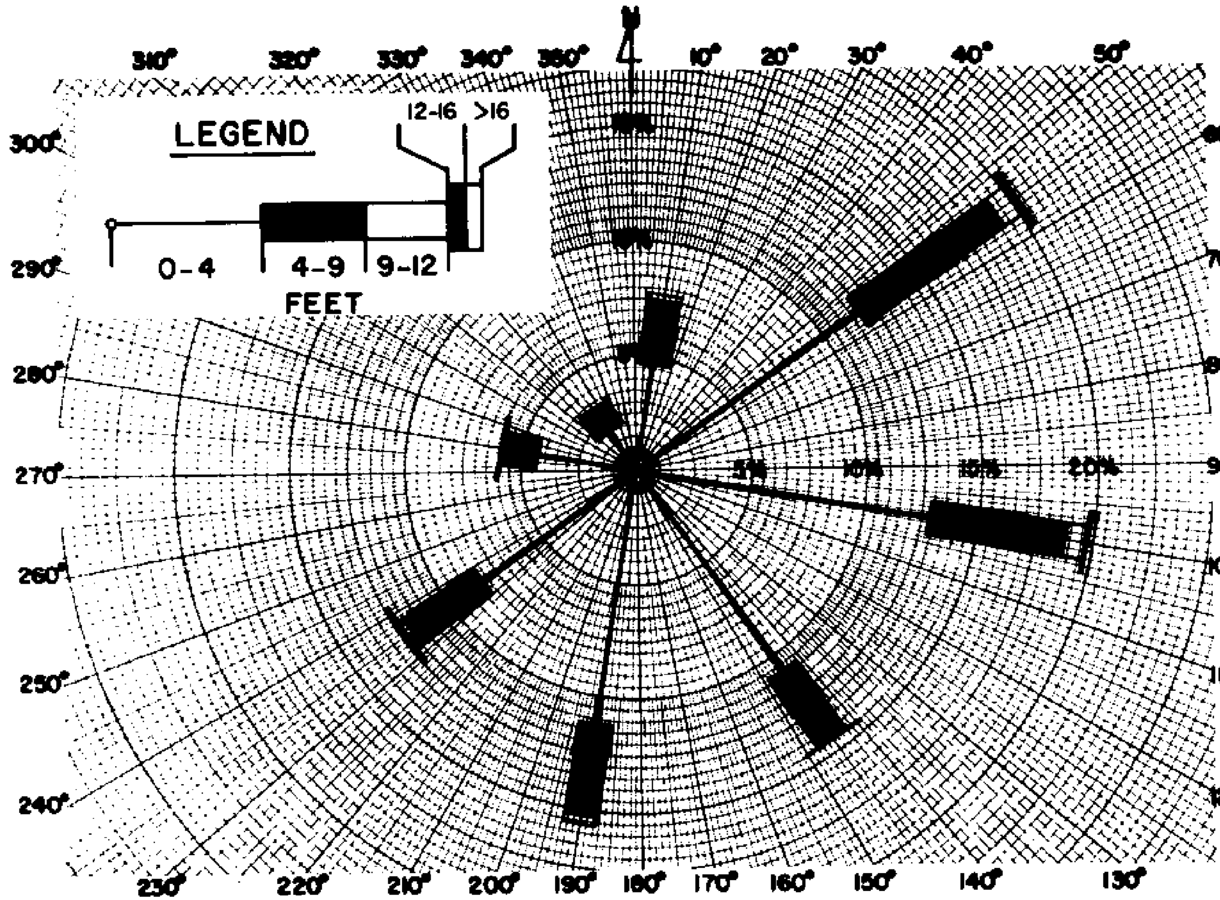

FIGURE D11. WAVE HEIGHT ROSE FOR OFFSHORE WAVE CLIMATE
SSMO DATA SQUARE NO. 11 - JUNE

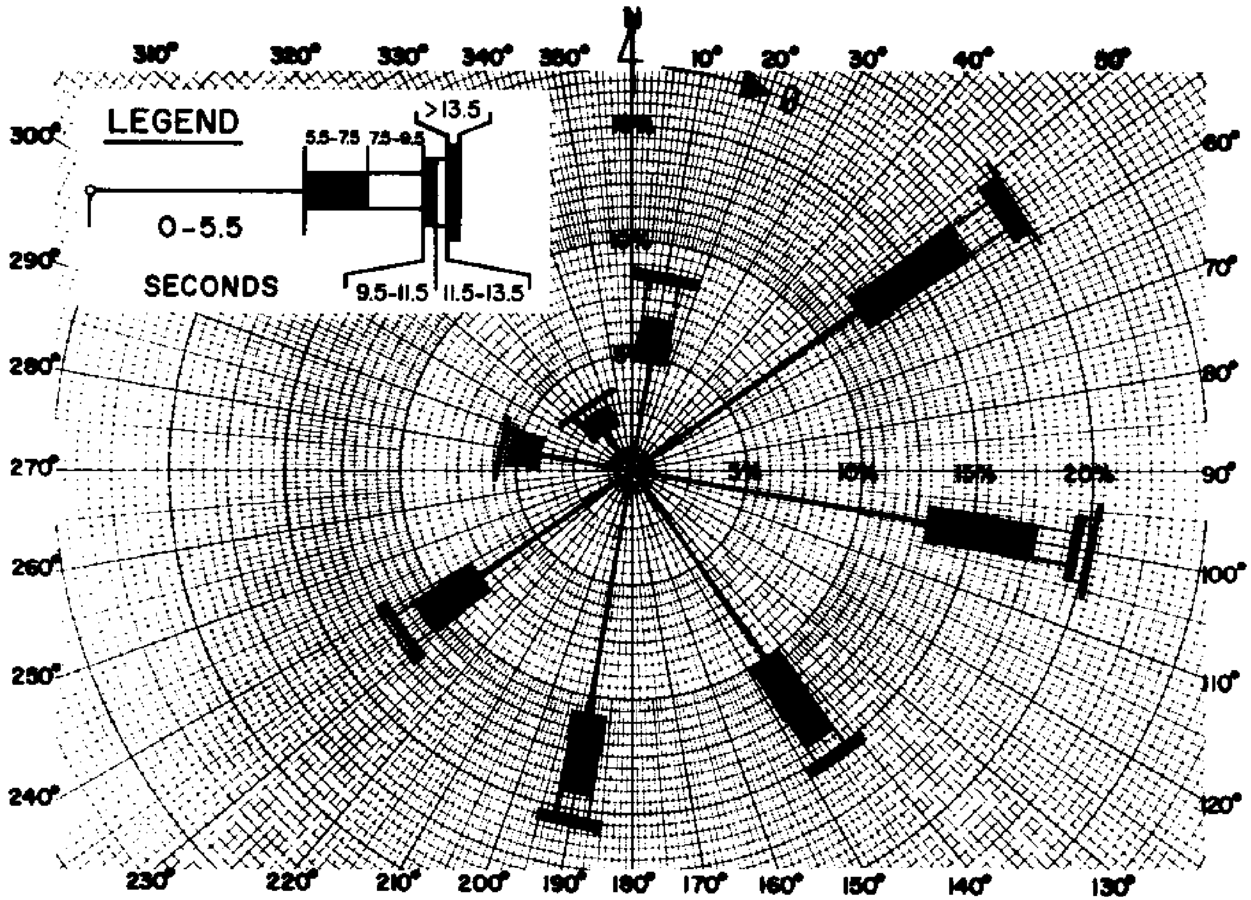

FIGURE D12. **WAVE** PERIOD **ROSE FOR OFFSHORE WAVE CLIMATE SSMO DATA SQUARE NO.** 11 - JUNE

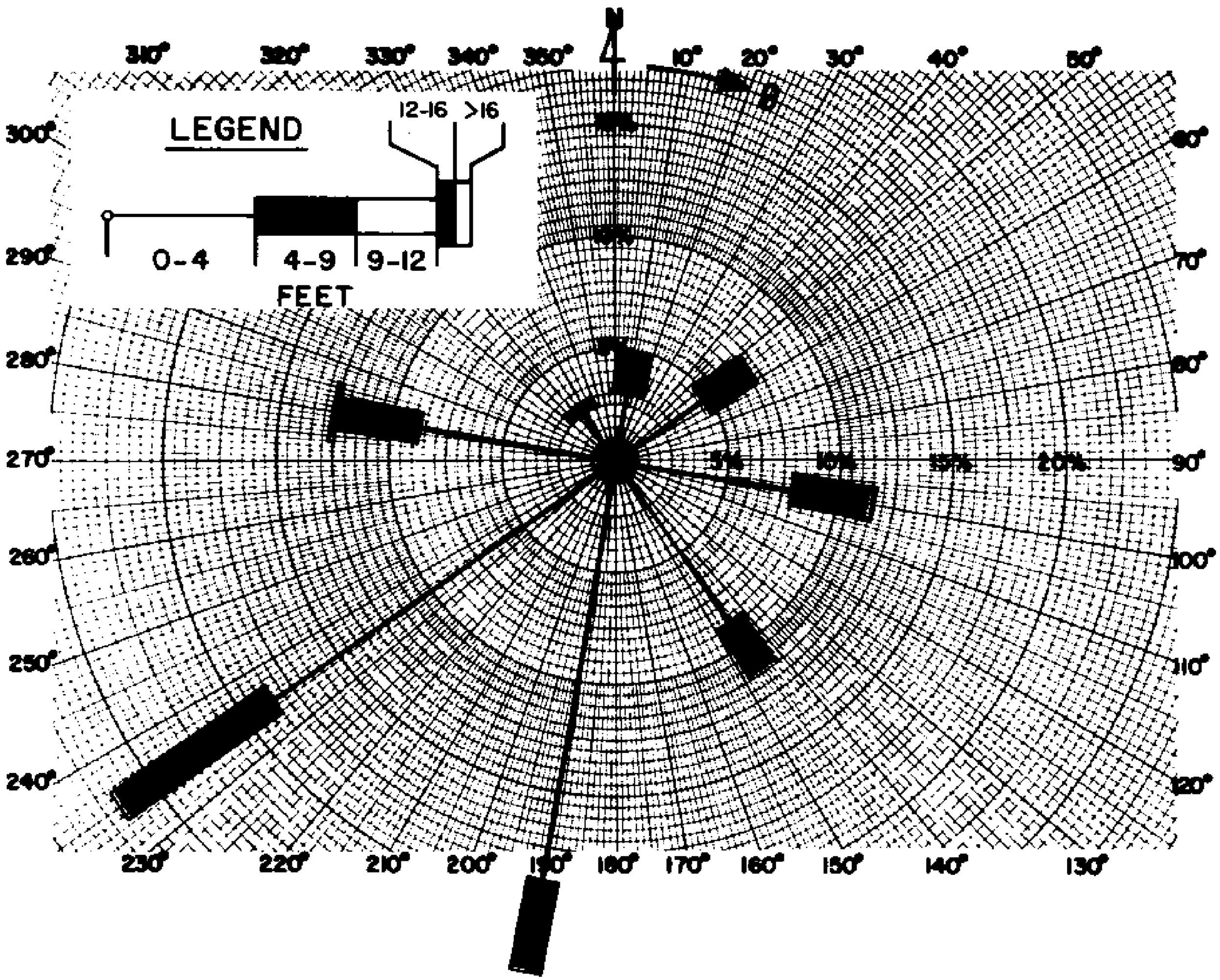

FIGURE D13. WAVE HEIGHT ROSE FOR OFFSHORE WAVE CLIMATE
SSMO DATA SQUARE NO. 11 - JULY

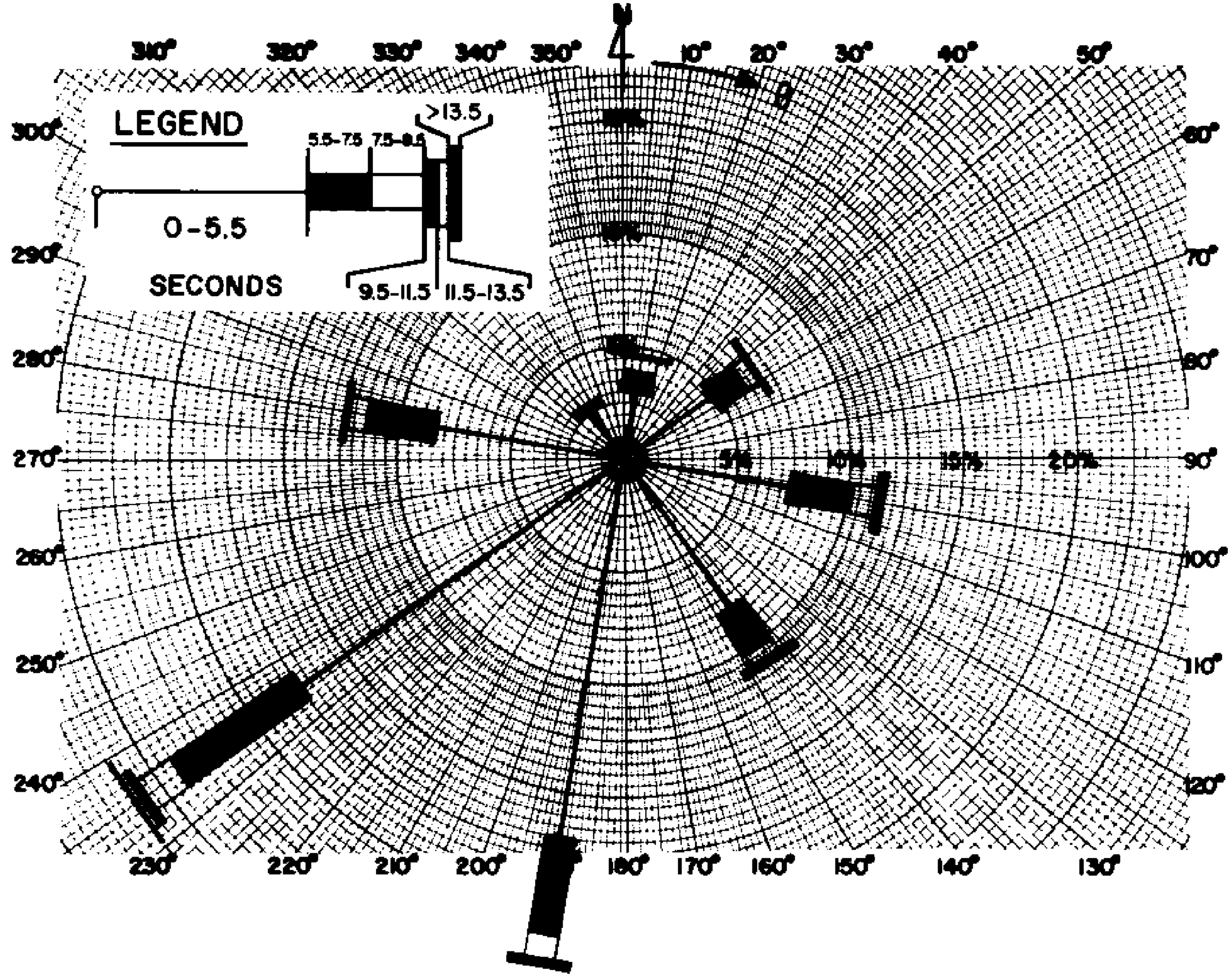

FIGURE D14. WAVE PERIOD ROSE FOR OFFSHORE WAVE CLIMATE SSMO DATA SQUARE NO. 11 - JULY

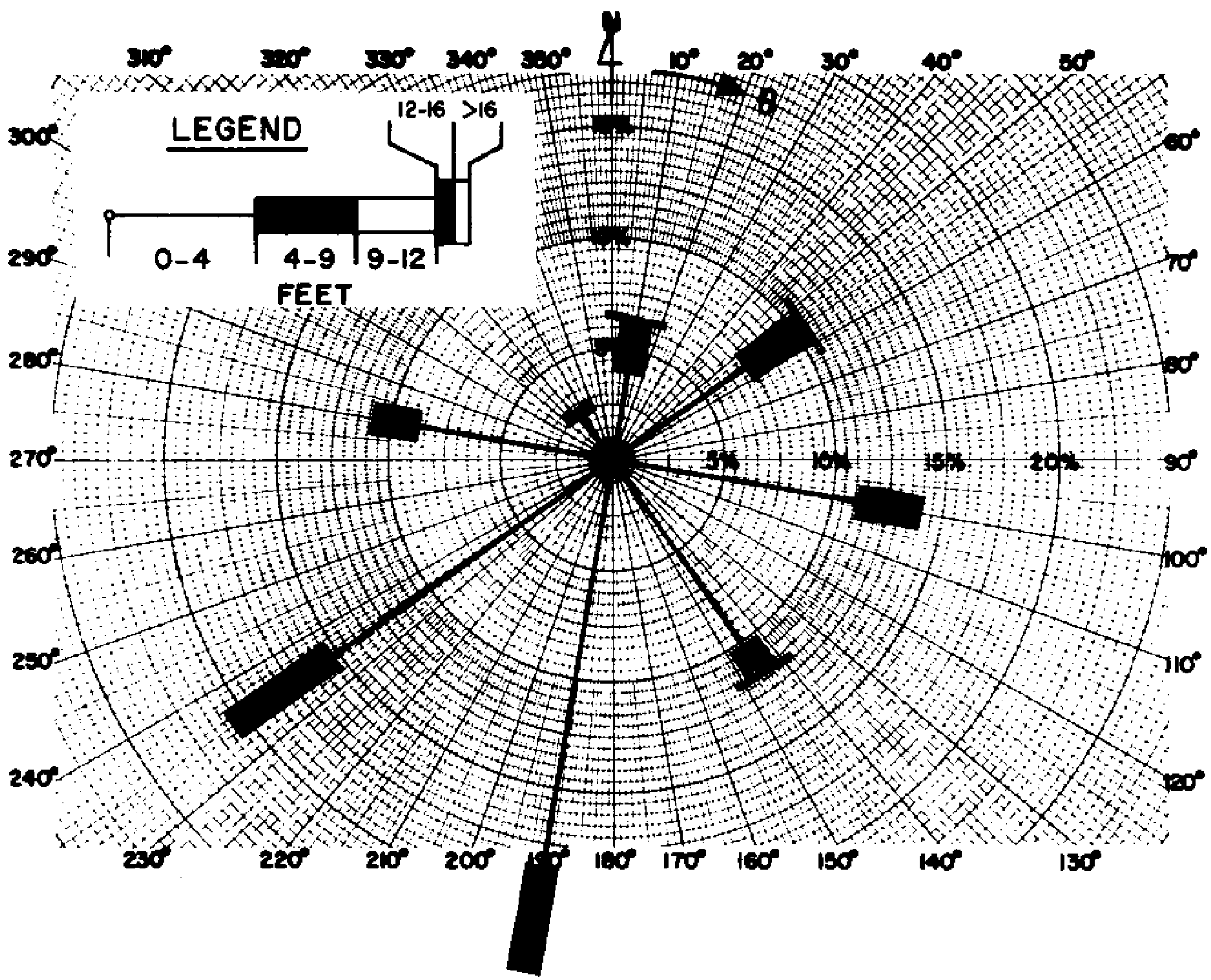

FIGURE D15. WAVE HEIGHT ROSE FOR OFFSHORE WAVE CLIMATE SSMO DATA SQUARE NO. 11 - AUGUST

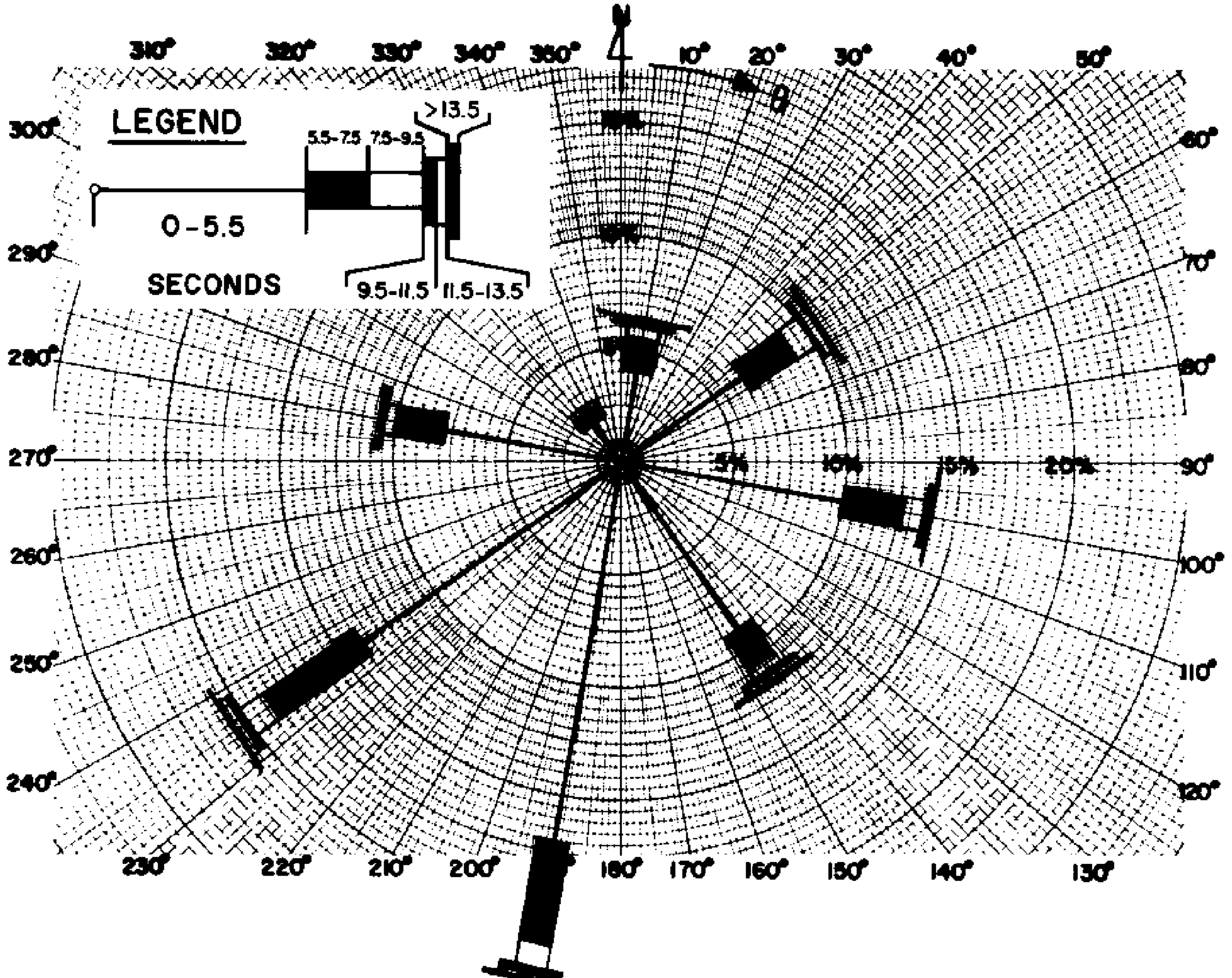

FIGURE D16. WAVE PERIOD ROSE FOR OFFSHORE WAVE CLIMATE
SSMO DATA SQUARE NO. 11 - AUGUST

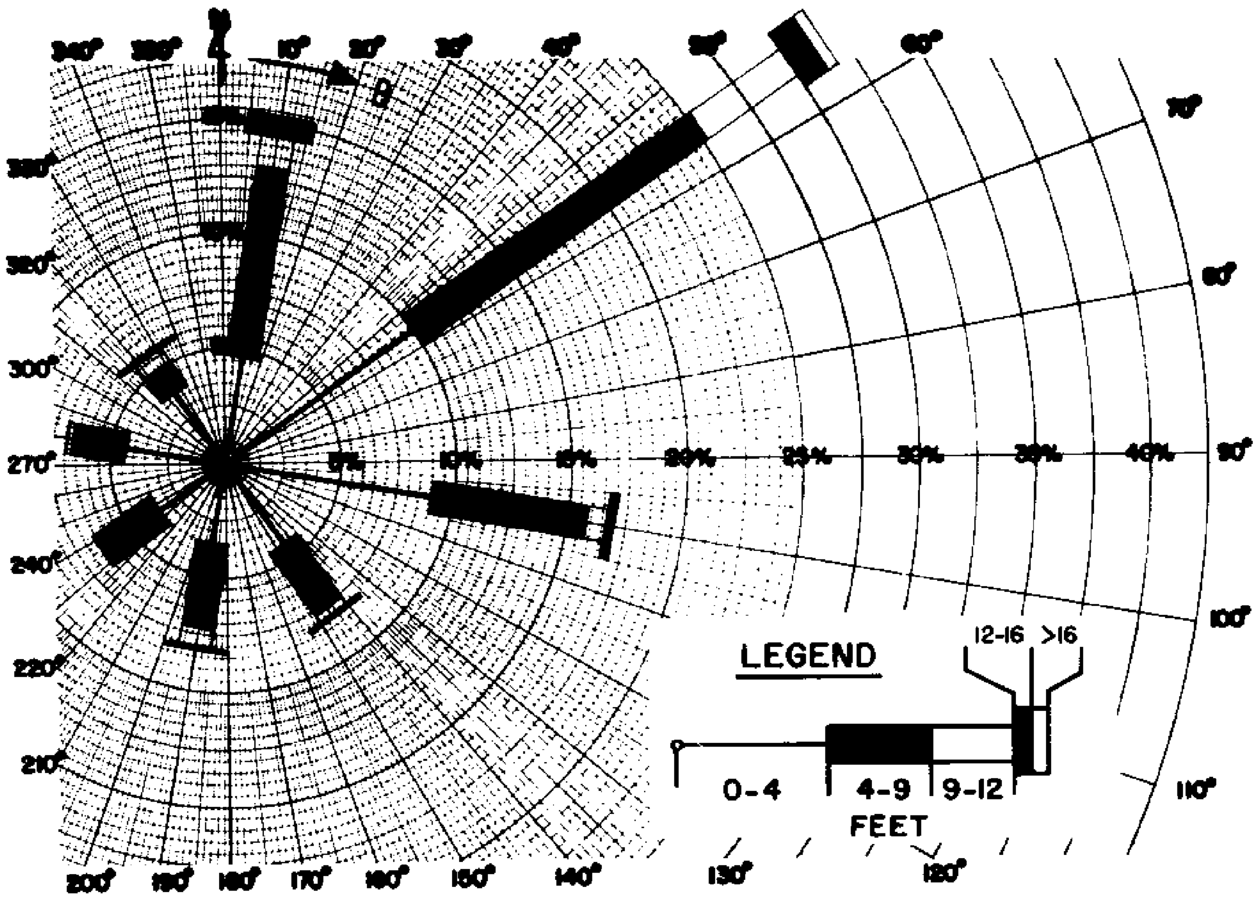

FIGURE D 17. WAVE HEIGHT ROSE FOR OFFSHORE WAVE CLIMATE SSMO DATA SQUARE NO. 11 - SEPTEMBER

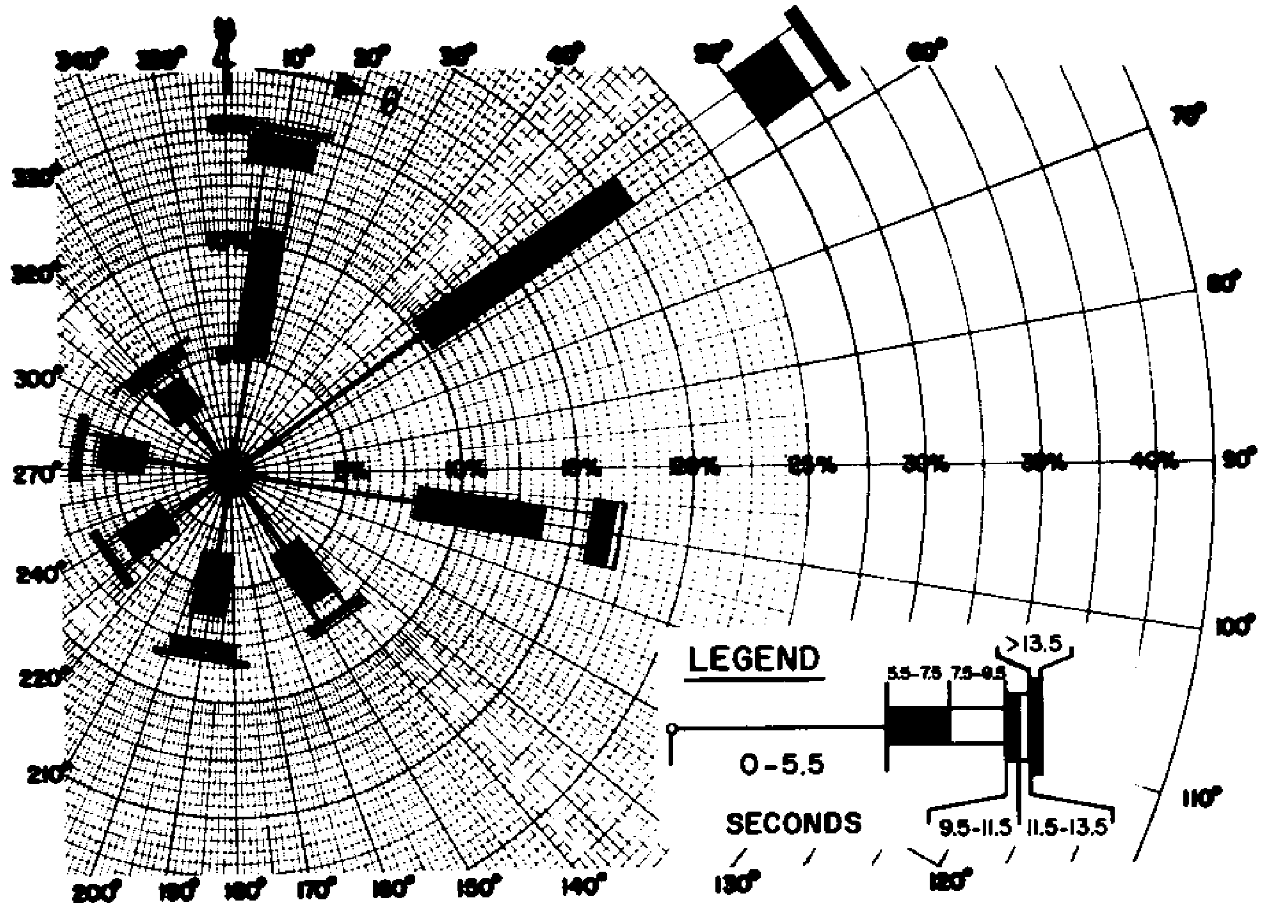

FIGURE D 18. WAVE PERIOD ROSE FOR OFFSHORE WAVE CLIMATE SSMO DATA SQUARE NO. 11 - SEPTEMBER

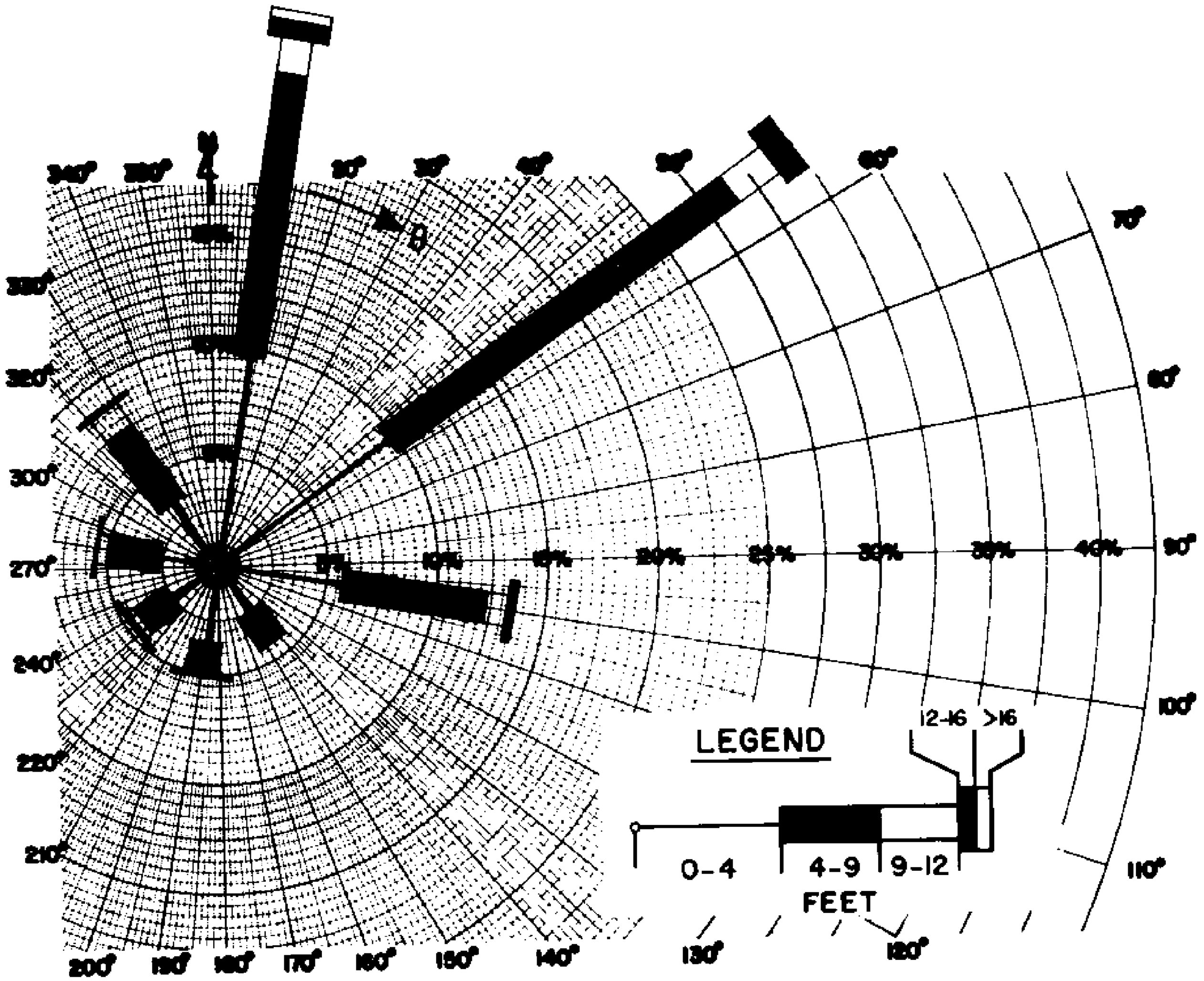

FIGURE D19. WAVE HEIGHT ROSE FOR OFFSHORE WAVE CLIMATE
SSMO DATA SQUARE NO. 11 - OCTOBER

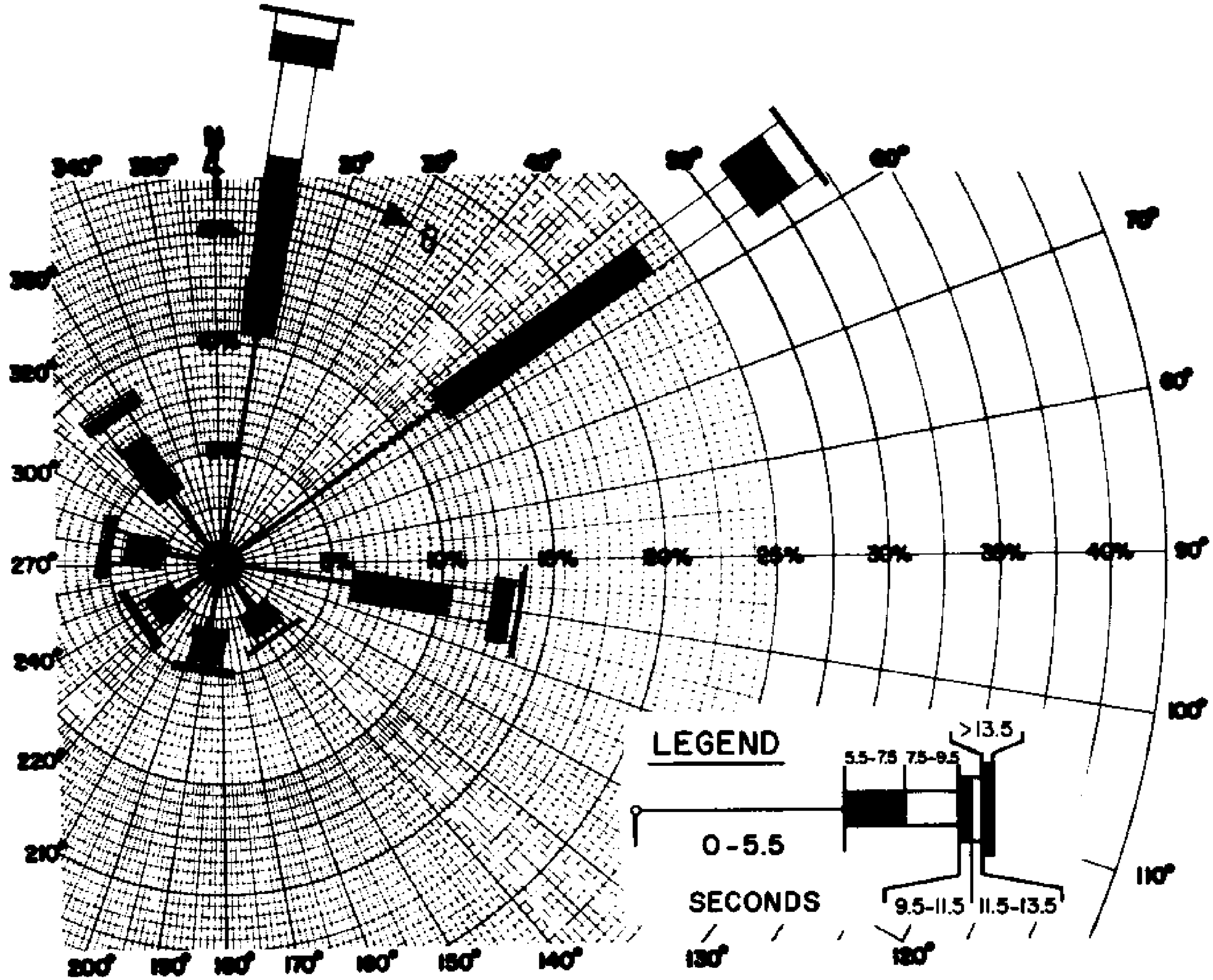

FIGURE D 20. WAVE PERIOD ROSE FOR OFFSHORE WAVE CLIMATE
SSMO DATA SQUARE NO. 11 - OCTOBER

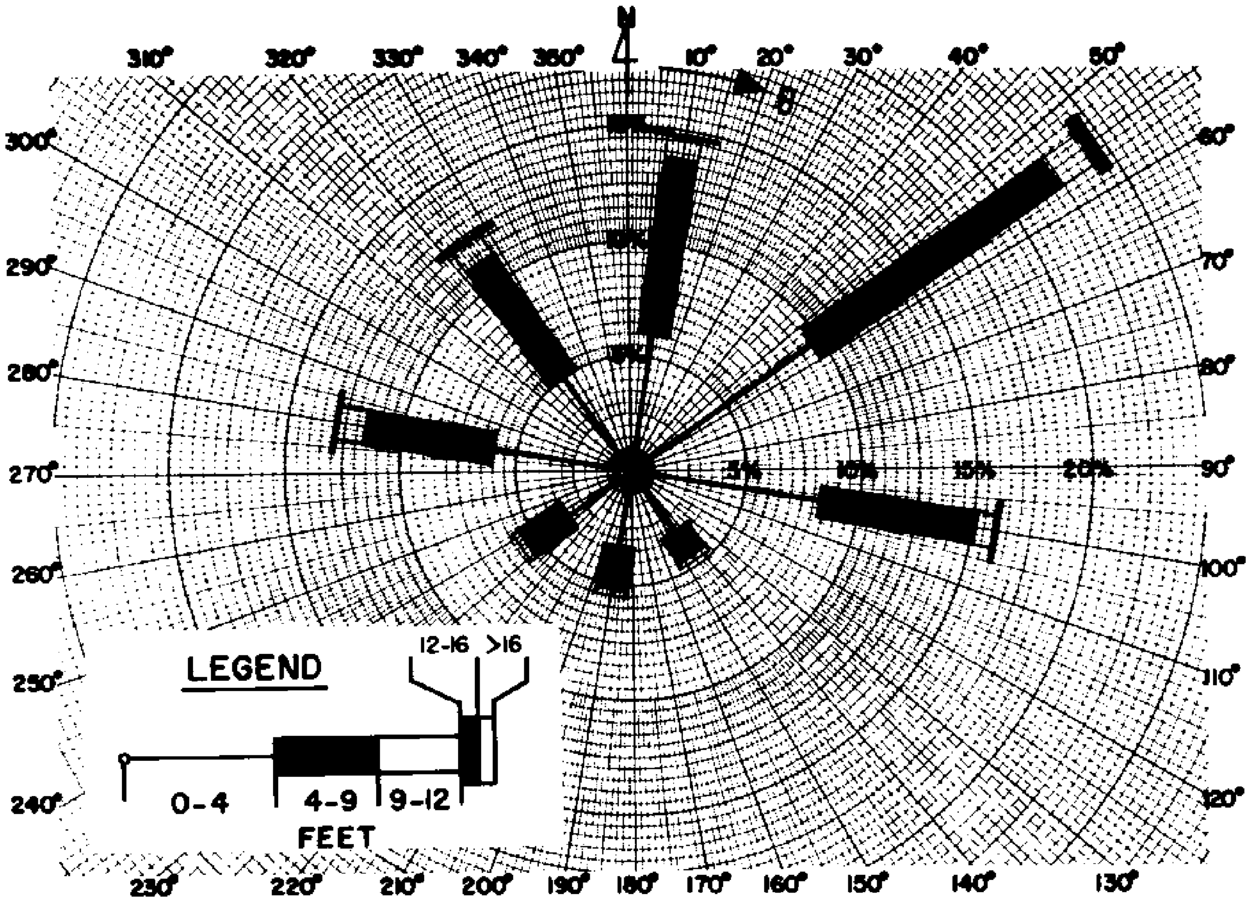

FIGURE D21. WAVE HEIGHT ROSE FOR OFFSHORE WAVE CLIMATE
SSMO DATA SQUARE NO. 11 - NOVEMBER

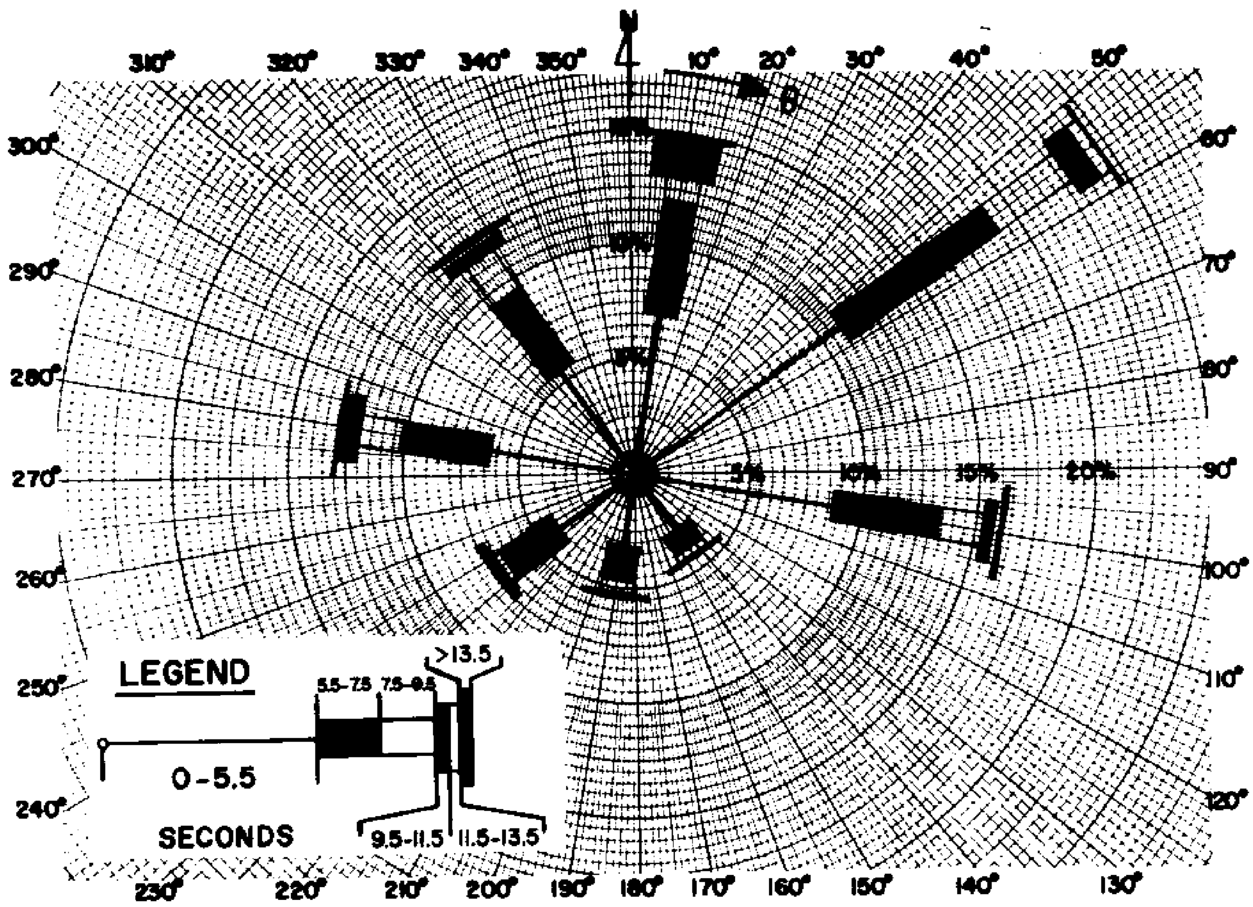

FIGURE D22. WAVE PERIOD ROSE FOR OFFSHORE WAVE CLIMATE SSMO DATA SQUARE NO. 11 - NOVEMBER

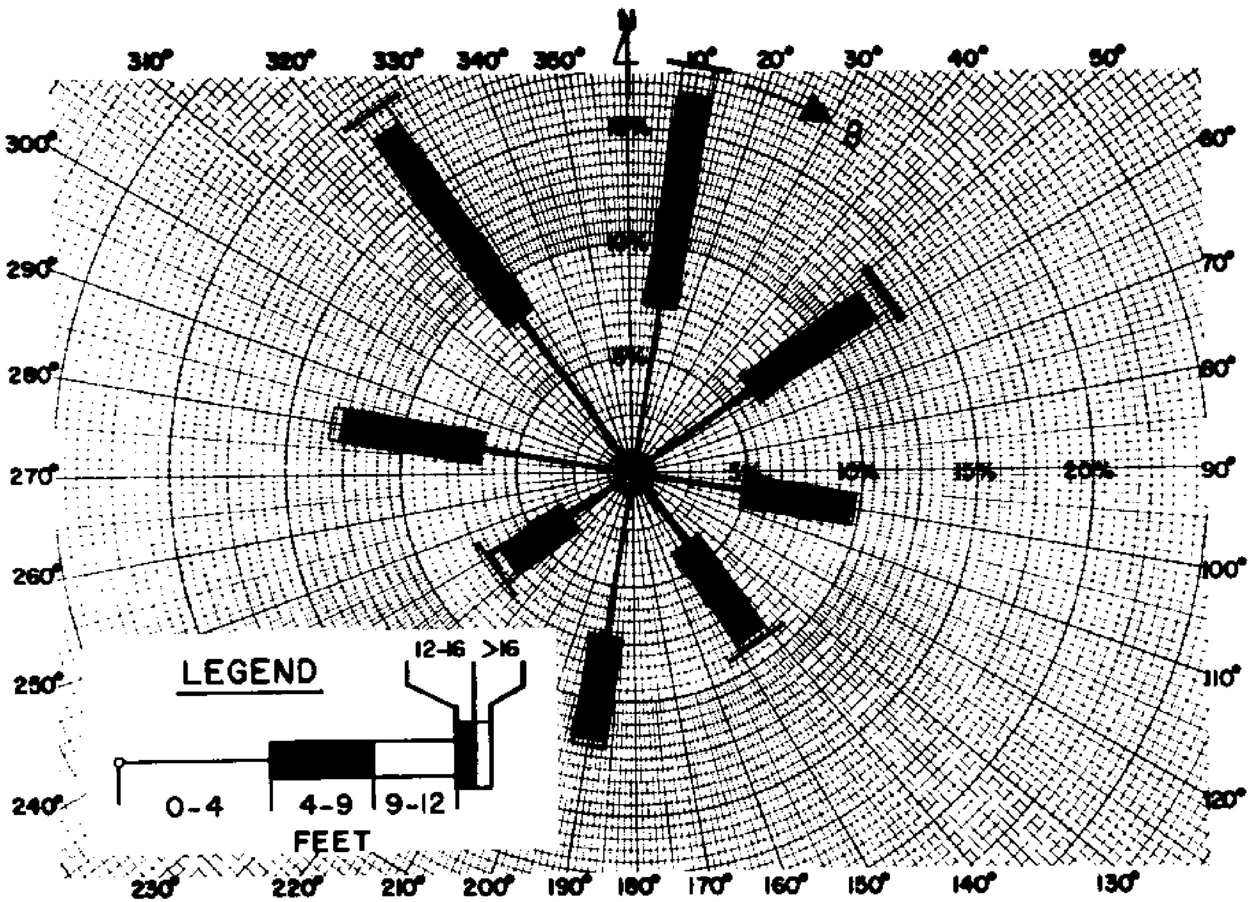

FIGURE D 23. WAVE HEIGHT ROSE FOR OFFSHORE WAVE CLIMATE SSMO DATA SQUARE NO. 11 - DECEMBER

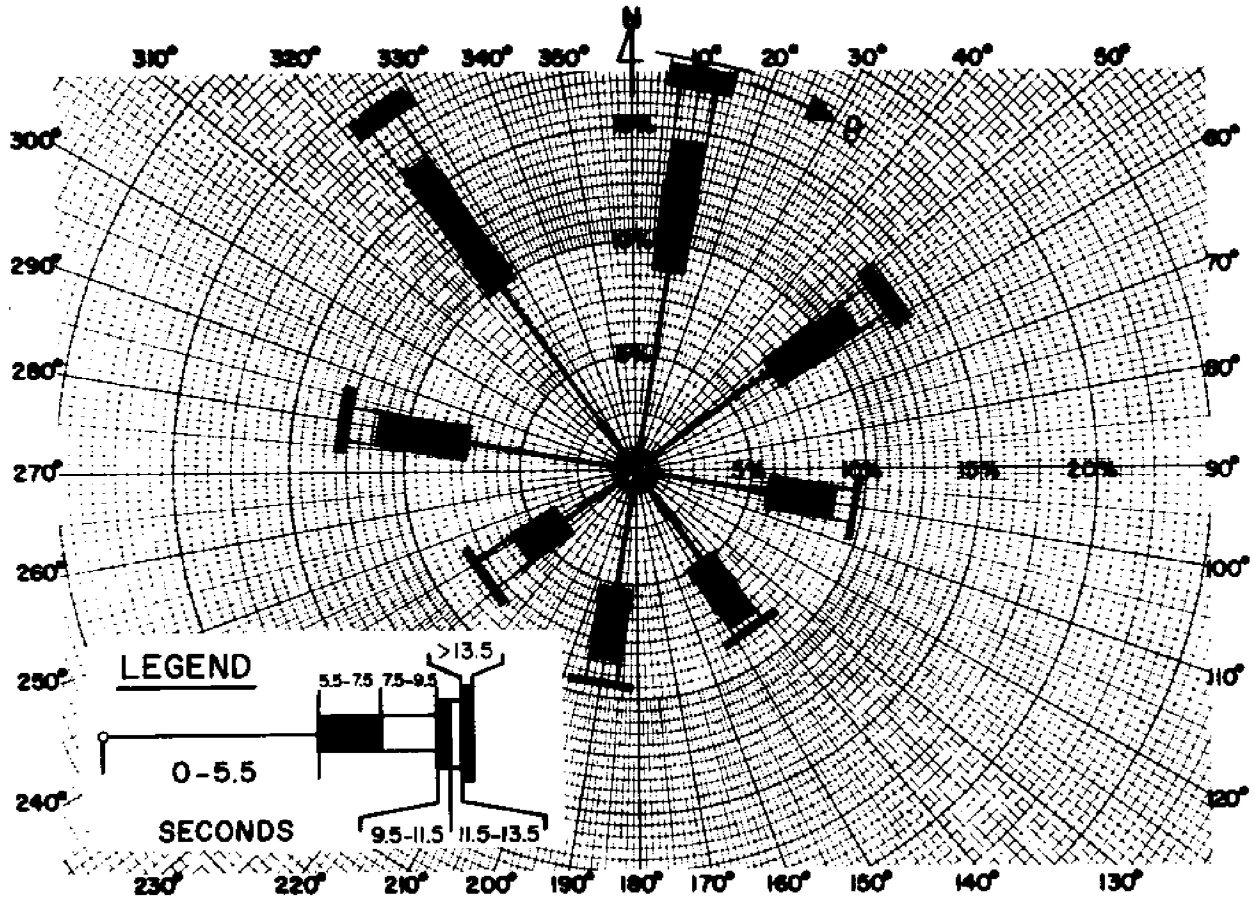

FIGURE D 24. WAVE PERIOD ROSE FOR OFFSHORE WAVE CLIMATE SSMO DATA SQUARE NO. 11 - DECEMBER

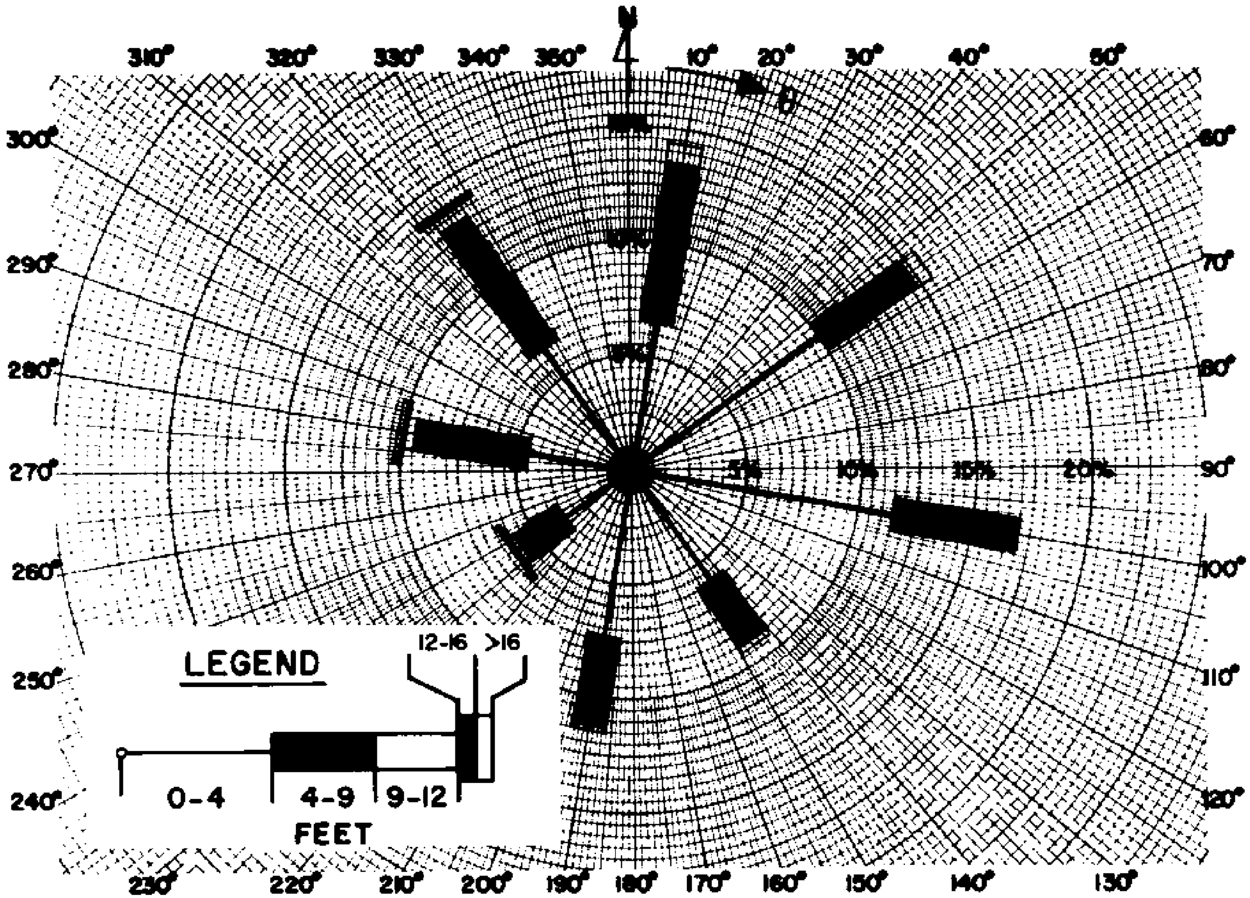

FIGURE D 25. WAVE HEIGHT ROSE FOR OFFSHORE WAVE CLIMATE
SSMO DATA SQUARE NO. 12 - JANUARY

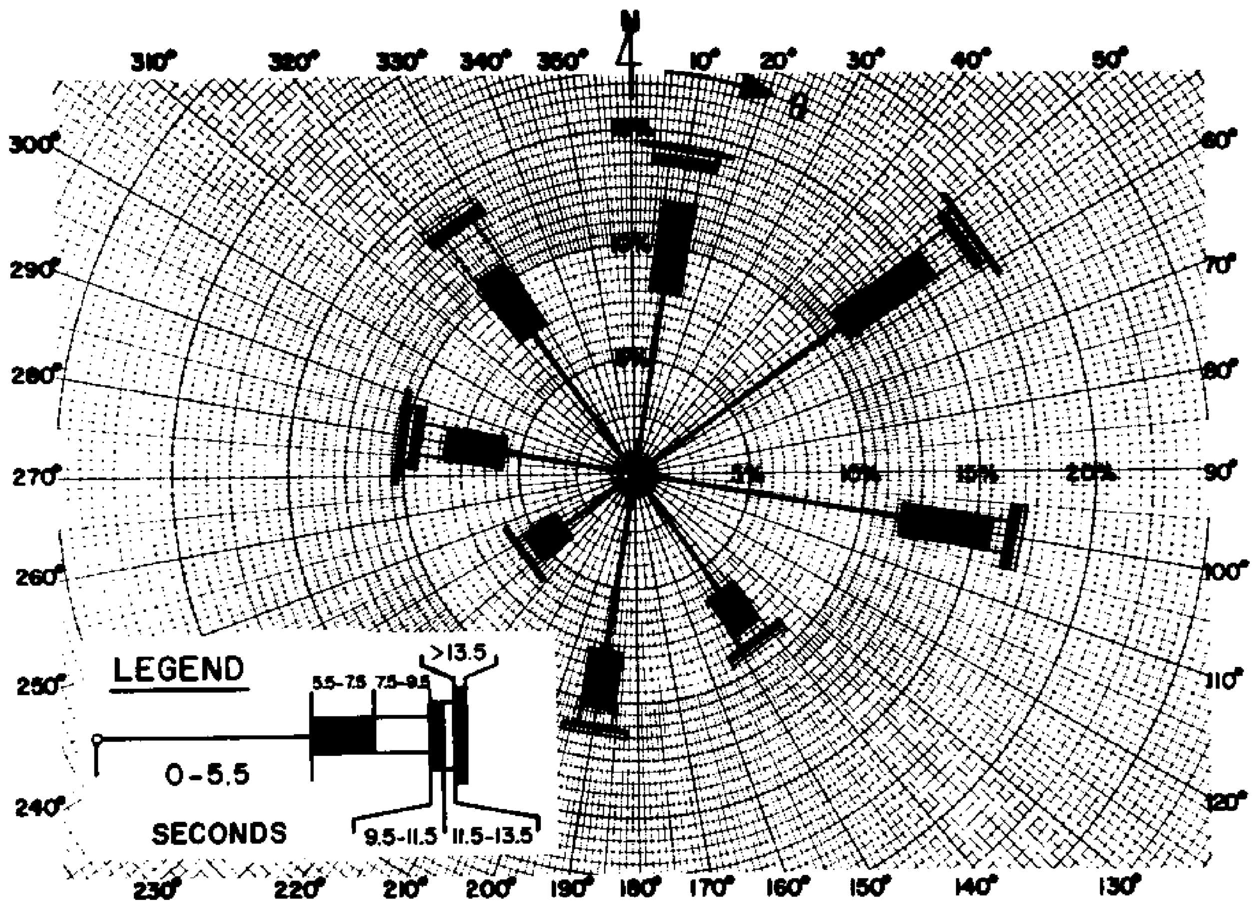

FIGURE D 26. WAVE PERIOD ROSE FOR OFFSHORE WAVE CLIMATE
SSMO DATA SQUARE NO. 12 - JANUARY

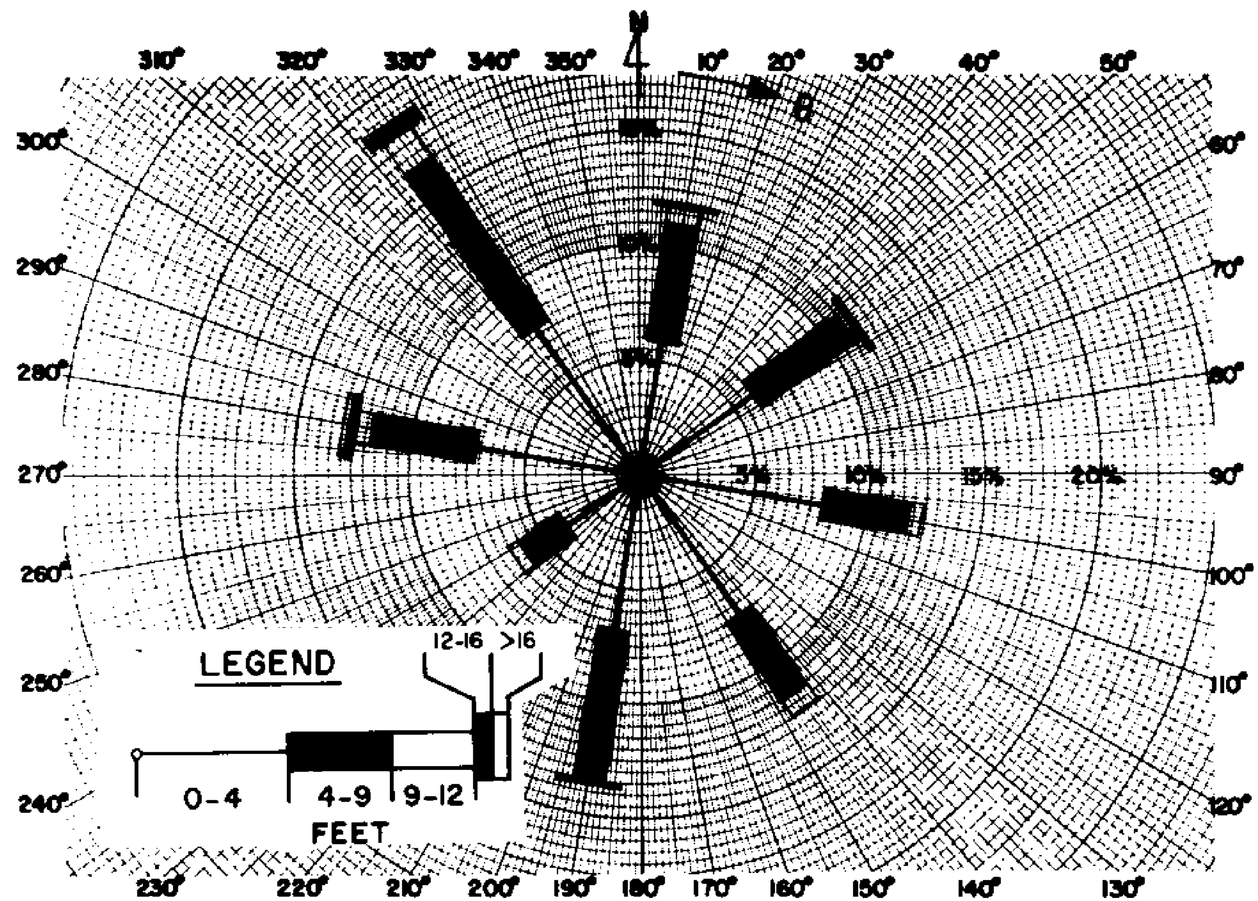

FIGURE D 27. WAVE HEIGHT ROSE FOR OFFSHORE WAVE CLIMATE
SSMO DATA SQUARE NO. 12 - FEBRUARY

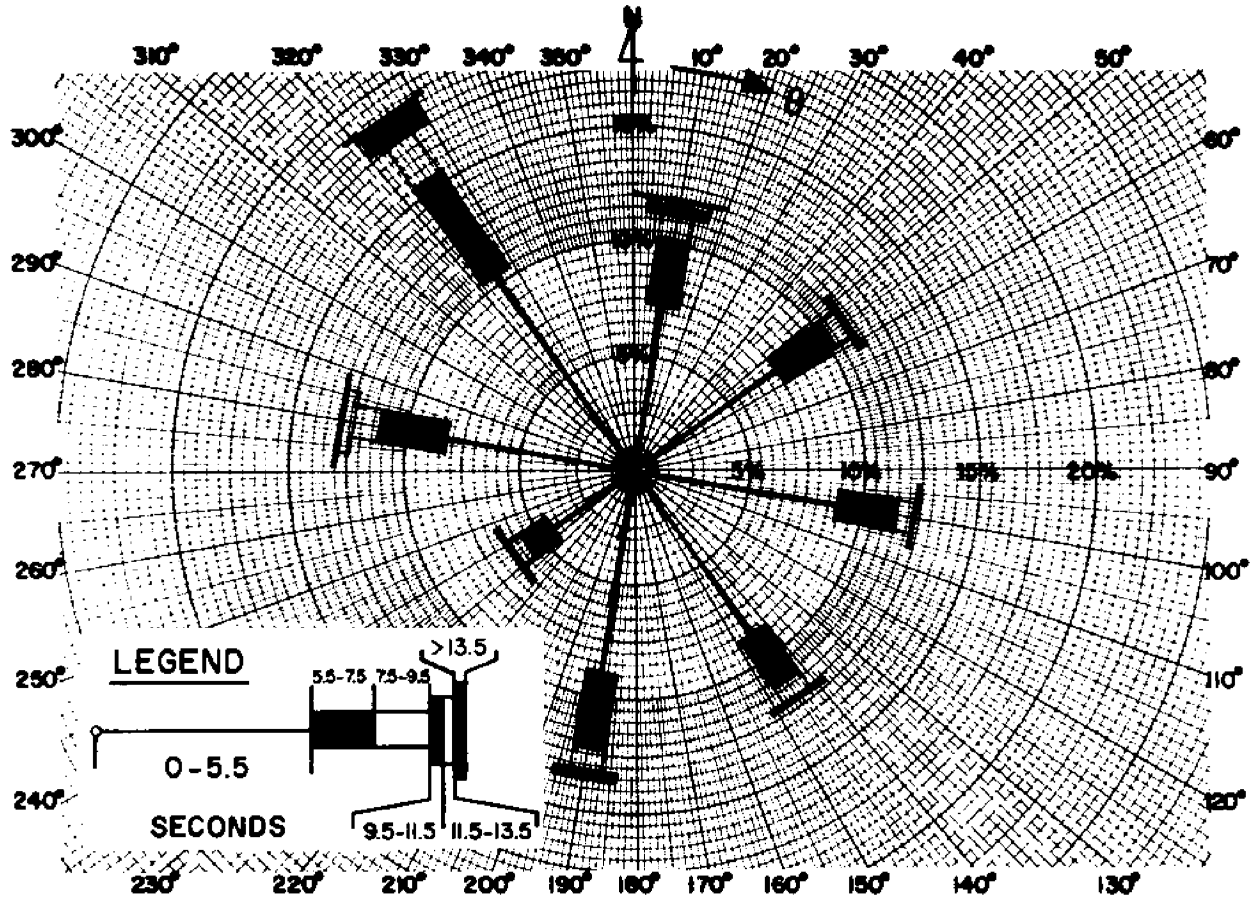

FIGURE D 28. WAVE PERIOD ROSE FOR OFFSHORE WAVE CLIMATE
SSMO DATA SQUARE NO. 12 - FEBRUARY

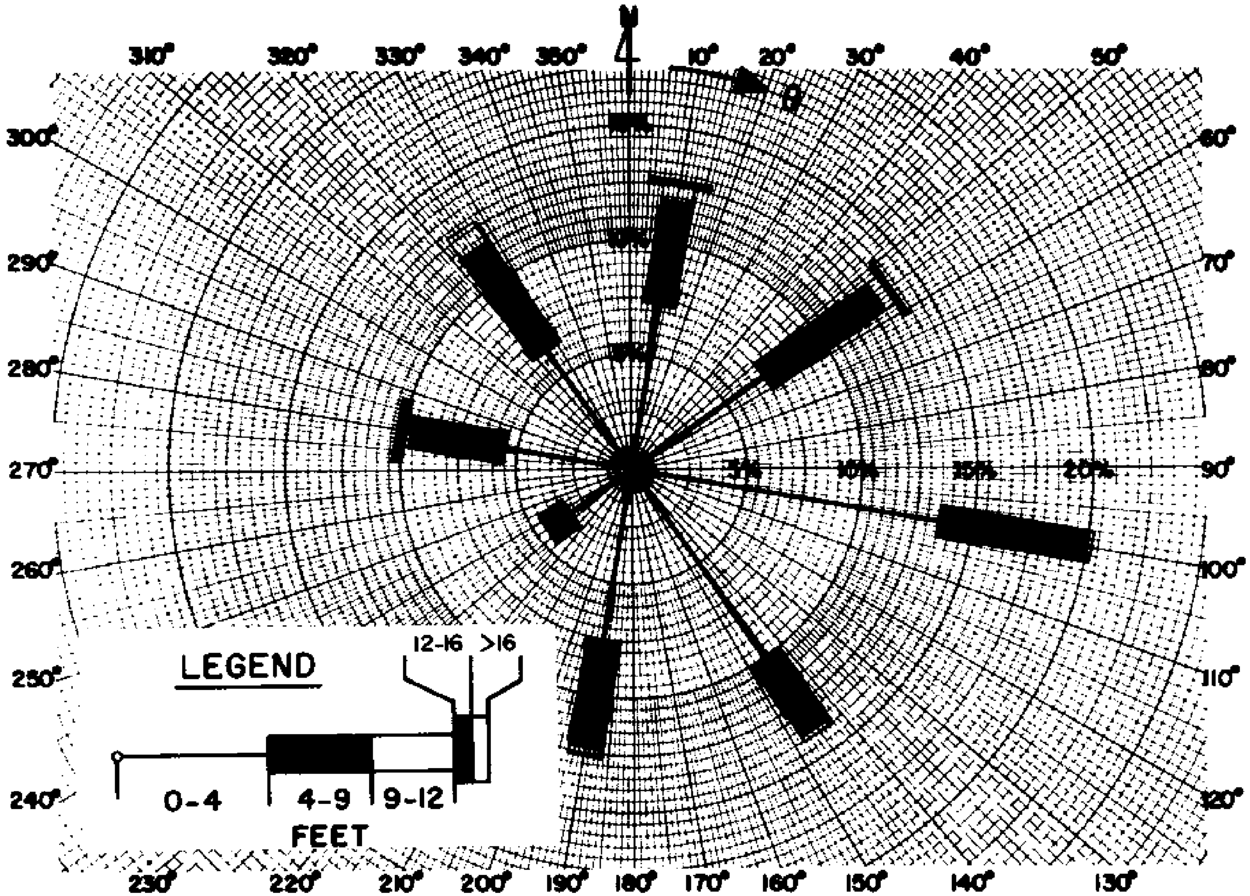

FIGURE D 29. WAVE HEIGHT ROSE FOR OFFSHORE WAVE CLIMATE SSMO DATA SQUARE NO. 12 - MARCH

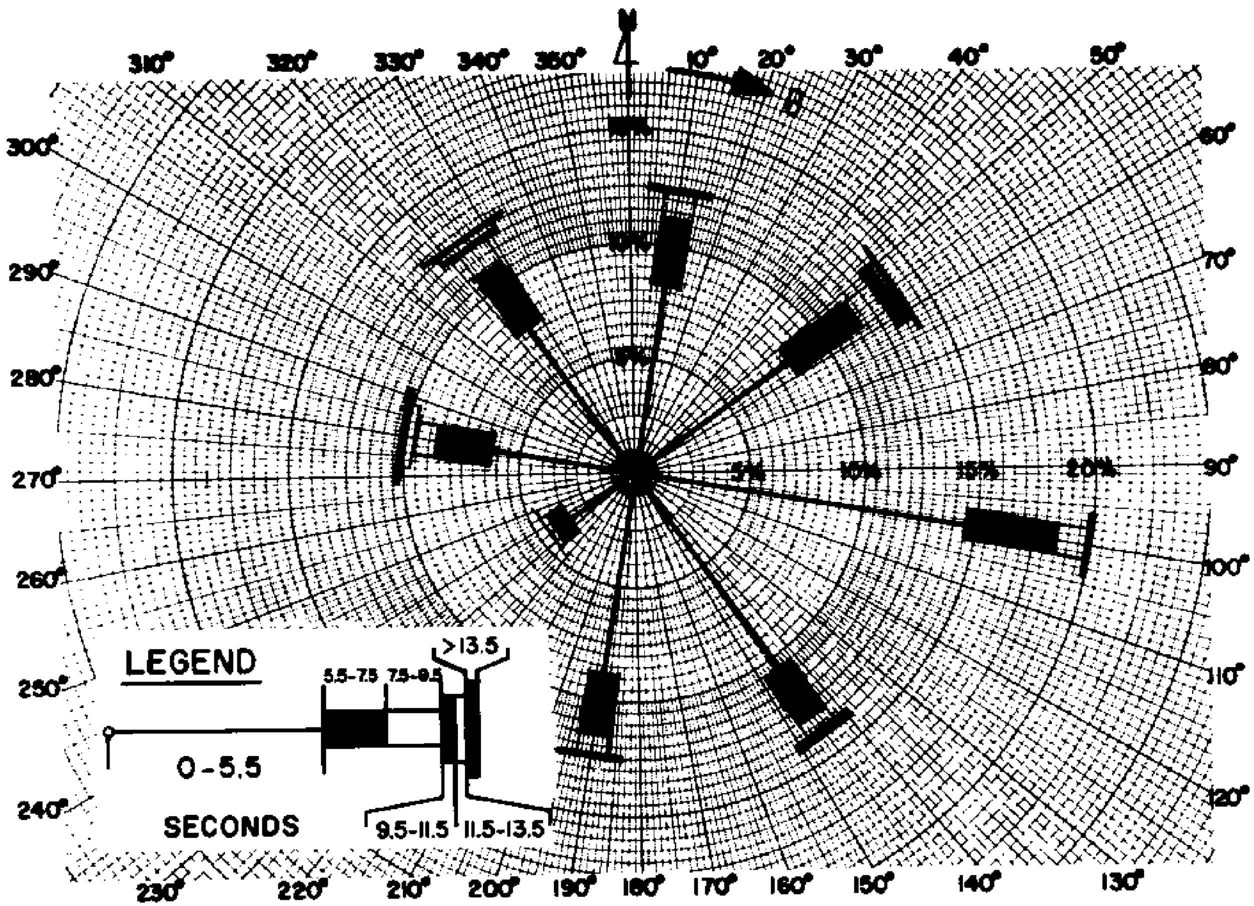

FIGURE D 30. WAVE PERIOD ROSE FOR OFFSHORE WAVE CLIMATE
SSMO DATA SQUARE NO. 12 - MARCH

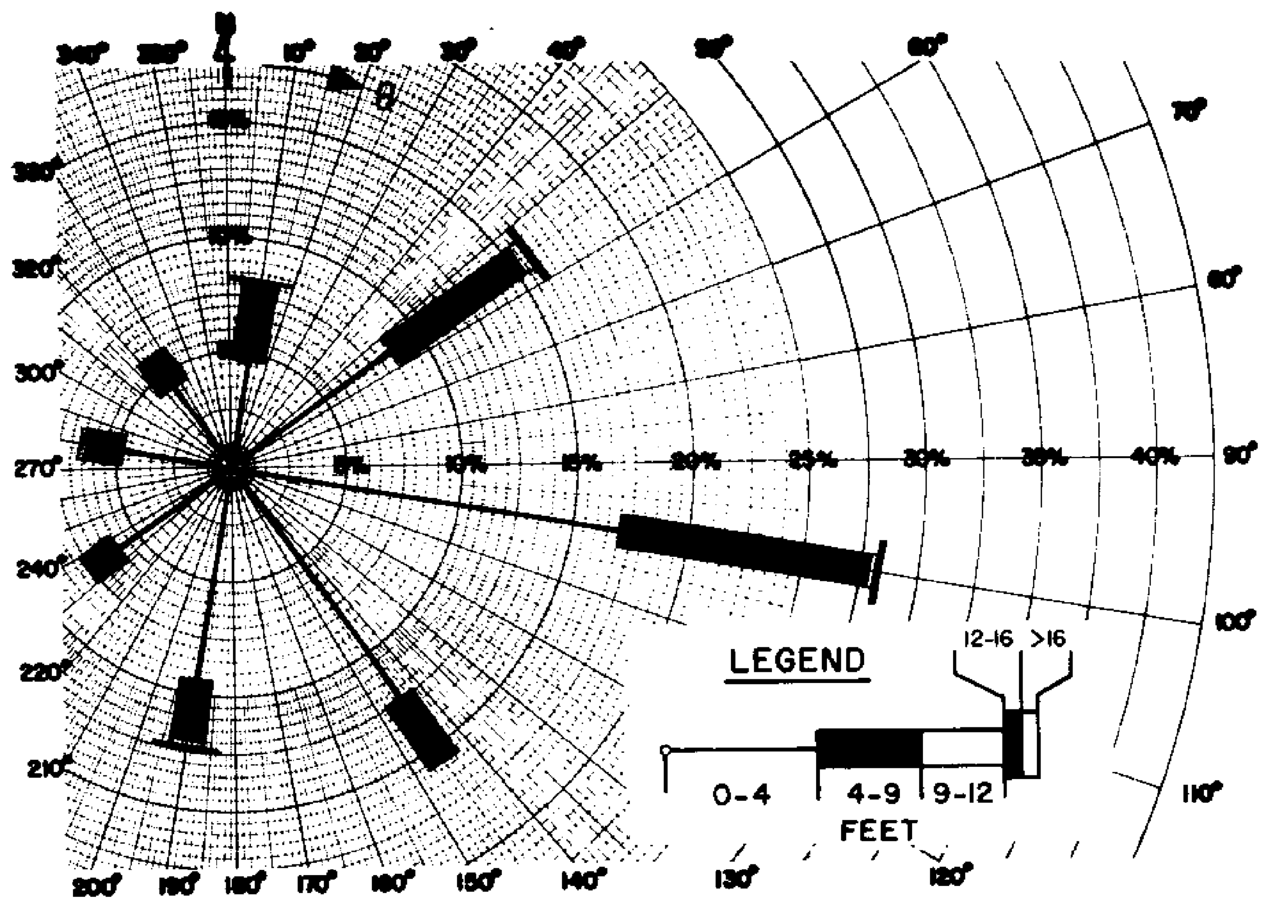

FIGURE D 31. WAVE HEIGHT ROSE FOR OFFSHORE WAVE CLIMATE SSMO DATA SQUARE NO. 12 - APRIL

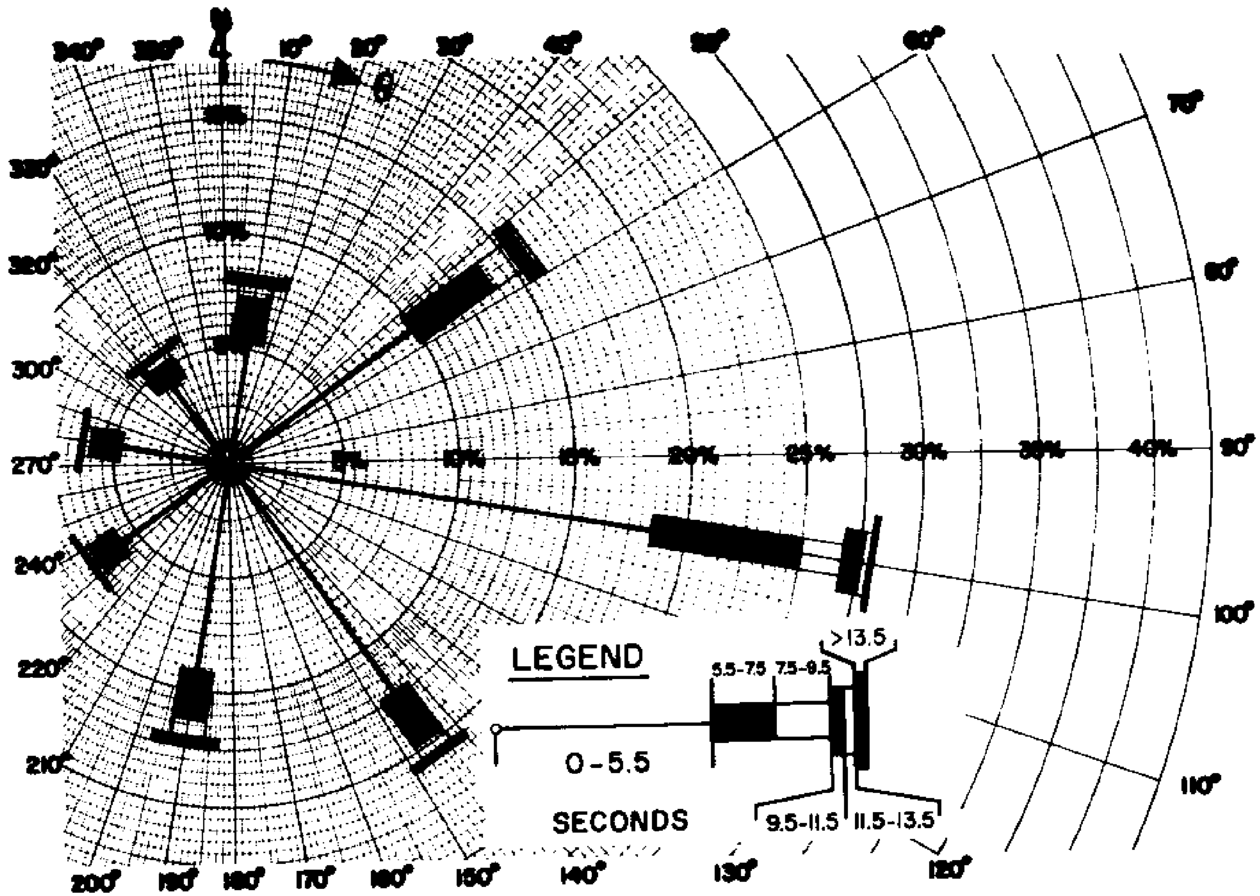

FIGURE D32. WAVE PERIOD ROSE FOR OFFSHORE WAVE CLIMATE
SSMO DATA SQUARE NO. 12 - APRIL

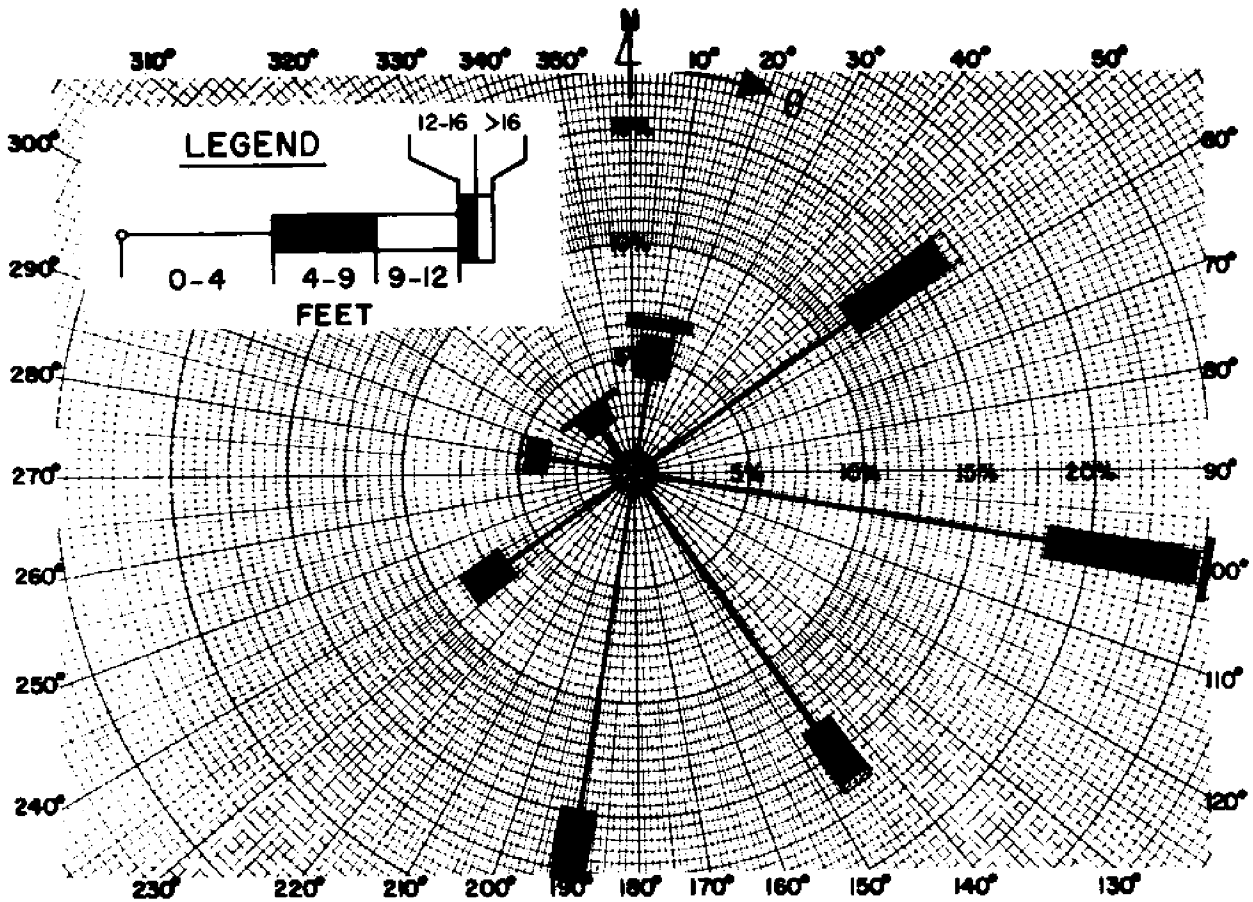

FIGURE D 33. WAVE HEIGHT ROSE FOR OFFSHORE WAVE CLIMATE
SSMO DATA SQUARE NO. 12 - MAY

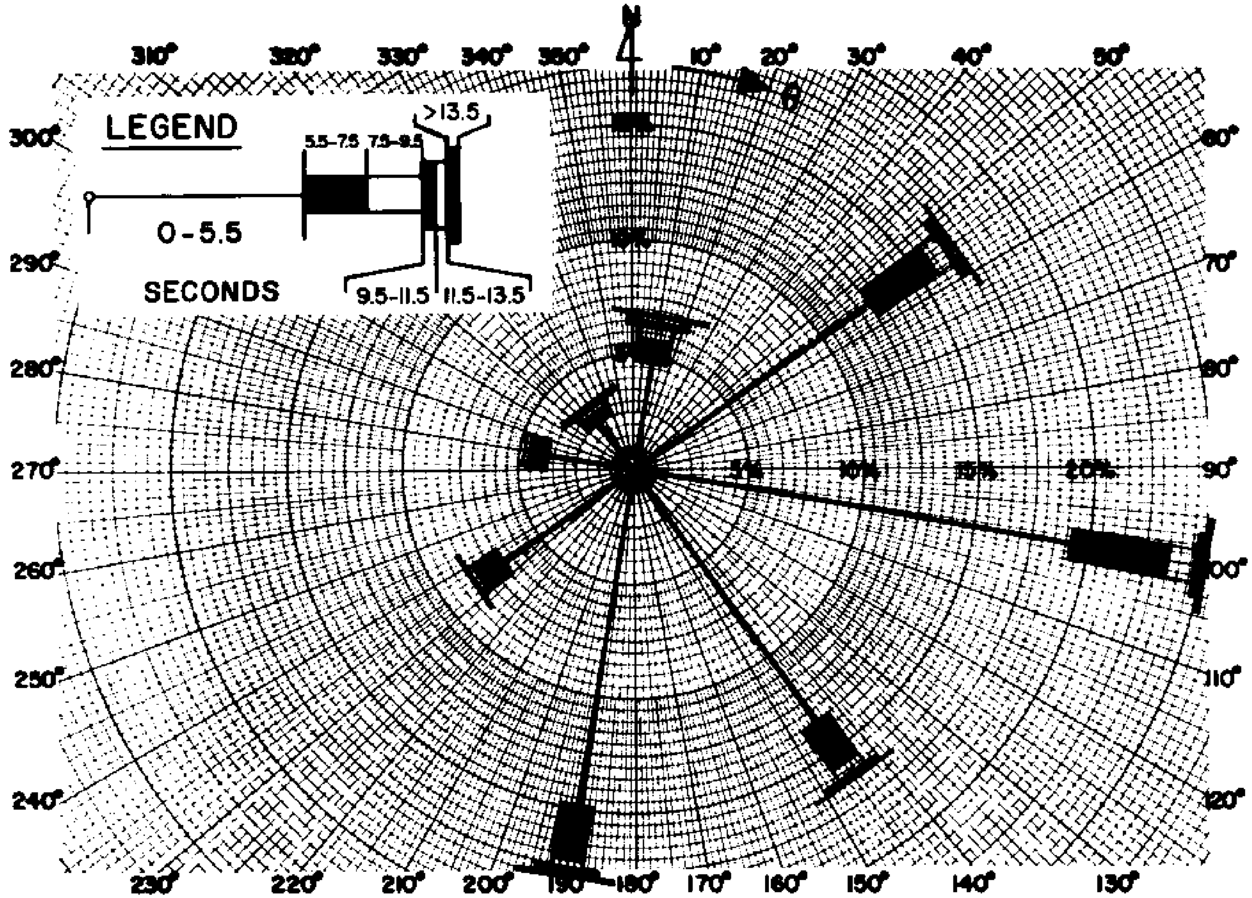

FIGURE D 34. WAVE PERIOD ROSE FOR OFFSHORE WAVE CLIMATE SSMO DATA SQUARE NO. 12 - MAY

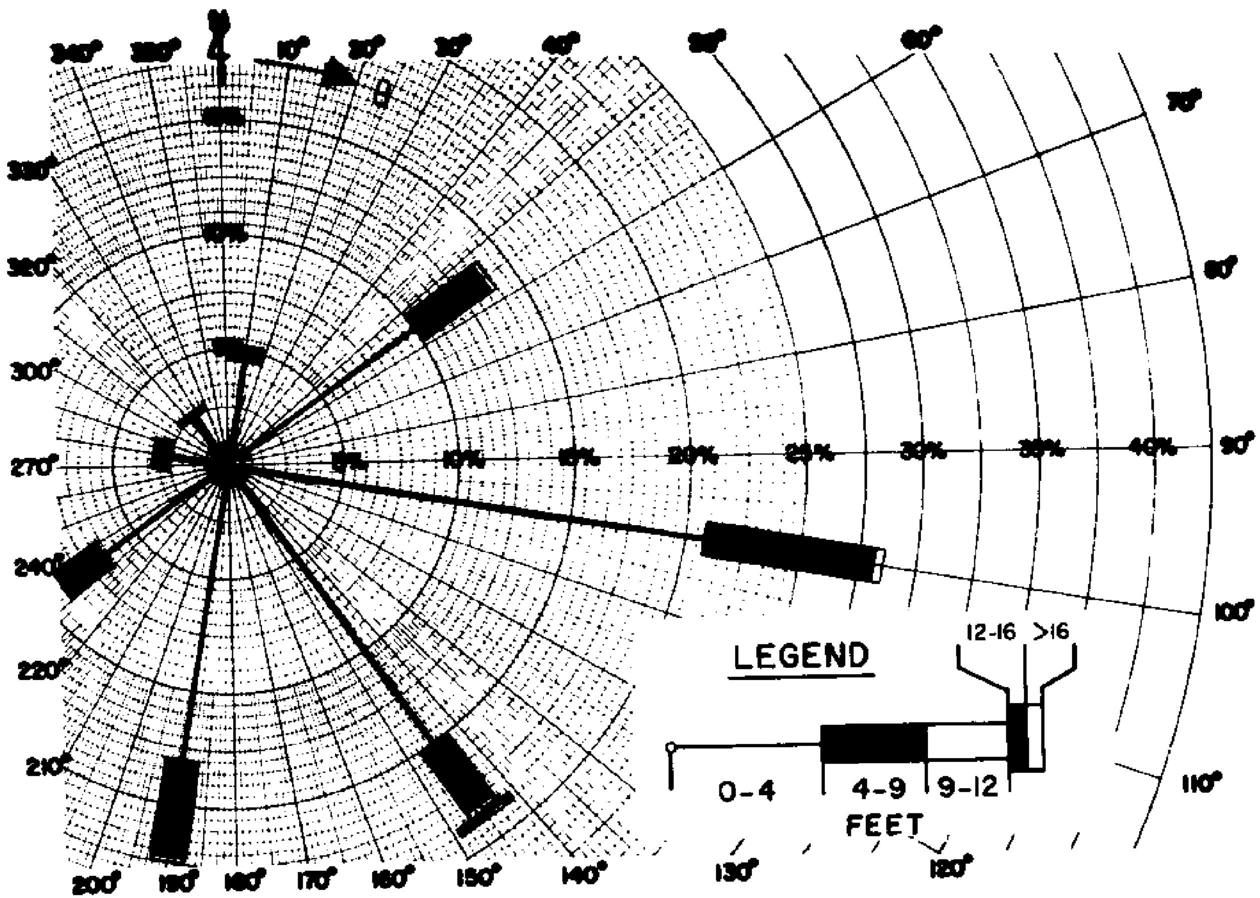

FIGURE D 35. WAVE HEIGHT ROSE FOR OFFSHORE WAVE CLIMATE SSMO DATA SQUARE NO. 12 - JUNE

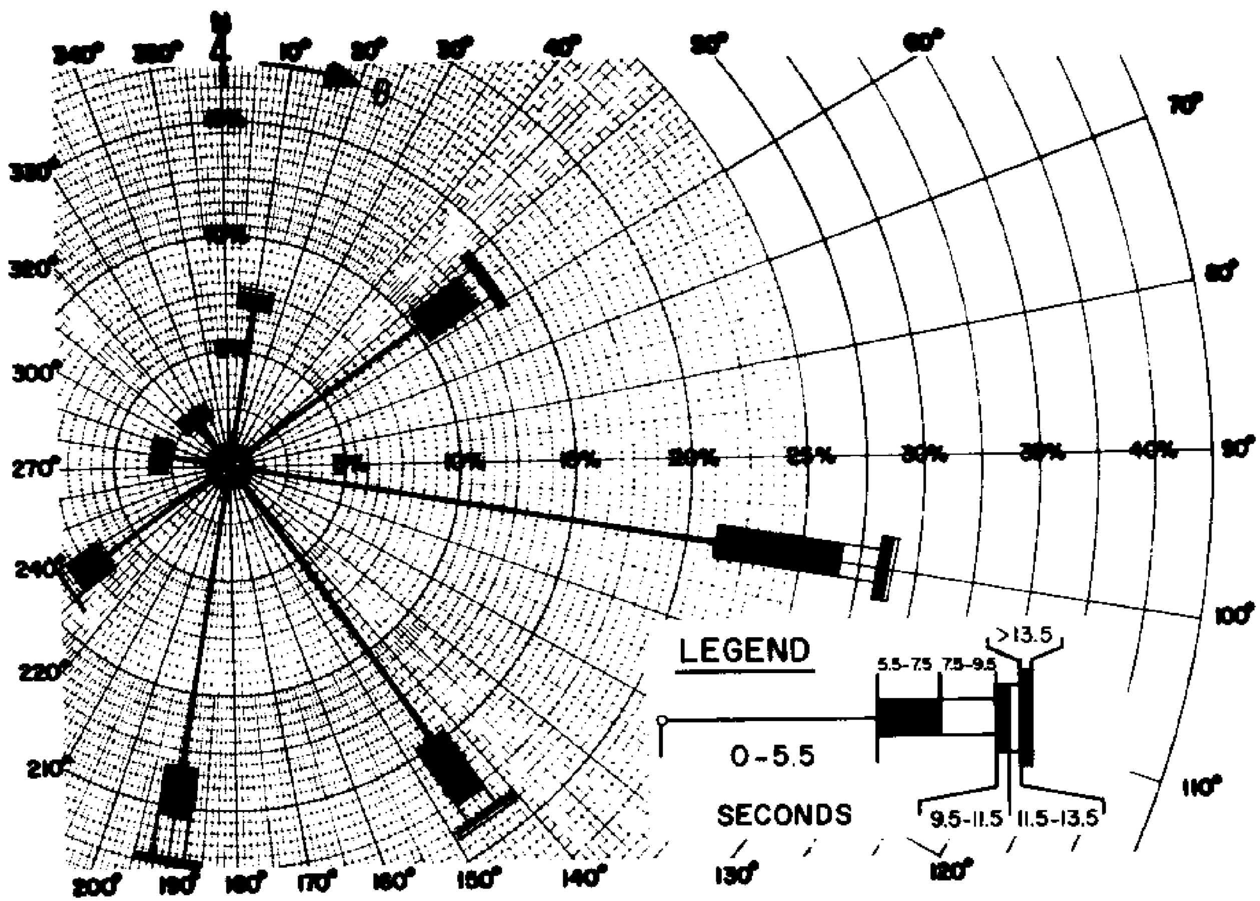

FIGURE D 36. WAVE PERIOD ROSE FOR OFFSHORE WAVE CLIMATE SSMO DATA SQUARE NO. 12 - JUNE

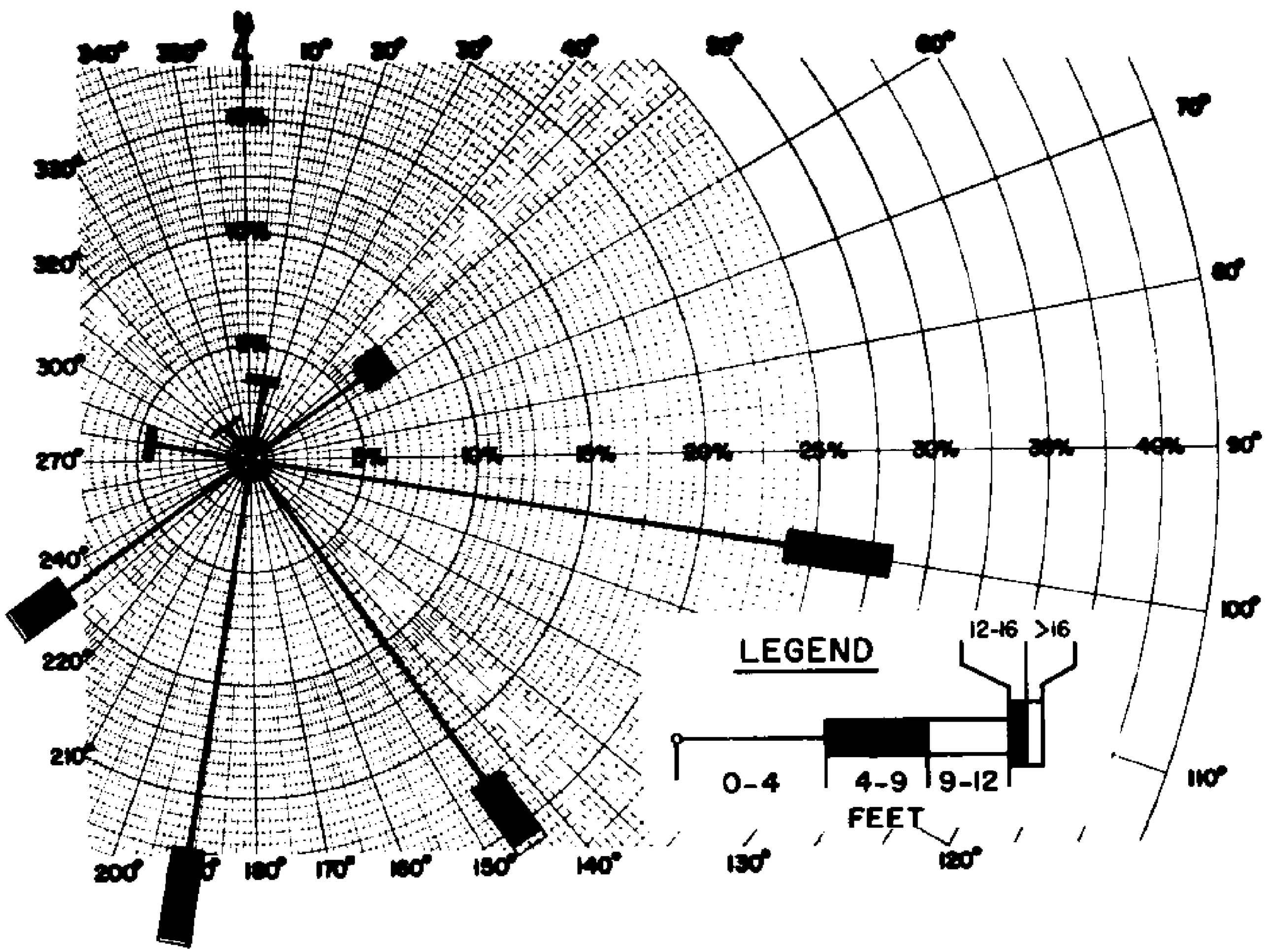

FIGURE D 37. WAVE HEIGHT ROSE FOR OFFSHORE WAVE CLIMATE
SSMO DATA SQUARE NO. 12 - JULY

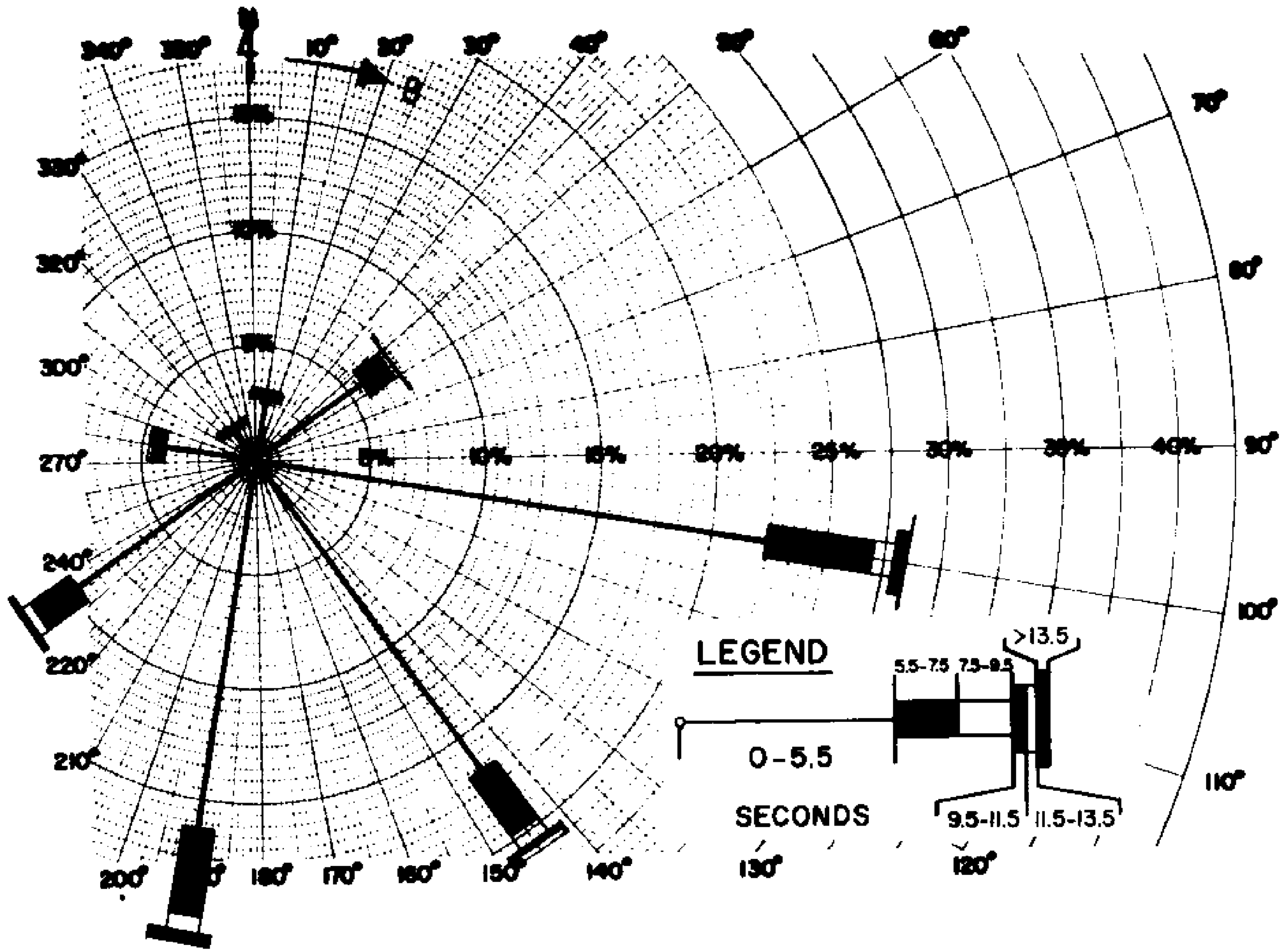

FIGURE D 38. WAVE PERIOD ROSE FOR OFFSHORE WAVE CLIMATE SSMO DATA SQUARE NO. 12 - JULY

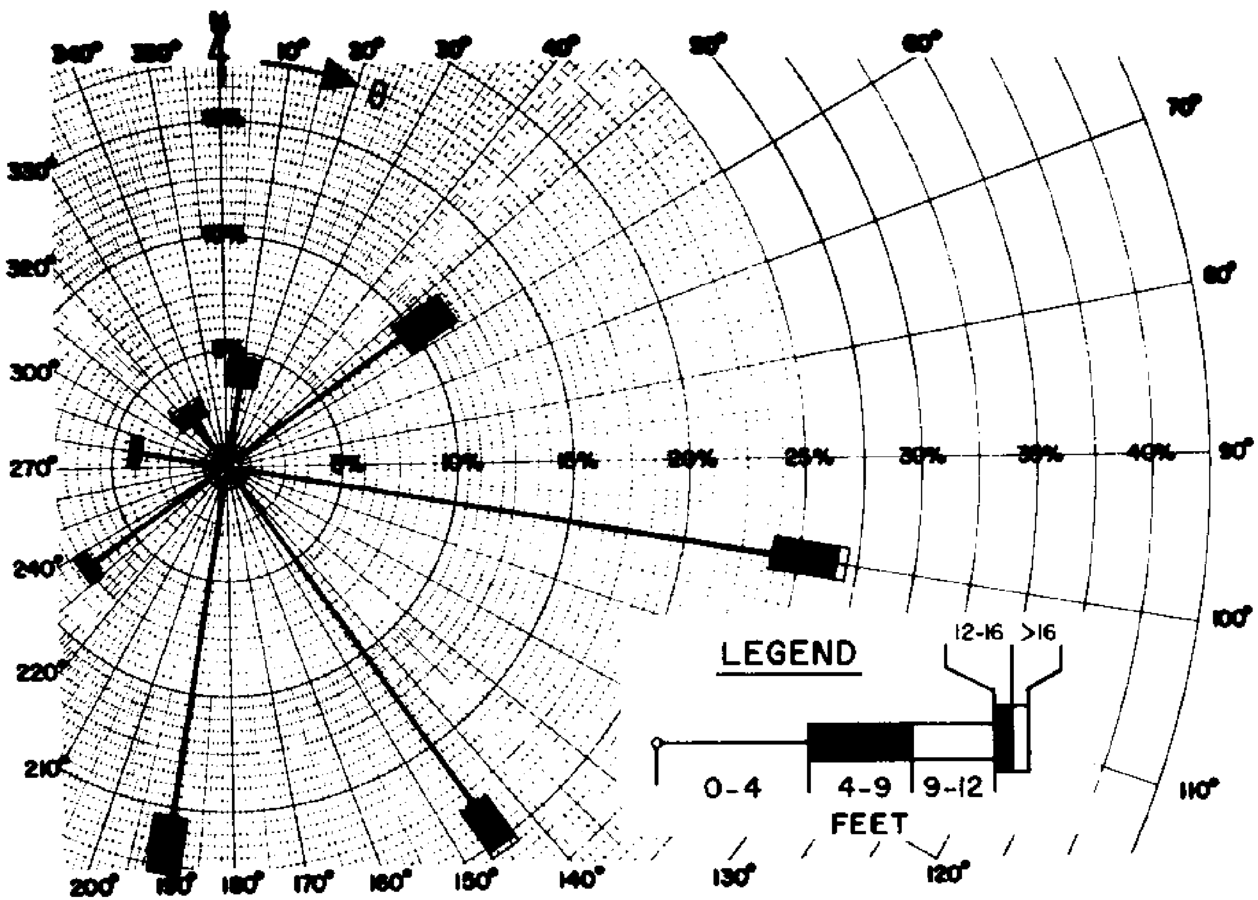

FIGURE D 39. WAVE HEIGHT ROSE FOR OFFSHORE WAVE CLIMATE
SSMO DATA SQUARE NO. 12 - AUGUST

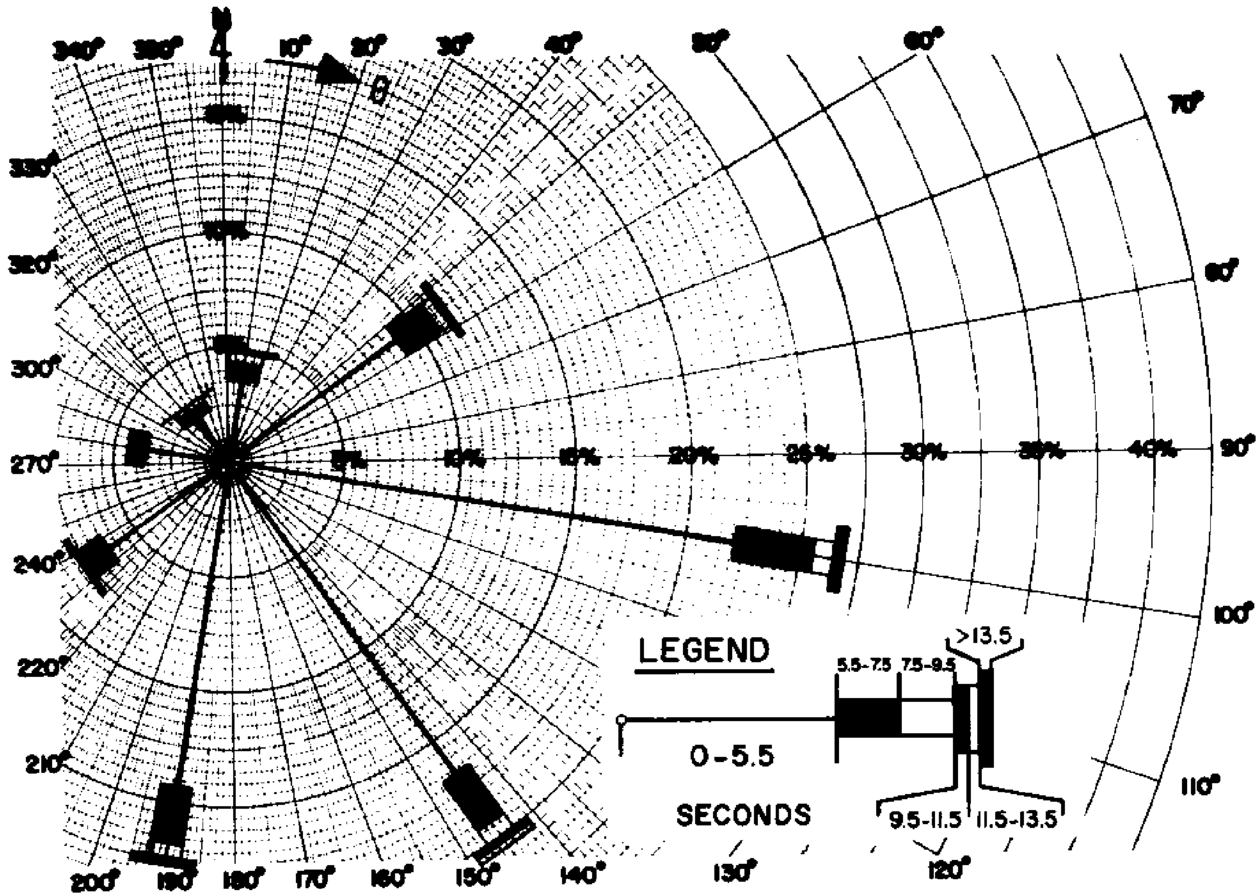

FIGURE D 40. WAVE PERIOD ROSE FOR OFFSHORE WAVE CLIMATE
SSMO DATA SQUARE NO. 12 - AUGUST

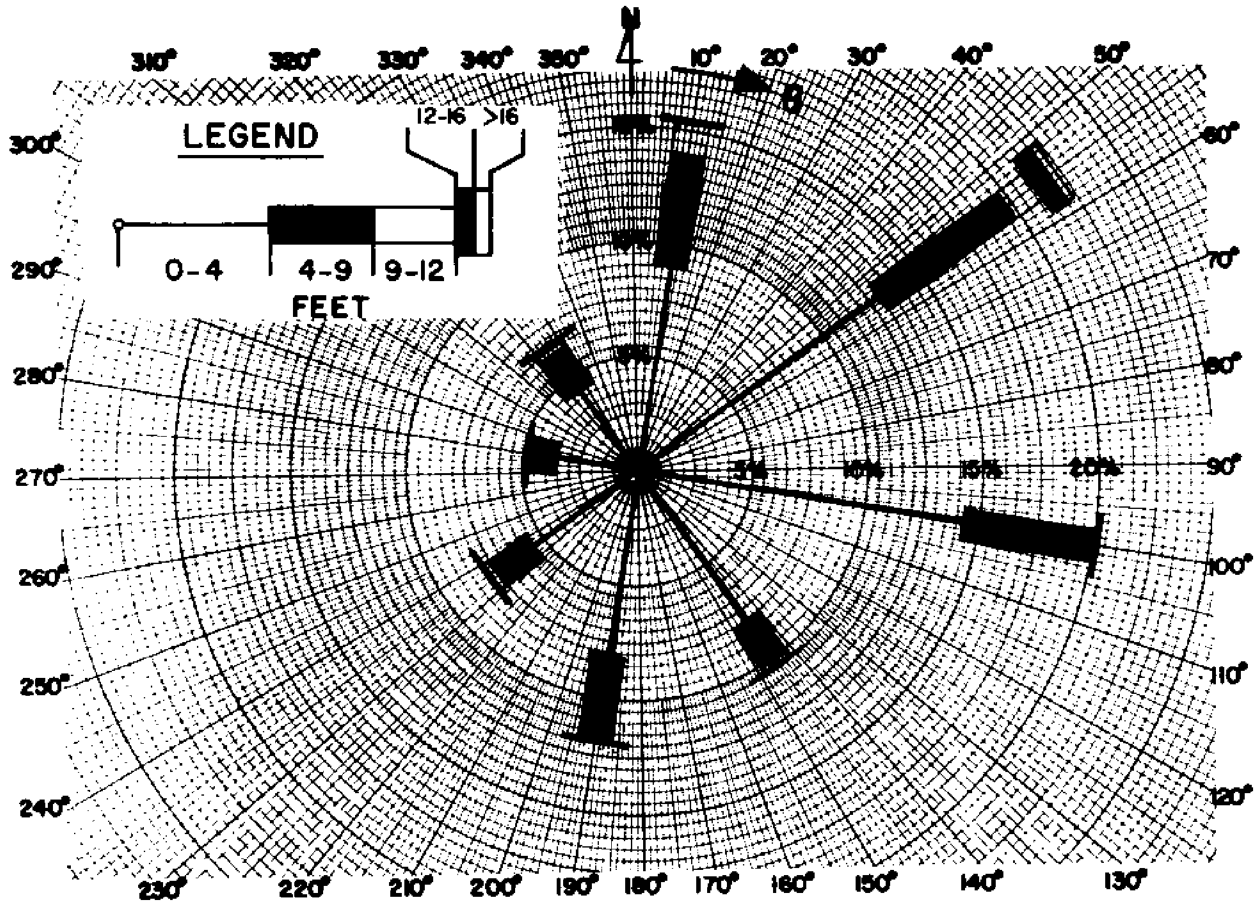

FIGURE D 41. WAVE HEIGHT ROSE FOR OFFSHORE WAVE CLIMATE
SSMO DATA SQUARE NO. 12 - SEPTEMBER

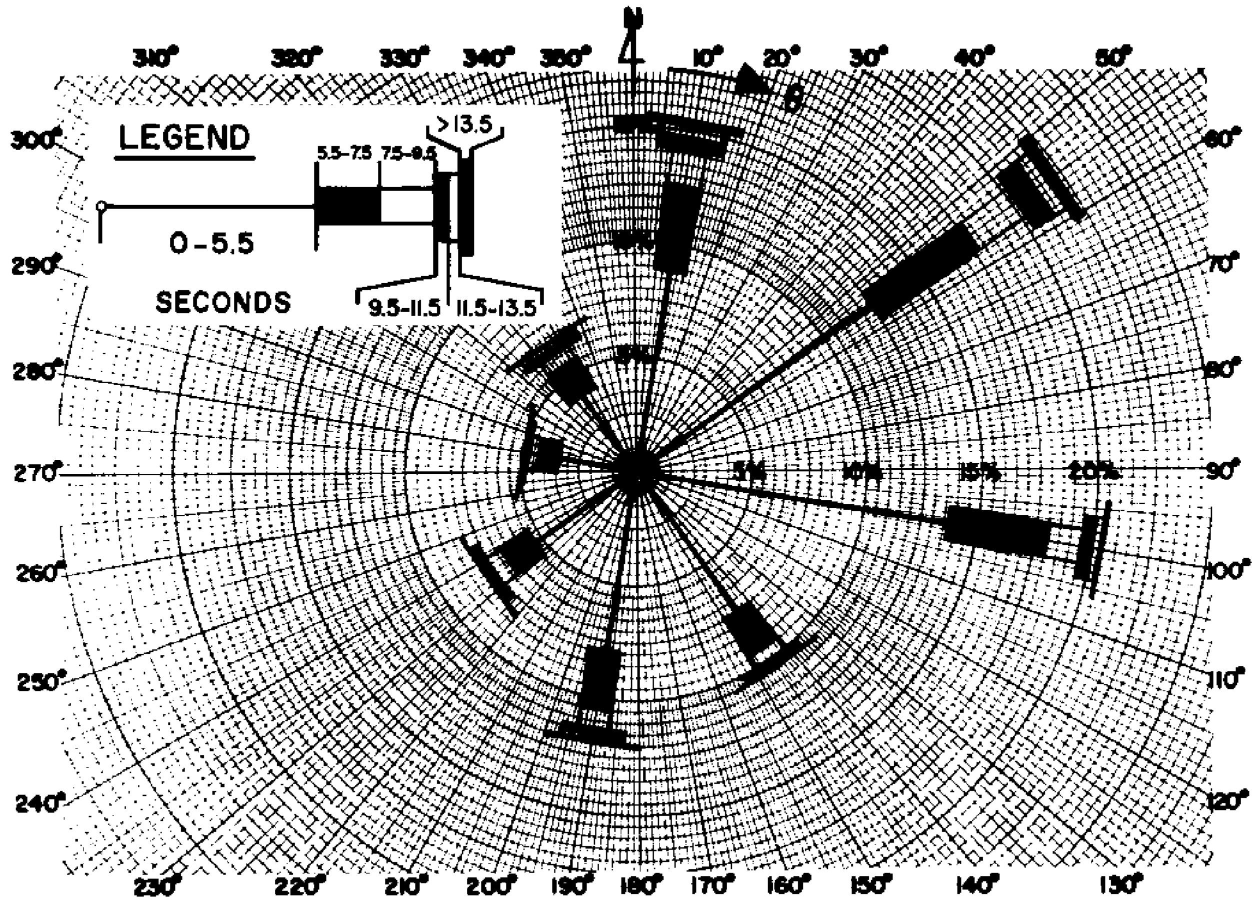

FIGURE D 42. WAVE PERIOD ROSE FOR OFFSHORE WAVE CLIMATE
SSMO DATA SQUARE NO. 12 - SEPTEMBER

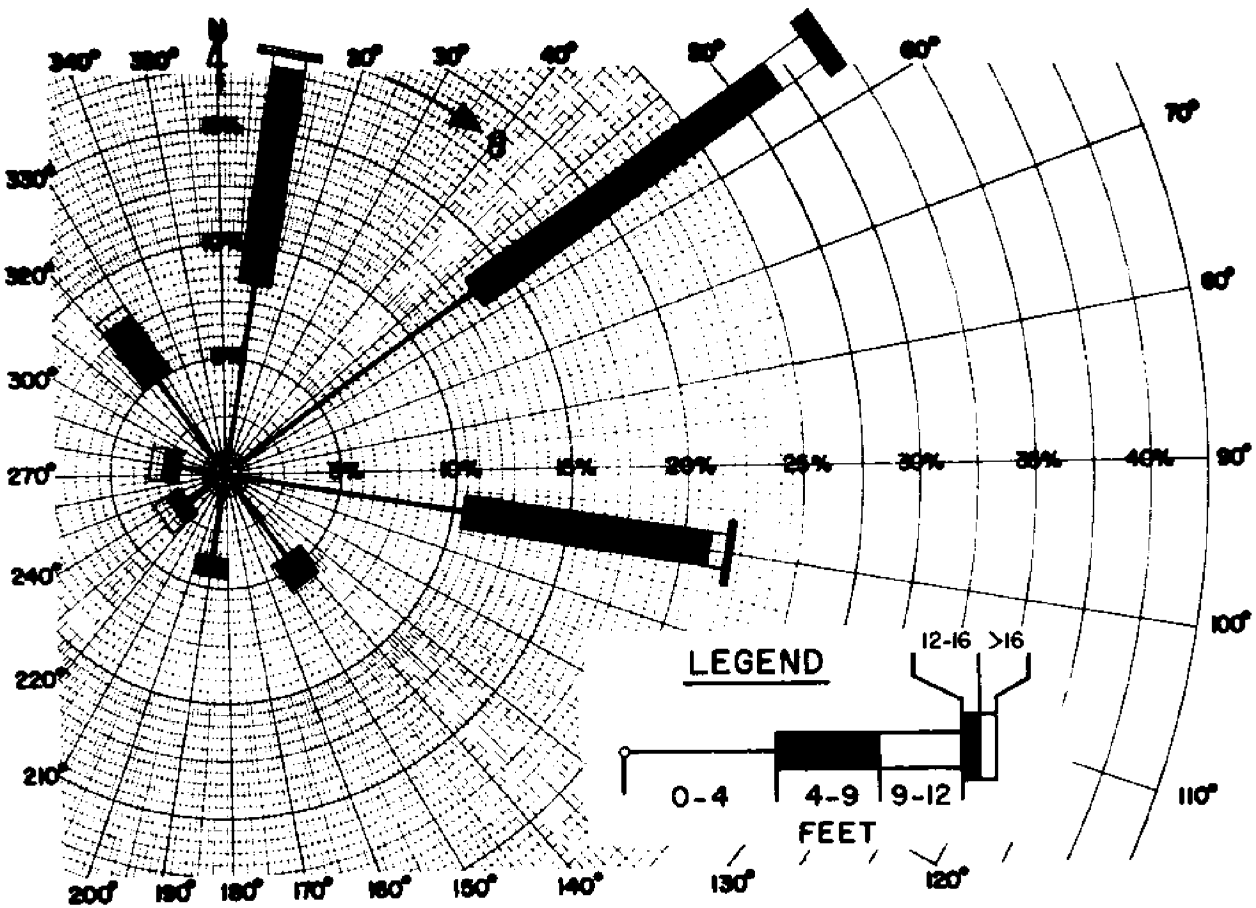

FIGURE D 43. WAVE HEIGHT ROSE FOR OFFSHORE WAVE CLIMATE
SSMO DATA SQUARE NO. 12 - OCTOBER

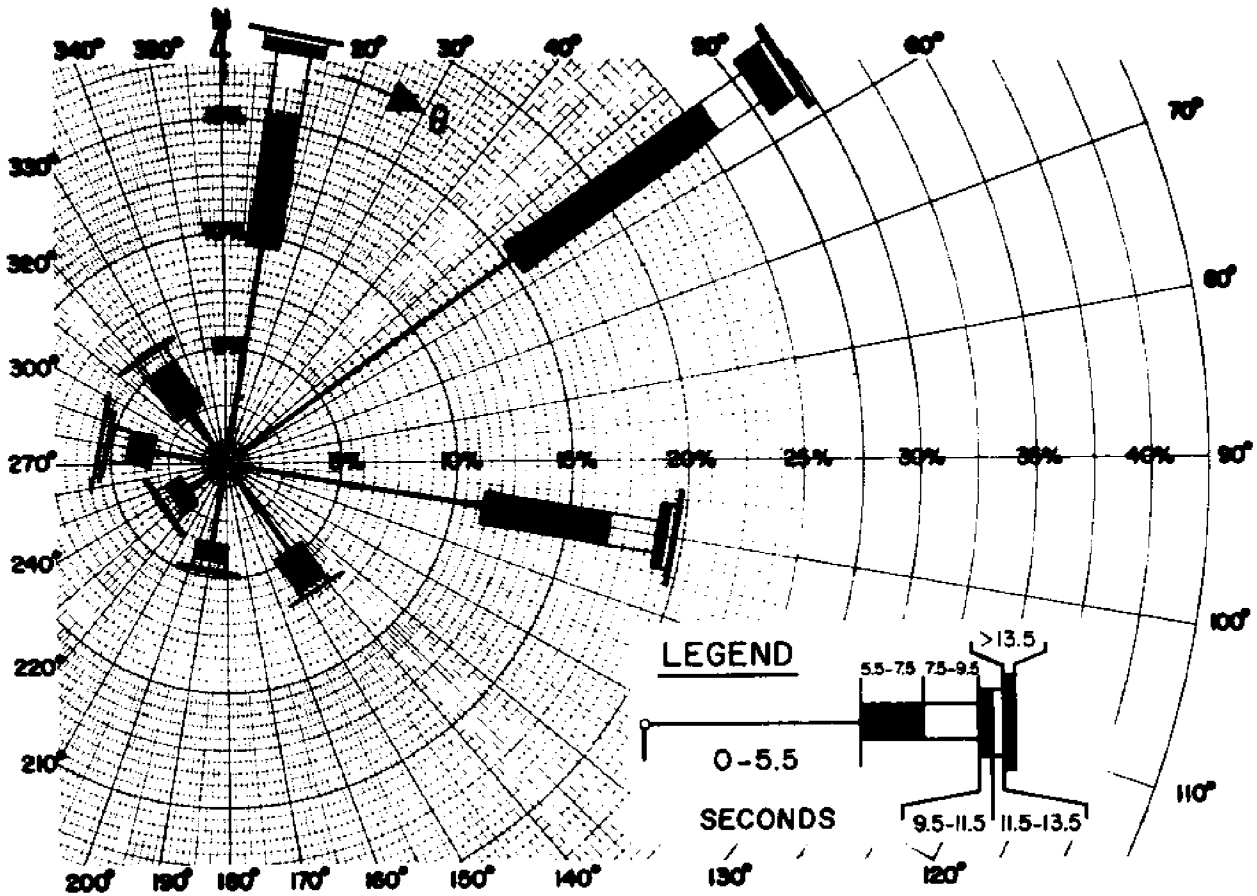

FIGURE D 44. WAVE PERIOD ROSE FOR OFFSHORE WAVE CLIMATE
SSMO DATA SQUARE NO. 12 - OCTOBER

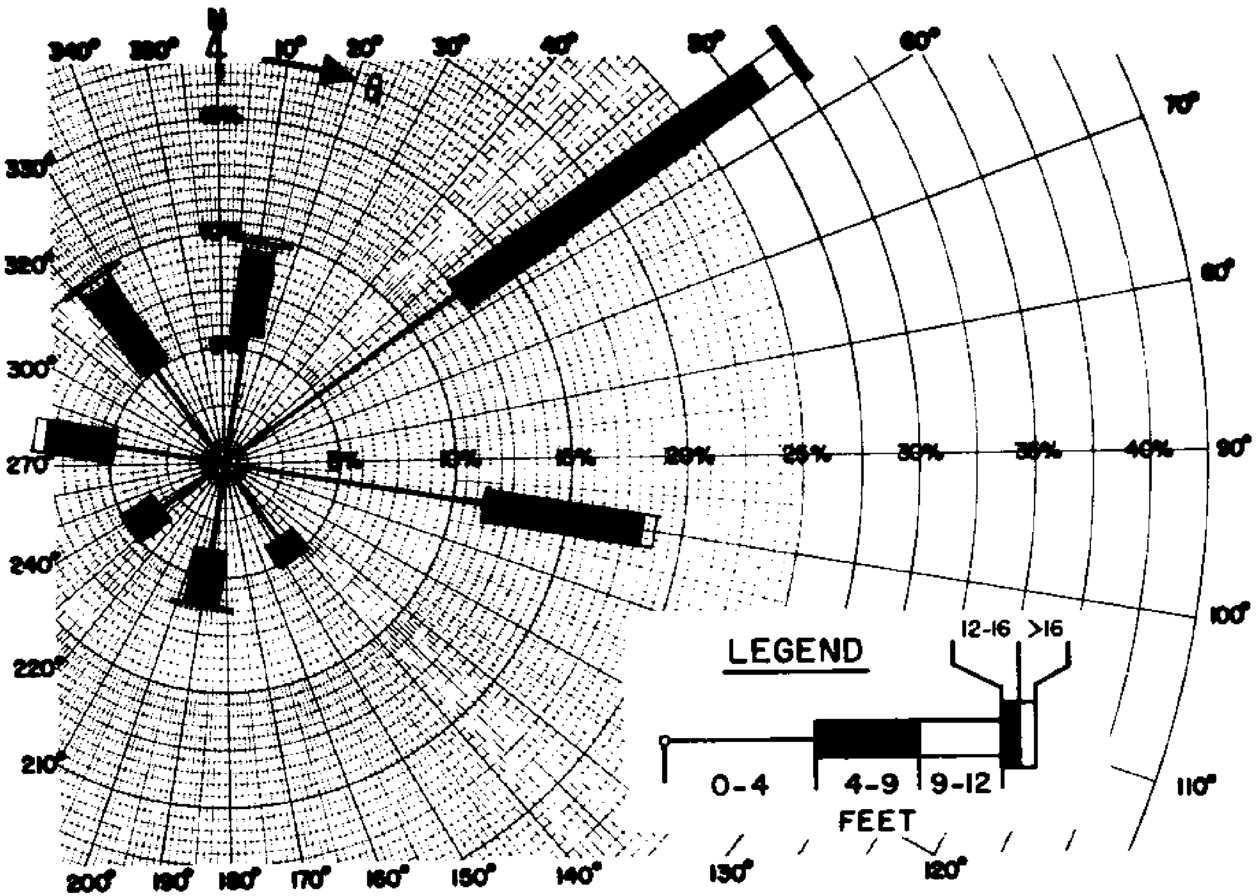

FIGURE D 45. **WAVE** HEIGHT **ROSE FOR OFFSHORE WAVE CLIMATE**
SSMO DATA SQUARE NO. 12 - NOVEMBER

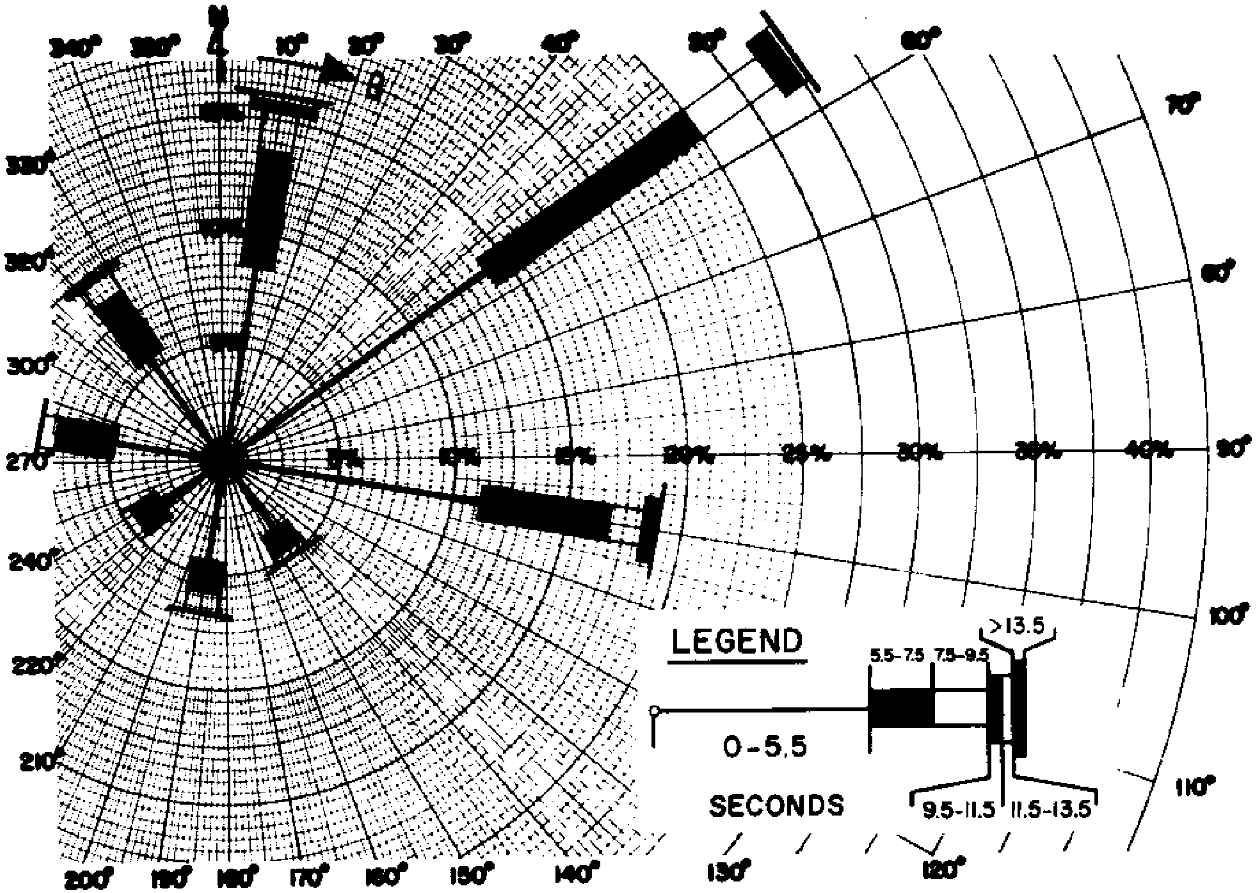

FIGURE D 46. WAVE PERIOD ROSE FOR OFFSHORE WAVE CLIMATE
SSMO DATA SQUARE NO. 12 - NOVEMBER

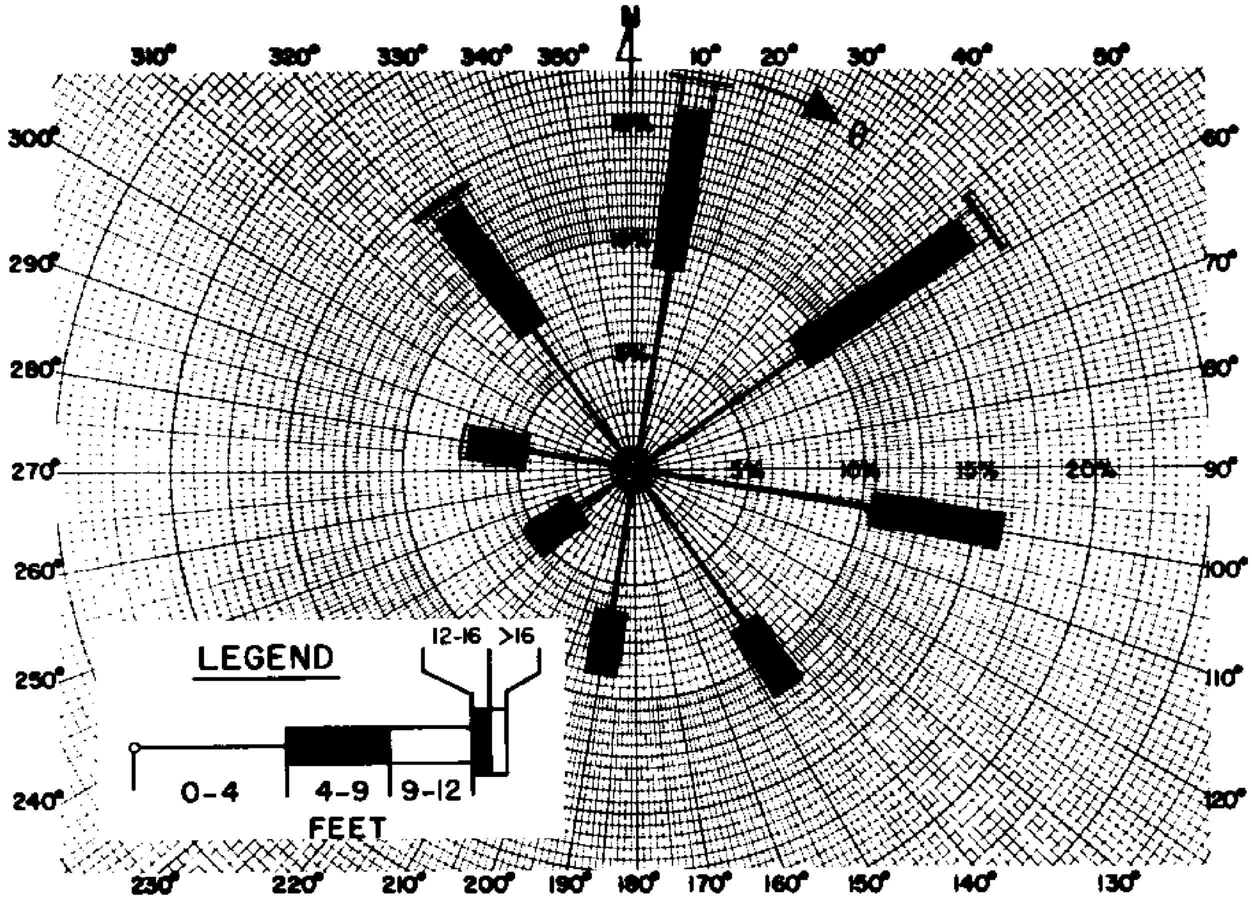

FIGURE D 47. WAVE HEIGHT ROSE FOR OFFSHORE WAVE CLIMATE SSMO DATA SQUARE NO. 12 - DECEMBER

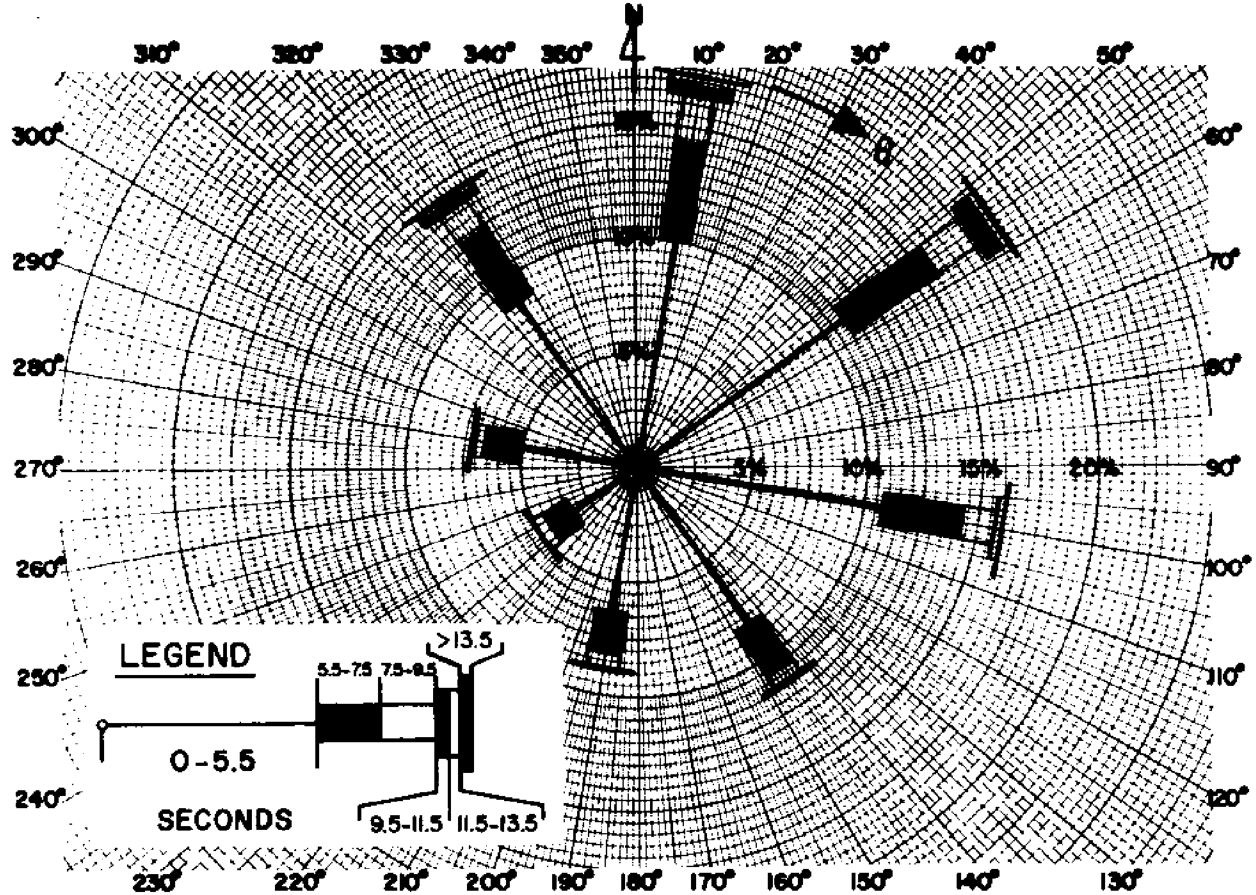

FIGURE D 48. WAVE PERIOD ROSE FOR OFFSHORE WAVE CLIMATE SSMO DATA SQUARE NO. 12 - DECEMBER